Advances in Clinical and Experimental Medicine

MONTHLY ISSN 1899-5276 (PRINT) ISSN 2451-2680 (ONLINE) advances.umw.edu.pl

2026, Vol. 35, No. 4 (April)

Impact Factor (IF) – 1.9
Ministry of Science and Higher Education – 70 pts
Index Copernicus (ICV) – 161.00 pts

Wroclaw Medical University

Advances
in Clinical and Experimental
Medicine

Advances
in Clinical and Experimental Medicine

ISSN 1899-5276 (PRINT) ISSN 2451-2680 (ONLINE) advances.umw.edu.pl

MONTHLY 2026
Vol. 35, No. 4
(April)

Advances in Clinical and Experimental Medicine (*Adv Clin Exp Med*) publishes high-quality original articles, research-in-progress, research letters and systematic reviews and meta-analyses of recognized scientists that deal with all clinical and experimental medicine.

Editorial Office
ul. Marcinkowskiego 2–6
50-368 Wrocław, Poland
Tel.: +48 71 784 12 05
E-mail: acem.journal@umw.edu.pl

Publisher
Wroclaw Medical University
Wybrzeże L. Pasteura 1
50-367 Wrocław, Poland

Online edition is the original version of the journal

Editorial Policy

Advances in Clinical and Experimental Medicine (Adv Clin Exp Med) is an independent multidisciplinary forum for exchange of scientific and clinical information, publishing original research and news encompassing all aspects of medicine, including molecular biology, biochemistry, genetics, biotechnology and other areas. During the review process, the Editorial Board conforms to the "Uniform Requirements for Manuscripts Submitted to Biomedical Journals: Writing and Editing for Biomedical Publication" approved by the International Committee of Medical Journal Editors (www.ICMJE.org). The journal publishes (in English only) original papers and reviews. Short works considered original, novel and significant are given priority. Experimental studies must include a statement that the experimental protocol and informed consent procedure were in compliance with the Helsinki Convention and were approved by an ethics committee.

For all subscription-related queries please contact our Editorial Office: acem.journal@umw.edu.pl
For more information visit the journal's website: advances.umw.edu.pl

Pursuant to the ordinance of the Rector of Wroclaw Medical University No. 37/XVI R/2024, from March 1, 2024, authors are required to pay a fee for each manuscript accepted for publication in the journal Advances in Clinical and Experimental Medicine. The fee amounts to 1600 EUR for all types of papers.

Indexed in: MEDLINE, Science Citation Index Expanded, Journal Citation Reports/Science Edition, Scopus, EMBASE/Excerpta Medica, Ulrich's™ International Periodicals Directory, Index Copernicus

Typographic design: Piotr Gil, Monika Kolęda
DTP: Wydawnictwo UMW
Cover: Monika Kolęda
Printing and binding: Agencja Wydawnicza "ARGI" s.c.

Advances
in Clinical and Experimental Medicine

MONTHLY 2026, Vol. 35, No. 4 (April)

ISSN 1899-5276 (PRINT)
ISSN 2451-2680 (ONLINE)
advances.umw.edu.pl

Contents

Editorials

Original papers

Research letters

Triglyceride-glucose (TyG) index in cardiovascular risk prediction: Clinical utility, guideline implications, and the need for outcome trials

Hongji Cheng[A–F]

Department of Cardiology, The Panyu District He Xian Memorial Hospital, Guangzhou, China

A – research concept and design; B – collection and/or assembly of data; C – data analysis and interpretation;
D – writing the article; E – critical revision of the article; F – final approval of the article

Advances in Clinical and Experimental Medicine, ISSN 1899–5276 (print), ISSN 2451–2680 (online) *Adv Clin Exp Med*. 2026;35(4):587–590

Address for correspondence
Hongji Cheng
E-mail: chenghongji@live.cn

Funding sources
This work was supported by the Medical and Health Project of the Panyu District Science and Technology Program, Guangzhou (grant No. 2025-Z04-46).

Conflict of interest
None declared

Received on March 26, 2025
Reviewed on June 7, 2025
Accepted on February 23, 2026

Published online on March 16, 2026

Abstract

The triglyceride-glucose (TyG) index, a simple surrogate marker integrating insulin resistance and atherogenic dyslipidemia, has attracted growing attention as a potential tool for addressing residual risk in cardiovascular disease (CVD) prediction. Robust observational evidence consistently links the TyG index to hard cardiovascular endpoints and subclinical atherosclerosis, positioning it as a strong candidate for clinical translation. However, its adoption in mainstream guidelines is constrained by a critical limitation: the current evidence is exclusively observational and lacks interventional data demonstrating that lowering the TyG index improves clinical outcomes. This editorial argues that, although the TyG index represents a practical and readily available risk-stratification adjunct, it has not yet evolved into a validated therapeutic target. We propose a dual-pathway strategy: provisional recognition within guidelines as a risk-enhancing factor, accompanied by a clear call for dedicated cardiovascular outcome trials. Such an approach would capitalize on its present utility while upholding the evidentiary standards required to inform clinical practice.

Key words: triglycerides, blood glucose, insulin resistance, cardiovascular disease, risk assessment

Cite as
Cheng H. Triglyceride-glucose (TyG) index in cardiovascular risk prediction: Clinical utility, guideline implications, and the need for outcome trials. *Adv Clin Exp Med*. 2026;35(4):587–590. doi:10.17219/acem/218470

DOI
10.17219/acem/218470

Highlights

- Triglyceride–glucose (TyG) index emerges as a strong cardiovascular risk marker: Robust observational studies link the TyG index to hard cardiovascular disease (CVD) outcomes and subclinical atherosclerosis, highlighting its value in residual risk prediction.
- Evidence gap limits guideline adoption: Despite consistent associations with cardiovascular events, the TyG index lacks interventional trials proving that lowering it improves clinical outcomes, preventing its recognition as a validated therapeutic target.
- Call for dual-pathway integration into CVD guidelines: Provisional inclusion of the TyG index as a risk-enhancing factor, combined with dedicated cardiovascular outcome trials, may accelerate its translation into evidence-based clinical practice.

Introduction

A consensus is emerging in preventive cardiology: the triglyceride-glucose (TyG) index is a remarkably strong, accessible, and independent marker of cardiovascular risk. Its calculation is seductively simple, its pathophysiological basis – integrating insulin resistance and atherogenic lipoproteins – is compelling, and its association with future events is consistently validated across diverse cohorts. It would seem, then, that its place in future clinical guidelines is all but assured.

However, the very ease of its adoption presents a danger. The translation of a risk marker into a guideline-recommended action is a process governed by rigorous evidentiary hierarchies, not merely by statistical association. The medical landscape is littered with biomarkers whose promising observational data never translated into improved patient outcomes when put to the interventional test. Thus, the critical question is not whether the TyG index is useful, but how it should be useful at this precise moment in its evidentiary evolution.

This editorial argues that we must resist the temptation to anoint the TyG index as a standalone intervention target prematurely. Its current, undeniable value lies in risk refinement – identifying the "hidden" high-risk individual within traditional intermediate-risk categories. I propose that guidelines should formally categorize it as a "risk-enhancing factor," a tool to prompt more personalized clinician–patient discussion and enhance lifestyle counseling. Concurrently, and with equal urgency, the research community must prioritize the definitive randomized trials that can probe its causal role. The TyG index is ready for a supporting role in risk assessment today, but its starring role in therapeutic guidance awaits the next act of scientific validation.

The guideline dilemma and the TyG opportunity

Despite the widespread application of existing risk prediction models based on traditional factors (e.g., blood pressure, low-density lipoprotein cholesterol [LDL-C]), the "residual risk" of cardiovascular disease (CVD) remains significant.[1] This drives the search for novel biomarkers that can more comprehensively and earlier reflect the essence of metabolic dysregulation. Insulin resistance and atherogenic dyslipoproteinemia are core pathophysiological mechanisms driving this residual risk,[2] yet current guidelines lack simple, cost-effective tools to routinely assess these dual pathways. The TyG index (Ln[fasting triglycerides (mg/dL) × fasting glucose (mg/dL)/2]) emerges precisely for this purpose. It ingeniously integrates these 2 mechanisms into a simple formula, representing a paradigm shift from assessing "single metrics" to evaluating "integrated pathways".[3] Faced with such a promising marker, what should be the stance of clinical guidelines: enthusiastic adoption or cautious vigilance?

Compelling evidence for TyG index usefulness

Large-scale, long-term follow-up studies have shown that the TyG index is significantly associated with myocardial infarction, stroke, and all-cause mortality.[4–6] Its predictive power is independent of traditional risk factors and often superior to single glycemic or lipid metrics.[7–9] Deeper investigation reveals that derivatives combining TyG with indices like body mass index (BMI) or waist circumference (WC) (e.g., TyG-BMI, TyG-WC) further enhance predictive accuracy, showcasing its excellent scalability.[10,11]

The TyG index integratively reflects the 2 key drivers of residual cardiovascular risk. First, as a valid surrogate for insulin resistance, its elevation signals abnormalities in glucose and fat metabolism, accompanied by increased free fatty acids and a pro-inflammatory state.[12] Second, elevated triglyceride levels per se are a marker for increased atherogenic triglyceride-rich lipoproteins (TRLs) and their remnants, which directly damage vasculature by inducing endothelial dysfunction and oxidative stress.[13] Thus, through a simple calculation, the TyG index captures

both the "upstream mechanism" (insulin resistance) and the "downstream effect" (TRLs).

The TyG index correlates strongly with subclinical atherosclerosis, providing a mechanistic bridge to hard endpoints. Substantial evidence confirms its strong association with key markers of subclinical atherosclerosis. At the vascular structural level, an elevated TyG index is independently associated with and is a significant risk factor for increased carotid intima-media thickness (CIMT).[14] At the coronary level, cross-sectional and intravascular ultrasound evidence indicates that a higher TyG index is significantly associated with the presence, extent, and unstable features (e.g., spotty calcification) of coronary artery calcification (CAC).[15] A meta-analysis of 41 studies concluded that individuals with a high TyG index are at significantly increased risk of coronary calcification, plaque progression, and multivessel disease.[16] These findings indicate that the insulin-resistant and dyslipidemic state captured by the TyG index directly promotes the initiation, progression, and destabilization of atherosclerotic lesions. Therefore, the TyG index is not merely a risk marker but a mechanistic link connecting metabolic dysregulation to structural vascular damage.

Finally, the calculation of the TyG index relies solely on the most routine, low-cost laboratory tests, obtainable at any level of healthcare facility. This grants it immense public health value, particularly in resource-limited settings.

The "critical gap" hindering TyG index guideline inclusion

However, a sober recognition is essential: Observational association is merely the first step. Changing clinical practice through guidelines requires the highest level of evidence – demonstrating that intervention on the marker yields clear clinical benefit. Currently, all evidence supporting the TyG index remains observational, proving "association" but not "causation" or "intervention benefit". This evidence chasm is precisely what separates a "risk marker" from a "clinical decision-making target." The historical trajectory of high-sensitivity C-reactive protein (hs-CRP) offers a profound lesson: Despite an immense body of evidence linking it to cardiovascular risk, and a positive trial (JUPITER) designed based on this link,[17] a subsequent trial specifically testing the "anti-inflammatory" benefit (CIRT) failed to improve cardiovascular outcomes.[18] This exposes a critical issue: Even if a marker can be lowered by an intervention, it does not equate to the efficacy of a direct, pathway-specific intervention. Consequently, hs-CRP has not been widely adopted as an independent target to initiate therapy.

In contrast, the transformative pathway of lipoprotein(a) (Lp(a)) points the way forward. Although its causal link to cardiovascular risk was long established through large-scale genetic studies, its fundamental change in clinical stature began when drugs targeting Lp(a) reduction (e.g., Zerlasiran) demonstrated safe and potent lowering of its levels by over 80% in clinical trials, with several phase III trials with cardiovascular endpoints underway.[19,20] It is precisely this progress that has led to Lp(a)'s recent inclusion in multiple international guidelines. In contrast, the TyG index stands at this decisive threshold: It urgently needs its own 'cardiovascular outcomes trial' to answer the pivotal question – can actively lowering a high TyG index ultimately reduce the incidence of myocardial infarction and stroke? Only with positive results from such prospective randomized controlled trials (RCTs) can the TyG index complete its transformation from an excellent risk predictor to an actionable clinical decision-making tool.

Furthermore, the distribution and optimal risk cut-off points for the TyG index vary across races, ages, and genders. Guidelines require a universal or stratified standard. As the index fluctuates with lifestyle and medication, should guidelines recommend a single measurement or an average/trend from multiple readings? In modern risk prediction models incorporating over a dozen variables (e.g., the U.S. Pooled Cohort Equations), is the Net Reclassification Improvement (NRI) or Integrated Discrimination Improvement (IDI) gained by adding the TyG index significant enough to justify the added complexity and change risk stratification? Finally, its routine use necessitates evaluation of "clinical net benefit" to prevent unnecessary additional testing or over-treatment of borderline cases.

A pragmatic pathway towards guideline inclusion

I propose that current guidelines formally include the TyG index within chapters dedicated to "Emerging Risk Markers" or "Risk-Enhancing Factors." Its role should be defined not as an independent standard to initiate therapy, but as a decision-aid for risk stratification and an alert indicator to intensify patient education. For instance, in individuals at intermediate traditional risk but with a significantly elevated TyG index, an escalation of intervention intensity could be considered.

There is a compelling need to launch TyG index-directed RCTs. These trials could enroll asymptomatic individuals at low-to-intermediate traditional risk but with a TyG index above a specific cut-point, randomizing them to standard care versus intensified intervention arms (e.g., early initiation of statins, GLP-1 receptor agonists, or intensive lifestyle management), with cardiovascular events as the primary endpoint.

We recommend that professional societies lead the development of expert consensus statements on the measurement and reporting of the TyG index to promote standardization.

Conclusions

Prudent integration of the TyG index into clinical context and the active pursuit of rigorous research are not mutually exclusive but embody the rigor and dynamism of evidence-based medicine. I embrace this promising tool but must validate it against the highest scientific standards, with the ultimate goal of patient benefit.

Use of AI and AI-assisted technologies

Not applicable.

ORCID iDs

Hongji Cheng https://orcid.org/0000-0002-5092-6560

References

1. Karakasis P, Theofilis P, Patoulias D, Vlachakis PK, Antoniadis AP, Fragakis N. Diabetes-driven atherosclerosis: Updated mechanistic insights and novel therapeutic strategies. *Int J Mol Sci*. 2025;26(5):2196. doi:10.3390/ijms26052196
2. Caselli C, Occhipinti M, Pane K, et al. Health improvements by understanding residual risk in coronary artery disease and new targets for prevention/treatment: Rationale and research protocol of the HURRICANE project. *Eur Heart J Open*. 2025;5(1):oeaf005. doi:10.1093/ehjopen/oeaf005
3. Zhong J, Liu D, Huang X, et al. Triglyceride glucose-waist circumference dynamics and cardiovascular risk: A national longitudinal study. *Lipids Health Dis*. 2025;24(1):354. doi:10.1186/s12944-025-02774-5
4. Alizargar J, Bai CH, Hsieh NC, Wu SFV. Use of the triglyceride-glucose index (TyG) in cardiovascular disease patients. *Cardiovasc Diabetol*. 2020;19(1):8, doi:10.1186/s12933-019-0982-2
5. Li J, Dong Z, Wu H, et al. The triglyceride-glucose index is associated with atherosclerosis in patients with symptomatic coronary artery disease, regardless of diabetes mellitus and hyperlipidaemia. *Cardiovasc Diabetol*. 2023;22(1):224. doi:10.1186/s12933-023-01919-z
6. Wang X, Xu W, Song Q, et al. Association between the triglyceride–glucose index and severity of coronary artery disease. *Cardiovasc Diabetol*. 2022;21(1):168. doi:10.1186/s12933-022-01606-5
7. Wu X, Qiu W, Yang H, Chen YJ, Liu J, Zhao G. Associations of the triglyceride-glucose index and atherogenic index of plasma with the severity of new-onset coronary artery disease in different glucose metabolic states. *Cardiovasc Diabetol*. 2024;23(1):76. doi:10.1186/s12933-024-02163-9
8. Polak M, Nowicki GJ, Chrzanowska-Wąsik M, Ślusarska BJ. Do sociodemographic and health predictors affect the non-insulin-based insulin resistance index? A cross-sectional study. *Adv Clin Exp Med*. 2024;34(7):1155–1163. doi:10.17219/acem/191200
9. Pan LY, Jin L. Association between triglyceride glucose index and biological aging in U.S. adults: National Health and Nutrition Examination Survey. *Cardiovasc Diabetol*. 2025;24(1):100. doi:10.1186/s12933-025-02631-w
10. Kochanowicz M, Rhaiem TB, Owczarek AJ, et al. The cut-off values for SHBG discriminating insulin resistance based on the TyG, TyG-BMI, and TyG-WC values in women with PCOS. *Biomedicines*. 2026;14(1):187. doi:10.3390/biomedicines14010187
11. He D, Huang Y, Ni X, Bao Z. Prospective associations of triglyceride-glucose related indices with cardiovascular disease and mortality in individuals with metabolic syndrome: Evidence from the UK biobank. *Cardiovasc Diabetol*. 2026;25(1):53. doi:10.1186/s12933-025-03070-3
12. Adams-Huet B, Jialal I. An increasing triglyceride–glucose index is associated with a pro-inflammatory and pro-oxidant phenotype. *J Clin Med*. 2024;13(13):3941. doi:10.3390/jcm13133941
13. Gounden V, Devaraj S, Jialal I. The role of the triglyceride-glucose index as a biomarker of cardio-metabolic syndromes. *Lipids Health Dis*. 2024;23(1):416. doi:10.1186/s12944-024-02412-6
14. Lin X, Xie S, Pu B, et al. Triglyceride-glucose index in the associations between chronic low-grade inflammation and carotid intima-media thickness: Mediation and effect-modification across triglyceride–glucose strata. *BMC Cardiovasc Disord*. 2025;25(1):725. doi:10.1186/s12872-025-05199-1
15. Zhou H, Chen X, Zhang Y, et al. The associations between pancreatic fat infiltration and its combination with the triglyceride-glucose index and the risk of coronary calcification: A multicenter study. *Clin Transl Gastroenterol*. 2025;16(11):e00905. doi:10.14309/ctg.0000000000000905
16. Liang S, Wang C, Zhang J, et al. Triglyceride-glucose index and coronary artery disease: A systematic review and meta-analysis of risk, severity, and prognosis. *Cardiovasc Diabetol*. 2023;22(1):170. doi:10.1186/s12933-023-01906-4
17. Ridker PM, Danielson E, Fonseca FAH, et al. Rosuvastatin to prevent vascular events in men and women with elevated C-reactive protein. *N Engl J Med*. 2008;359(21):2195–2207. doi:10.1056/NEJMoa0807646
18. Ridker PM, Everett BM, Pradhan A, et al. Low-dose methotrexate for the prevention of atherosclerotic events. *N Engl J Med*. 2019;380(8):752–762. doi:10.1056/NEJMoa1809798
19. Di Costanzo A, Indolfi C, Franzone A, Esposito G, Spaccarotella CAM. Lp(a) in the pathogenesis of aortic stenosis and approach to therapy with antisense oligonucleotides or short interfering RNA. *Int J Mol Sci*. 2023;24(19):14939. doi:10.3390/ijms241914939
20. Kronenberg F, Mora S, Stroes ESG. Consensus and guidelines on lipoprotein(a): Seeing the forest through the trees. *Curr Opin Lipidol*. 2022;33(6):342–352. doi:10.1097/MOL.0000000000000855

Measurement of platelet reactivity in thrombocytopenic patients on dual antiplatelet therapy after percutaneous coronary intervention

Daiwa Wilczewska[1,A–F], Mikołaj Błaziak[1,D], Kornelia Gajek[2,B,C], Bożena Karolko[1,B,C], Magdalena Cielecka[1,B,D,E], Kamila Florek[3,D], Weronika Wietrzyk[3,D], Wojciech Stefaniak[3,B], Jakub Sokołowski[3,B], Urszula Woźniak[3,B], Dominik Mendyka[3,B,C], Andrzej Mysiak[1,A,E,F], Wiktor Kuliczkowski[1,A–F]

[1] Institute for Heart Diseases, Wroclaw Medical University, Poland
[2] Department of Pediatric Oncology, Haematology and Bone Marrow Transplantation, Wroclaw Medical University, Poland
[3] Students' Scientific Group of Invasive Cardiology, Institute for Heart Diseases, Wroclaw Medical University, Poland

A – research concept and design; B – collection and/or assembly of data; C – data analysis and interpretation; D – writing the article; E – critical revision of the article; F – final approval of the article

Advances in Clinical and Experimental Medicine, ISSN 1899–5276 (print), ISSN 2451–2680 (online) *Adv Clin Exp Med*. 2026;35(4):591–597

Address for correspondence
Mikołaj Błaziak
E-mail: blaziak.mikolaj@gmail.com

Funding sources
This work was supported by Wroclaw Medical University, grant No. SUB.C150.20.017.

Conflict of interest
None declared

Received on December 9, 2024
Reviewed on January 21, 2025
Accepted on July 2, 2025

Published online on April 21, 2026

Abstract

Background. Thrombocytopenia remains a significant problem in patients with cardiovascular disease (CVD) due to the indispensable use of antiplatelet therapy.

Objectives. The aim of this study was to establish a novel flow cytometry (FC)-based method for measuring platelet reactivity during dual antiplatelet therapy (DAPT) and to compare it with impedance aggregometry (IA) in thrombocytopenic patients undergoing percutaneous coronary intervention (PCI).

Materials and methods. This prospective cross-sectional study included 30 patients with thrombocytopenia. Platelet aggregation was assessed using IA and FC.

Results. A similar response to arachidonic acid (AA), reflecting the effect of acetylsalicylic acid (ASA), was observed in both groups. Responses to thrombin receptor agonist peptide (TRAP) and adenosine diphosphate (ADP), measured with aggregometry, were significantly higher in thrombocytopenic patients than in patients with normal platelet counts. When the FC method was used, the response to AA was significantly higher in thrombocytopenic patients. The optimal cut-off value for the FC method to define adequate platelet reactivity inhibition with clopidogrel in thrombocytopenic patients was <25.7%.

Conclusions. In patients with thrombocytopenia, IA is useful for assessing ASA response, whereas the presented FC method may be more accurate for evaluating response to clopidogrel.

Key words: percutaneous coronary intervention, thrombocytopenia, dual antiplatelet therapy

Cite as
Wilczewska D, Błaziak M, Gajek K, et al. Measurement of platelet reactivity in thrombocytopenic patients on dual antiplatelet therapy after percutaneous coronary intervention. *Adv Clin Exp Med*. 2026;35(4):591–597. doi:10.17219/acem/207803

DOI
10.17219/acem/207803

Highlights

- Flow cytometry (FC) provides a more accurate assessment of platelet reactivity to clopidogrel in thrombocytopenic patients undergoing percutaneous coronary intervention (PCI).
- Impedance aggregometry remains reliable for evaluating acetylsalicylic acid (ASA) response in patients on dual antiplatelet therapy (DAPT).
- Thrombocytopenic patients show enhanced platelet reactivity to ADP and TRAP, indicating altered platelet function despite reduced platelet counts.
- A flow cytometry cut-off below 25.7% may optimize monitoring of clopidogrel effectiveness in thrombocytopenic patients.

Background

Antiplatelet therapy is a key component of pharmacologic treatment in patients with atherosclerotic vascular disease, as it reduces platelet activation and aggregation and thereby lowers the risk of thrombotic events. However, this approach is inherently associated with an increased risk of bleeding, making the balance between thrombotic protection and hemorrhagic complications particularly challenging in high-risk populations with thrombocytopenia. This issue is especially pronounced after percutaneous coronary intervention (PCI) with stent implantation, where dual antiplatelet therapy (DAPT) with acetylsalicylic acid (ASA) and clopidogrel is recommended for 6 months. However, robust evidence to guide DAPT management in patients with thrombocytopenia is lacking. The available literature is largely limited to individual case reports, small case series, and expert opinions, with a notable lack of evidence-based guidelines or randomized controlled trials (RCTs) supporting tailored long-term antiplatelet therapy in this population.[1–6]

One proposed approach to optimize ASA and clopidogrel therapy involves monitoring platelet inhibition using aggregometry.[7] This technique has been extensively studied in patients with normal platelet counts and has demonstrated robust utility in characterizing platelet function and assessing responsiveness to antiplatelet therapy. However, current clinical guidelines do not recommend its routine use after PCI. Instead, platelet reactivity assessment is reserved for selected high-risk populations, such as patients undergoing urgent coronary artery bypass grafting while receiving DAPT.[8] Although thrombocytopenia is relatively uncommon among patients undergoing coronary interventions, platelet function monitoring may be justified in this subgroup to achieve an appropriate balance between antithrombotic efficacy and bleeding risk. This consideration is particularly relevant because thrombocytopenia is independently associated with adverse outcomes in patients hospitalized with cardiovascular disease (CVD).[9]

A major limitation of conventional aggregometry is that commercially available systems are validated only for platelet counts from 150,000/mm^3 to 450,000/mm^3. An alternative approach to address this limitation is the use of flow cytometry (FC)-based platelet reactivity assessment, which allows for evaluation of platelet activation independently of the absolute platelet count. Although FC remains technically demanding and has not yet been implemented as a point-of-care assay, it has consistently demonstrated superior sensitivity for detecting alterations in platelet reactivity.

Objectives

This study aimed to establish a novel FC-based method for assessing platelet reactivity during DAPT and to compare its performance with impedance aggregometry (IA) in patients with thrombocytopenia undergoing PCI.

Materials and methods

Patients selection

This prospective cross-sectional study was conducted in patients with thrombocytopenia undergoing PCI. Inclusion criteria were a platelet count <150,000/mm^3, recent PCI, and treatment with DAPT. Exclusion criteria included the use of additional systemic anticoagulation. Patients who met all inclusion criteria, had no exclusion criteria, and provided written informed consent were enrolled. The control group comprised healthy volunteers not receiving antiplatelet therapy and patients with normal platelet counts who had recently undergone PCI and were treated with DAPT. All participants had blood samples collected in the early morning after fasting for at least 6 h.

Impedance aggregometry

Blood samples for platelet aggregation assessment were collected at the following time points: pre-PCI and at 24 h, 7 days, and 30 days after the procedure. Platelet aggregation was measured using a Multiplate® impedance aggregometer (Roche Diagnostics, Basel, Switzerland). Blood

was collected into tubes containing hirudin (25 µg/mL) as an anticoagulant (Roche Diagnostics). The agonists used for aggregation were arachidonic acid (AA) 0.5 mM, adenosine diphosphate (ADP) 6.4 µM, collagen (COL) 3.2 µg/mL, and thrombin receptor agonist peptide (TRAP) 32 µM. All reagents were provided by the manufacturer (Roche Diagnostics). Aggregation was performed within 2 h of blood collection and recorded as the area under the curve (AUC). Each test was performed in duplicate, and the mean value was used for analysis. If the difference between the 2 measurements exceeded 10%, the result was discarded and the measurement was repeated. Response to ASA was evaluated using AA-induced platelet aggregation, whereas response to clopidogrel was assessed using ADP-induced aggregation. Based on previously published thresholds, incomplete response to clopidogrel was defined as aggregation >48 AU and incomplete response to ASA as aggregation >30 AU.[10,11]

Flow cytometry method

Plasma from a single male donor (blood group AB, RhD positive) was used as the matrix for all flow cytometric platelet aggregation experiments, following the protocol described by Vinholt et al.[12] Donor plasma was obtained by double centrifugation of citrate-anticoagulated whole blood at 1,000 × g for 10 min. The resulting plasma was aliquoted into 150-µL portions and stored at –80°C. Peripheral blood from study participants was collected into BD Vacutainer® tubes (BD Biosciences, Franklin Lakes, USA)containing 0.109 M trisodium citrate for platelet function testing or ethylenediaminetetraacetic acid (EDTA) for hematologic analysis. Platelet-rich plasma (PRP) was prepared by centrifuging citrate-anticoagulated blood at 200 × g for 15 min at 37°C. Platelet counts in PRP were measured using a Sysmex XN-2000 analyzer (Sysmex Corporation, Kobe, Japan).

Platelet-rich plasma was subsequently divided into 2 fractions containing 144 × 10^3/µL and 16 × 10^3/µL platelets, respectively. In patients with peripheral platelet counts <150 × 10^3/µL, proportional reductions in fraction volumes were applied (eg, 72 × 10^3/µL and 8 × 10^3/µL). The PRP fractions were diluted to the target platelet concentration with a physiologic buffer (NaCl 134 mM, KCl 2.9 mM, $MgCl_2$ 1 mM, glucose 5.6 mM, and HEPES 20 mM; pH 7.4) and labeled with either calcein-AM ultrapure grade (CAMU; detected in fluorescein isothiocyanate (FITC)) or calcein-AM Violet 450 (CV450; detected in V450) (both from eBioscience, San Diego, USA). A 500-µL aliquot of the 144 × 10^3/µL fraction was stained with 10 µL of CV450 (working solution, 0.2 µM in dimethyl sulfoxide (DMSO)), and a 500-µL aliquot of the 16 × 10^3/µL fraction was stained with 10 µL of CAMU (working solution, 10 µM in DMSO). Labeling was performed for 15 min at 37°C in the dark with shaking at 600 rpm (BioSan Thermo-Shaker TS-100; Biosan, Riga, Latvia).

For the FC aggregation assay, 35 µL of thawed donor plasma was mixed with 17.5 µL of each labeled platelet fraction in 1.5-mL Eppendorf® tubes (Eppendorf SE, Hamburg, Germany). Subsequently, 2.5 µL of ADP, 2.5 µL of TRAP, or 25 µL of AA (Roche ADPtest, TRAPtest, and ASPItest, respectively; Roche Diagnostics) was added, yielding a final concentrations of ADP 6.5 µM, TRAP 32 µM, and AA 0.56 mM. Samples were incubated for 5 min at 37°C with shaking at 600 rpm. A 4th tube, processed identically but without agonist, served as a negative control (NC).

After incubation, 1 mL of fixation buffer (0.2% formaldehyde in dilution buffer) was added, and samples were transferred to FC tubes. Acquisition was performed using a FACSCanto 10-color (uncompensated) flow cytometer, and data were analyzed using FACSDiva software (both from BD Biosciences).

Gating strategy

The platelet population was initially identified on a forward scatter (FSC) vs side scatter (SSC) plot and subsequently confirmed on an FSC vs FITC plot corresponding to CAMU-labeled platelets (Fig. 1). The platelet gate (P3)

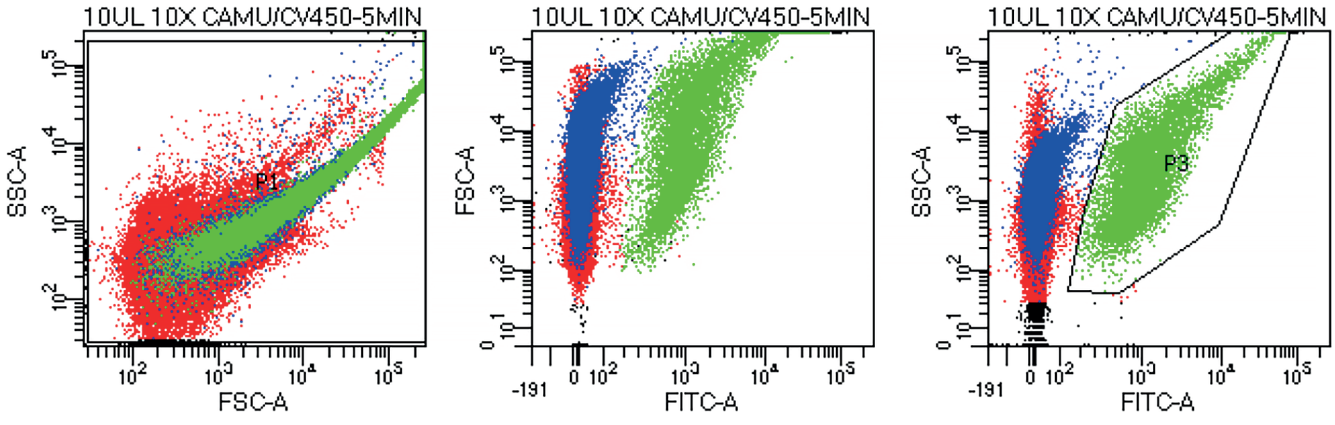

Fig. 1. Identification of the platelet population using FC

FC – flow cytometry; FITC-A – fluorescein isothiocyanate area; FSC – forward scatter; SSC – side scatter.

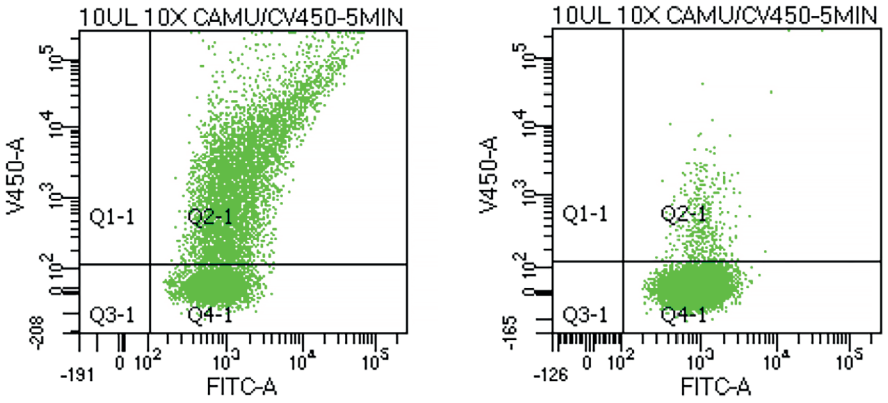

Fig. 2. Platelet aggregation with (right) and without (left) ADP stimulation

AA – arachidonic acid; ADP – adenosine diphosphate; CAMU – calcein-acetoxymethyl ester ultrapure grade; V450-A,c – alcein-AM Violet 450.

was defined on the SSC vs FITC plot, and 10,000 events were acquired within this gate. Platelet aggregation was quantified as the proportion of double-positive ($CAMU^+$/$CV450^+$) events relative to all CAMU-positive platelets. Representative results showed 60.8% aggregation following ADP stimulation and 4.6% in the unstimulated control (Fig. 2).

Statistical analyses

Statistical analysis was performed using Statistica v. 9.0 (StatSoft Inc., Tulsa, USA). For all patients, means and standard deviations (SDs) were calculated, and the distribution of variables was assessed using the Shapiro–Wilk test (Supplementary Table 1). Levene's test was used to evaluate homogeneity of variance. Differences between independent groups were analyzed using the Student's t-test for normally distributed variables and the Mann–Whitney U test for non-normally distributed variables (Supplementary Table 2). For dichotomous variables, differences between groups were assessed using the χ^2 test with Yates' correction or the Fisher's exact test, as appropriate. Receiver operating characteristic (ROC) curve analysis was also performed. Correlations between variables were assessed using the Pearson's and the Spearman's test, as appropriate.

Results

The study included 30 patients with thrombocytopenia and 24 patients with normal platelet counts. Detailed characteristics of both groups are presented in Table 1. Patients with thrombocytopenia had significantly lower platelet counts ($p < 0.001$) and were more likely to have kidney failure ($p = 0.014$) and a history of coronary artery bypass grafting (CABG; $p = 0.042$) than patients with normal platelet counts, whereas other clinical characteristics were similar.

The control cohort (healthy volunteers) had a mean (±SD) age of 29 (±5) years and a mean platelet count of 225,000 (48,000)/mm^3. The predominant causes of thrombocytopenia were idiopathic thrombocytopenia (n = 11), chronic leukemia (n = 1), and thrombocytopenia of unknown origin or under diagnostic evaluation (n = 18). Platelet reactivity findings are summarized in Table 2. AA-induced

Table 1. General characteristics of the study population

Variable		Patients with thrombocytopenia (n = 30)	Patients with normal platelet count (n = 24)	p-value
Age [years], mean ±SD		73 ±12	72 ±9	0.712
Sex, M/F (n)		26/4	20/4	0.780
Platelet count, ($\times 10^5$/mm^3), median (Q1–Q3)		107.5 (88–116)	214.0 (184.5–242.0)	<0.001
PCI indication	ACS, n	13	9	0.804
	CCS, n	17	15	0.580
Arterial hypertension, n (%)		28 (93)	21 (87)	0.439
Diabetes, n (%)		12 (40)	12 (50)	0.551
Chronic kidney disease, n (%)		17 (56)	6 (25)	0.014
Hyperlipidemia, n (%)		27 (90)	22 (84)	0.797
History of CABG, n (%)		7 (23)	1 (4)	0.042
History of PCI, n (%)		25 (83.3)	20 (83.3)	0.941

ACS – acute coronary syndrome; CABG – coronary artery bypass grafting; CCS – chronic coronary syndrome; PCI – percutaneous coronary intervention; SD – standard deviation; Q1 – 1st quartile; Q3 – 3rd quartile.

Table 2. Platelet reactivity results

Variable (mean ±SD)	Patients with thrombocytopenia (n = 29)	Patients with normal platelet count (n = 26)	p-value
AA AUC, median (Q1–Q2)	12.5 (5.0–21.0)	15.0 (5.5–22.0)	0.237
AA AGG, median (Q1–Q2)	31.1 (15.6–46.1)	35.15 (16.25–48.65)	0.237
AA VEL, median (Q1–Q2)	4.5 (3.0–5.8)	4.9 (2.95–6.1)	0.167
ADP AUC, mean ±SD	18.5 ±10.1	27.3 ±12.7	<0.01
ADP AGG, mean ±SD	35.9 ±17.2	49.3 ±21.1	<0.05
ADP VEL, mean ±SD	5.1 ±2.5	6.8 ±2.7	<0.05
TRAP AUC, median (Q1–Q2)	45.0 (26.0–54.0)	69.5 (50.5–93.5)	<0.01
TRAP AGG, median (Q1–Q2)	68.7 (42.4–81.9)	107.45 (77.35–142.4)	<0.01
TRAP VEL, median (Q1–Q2)	12.0 (7.7–15.0)	17.45 (13.25–23.95)	<0.01
K-FLC, median (Q1–Q2)	1.25 (0.7–3.4)	1.55 (1.35–2.95)	0.337
ADP-FLC, median (Q1–Q2)	10.5 (4.7–23.4)	12.95 (4.05–22.85)	0.653
TRAP-FLC, median (Q1–Q2)	11.45 (7.4–21.0)	17.34 (10.0–26.75)	0.277
AA-FLC, median (Q1–Q2)	3.7 (1.3–14.1)	32.5 ±20.9	<0.01

AA – arachidonic acid; AA-FLC – arachidonic acid platelet reactivity in flow cytometry method; ADP – adenosine diphosphate; ADP-FLC – adenosine diphosphate platelet reactivity in flow cytometry method; AGG – aggregation; AUC – area under the curve; K-FLC – controls for flow cytometry method; TRAP – thrombin receptor agonist protein; TRAP-FLC – thrombin receptor agonist protein platelet reactivity in flow cytometry method; VEL – velocity of aggregation; SD – standard deviation; Q1 – 1st quartile; Q2 – 2nd quartile.

aggregation (reflecting ASA effect) did not differ significantly between the 2 groups. In contrast, TRAP- and ADP-induced aggregation measured with IA was significantly higher in patients with thrombocytopenia than in those with normal platelet counts.

In the FC assay, ADP- and TRAP-induced responses were comparable between groups, whereas the AA-induced response was significantly higher in patients with thrombocytopenia. In patients with normal platelet counts, an optimal response to clopidogrel assessed using Multiplate aggregometry was defined as <48 AU. Receiver operating characteristic analysis showed that in patients with thrombocytopenia, the optimal FC cut-off indicating adequate $P2Y_{12}$ inhibition was <25.7% (AUC = 0.75; sensitivity 60%; specificity 80%) (Fig. 3). Using this threshold, 7 patients (23%) with thrombocytopenia had an inadequate response to clopidogrel despite low platelet counts. Correlation analysis showed a moderate association between platelet count and TRAP-induced aggregation in the pooled cohort ($r = 0.62$ for TRAP AUC; $p < 0.05$) and a weak association between platelet count and ADP-induced aggregation ($r = 0.33$ for ADP AUC; $p < 0.05$) (Fig. 4).

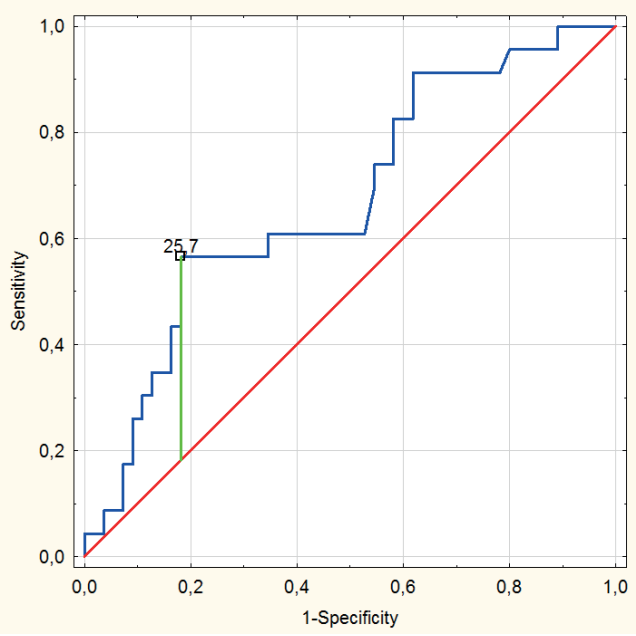

Fig. 3. Clopidogrel response assessed with Multiplate® aggregometry. An optimal platelet reactivity blockade is suggested at <25.7%. The cut-off value determined using Youden's J statistic

Discussion

Our results indicate no significant difference in ASA response measured using IA between patients with thrombocytopenia and controls. Similarly, clopidogrel response assessed using the FC-based aggregation method did not differ between groups. In contrast, ASA responsiveness differed significantly when evaluated with FC, whereas clopidogrel responsiveness differed significantly when assessed using IA. These findings suggest that in patients with thrombocytopenia, ASA reactivity is more reliably assessed using IA, whereas clopidogrel reactivity is better evaluated using the FC-based assay. Currently available aggregometers are not fully adapted for use in patients with low platelet counts. To address this limitation, several investigators have proposed correction formulas to adjust IA results in thrombocytopenia. Shultz-Lebahn et al. diluted healthy donor blood to simulate thrombocytopenia and demonstrated strong correlations between

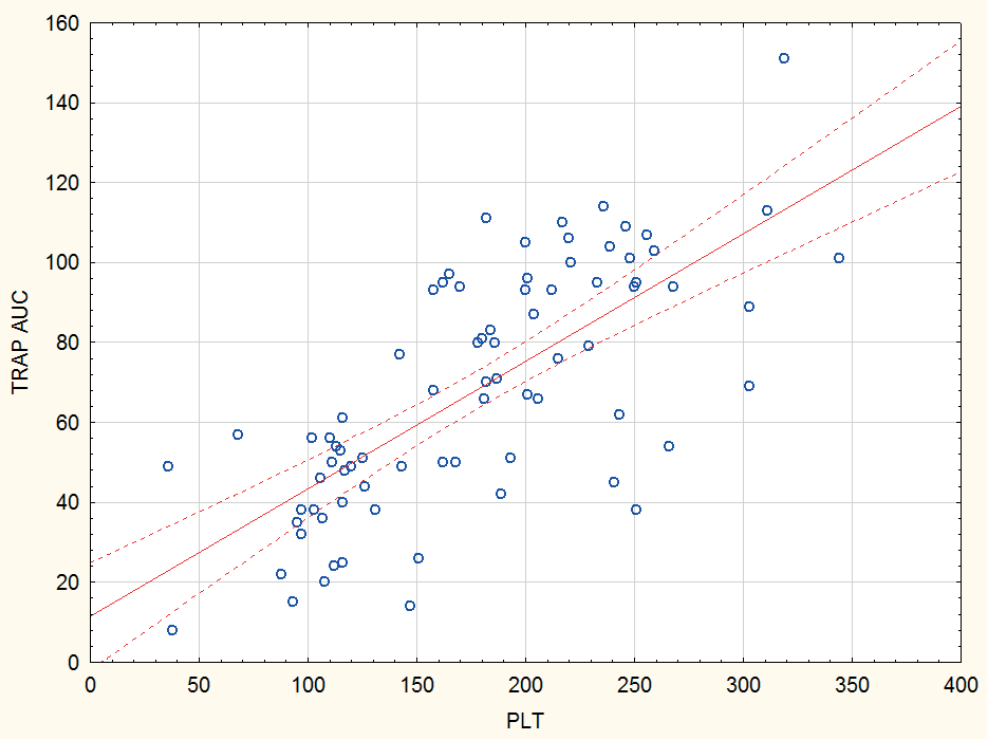

Fig. 4. Correlation between platelet count and TRAP-induced aggregation. The Pearson's correlation coefficient was used to assess the relationship between variables

AUC – area under the curve; PLT – platelet count; TRAP – thrombin receptor agonist peptide.

platelet count and aggregation responses to COL, ADP, and TRAP.[13] A similar approach was reported by Rubak et al.[14] Previous studies suggest that FC-based methods are largely independent of platelet count.[15] Skipper et al. demonstrated that platelet function assessed by FC showed minimal variability across platelet count ranges.[16] Likewise, Frelinger et al. reported that in immune thrombocytopenia, FC-based platelet function remained stable across platelet count ranges.[17] In this study, a moderate correlation was observed between TRAP-induced aggregation and platelet count, whereas weak or no correlation was found for ADP- and AA-induced aggregation, respectively. This finding may reflect the inclusion of patients with true clinical thrombocytopenia, as well as the influence of DAPT. TRAP-induced aggregation assesses platelet reactivity independently of $P2Y_{12}$ or COX-1 blockade and therefore shows a continuous relationship between platelet count and aggregation amplitude. Skipper et al. developed mathematical formulas in a mixed cohort of patients with normal and low platelet counts to adjust IA results to equivalent values at normal platelet counts[11]; however, this approach requires further clinical validation. In this study, we used the FC method described by Vinholt et al.[12], as it appears to circumvent the technical limitations of IA by evaluating washed platelet populations with count-independent analytical performance. Based on published evidence and our data, we established a cut-off value for clopidogrel-induced platelet reactivity in patients with thrombocytopenia.[18] Despite low platelet counts, 7 patients (24%) demonstrated inadequate $P2Y_{12}$ receptor inhibition according to this FC-derived threshold. This finding is clinically relevant, as patients with thrombocytopenia are known to have an elevated risk of recurrent cardiovascular events.[19]

Limitations of the study

Because thrombocytopenia is relatively uncommon in the general population, including patients with CVD, the study group was small. Nevertheless, the study provides clinically relevant insights into DAPT monitoring in patients with thrombocytopenia.

Although the FC method may appear complex, it was performed in a hematology laboratory where FC is routinely used, and once established, the analyses proceeded without difficulty.

Finally, these findings should be considered hypothesis-generating and require further study to confirm their applicability in routine clinical practice.

Conclusions

In patients with thrombocytopenia, IA appears appropriate for assessing ASA response, whereas the FC-based aggregation method may provide a more accurate evaluation of clopidogrel responsiveness, with optimal $P2Y_{12}$ inhibition defined as <25.7%.

Supplementary data

The supplementary materials are available at https://doi.org/10.5281/zenodo.19235950. The package contains the following files:

Supplementary Table 1. Results of checking the normality of the data distribution (Shapiro–Wilk test) of the variables.

Supplementary Table 2. Results of the statistical analyses.

Data Availability Statement

The participants of this study did not give written consent for their data to be shared publicly, so due to the sensitive nature of the research, the supporting data are not available.

Consent for publication

Not applicable.

Use of AI and AI-assisted technologies

Not applicable.

ORCID iDs

Mikołaj Błaziak https://orcid.org/0000-0001-8207-1723
Kornelia Gajek https://orcid.org/0000-0003-0073-7769
Bożena Karolko https://orcid.org/0000-0001-6253-1817
Magdalena Cielecka https://orcid.org/0000-0003-3779-6658
Kamila Florek https://orcid.org/0009-0002-0256-2421
Dominik Mendyka https://orcid.org/0009-0009-1189-0065
Andrzej Mysiak https://orcid.org/0000-0002-4728-2565
Wiktor Kuliczkowski https://orcid.org/0000-0001-6284-0820

References

1. Kearon C, Akl EA, Ornelas J, et al. Antithrombotic therapy for VTE disease. *Chest*. 2016;149(2):315–352. doi:10.1016/j.chest.2015.11.026
2. Iliescu CA, Grines CL, Herrmann J, et al. SCAI Expert Consensus Statement: Evaluation, management, and special considerations of cardio-oncology patients in the cardiac catheterization laboratory (endorsed by the Cardiological Society of India, and Sociedad Latino Americana de Cardiologia Intervencionista). *Catheter Cardiovasc Interv*. 2016;87(5):E202–223. doi:10.1002/ccd.26379
3. Liu R, Liu J, Yang J, et al. Association of thrombocytopenia with in-hospital outcome in patients with acute ST-segment elevated myocardial infarction. *Platelets*. 2019;30(7):844–853. doi:10.1080/09537104.2018.1529298
4. Jiang P, Gao Z, Zhao W, et al. Prognostic significance of in-hospital acquired thrombocytopenia in stable coronary artery disease undergoing percutaneous coronary intervention. *Am J Med Sci*. 2019;358(1):19–25. doi:10.1016/j.amjms.2019.04.008
5. Morici N, Cantoni S, Savonitto S. Antiplatelet therapy for patients with stable ischemic heart disease and baseline thrombocytopenia: Ask the hematologist. *Platelets*. 2014;25(6):455–460. doi:10.3109/09537104.2013.828029
6. McCarthy CP, Steg G, Bhatt DL. The management of antiplatelet therapy in acute coronary syndrome patients with thrombocytopenia: A clinical conundrum. *Eur Heart J*. 2017;38(47):3488–3492. doi:10.1093/eurheartj/ehx531
7. Aradi D, Storey RF, Komócsi A, et al. Expert position paper on the role of platelet function testing in patients undergoing percutaneous coronary intervention. *Eur Heart J*. 2014;35(4):209–215. doi:10.1093/eurheartj/eht375
8. Vrints C, Andreotti F, Koskinas KC, et al. 2024 ESC Guidelines for the management of chronic coronary syndromes. *Eur Heart J*. 2024;45(36):3415–3537. doi:10.1093/eurheartj/ehae177
9. Hakim DA, Dangas GD, Caixeta A, et al. Impact of baseline thrombocytopenia on the early and late outcomes after ST-elevation myocardial infarction treated with primary angioplasty: Analysis from the Harmonizing Outcomes with Revascularization and Stents in Acute Myocardial Infarction (HORIZONS-AMI) trial. *Am Heart J*. 2011;161(2):391–396. doi:10.1016/j.ahj.2010.11.001
10. Kuliczkowski W, Żurawska-Płaksej E, Podolak-Dawidziak M, et al. Platelet reactivity and response to aspirin and clopidogrel in patients with platelet count disorders. *Cardiol Res Pract*. 2021;2021:6637799. doi:10.1155/2021/6637799
11. Skipper MT, Rubak P, Stentoft J, Hvas AM, Larsen OH. Evaluation of platelet function in thrombocytopenia. *Platelets*. 2018;29(3):270–276. doi:10.1080/09537104.2017.1296566
12. Vinholt PJ, Frederiksen H, Hvas AM, Sprogøe U, Nielsen C. Measurement of platelet aggregation, independently of patient platelet count: A flow-cytometric approach. *J Thromb Haemost*. 2017;15(6):1191–1202. doi:10.1111/jth.13675
13. Schultz-Lebahn A, Skipper MT, Hvas AM, Larsen OH. Optimized tool for evaluation of platelet function measured by impedance aggregometry. *Platelets*. 2021;32(6):842–845. doi:10.1080/09537104.2020.1809644
14. Rubak P, Villadsen K, Hvas AM. Reference intervals for platelet aggregation assessed by multiple electrode platelet aggregometry. *Thromb Res*. 2012;130(3):420–423. doi:10.1016/j.thromres.2012.06.017
15. Dovlatova N. Current status and future prospects for platelet function testing in the diagnosis of inherited bleeding disorders. *Br J Haematol*. 2015;170(2):150–161. doi:10.1111/bjh.13405
16. Skipper MT, Rubak P, Larsen OH, Hvas AM. Thrombocytopenia model with minimal manipulation of blood cells allowing whole blood assessment of platelet function. *Platelets*. 2016;27(4):295–300. doi:10.3109/09537104.2015.1095873
17. Frelinger AL, Grace RF, Gerrits AJ, et al. Platelet function tests, independent of platelet count, are associated with bleeding severity in ITP. *Blood*. 2015;126(7):873–879. doi:10.1182/blood-2015-02-628461
18. Gross L, Aradi D, Sibbing D. Platelet function testing in patients on antiplatelet medications. *Semin Thromb Hemost*. 2016;42(3):306–320. doi:10.1055/s-0035-1570083
19. Iakovis N, Xanthopoulos A, Chamaidi A, et al. Recurrent acute coronary syndromes in a patient with idiopathic thrombocytopenic purpura. *Case Rep Cardiol*. 2020;2020:6738348. doi:10.1155/2020/6738348

INNODIA screening for early-stage type 1 diabetes: Insights from Polish first-degree relatives of T1D patients (2015–2023, EU115797)

Magdalena Małachowska[1,A–D], Kamil Kosiorowski[1,2,A–D], Paulina Pokrywka[1,A–D], Eliza Skała-Zamorowska[3,A–F], Ewa Rusak[3,A–F], Halla Kamińska[3,A–F], Sebastian Jacek Seget[3,A–F], Aleksandra Pyziak-Skupień[4,A–F], Grażyna Deja[3,A–F], Przemysława Jarosz-Chobot[3,A–F]

[1] Students' Scientific Association at the Department of Children's Diabetology and Lifestyle Medicine, Medical University of Silesia, Katowice, Poland
[2] College of Interdisciplinary Studies at the University of Silesia in Katowice, Poland
[3] Department of Children's Diabetology and Lifestyle Medicine, Medical University of Silesia, Katowice, Poland
[4] Department of Children's Diabetology and Pediatrics, Upper Silesian Centre for Child Health, Katowice, Poland

A – research concept and design; B – collection and/or assembly of data; C – data analysis and interpretation; D – writing the article; E – critical revision of the article; F – final approval of the article

Advances in Clinical and Experimental Medicine, ISSN 1899–5276 (print), ISSN 2451–2680 (online) *Adv Clin Exp Med*. 2026;35(4):599–609

Address for correspondence
Magdalena Małachowska
E-mail: mmalachowska25@gmail.com

Funding sources
INNODIA has received funding from the Innovative Medicines Initiative 2 Joint Undertaking under grant agreement No. 115797. This Joint Undertaking is supported by the European Union's Horizon 2020 research and innovation program, EFPIA, JDRF, and The Leona M. and Harry B. Helmsley Charitable Trust.

Conflict of interest
None declared

Received on May 18, 2025
Reviewed on July 28, 2025
Accepted on July 31, 2025

Published online on January 13, 2026

Cite as
Małachowska M, Kosiorowski K, Pokrywka P, et al. INNODIA screening for early stage type 1 diabetes: Insights from Polish first-degree relatives of T1D patients (2015–2023, EU115797). *Adv Clin Exp Med*. 2026;35(4):599–609. doi:10.17219/acem/208837

DOI
10.17219/acem/208837

Abstract

Background. Early identification of individuals at increased risk for type 1 diabetes (T1D) is essential to prevent diabetic ketoacidosis (DKA) at onset and to facilitate the development of disease-modifying therapies. The INNODIA EU115797 project (2015–2023) conducted a Europe-wide screening of individuals with recent-onset T1D (<6 weeks) and their first-degree relatives (aged 1–45 years).

Objectives. To evaluate the risk of T1D development among first-degree relatives of individuals with T1D, based on data from the Polish INNODIA center at the Medical University of Silesia in Katowice, Poland.

Materials and methods. Data on the incidence of autoantibodies were obtained from the INNODIA project platform. The analysis included first-degree relatives of individuals with T1D, aged 1–45 years, who met the inclusion criteria and were recruited at the Polish center. Samples were collected at the Medical University of Silesia in accordance with the INNODIA protocol. Participants were stratified based on the number of autoantibodies detected (1 or ≥2). The analysis considered age, sex, prevalence of specific autoantibodies (GAD65, IAA, IA-2A, ZnT8), and familial relationship.

Results. Among 817 screened individuals, 65 (7.96%) tested positive for autoantibodies (AA): 48 (5.88%) had 1AA and 17 (2.08%) had ≥2AA. The highest prevalence was observed in the 10–23-year age group (27.7%, 18/65). In this subgroup, 11.04% (18/163) were autoantibody-positive, whereas prevalence in other age groups (1–9, 24–36, 37–40, and 41–45 years) ranged from 5.98% to 8.97%. GAD65 (5.51%) and IAA (3.43%) were the most frequent autoantibodies. Individuals with 1AA were predominantly parents (32/48; 66.7%), while ≥2AA were more common among siblings (13/17; 72.2%). During follow-up, 2 participants progressed to stage 3 T1D.

Conclusions. In the Polish cohort of the INNODIA study, autoantibodies were detected in 7.96% of first-degree relatives of individuals with T1D. Early screening is crucial for accurate risk stratification, guiding the development of therapeutic interventions and reducing the risk of severe complications at disease onset.

Key words: autoantibodies, diabetes mellitus type 1/diagnosis and immunology, mass screening/methods, autoimmune diseases/diagnosis, autoimmune diabetes mellitus

Acknowledgements
We would like to express our sincere gratitude to the INNODIA investigators and participants of the INNODIA program for their courage and for making this study possible. Special thanks go to Hanna Szczudło M.Sc., Urszula Bielec M.Sc., Lillianna Gremlowska M.Sc., Agnieszka Straszewska M.Sc., and Piotr Kusa M.Sc. for their essential roles in ensuring the smooth organization and success of the program at the Polish site. We also extend our gratitude to all the associates, researchers, healthcare professionals, and collaborators whose collective efforts made this work possible.

Highlights

- Polish INNODIA data align with European trends: Autoantibody prevalence in first-degree relatives of type 1 diabetes (T1D) patients mirrors findings from other European cohorts.
- 7.96% of first-degree relatives tested positive for T1D-related autoantibodies: GAD65 and IAA were the most frequently detected markers across all subgroups.
- Highest autoantibody positivity in youth and siblings: Rates peaked in the 10–23 age group and among siblings of individuals with T1D.
- Progression without DKA observed: Two children advanced to stage 3 T1D without developing diabetic ketoacidosis, underscoring benefits of early monitoring.
- Early recognition and supportive care are critical: Integrating prompt symptom identification into protocols can improve outcomes in early-stage T1D.

Background

Type 1 diabetes (T1D) is the most common type of diabetes in the European pediatric population, with nearly 129,000 new diagnoses each year globally in children and adolescents under 20 years of age.[1,2] According to the T1D Index, the estimated number of people living with T1D in 2024 was 9.4 million, and with the continued rise in its incidence, this number is expected to reach 16.4 million by 2040 ((Type 1 Diabetes Index; https://www.t1dindex.org).

Thanks to ongoing T1D research, remarkable progress has been made in staging the early phases of the disease and refining its definitions. It is now well established that autoantibodies, which serve as markers of T-cell-mediated β-cell destruction, may appear years before the clinical onset of T1D. Identification of T1D-related autoantibodies – such as GAD65 (glutamic acid decarboxylase), IAA (insulin autoantibody), IA-2A (islet antigen-2 antibody), and ZnT8 (zinc transporter-8 antibody) – in combination with glucose metabolism monitoring enables classification of preclinical stages of T1D: stage 1 (≥2 autoantibodies and normoglycemia), stage 2 (≥2 autoantibodies and dysglycemia) and stage 3 (≥2 autoantibodies and clinical onset).[3–6] The International Society for Pediatric and Adolescent Diabetes (ISPAD) 2024 Guidelines provide more detailed subdivision of these stages, reflecting advances in understanding of the disease.[5]

In recent years, initiatives to identify individuals in the early stages of T1D have laid the foundation for ongoing screening efforts to reduce the incidence of diabetic ketoacidosis (DKA) at T1D onset, as well as to minimize short and long-term morbidity, mortality, prolonged hospitalization, weight loss, and psychological burden associated with T1D onset.[7] These endeavors also provide participants with the opportunity to enroll in clinical trials investigating disease-modifying therapies aimed at delaying the onset of T1D. Islet autoantibody testing has proven to be an effective method for detecting early-stage T1D and may be preferred over genetic testing due to lower participant dropout rates and its predictive value in stratifying the rate of progression to stage 3 T1D once autoantibodies are developed.[5] Moreover, genetic risk is frequently perceived as abstract and difficult for parents to fully understand and accept.[8] In accordance with the most recent ISPAD guidelines, population-based screening for T1D is optimally performed between 3 and 5 years of age, with maximal sensitivity achieved by 2 examinations at 2 and 6 years of age.[5] When screening is deferred until adolescence, the preferred time points are 10 and 14 years of age.[5] However, it should be emphasized that despite the ongoing efforts to integrate T1D screening into national healthcare systems, still only a minority of countries currently maintain nationwide programs. In Poland, the majority of children who present with – or are likely to develop – stage 3 T1D have not undergone prior T1D screening. Therefore, if the standard, age-based screening windows cannot be met, it is reasonable to offer T1D screening independently of a child's age.

In 2015 the INNODIA (now an international non-profit organization, formerly a European-based public-private partnership) launched the project (EU115797) titled Translational Approaches to Disease-Modifying Therapy of Type 1 Diabetes: An Innovative Approach Towards Understanding and Arresting Type 1 Diabetes.[9] The study protocol was approved by the Bioethics Committee of the Medical University of Silesia (Katowice, Poland; approval No. KNW/0022/KB1/25/I/17 issued on May 16, 2017). As the largest program of its kind at the time, this European-wide initiative conducted a screening of individuals with newly diagnosed T1D (diagnosed less than 6 weeks prior) as well as first-degree relatives of individuals living with T1D. The study ran from November 1, 2015, to October 31, 2023, and included participants from 13 European countries, including Poland with the reference site at the Medical University of Silesia, which became an accredited clinical trial site. The project was carried out under the framework of the Innovative Medicines Initiative – Joint Undertaking (IMI-JU) and involved a global partnership between academic researchers and industrial partners, all working towards combating T1D.[9]

It has been well established that first-degree relatives of individuals with T1D face a markedly higher (up to 15 times) risk of developing T1D than the general population, with the prevalence of T1D in the first-degree relatives equal to 5% by the age of 20, compared to 0.3–0.4% in the general population.[5,10–12]

Children of mothers with T1D have a 1.3–4% risk of developing the disease, whereas children of fathers with T1D have a higher risk of 6–9%. In siblings of individuals with T1D, the lifetime risk is estimated at approx. 6–7%.[10–12] Relatives of individuals with T1D should certainly be included in early screening; however, population-wide screening is also warranted, as it is reasonable to state that everyone is at risk of developing T1D. This is supported by evidence showing that approx. 90% of individuals with recent-onset T1D have no known family history of the disease.[5]

Objectives

The aim of this study was to describe and characterize the risk of type T1D development in the Polish population, based on data from the INNODIA screening project, which focused on first-degree relatives of individuals with T1D.

Materials and methods

Between 2018 and 2023, all first-degree relatives (aged 1–45 years) of individuals either newly diagnosed with T1D or already receiving care at the Outpatient Department of Children's Diabetology and Lifestyle Medicine at the Independent Public Clinical Hospital No. 6 of the Silesian Medical University in Katowice (Upper Silesian Child Health Centre) were invited to participate in the INNODIA study conducted at the Medical University of Silesia.

In addition to serving as an INNODIA clinical site, this center is accredited as a certified SWEET (Better control in Pediatric and Adolescent diabeteS: Working to crEate CEnTers of Reference) reference center and participates in international projects, including the European Action for the Early Diagnosis of Early Non-Clinical Type 1 Diabetes for Disease Interception (EDENT1FI).[13]

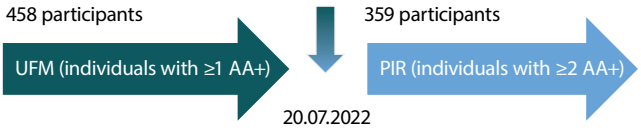

Fig. 1. Allocation of participants to the Unaffected Family Member (UFM) and People at Increased Risk (PIR) groups

To be enrolled, participants were required to meet the inclusion and exclusion criteria outlined in Table 1. Eligible individuals were invited for a screening visit, which included a blood test for the presence of T1D-specific autoantibodies (GADA, IAA, IA-2A, ZnT8A). Three autoantibodies (GADA, IA-2A and ZnT8A) were analyzed at the PEDIA (Pediatric Diabetes Research Group) laboratory at the University of Helsinki, Finland, while IAA was measured using a specific radiobinding assay.[14]

If participants tested positive for autoantibodies (AA), they were assigned to either the Unaffected Family Member (UFM) or People at Increased Risk (PIR) group, depending on the year of enrollment. Individuals who were screened up until the July 20, 2022, were assigned to the UFM group. If the screening resulted in at least 1 positive autoantibody, participants continued in the study and followed a specific visit schedule to ensure they received specialized medical care. Consecutively, every patient enrolled in the study after July 20, 2022, was assigned to the PIR group. In this case, further medical care was provided only if the individual was found to have at least 2 autoantibodies present (Fig. 1).

Participants in both the UFM and PIR groups received medical care through regular follow-up visits, which included eligibility screening, medical history review, anthropometric measurements, assessment of glycemic control (oral glucose tolerance test (OGTT) and glycated hemoglobin (HbA1c)), immunological testing, and biobanking. Detailed schedule for visits and performed tests are presented in the Tables 2,3. If required, any additional tests were performed in order to provide the best possible care following then-current ISPAD guidelines. At the time of the INNODIA study, the clinical site at the Medical University of Silesia was not conducting any kind of trials aimed at people at an early stage of T1D. Therefore, participants were not offered enrolment to the clinical trials but were

Table 1. Inclusion and exclusion criteria for participants in the Unaffected Family Member (UFM) and People at Increased Risk (PIR) groups

Criteria	UFM and PIR
Inclusion	• Have given written informed consent to participate. • Aged between 1 year and <45 years. • Have a first-degree relative with T1D (parent, child, full or half siblings) diagnosed at <45 years of age.
Exclusion	• The affected first degree relative has type 2 diabetes, monogenic diabetes or diabetes secondary to another medical condition. • Concurrent use of long-term immunosuppressive agents (including oral steroids) or medication likely to confound the interpretation of study results. • Any medical history or clinically relevant abnormality that is deemed by the principal investigator and/or co-investigator to make the participant ineligible for inclusion because of problems in data interpretation or safety concerns. • Participating in an interventional or other drug research which could affect the primary objectives of the study.

Table 2. Schedule of visits for the Unaffected Family Member (UFM) group

Assessments and procedures	Baseline visit 1	Visit 2	Visit 3	Visit 4	Visit 5	Visit 6	Visit 7
Time point	0 months*	6 months	12 months	18 months	24 months	36 months	48 months
Inclusion/exclusion	x	x	x	x	x	x	x
Update medical and family history	x	x	x	x	x	x	x
Concomitant medication	x	x	x	x	x	x	x
Height [cm] and weight [kg]	x	x	x	x	x	x	x
Autoantibodies	x	–	x	–	x	x	x
HbA1c	x	x	x	x	x	x	x
PBMC	x	x	x	x	x	x	x
Blood samples for storage	x	x	x	x	x	x	x
Urine (biomarkers)	x	–	x	–	x	x	x
Stool (microbiome)	x	x	x	x	x	x	x
OGTT	x	x	x	x	x	x	x
CGM**	x	x	x	x	x	x	x
Allocation of glucose meter at visit 1	x	–	–	–	–	–	–
Home collection of monthly C-peptide DBS and BG measurements	x	x	x	x	x	x	x
Retention of contact details for all participants at clinical site	–	–	–	–	–	–	x

*Visit to be scheduled ideally within 3 months following receipt of their autoantibody test results. ** If dysglycemia at OGTT.
HbA1c – hemoglobin A1c (%); PBMC – peripheral blood mononuclear cells; OGTT – oral glucose tolerance test; CGM – constant glucose monitoring; DBS – dried blood spot; BG – blood glucose.

Table 3. Schedule of visits for the People at Increased Risk (PIR) group

Assessments and procedures	Baseline visit 1	Visit 2	Visit 3	Visit 4	Visit 5
Time point	0 months*	6 months	12 months	18 months	24 months
Inclusion/exclusion	x	x	x	x	x
Update medical and family history	x	x	x	x	x
Concomitant medication	x	x	x	x	x
Height [cm] and weight [kg]	x	x	x	x	x
Autoantibodies	x	–	x	–	x
HbA1c	x	x	x	x	x
Blood samples for storage	x	x	x	x	x
OGTT	x	x	x	x	x
CGM**	x	x	x	x	x
Retention of contact details for all participants at clinical site	–	–	–	–	x

*Visit to be scheduled ideally within 3 months following receipt of their autoantibody test results. ** If dysglycemia at OGTT.
HbA1c – hemoglobin A1c (%); OGTT – oral glucose tolerance test; CGM – constant glucose monitoring.

informed of the potential opportunities to join clinical trials at other sites. All participants received education on the symptoms of T1D onset and the disease management, which contributed to the prevention of DKA development at the onset of symptomatic T1D.

Unfortunately, data on potential reasons for reluctance or concerns about participating in and continuing the study were not collected, as well as mental health assessment was not performed; therefore there were no data enabling assessment of the direct impact of screening on individuals' mental wellbeing. This illustrates the shift in perception of the T1D screening process and the movement towards a holistic and patient-centered model that incorporates psychological wellbeing assessment as a key component.

However, it is important to note that most participants – being First-degree relatives of individuals living with T1D – already had substantial disease awareness and understanding, which may have influenced how they perceived and accepted the final diagnosis. Nonetheless, any individual in need of psychological support was offered assistance from a qualified psychologist at the Medical University of Silesia site.

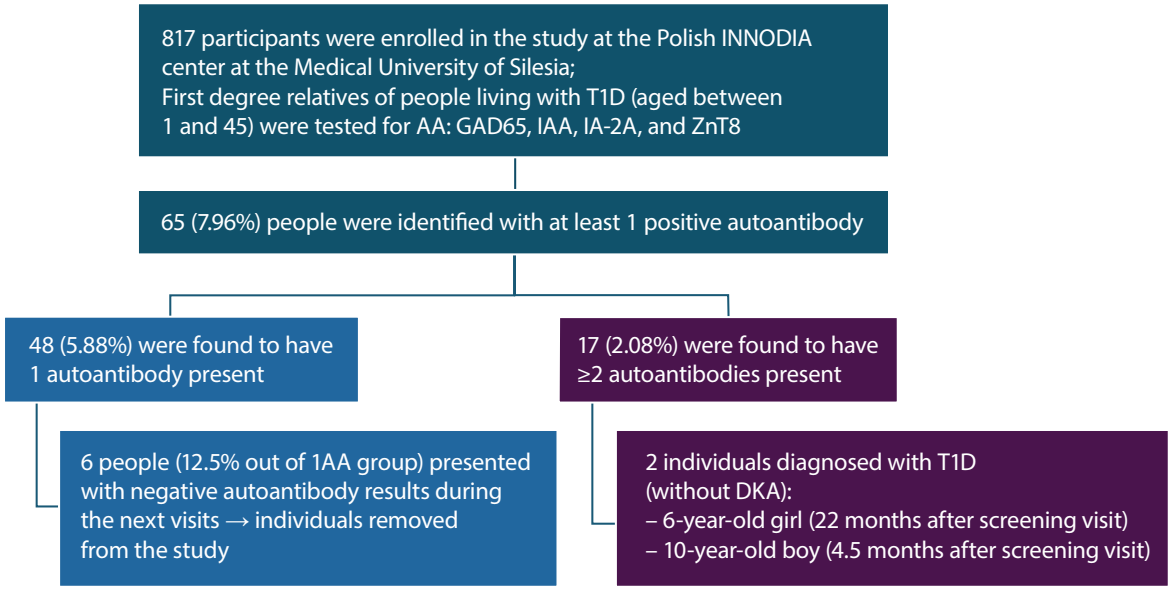

Fig. 2. Classification of screened individuals according to autoantibody status

T1D – type 1 diabetes; GAD65 – autoantibodies to glutamic acid decarboxylase 65; IAA – autoantibodies to insulin; IA-2A – autoantibodies to tyrosine phosphatase-like protein; ZnT8 – autoantibodies to zinc transporter 8; 1AA group – individuals with 1 autoantibody present; DKA – diabetic ketoacidosis.

Results

Among 817 first-degree relatives of individuals with T1D, 7.96% (n = 65) tested positive for at least 1 autoantibody. Of these, 5.87% (n = 48) had a single autoantibody, corresponding to an estimated 15% risk of developing T1D within 15 years, with most progression occurring within 2 years of seroconversion. The remaining 2.08% (n = 17) had ≥2 autoantibodies, associated with a 44% risk of progression to stage 3 T1D within 5 years and an almost 100% lifetime risk.[5,6,10]

Among the 48 individuals with a single autoantibody, 6 (12.5%) subsequently reverted to seronegative status. In 5 cases the autoantibody was GAD65, and in 1 case IAA. These individuals represented a wide age range (3, 8, 15, 17, 34, and 39 years), with no discernible pattern related to age at seroreversion. Four were siblings and 2 were parents of a child with T1D.

Additionally, 15 of the 48 participants with a single autoantibody were initially recruited as PIR rather than UFM. At that time, eligibility for follow-up required the presence of at least 2 autoantibodies. Since these participants did not meet the follow-up criteria and no subsequent data regarding their autoantibody status were available, the true incidence of transient autoantibody positivity may be underestimated. Over the course of the study, 2 children progressed to symptomatic stage 3 T1D. In both cases, DKA was not observed at the time of onset (see Fig. 2 for details).

Autoantibody identification stratified by age

Individuals were divided into 5 age groups: 0–9, 10–23, 24–36, 37–40, and 41–45 years, each accounting for approx. 20% of the total PIR and UFM study population (n = 817). The largest group was the 41–45 age range (184 participants, 22.52%), while the least populous group was the 37–40 age range (146 participants, 17.75%) (Table 4).

Most participants with positive autoantibodies had only 1 autoantibody (73.85% of the total AA+ group; n = 48). Seventeen (26.15%) were found having 2 or more autoantibodies, with 8 (12.31%) having 2 autoantibodies, 6 (9.23%)

Table 4. Age categories for study participants

Age range [years]	Number of people in this age range	% of all participants (PIR and UFM; 817)	Number of people with AA+	% of AA+ within this age category	% of AA+ in this age group out of all AA (+)
1–9	163	19.95%	12	7.36%	18.46%
10–23	163	19.95%	18	11.04%	27.69%
24–36	162	19.83%	11	6.79%	16.92%
37–40	145	17.75%	13	8.97%	20.00%
41–45	184	22.52%	11	5.98%	16.92%

PIR – People at Increased Risk; UFM – Unaffected Family Member; AA – autoantibodies.

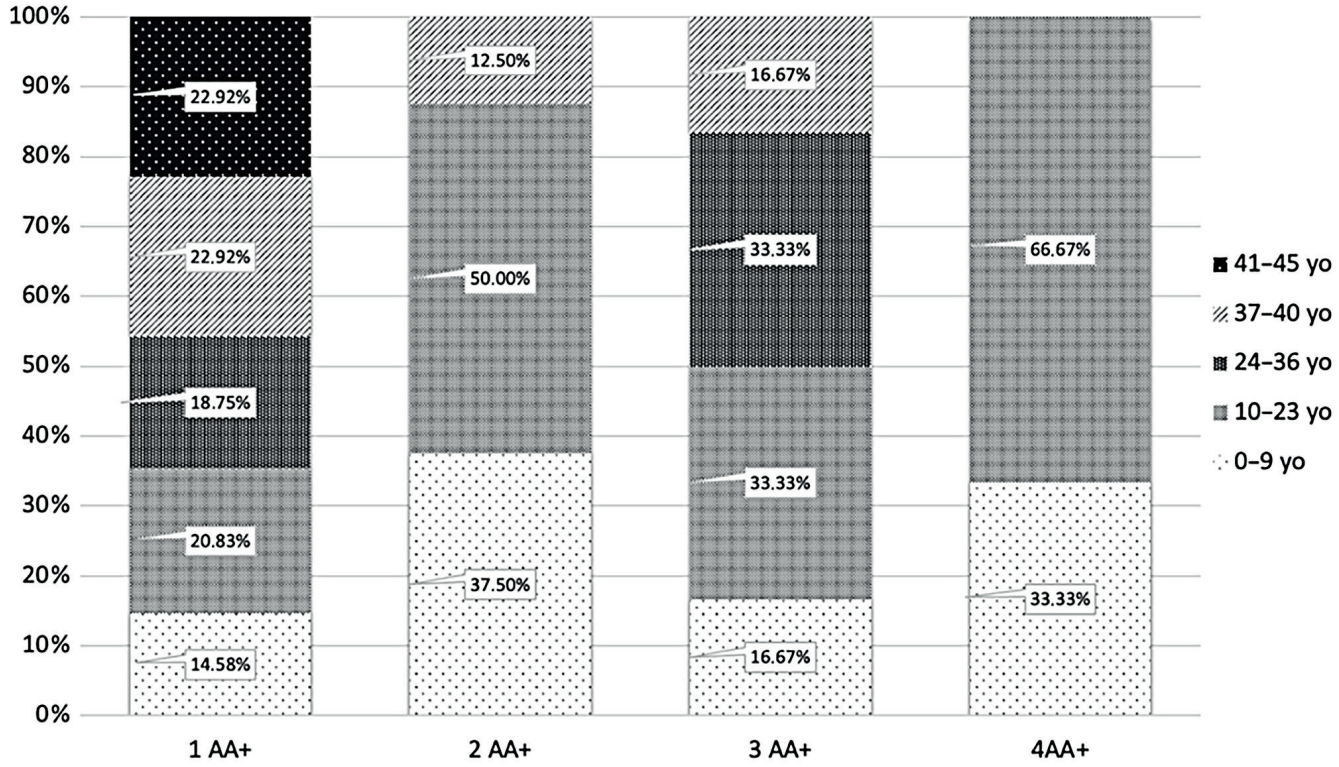

Fig. 3. Age-group distribution (%) of individuals by autoantibody count

having 3 autoantibodies and 3 (4.62%) with 4 autoantibodies. The majority of AA+ individuals were aged 10–23, accounting for 27.69% of all AA+ (18 of 65).

Consequently, 11.04% (18 of 163) of participants in this age group had at least 1 autoantibody, while the percentage for other age categories ranged from 5.98% to 8.97%. The 10–23 age group also had the highest prevalence of 2 autoantibodies (2.5%, n = 4) and 4 autoantibodies (1.2%, n = 2). There were 2 individuals with 3 autoantibodies (1.2%, n = 2) both for the 10–23 and 24–36 age category. People between the age 10–23 accounted for 50.00% (n = 4) of cases with 2 autoantibodies, for 33.33% (n = 2) with 3 autoantibodies and for 66.67% (n = 2) with 4 autoantibodies.

There is a predominance of younger individuals with 2 autoantibodies, which can be observed in Fig. 3. However, this pattern was not observed in the group with only 1 autoantibody. In contrast, participants aged 37–45 accounted for approx. 46% (n=22) of the 1AA group. Additionally, 20.83% (n = 10) of individuals with 1 autoantibody were between 10 and 23 years old, while 18.75% (n = 9) were aged 24–36. The lowest percent of people with 1 autoantibody was in the 0–9 age group (14.58%, n = 7). Single-autoantibody cases demonstrated a more balanced age-profile than cases with 2 autoantibodies; however, the aspect of a very small sample must be taken into consideration (Fig. 3). In the 37–40 age group, 7.59% of participants had 1 autoantibody, while the percentage for 2 autoantibodies and 3 autoantibodies was 0.69% in both cases, and none was found having 4 autoantibodies. Although there is a slight predominance of positive autoantibodies in younger individuals, it is important to note that autoantibodies were detected in all age groups, supporting the rationale for including adults (>18 years) in T1D screening programs.

Figure 4 shows that the occurrence of specific autoantibodies is in overall similar across age groups. However, 66.7% (n = 6) of IA-2A cases were in the 10–23 age group, while this group accounted for 25% (n = 3 for ZnT8) to 35% (n = 10 for IAA) of cases for other autoantibodies. Certainly, due to the small sample size, no firm conclusions can be drawn at this point.

Autoantibody identification stratified by sex

As noted, 65 participants (7.96%) had at least 1 autoantibody (Fig. 2). GAD65 was the most common, found in 69.23% (n = 45) of all AA+ cases and 5.51% of all screened (Fig. 5). IAA was found in 43.08% (n = 28; 3.43% of UFM and PIR), followed by ZnT8 in 18.46% (n = 12; 1.47% of UFM and PIR) and IA-2A in 13.85% (n = 9; 1.10% of UFM and PIR).

The stratification of autoantibodies by sex (Fig. 6) mirrored the overall incidence, with women marginally higher (53.85%, n = 35) than men (46.15%, n = 30), which is consistent with the study's overall sex ratio (56.55% women). In general, 7.58% of women (n = 35) in the study had positive autoantibodies, compared to 8.45% (n = 30) of men. Therefore, although a greater number of women tested positive for autoantibodies, the detection rate relative to the number

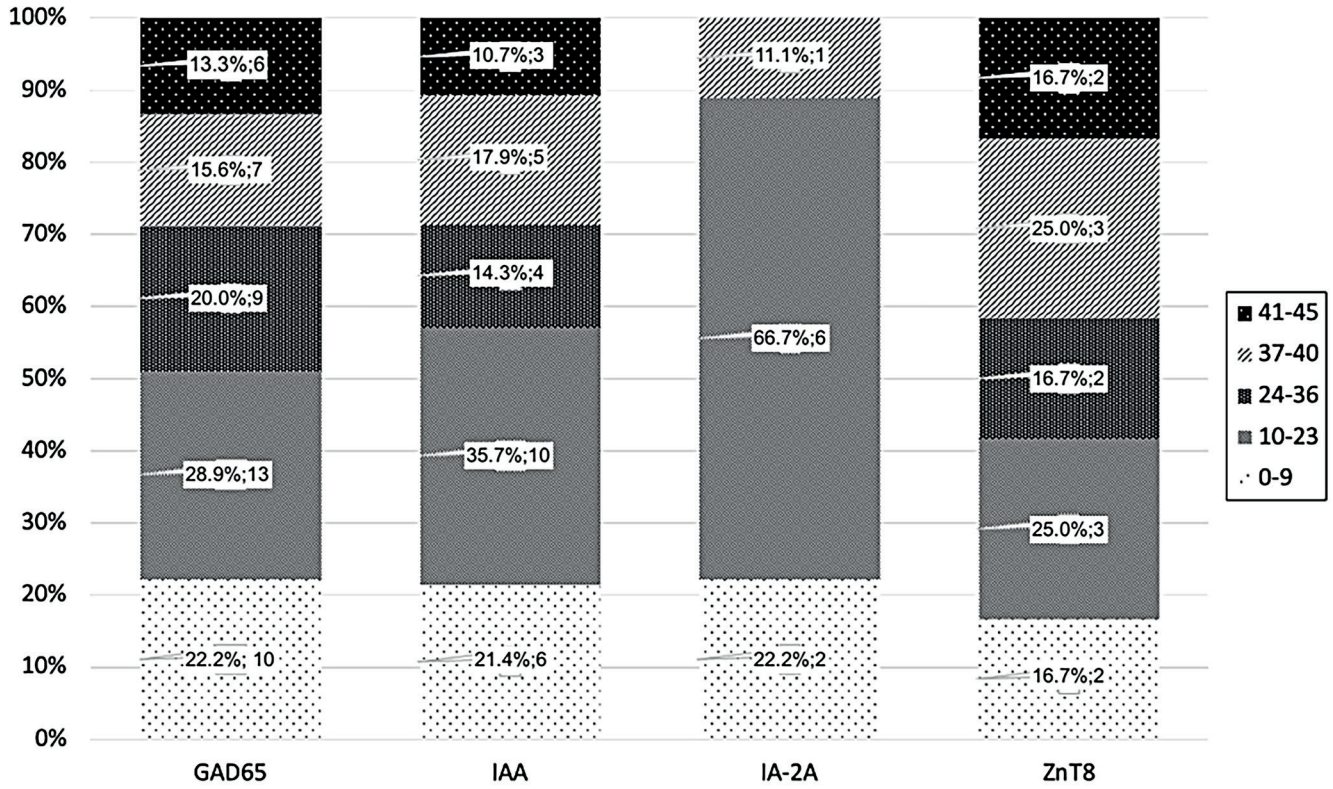

Fig. 4. Age-group distribution (%) and number of individuals with a specific autoantibody

of participants was higher in men. Women also represented the majority of those with 1 autoantibody (60.42%, n = 29). In contrast, the majority of those with ≥2 autoantibodies were male: 62.50% (n = 5) for 2 autoantibodies, 66.67% (n = 4) for 3 autoantibodies and 66.67% (n = 2) for 4 autoantibodies. Despite predominance of women in the study, GAD65 incidence was similar: 5.19% (n = 24) in women and 5.92% (n = 21) in men. IAA was more frequent in men (4.23%, n = 15) than women (2.81%, n = 13), while IA-2A was even 4 times more frequent in men (1.97%, n = 7) than women (0.43%, n = 2). Again, no definite conclusions can be drawn about the prevalence of specific autoantibodies across age groups due to the limited number of cases in each group.

Participants with 2 or more autoantibodies

Type 1 diabetes screening enables to identify individuals at an early stage of T1D. Those in stage 1 face a nearly 100% lifetime risk of progressing to stage 3 T1D.[5,6,10,15] Given the importance of early detection and monitoring, data

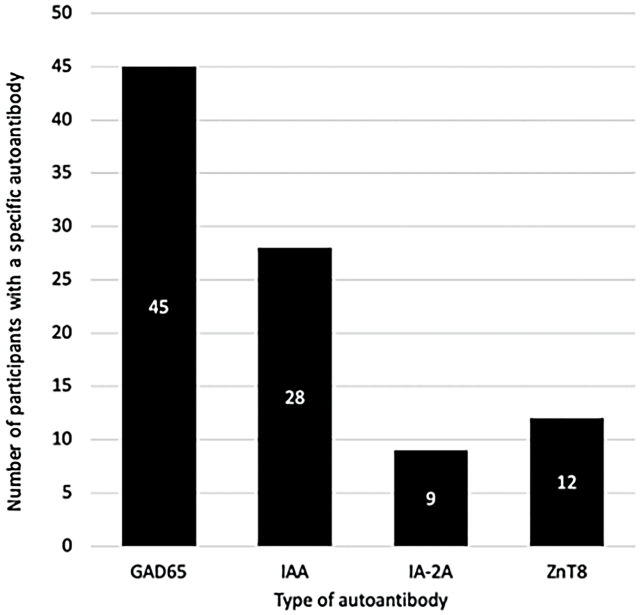

Fig. 5. Distribution of specific autoantibodies identified among study participants

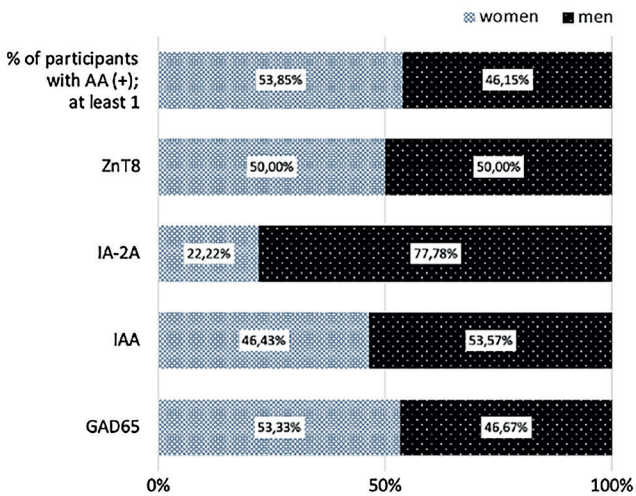

Fig. 6. Sex-based distribution (%) of individuals with a specific autoantibody

Table 5. Description of (2 or more AA+) group of study participants

Type of A	Prevalence of specific AA in ≥2AA (+) group	Number of detected AA to the total number of screened participants (817)	% of detected specific AA in (+) group to all 65 cases of AA (+)	% of detected specific AA in ≥2AA (+) group to all 17 cases of the 2AA (+) group
GAD65	16	1.96%	24.62%	94.12%
IAA	13	1.59%	20.00%	76.47%
IA-2A	9	1.10%	13.85%	52.94%
ZnT8	8	0.98%	12.31%	47.06%

AA – autoantibodies; ** 2AA (+) group – individuals with autoantibodies present; GAD65 – autoantibodies to glutamic acid decarboxylase 65; IAA – autoantibodies to insulin; IA-2A – autoantibodies to tyrosine phosphatase-like protein; ZnT8 – autoantibodies to zinc transporter 8.

Table 6. Autoantibodies combinations in the (2 or more AA+) group

GAD65	IAA	IA-2A	ZnT8	Frequency of given AA configuration in the group of study participants with (+)
+	+	–	+	4
+	+	–	–	4
+	+	+	+	3
+	–	+	–	3
+	+	+	–	2
–	–	+	+	1

AA – autoantibodies; ** 2AA (+) group – individuals with autoantibodies present; GAD65 – autoantibodies to glutamic acid decarboxylase 65; IAA – autoantibodies to insulin; IA-2A – autoantibodies to tyrosine phosphatase-like protein; ZnT8 – autoantibodies to zinc transporter 8.

for participants with multiple (2 or more) autoantibodies were analyzed separately (Table 5).

Seventeen participants (1.96% of the UFM and PIR group, n = 817) had multiple (2 or more) autoantibodies, representing 26.15% of all those with AA+. These individuals were classified as stage 1 T1D, as all had normoglycemia, and back then no continuous glucose monitoring (CGM) was required for them.

In both the AA+ group and the ≥ 2AA group, GAD65 and IAA occurred with the highest prevalence. For people with ≥ 2 autoantibodies, IA-2A was 3rd most frequent (9 out of 17), while in the overall AA+ group, it was ZnT8.

Six out of the 17 participants with ≥ 2 autoantibodies were female, with age ranging from 1 to 37 years (1, 6, 11, 13, 35, 37). The remaining 11 participants were male, with age ranging from 2 to 40 years (2 (n = 2), 3, 10, 11 (n = 2), 12, 12, 15, 33, 40).

To observe the co-occurrence of autoantibodies and their combinations in the study participants, all configurations and their frequencies are presented in the Table 6.

Follow-up diagnoses of stage 3 T1D in study participants

Within this group, a 6-year-old girl and a 10-year-old boy progressed to stage 3 T1D, both without developing DKA at diagnosis (Table 7).

The 6-year-old girl tested positive for 2 autoantibodies – GAD65 and IAA – at screening visit and progressed to stage 3 T1D after 22 months. At her last follow-up visit, 53 days before clinical onset, there were no signs of dysglycemia (HbA1c: 36.64 mmol/mol). She began regular visits at the Diabetes Outpatient Department and, 21 months post-diagnosis, is being treated with insulin injections twice a day. Her current HbA1c is 5.2%, with a time in range (TIR) of 93%.

The 9-year-old boy, positive for GAD65, IAA and IA-2A at screening, progressed to stage 3 T1D within only 4.5 months. IA-2A presence, high autoantibody levels and high-affinity screening have been shown to predict rapid progression to clinical T1D.[9,10] Similarly to the 6-year-old girl, his follow-up visit took place 50 days before disease onset and presented no dysglycemia (HbA1c: 36.62 mmol/mol). Now 13 years old, he attends follow-up visits, using

Table 7. Description of individuals diagnosed with type 1 diabetes (T1D) during the study

Variable	6-year-old girl	10-year-old boy
Family history	sibling living with T1D	sibling living with T1D
AA preset at screening	GAD65, IAA	GAD65, IAA, IA-2A
Time of diagnosis	22 months after screening visit	4.5 months after screening visit
DKA	no DKA at diagnosis	no DKA at diagnosis
HbA1c at last follow-up visit	36.64 mmol/mol (53 days before diagnosis)	36.62 mmol/mol (50 days before diagnosis)
Current data	10 years old, HbA1c 5.7%; TIR 93%, insulin injection twice a day	13 years old, HbA1c 7.4%, TIR 58%, insulin pump 0.8 u/h

GAD65 – autoantibodies to glutamic acid decarboxylase 65; IAA – autoantibodies to insulin; IA-2A – autoantibodies to tyrosine phosphatase-like protein; DKA – diabetic ketoacidosis; HbA1c – hemoglobin A1c (%); TIR – time in range (%).

an insulin pump (0.8 units/h), with a TIR of 58% and an HbA1c of 7.4% At times, he may question or be reluctant to follow his treatment plan, which is not uncommon for individuals his age.

Autoantibody profiles stratified by family relationship

The largest group of participants were parents of individuals with T1D (60.59%, 495), followed by siblings (38.19%, 312) and children of parents with T1D (4.41%, 36). It is important to note that individuals may be counted more than once if they fit multiple categories. Among children with a parent diagnosed with T1D, 8.33% (3/36) were positive for at least 1 autoantibody, while for parents of children with T1D it was 7.27% (36/495). The highest percentage of autoantibodies was found in siblings, at 9.62% (30/312).

Among those with 1 autoantibody, 66.67% (n = 32) were parents of children with T1D, 35.42% (n = 17) were siblings and 4.17% (n = 2) were children of a parent with T1D. The highest incidence of 2 autoantibodies was found in siblings of individuals with T1D, who accounted for 75% (6 out of 8) of all individuals with 2 autoantibodies.

Three autoantibodies were only found in siblings (n = 4, 66.67%) and parents of children with T1D (n = 3, 50.00%), while 4 autoantibodies were observed exclusively in 3 individuals, all of whom were siblings of a person with T1D.

When examining autoantibody prevalence by the familial relationships, GAD65 was most common in both siblings and parents. Of the 45 individuals with positive GAD65, 53.33% were siblings and 48.89% were parents. Only 4.44% were children of parent with T1D. It is important to consider that individuals may have multiple familial connections to an individual with T1D.

Similarly, IAA was most often found in siblings (53.57%; n = 15) and parents of individuals with T1D (42.86%; n = 12). Interestingly, 88.9% (n = 9) of those with IA-2A were siblings and 11.10% (n = 1) were parents. No cases of IA-2A were observed in children of T1D parents. The same pattern was seen for ZnT8, which was found only in siblings (50.00%; n = 6) and parents (66.67%; n = 8).

Discussion

The Polish INNODIA cohort provides insight into T1D development risk in the first-degree relatives of people living with T1D. Among the 65 participants with autoantibodies, 73.8% (n = 48) had 1 positive autoantibody, with GAD65 and IAA being most common. Despite the smaller sample size (n = 817), the findings are consistent with the broader INNODIA dataset (n > 4,400) and with the Type 1 Diabetes TrialNet Pathway to Prevention Study (TN01), a USA-based consortium (n > 250,000), both of which focus on screening first-degree relatives of individuals with T1D.[10,16]

Although both studies were still ongoing as of 2022 and had not yet reported final results, they demonstrated similar patterns in autoantibody prevalence, with GAD65 and IAA being the most frequently observed.[16] In the Polish INNODIA cohort, 7.96% of first-degree relatives tested positive for at least 1 autoantibody, compared to 5.00% in TrialNet TN01. The prevalence of ≥2 autoantibodies in the Polish cohort (2.08%) was comparable to that reported in the overall INNODIA (2.6%) and TrialNet TN01 (2.5%) studies.[10,16]

These similarities suggest that autoantibody patterns in the Polish data align with those in larger international cohorts, though caution is needed due to the limited sample size. Despite differences in number of participants and regions, these studies indicate consistent T1D risk in first-degree relatives across populations. While Poland lacks a national T1D screening program, a study performed by the Medical University of Bialystok reported that 7.78% of 3,575 children screened had at least 1 autoantibody, with markedly higher prevalence of a single autoantibody (6.60%; n = 236) compared to multiple autoantibodies (1.17%, n = 42). It is important to note, however, that this study focused on children aged 1–9 years, a younger cohort than that examined in the INNODIA study, and included a broader population, not limited to first-degree relatives.[17]

Type 1 diabetes mellitus screening in clinical practice enables the detection of early-stage disease, reducing the incidence of DKA and facilitating enrollment in clinical trials for disease-modifying therapies. Early diagnosis through screening reduces DKA rates at onset to below 5%, whereas in Poland, 30–40% of children with newly diagnosed T1D present with DKA.[5,15,18–20]

Prior screening, metabolic staging and education help eliminate clinical differences between individuals with and without a family history of T1D.[18,21] In the Fr1da study, participants who did not receive early intervention – including education – had higher HbA1c levels and more frequent hospitalizations compared with those who did.[7] Similarly, individuals with a family history had lower HbA1c levels (9.3% vs 10.6%) and fewer cases of severe ketonuria compared to those without a family history. These studies emphasize the importance of awareness and early detection through screening and proper education.[8]

In the Polish INNODIA study, most AA-positive individuals (73.8%, n = 48) presented with a single autoantibody. Although their risk of progressing to T1D is comparatively lower – with approx. 50% of children showing transient positivity – they still require careful monitoring, particularly younger individuals and those within the first 2 years of seroconversion.[6]

Type 1 diabetes screening is a complex process, with various factors potentially influencing the decision to participate such as fear of positive result or inability to prevent T1D.[22,23] To improve participation, it is essential to address

the emotional challenge associated with screening and to provide appropriate psychological support, particularly for individuals experiencing anxiety about the results. Providing support and educating individuals on T1D, its autoimmune causes, symptoms, and the importance of early detection can reduce stress and encourage continued involvement. A balanced approach combining medical information and emotional support is a key to motivating participation.

Limitations of the study

In Poland, over 1/3 of children newly diagnosed with T1D present with DKA.[18,19] The INNODIA study, which focused on first-degree relatives of individuals with T1D, does not fully represent the general population. Accordingly, broader screening and early detection initiatives should be implemented to encompass the general public. A proactive approach, emphasizing early recognition of symptoms and timely support, should be incorporated into care protocols for individuals at the earliest stages of T1D. Additional analyses, such as the influence of birth order and sibling sex, may provide further insights, although the relatively small sample size in this study limits the reliability of such conclusions.

Conclusions

Analysis of the Polish INNODIA results reveals a similar occurrence of autoantibodies in first-degree relatives of people with T1D when compared to other European countries. Early detection of T1D is an evolving initiative that offers valuable medical care not only to relatives of people living with T1D but also to the broader population.

Although the process is complex and optimal strategies are still under development, substantial progress has been achieved since the early phases of the INNODIA screening program. These advances provide a solid foundation for the potential implementation of national screening initiatives, with the ultimate goal of improving patient care.

Data Availability Statement

The datasets supporting the findings of the current study are openly available in the Zenodo repository at https://doi.org/10.5281/zenodo.15574493.

Consent for publication

Not applicable.

Use of AI and AI-assisted technologies

Not applicable.

ORCID iDs

Magdalena Małachowska https://orcid.org/0009-0008-2147-4316
Kamil Kosiorowski https://orcid.org/0009-0009-4020-2188
Eliza Skała-Zamorowska https://orcid.org/0000-0002-9140-3686
Przemysława Jarosz-Chobot https://orcid.org/0000-0002-1120-0994
Sebastian Seget https://orcid.org/0000-0002-1917-6351
Ewa Rusak https://orcid.org/0000-0002-4422-7704
Halla Kamińska https://orcid.org/0000-0003-0960-8365
Grażyna Deja https://orcid.org/0000-0001-6779-4966
Aleksandra Pyziak-Skupień https://orcid.org/0000-0002-7520-8506

References

1. Tekielak A, Otto-Buczkowska E, Rusak E. Less common forms of diabetes in young population. *Pediatr Endocrinol Diabetes Metab*. 2024;30(1):29–35. doi:10.5114/pedm.2024.136279
2. Bauer W, Gyenesei A, Krętowski A. The multifactorial progression from the islet autoimmunity to type 1 diabetes in children. *Int J Mol Sci*. 2021;22(14):7493. doi:10.3390/ijms22147493
3. Tatovic D, Narendran P, Dayan CM. A perspective on treating type 1 diabetes mellitus before insulin is needed. *Nat Rev Endocrinol*. 2023;19(6):361–370. doi:10.1038/s41574-023-00816-5
4. Quinn LM, Dias RP, Bidder C, et al. Presentation and characteristics of children with screen-detected type 1 diabetes: Learnings from the ELSA general population pediatric screening study. *BMJ Open Diab Res Care*. 2024;12(5):e004480. doi:10.1136/bmjdrc-2024-004480
5. Haller MJ, Bell KJ, Besser REJ, et al. ISPAD Clinical Practice Consensus Guidelines 2024: Screening, Staging, and Strategies to Preserve Beta-Cell Function in Children and Adolescents with Type 1 Diabetes. *Horm Res Paediatr*. 2024;97(6):529–545. doi:10.1159/000543035
6. Phillip M, Achenbach P, Addala A, et al. Consensus guidance for monitoring individuals with islet autoantibody-positive pre-stage 3 type 1 diabetes. *Diabetes Care*. 2024;47(8):1276–1298. doi:10.2337/dci24-0042
7. Hummel S, Carl J, Friedl N, et al. Children diagnosed with presymptomatic type 1 diabetes through public health screening have milder diabetes at clinical manifestation. *Diabetologia*. 2023;66(9):1633–1642. doi:10.1007/s00125-023-05953-0
8. Bonifacio E, Coelho R, Ewald DA, et al. The efficacy of islet autoantibody screening with or without genetic pre-screening strategies for the identification of presymptomatic type 1 diabetes. *Diabetologia*. 2025;68(6):1101–1107. doi:10.1007/s00125-025-06408-4
9. European Commission. Translational approaches to disease modifying therapy of type 1 diabetes: An innovative approach towards understanding and arresting type 1 diabetes. Sofia ref. 115797. Brussels, Belgium: European Commission; 2015. doi:10.3030/115797
10. Sims EK, Besser REJ, Dayan C, et al. Screening for type 1 diabetes in the general population: A status report and perspective. *Diabetes*. 2022;71(4):610–623. doi:10.2337/dbi20-0054
11. Redondo MJ, Steck AK, Pugliese A. Genetics of type 1 diabetes. *Pediatr Diabetes*. 2018;19(3):346–353. doi:10.1111/pedi.12597
12. Dorman J, Steenkiste A, O'Leary L, McCarthy B, Lorenzen T, Foley T. Type 1 diabetes in offspring of parents with type 1 diabetes: The tip of an autoimmune iceberg? *Pediatr Diabetes*. 2000;1(1):17–22. doi:10.1034/j.1399-5448.2000.010104.x
13. Hoffmann L, Kohls M, Arnolds S, et al. EDENT1FI Master Protocol for screening of presymptomatic early-stage type 1 diabetes in children and adolescents. *BMJ Open*. 2025;15(1):e088522. doi:10.1136/bmjopen-2024-088522
14. Marcovecchio ML, Hendriks AEJ, Delfin C, et al. The INNODIA Type 1 Diabetes Natural History Study: A European cohort of newly diagnosed children, adolescents and adults. *Diabetologia*. 2024;67(6):995–1008. doi:10.1007/s00125-024-06124-5
15. Simmons KM, Sims EK. Screening and prevention of type 1 diabetes: Where are we? *J Clin Endocrinol Metab*. 2023;108(12):3067–3079. doi:10.1210/clinem/dgad328
16. Battaglia M, Anderson MS, Buckner JH, et al. Understanding and preventing type 1 diabetes through the unique working model of TrialNet. *Diabetologia*. 2017;60(11):2139–2147. doi:10.1007/s00125-017-4384-2
17. Jamiołkowska-Sztabkowska M, Noiszewska K, Polkowska A, et al. Get ahead of the disease: Islet cell autoimmunity and preclinical phase of type 1 diabetes in general population of 1–9 year-old children in the north-eastern region of Poland: A summary of the first 18 months of the study. *Diabetes Obes Metab*. 2025;27(9):5108–5117. doi:10.1111/dom.16560

18. Pietrzak I, Michalak A, Seget S, et al. Diabetic ketoacidosis incidence among children with new-onset type 1 diabetes in Poland and its association with COVID-19 outbreak: Two-year cross-sectional national observation by PolPeDiab Study Group. *Pediatr Diabetes*. 2022;23(7): 944–955. doi:10.1111/pedi.13379
19. Rusak E, Seget S, Macherski M, Furgał N, Dyś P, Jarosz-Chobot P. Has the COVID-19 pandemic affected the prevalence of diabetic ketoacidosis in Polish children with newly diagnosed type 1 diabetes? An example of the largest Polish pediatric diabetes center (Upper Silesia, Katowice, Poland). *Healthcare (Basel)*. 2022;10(2):348. doi:10.3390/healthcare10020348
20. DiMeglio LA, Evans-Molina C, Oram RA. Type 1 diabetes. *Lancet*. 2018; 391(10138):2449–2462. doi:10.1016/S0140-6736(18)31320-5
21. Neuman V, Piona C, Cudizio L, et al. Are we ready to screen for type 1 diabetes? A structured worldwide survey among healthcare providers involved in paediatric diabetes care. *Diabet Med*. 2024; 41(6):e15329. doi:10.1111/dme.15329
22. Scudder C, Townson J, Bowen-Morris J, et al. General population screening for type 1 diabetes using islet autoantibodies at the preschool vaccination visit: A proof-of-concept study (the T1Early study). *Arch Dis Child*. 2024;109(10):812–817. doi:10.1136/archdischild-2023-326697
23. Kelly CS, Wolf WA, Cornelius EM, Peter ME, Chapman KS, Dunne JL. Insights into knowledge and attitudes about autoantibody screening from people affected by type 1 diabetes: A brief report. *Diabetes Ther*. 2024;15(10):2249–2261. doi:10.1007/s13300-024-01637-z

Heart failure in Poland: Epidemiology, hospitalizations, and trends from 2014 to 2021

Małgorzata Lelonek[1,A–F], Jadwiga Maria Nessler[2,A,E,F], Michał Bohdan[3,A,E,F], Tomasz Hryniewiecki[4,A,E,F], Magdalena Władysiuk[5,6,B–D,F], Grzegorz Niesyczyński[6,B–D], Urszula Cegłowska[7,8,B,E,F], Kacper Hałgas[7,B,E,F], Agata Śmiglewska[7,B,E,F], Anna Wiśniewska[7,B,E,F], Aleksander Siniarski[2,A,C–F]

[1] Department of Noninvasive Cardiology, Medical University of Lodz, Poland
[2] Department of Coronary Artery Disease and Heart Failure, Institute of Cardiology, Faculty of Medicine, Jagiellonian University Medical College St. John Paul II Hospital, Cracow, Poland
[3] First Department of Cardiology, Medical University of Gdansk, Poland
[4] Department of Valvular Heart Disease, National Institute of Cardiology, Warsaw, Poland
[5] Chair of Epidemiology and Preventive Medicine, Jagiellonian University Medical College, Cracow, Poland
[6] HTA Consulting, Cracow, Poland
[7] Department of Analysis and Strategy, Ministry of Health of the Republic of Poland, Warsaw, Poland
[8] Department of Epidemiology and Health Promotion, School of Public Health, Centre of Postgraduate Medical Education, Warsaw, Poland

A – research concept and design; B – collection and/or assembly of data; C – data analysis and interpretation; D – writing the article; E – critical revision of the article; F – final approval of the article

Advances in Clinical and Experimental Medicine, ISSN 1899–5276 (print), ISSN 2451–2680 (online) *Adv Clin Exp Med*. 2026;35(4):611–619

Address for correspondence
Aleksander Siniarski
E-mail: aleksandersiniarski@gmail.com

Funding sources
None declared

Conflict of interest
None declared

Received on May 6, 2025
Reviewed on June 22, 2025
Accepted on July 30, 2025

Published online on January 23, 2026

Cite as
Lelonek M, Nessler JM, Bohdan M, et al. Heart failure in Poland: Epidemiology, hospitalizations, and trends from 2014 to 2021. *Adv Clin Exp Med*. 2026;35(4):611–619. doi:10.17219/acem/208786

DOI
10.17219/acem/208786

Abstract

Background. Heart failure (HF) is marked by a poor prognosis, heightened mortality risk, and recurrent hospitalizations. Poland consistently ranks among the highest of all Organization for Economic Co-operation and Development (OECD) countries, with a hospitalization rate of 616 per 100,000 citizens in 2019 – nearly 3 times the 34-country average.

Objectives. This study aims to provide essential insights into the management of HF patients in Poland, with a particular focus on individuals experiencing recurrent hospitalizations, over the period 2014–2021.

Materials and methods. This observational study analyzes long-term registry data from the Polish Ministry of Health and the Health Needs Map. It includes more than 1,000,000 patients diagnosed with HF (ICD-10: I50) or pulmonary edema (ICD-10: J81), treated across all medical facilities operating under a uniform national healthcare system. This study inherently employs a population-based approach, encompassing all medical facilities that treat patients with these ICD-10 codes.

Results. Here, we present data on HF prevalence, incidence, and the healthcare pathway. The number of diagnosed HF cases in Poland increased to 1.02 million by December 31, 2019. In 2021, the standardized HF prevalence rate reached 2,626 per 100,000 population, with the highest prevalence observed in individuals aged 80–89 years (32%). Heart failure hospitalizations (HFH) in 2019 were 1022 per 100,000, decreasing to 205,000 in 2021. Notably, the number of hospitalizations exceeded the number of patients receiving treatment by 18–25%. Between 2014 and 2021, more than 9.2 million healthcare services were recorded, accounting for 48% of all HF-related encounters.

Conclusions. This study, relevant to both Polish and international cardiologists, provides a comprehensive overview of HF trends and associated risks, offering insights that may help refine diagnosis and treatment strategies in Central and Eastern European populations.

Key words: heart failure, hospitalization, registries, epidemiology in Poland, population surveillance

Highlights

- Over 1 million heart failure (HF) patients were registered in Poland by 2019, with a standardized prevalence rate of 2,626 per 100,000 in 2021.
- The highest HF burden was observed in the 80–89 age group, comprising 32% of all diagnosed cases.
- Despite declining hospitalizations, healthcare utilization remained high with 9.2 million HF-related services recorded between 2014 and 2021.
- The study reveals an 18–25% gap between HF hospitalizations and outpatient treatment, underscoring significant care-coordination challenges.

Background

Heart failure (HF) is a clinical syndrome characterized by a poor prognosis and a high risk of death and heart failure hospitalizations (HFH).[1] In Poland, the overall number of patients with HF has been systematically increasing.[2,3] Poland consistently ranks among the highest of all Organization for Economic Co-operation and Development (OECD) countries, with a HFH rate of 616 per 100,000 citizens in 2019 – nearly 3 times the 34-country average of 220.[4] This rate has been rising since 2009, in contrast to global trends showing a decline.

Beyond its epidemiological magnitude, HF represents a major and growing public health challenge in Poland, exerting a substantial clinical, organizational, and economic burden on the healthcare system.[1] The persistently high rates of hospitalization reflect not only the aging of the population and improved survival after acute cardiovascular events, but also a high prevalence of cardiovascular risk factors, multimorbidity, and suboptimal implementation of evidence-based therapies across the continuum of care.[1–3] Recurrent HF hospitalizations are associated with accelerated disease progression, impaired quality of life, and markedly increased mortality risk, underscoring the vicious cycle of decompensation and readmission.[1–3] In this context, the unfavorable Polish trends, diverging from those observed in many other OECD countries, highlight an urgent need for more effective prevention strategies, earlier diagnosis, optimized outpatient management, and coordinated, system-level interventions aimed at reducing HF-related morbidity and mortality.[1–3]

Objectives

The primary objective of this study was to generate comprehensive insights into the management of patients with HF in Poland, with particular emphasis on individuals experiencing recurrent hospitalizations. By analyzing data from 2014 to 2021, the study characterizes temporal trends, treatment patterns and healthcare utilization within this high-risk population. The findings aim to inform clinical practice, optimize resource allocation, and support the development of targeted strategies to reduce hospital readmissions and improve outcomes in HF care in Poland.

Materials and methods

Description of the studied population

This study is an observational long-term registry analysis using data from the Polish Ministry of Health spanning from 2014 to 2021. The study population reflects a diverse and extensive national cohort. Data obtained from the National Health Fund included patients diagnosed with HF (ICD-10: I50) and pulmonary edema (ICD-10: J81). A total of more than 1,000,000 patients with a primary or secondary diagnosis of HF were included in the analysis, the majority of whom were treated within a single type of medical service. Given the volume of cases, the study is population-based and encompasses all medical facilities providing care for conditions classified under ICD-10 codes I50 and J81.

Definitions of analyzed endpoints

Heart failure recorded as the main diagnosis in primary healthcare (PHC), outpatient specialist care (OSC), or hospital treatment indicates that the ICD-10 code for HF (I50 or J81) was listed as the first diagnosis (the primary reason for admission). In contrast, "HF overall" denotes cases in which the HF diagnosis appeared in the medical record as an additional or secondary condition. Hospitalization was defined as any inpatient stay with the relevant ICD-10 codes, including a diagnosis of HF. Heart failure hospitalization referred specifically to inpatient admissions directly associated with exacerbation or decompensation of HF. Hospital treatment, by contrast, denoted any other hospitalization occurring in patients with an HF diagnosis.

Statistical analyses

All described data regarding the healthcare services was derived from the following sources: 1) data provided by the Polish Ministry of Health specifically for the authors

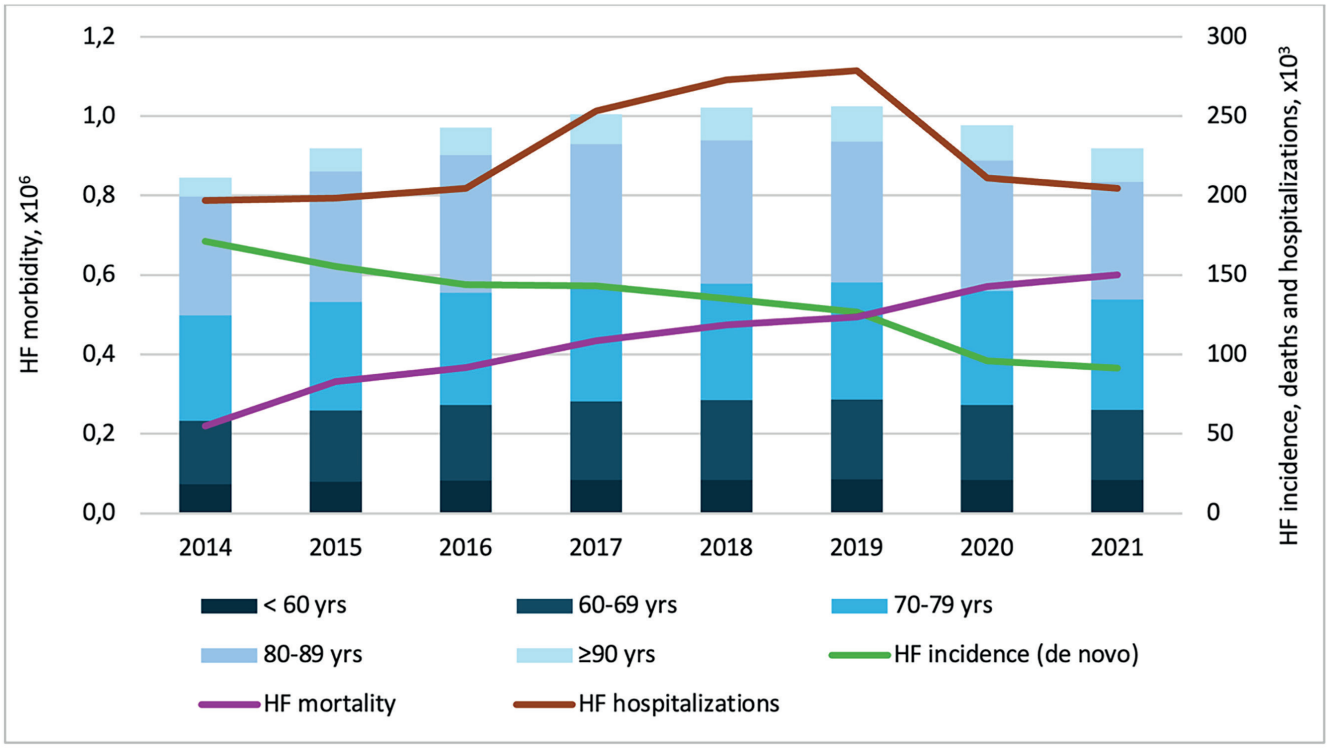

Fig. 1. Epidemiology of heart failure (HF) in Poland in 2014–2021: analysis based on data prepared by the Ministry of Health of the Republic of Poland. The graphical presentation utilizes colored bars to illustrate the frequency of the specified endpoint over the study years. Blue columns indicate on HF prevalence according to age groups. Green and purple denote incidence and deaths rates, respectively, while a brown line represents HF hospitalization (HFH) trends

of this report; 2) Health Needs Map for the years 2022–2026[5]; 3) analysis of the health problem of HF included in the Systemic and Implementation Analyses Base[3]; 4) statistics from the Polish National Health Fund; 5) selected data from the www.ezdrowie.gov.pl portal. All data was delivered anonymously, ensuring the highest level of data protection. A descriptive analysis was undertaken employing numerical values and/or percentages within each group, including the data presented as counts per 100,000 patients in the population.

Based on available data for pre-pandemic years (2014–2019), we performed a linear trend analysis, using the least-squares method, forecasting the trend for 2020–2021. Based on this analysis it is possible to compare the forecasted values with the data available for 2 pandemic years (2020–2021). The p-values for linear trend based on pre-pandemic data were also estimated. Data were analyzed using Microsoft Excel 2013 (Microsoft Corp., Redmond, USA).

Results

Epidemiology: prevalence and incidence of HF

Figure 1 summarizes HF morbidity, incidence, and hospitalizations, with colored bars depicting trends across calendar years and columns representing specific age groups. According to the latest Ministry of Health data, the number of diagnosed HF cases in Poland increased steadily from 2014 to 2019, reaching 1.02 million by December 31, 2019. Across the years analyzed, we observed a significant upward trend in HF prevalence accompanied by a simultaneous and significant decline in HF incidence (de novo HF) (Fig. 2A,B). During this period, de novo HF diagnoses decreased notably, with 127,000 cases reported in 2019 – representing a 26% reduction compared with 2014. Conversely, the total number of HF-related deaths increased markedly, reaching 124,000 in 2019 – nearly equaling the number of new HF cases (Fig. 2B–D). In 2020–2021, although new HF diagnoses declined, HF-related deaths continued to rise, leading to a reduction in registered morbidity (Fig. 2C). The current analysis shows that the HF prevalence rate in 2021 was 2,413 per 100,000, increasing to 2,626 per 100,000 after standardization for age, sex, and place of residence. The highest prevalence was observed among individuals aged 80–89 years (32%), followed by those aged 70–79 years (30%). Overall, approx. 90% of patients were aged 60 years or older (Table 1).

The age distribution of HF patients reflects a marked increase in morbidity after age 60, reaching 431 per 100,000, with a continued rise in each successive age group (Table 1). The average age at HF diagnosis was 71.8 years, while the mean age across all HF patients was 75.2 years. Although the proportion of HF-related deaths within total mortality gradually decreased, the absolute number

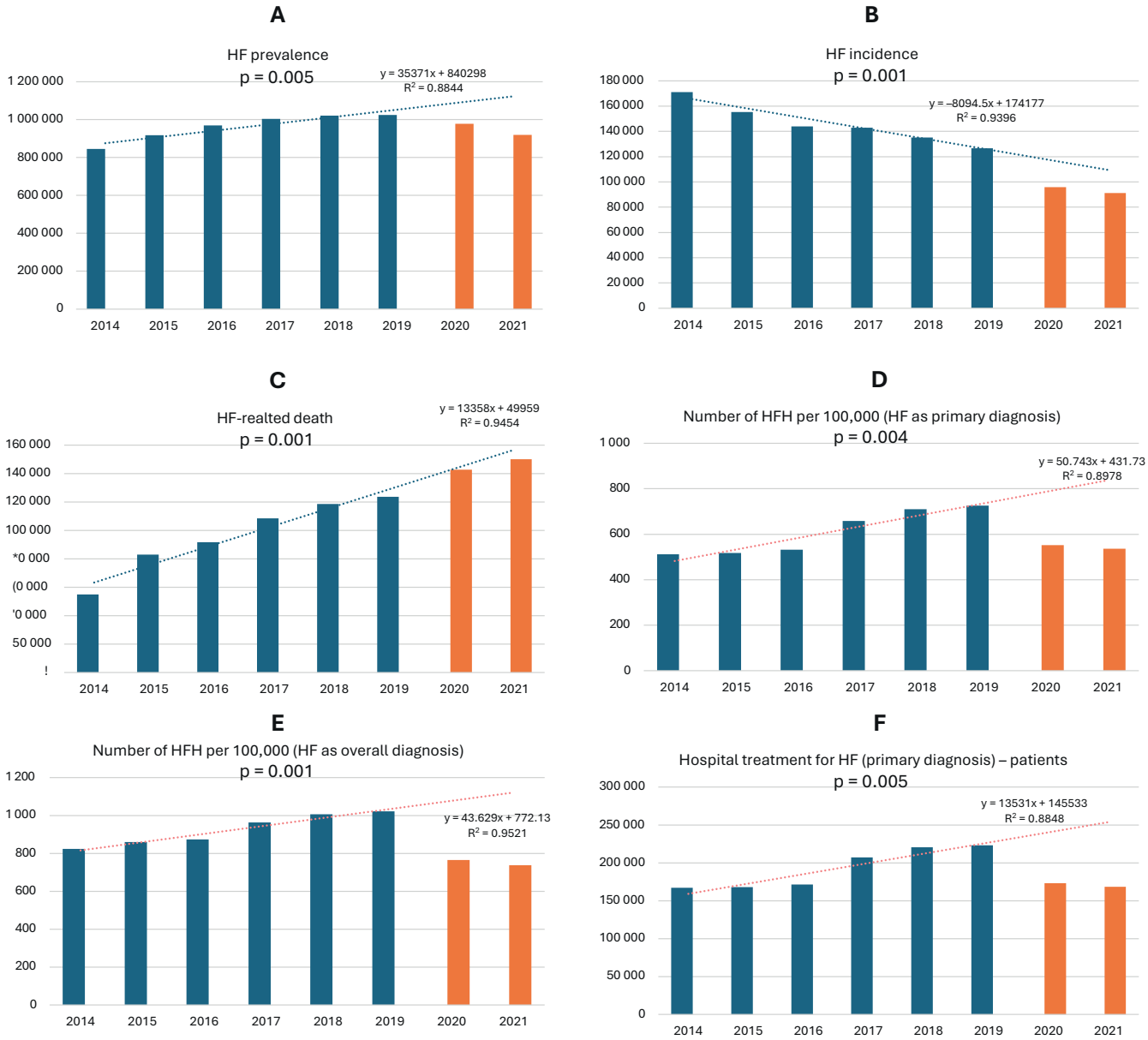

Fig. 2. Trends in heart failure prevalence, incidence, hospitalizations, and mortality from 2014 to 2021 in Poland. Data demonstrated as columns in each calendar year (2014–2021). The figure shows HF prevalence (A); HF incidence (B); HF-related deaths (C); HFH with HF as a primary (D) or overall diagnosis (E) per 100,000 population; hospital treatment for HF as a primary diagnosis calculated per patients (F)

HF – heart failure; HFH – heart failure hospitalization.

of such deaths increased from 2014 to 2021 – most notably in 2020–2021 – mirroring the overall rise in population mortality (Table 2).

Heart failure hospitalizations

During the analyzed years, the HFH rate in 2019 reached 1,022 per 100,000 individuals (primary or additional diagnosis), including 726 per 100,000 for HFH listed as the primary diagnosis. Across 2014–2021, HFH with a primary diagnosis ranged from 197,000 to 278,000,

Table 1. Epidemiological rates per 100,000 in Polish population and contribution of age group to morbidity in 2021

Age group [years]	Number per 100,000 population		Contribution of age group to morbidity
	incidence	morbidity	
0–9	3	21	1%
10–19	2	13	
20–29	9	57	
30–39	24	126	
40–49	60	335	2%
50–59	176	1,142	6%
60–69	431	3,476	19%
70–79	914	8,994	30%
80–89	1,625	21,722	32%
≥90	1,909	29,763	9%

Data presented as morbidity and incidence number per 100,000 population in each age group.

Table 2. Number of heart failure (HF)-related deaths and their percentage in the total number of deaths in 2014–2021

Year	2014	2015	2016	2017	2018	2019	2020	2021
HF-related deaths	55,003	82,911	91,582	108,446	118,619	123,711	142,774	149,963
Contribution of HF to the total number of deaths [%]	14.6	21.0	23.6	26.9	28.6	30.2	29.9	28.9

The data show the number of HF-related deaths and the percentage contribution of HF to the total number of deaths for each year.

declining to 211,000 and 205,000 in 2020 and 2021, respectively (Fig. 2E,F). There were significant increasing trends in HFH per 100,000 population from 2014 to 2019 for both HF as a primary diagnosis and HF as an overall diagnosis (Fig. 2D, Fig. 2E, respectively). Each year, HF-related hospitalizations exceeded the number of patients receiving treatment services (167,000–223,000) by 18–25%, resulting in an average of 1.18 to 1.25 hospitalizations per patient with at least one HFH in a given calendar year.

From 2014 to 2019, there was a 21% increase in HF patients experiencing ≥1 urgent HFH, rising from 36,300 to 44,000. Over the same period, the number of patients with ≥2 HFH within 12 months increased from 33,200–45,100 in 2014 to 38,700–54,700 in 2019. In 2020–2021, HFH numbers declined (24,700–38,400), most likely due to restricted access to the healthcare system during the COVID-19 pandemic. In terms of overall HF prevalence, individuals with ≥2 HFH represented 20% of all patients, totaling 181,100 of 918,800 in 2021.

Hospital treatment

From 2014 to 2019, hospital treatment for HF as the main diagnosis increased by 34%, reaching 223,000 cases; however, in 2020–2021 it declined by 22–24% to 168,000–173,000. Health services for HF, whether recorded as the primary or a concomitant diagnosis, followed similar patterns. Between 2014 and 2019, visits for HF as the main diagnosis rose by 41% to 298,000, then decreased by 24–27% to 226,000–219,000 in 2020–2021. In 2021, the average number of visits per patient with at least one HFH was 1.30, and 1.44 for patients with HF overall. Heart failure hospitalizations exceeded 250,000 annually until 2018, amounting to more than 1.6 million admissions between 2012 and 2018. This pattern corresponded with a significant upward trend in both the number of patients and the volume of HF-related services throughout the analyzed period (Fig. 2F, Fig. 3A).

Notably, 82% of these hospitalizations were emergency admissions, underscoring HF progression or limitations in OSC. Moreover, 60% of admissions occurred in internal medicine departments, whereas only 30% took place in cardiology departments. Only 1 in 12 hospitalizations (8.3%) involved patients younger than 60 years. Hospitalizations peaked in 2019, with 278,000 admissions for HF and more than 392,000 for overall HF diagnoses. Thereafter, the number of hospitalizations declined significantly, reaching 281,000 in 2021.

Healthcare pathway of patients with HF

From 2014 to 2021, a total of 9.2 million healthcare services were recorded, most of which occurred in PHC (48%), followed by hospital treatments (22%) and nursing/care services (15%). Services provided in OSC amounted to nearly half the volume of those delivered in hospital settings. The healthcare pathway was analyzed for 1,062,157 HF patients, including those treated exclusively within a single healthcare service (n = 446,224), those receiving repeated care within the same service (n = 289,067), and those managed across multiple services (n = 615,933). Overall, the median number of healthcare services per HF patient was 4.

From 2014 to 2021, the proportion of initial HF diagnoses made in PHC declined from 44% to 29%, while hospital-based diagnoses increased. This shift occurred despite a relatively stable proportion of patients receiving PHC services, and was accompanied by a significant downward trend in HF-related PHC visits. Outpatient specialist care accounted for only 12–15% of HF diagnoses, and other healthcare services for approx. 4%. Following an HFH, patients most commonly return either to the hospital (39%) or to PHC (34%). After hospitalization or OSC visits, PHC accounts for the largest share of subsequent encounters – 50.3% and 24.5%, respectively. These findings underscore the central role of PHC in the management of HF in Poland, where PHC physicians oversee the majority of patient care, constituting 62% of all visits (n = 1,459,619).

Primary healthcare

Between 2014 and 2021, both the number of patients diagnosed with HF and the volume of HF-related services provided in PHC declined, for both primary and overall HF diagnoses (Fig. 3B,C). Despite this, the number of medical centers providing HF services increased from 7,400 in 2014 to 7,700 in 2021 (Table 3).

The mean annual number of PHC visits per patient diagnosed with HF remained stable at 3 between 2014 and 2021. From 2014 to 2019, PHC physicians diagnosed an average of 458,000 HF patients annually, with a peak of 464,000 in 2016. However, in 2020–2021, this number declined by 10%, to an average of 413,000 patients. The total number of HF-related health services also decreased from 1.54 million in 2014 to 1.26 million in 2021, representing an 18% reduction.

Table 3. Primary healthcare for overall patients with heart failure (HF)

Year	2014	2015	2016	2017	2018	2019	2020	2021
Number of patients	451,116	460,706	463,884	462,831	452,613	458,675	421,056	405,730
Number of HF visits	1,539,451	1,445,649	1,439,753	1,420,677	1,356,172	1,384,048	1,270,183	1,261,125
Visits per patient ratio	3.41	3.14	3.10	3.07	3.00	3.02	3.02	3.11
Number of HF sites	7,395	7,393	7,503	7,693	7,649	7,690	7,625	7,650

Analysis was performed using data from the Ministry of Health of the Republic of Poland. Heart failure was defined according to ICD-10 codes I50 and J81.

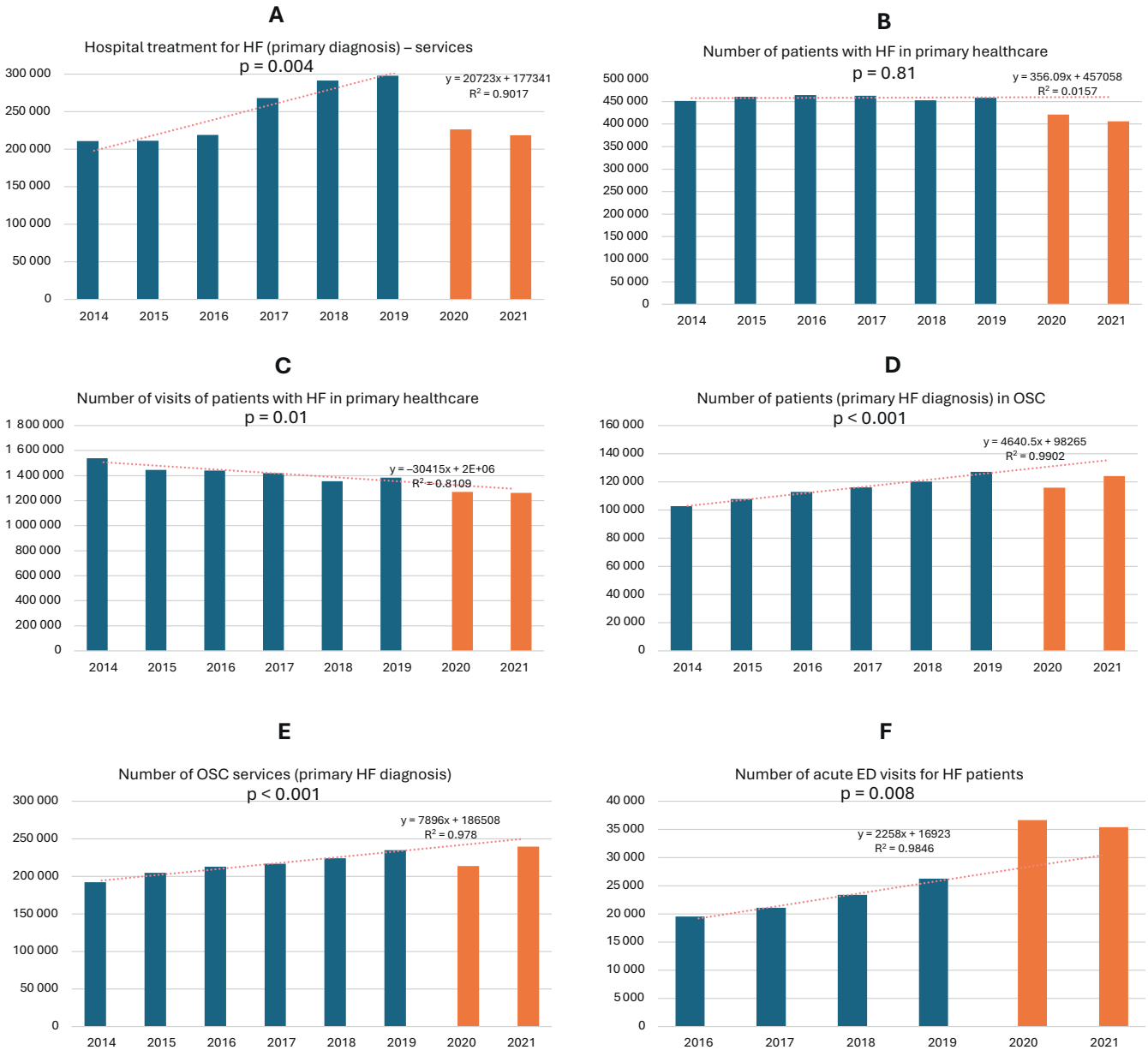

Fig. 3. Trends in heart failure (HF) hospitalizations, outpatients specialist care, and emergency visits. Data demonstrated as columns in each calendar year (2014–2021). The figure shows hospital treatment for HF as a primary diagnosis (A); Number of patients with HF in primary healthcare (B); Number of visits of patients with HF in primary healthcare (C); Number of patients (primary HF diagnosis) in outpatient specialist care center (D); number of outpatient specialist care services fof HF as a primary diagnosis (E); and number of acute ED visits for HF patients (F)

ED – emergency department; HF – heart failure; OSC – outpatient specialist care.

Outpatient specialist care

The OSC health services for patients with HF increased steadily from 192,000 in 2014 to 235,000 in 2019, representing an average annual rise of approx. 8,600 visits and a significant upward trend over the observed period (Fig. 3D,E). The COVID-19 pandemic resulted in a reduction of HF-related visits in 2020 (by approx. 21,000),

decreasing to 214,000 visits. Notably, in 2021 – despite ongoing pandemic conditions – healthcare services increased to 239,700, surpassing the 2019 peak (Fig. 3D,E). Furthermore, our data show that the number of patients utilizing OSC across all medical specialties exceeded the number of those with HF as the main diagnosis by more than 30% when considering all patients diagnosed with HF. Additionally, when comparing the volume of healthcare services provided, the difference was approx. 40%. These findings suggest that HF patients treated in OSC settings have clinically significant comorbidities and a more complex clinical profile.

Emergency department

Analysis of Ministry of Health data from 2016 to 2021 on emergency department (ED) visits by HF patients revealed a recent upward trend. In the last 2 years, acute ED visits among HF patients exceeded 35,000 annually, compared with 19,500–26,300 in 2016–2019. This trend was further supported by an increase in the proportion of ED visits resulting in HFH, which rose to 61–63% in 2020–2021, in contrast to 29–38% during 2016–2019. This was reflected in a significant upward trend in HF-related medical services provided in the ED (Fig. 3F). Notably, the percentage of ED visits resulting in death remained stable throughout 2014–2021 (2–3%).

Discussion

The study cohort, covering the years from 2014 to 2021, accurately reflects the diverse demographic and geographic characteristics of the Polish population with HF. It includes patients across a wide range of ages, socioeconomic backgrounds, and regions, ensuring comprehensive national representation. Based on data from the Ministry of Health and the Health Needs Map, the study offers essential insights into the evolving healthcare landscape in Poland over this 7-year period.

Epidemiology of HF in Poland

In Poland, nearly 150,000 HF-related deaths occur annually, corresponding to a population of more than 1 million individuals living with HF.[2] This elevated mortality is driven by the substantial number of newly diagnosed HF cases and the poor prognosis observed in older adults, particularly those aged 75 years and above. Another Polish study reported that only 57% of individuals diagnosed with HF survived beyond 5 years.[3] Furthermore, among individuals aged 75 years and older, the average survival period was approx. 4 years.[6,7]

Previous HF studies reported an age-standardized prevalence of 1,130 per 100,000 population in Poland, the 5th highest among EU countries.[8] In this study, even after standardization for age, sex, and place of residence, the prevalence was more than twice as high. Epidemiological projections suggest that HF incidence may continue to rise in the coming years, particularly between 2022 and 2031.[9] Based on available data, the number of new HF cases is projected to rise from 120,200–207,300 in 2022 to 133,500–229,800 in 2031, representing an approx. 11% increase across projected scenarios.[9] Consequently, a further increase in the total number of patients with HF cannot be excluded in the coming years, largely driven by demographic trends. According to Statistics Poland, the largest age groups affected by HF in Poland are currently individuals aged 60–69 years and 30–49 years.[10]

Finally, cardiovascular death – a predominant cause of mortality in Poland, accounting for 35% of all deaths in 2021, particularly among individuals aged 65 and older – now occurs at an estimated annual rate of approx. 175,000–180,000.[9,10]

HF hospitalizations

Poland has consistently ranked among OECD countries with the highest number of HF hospitalizations, reporting 616 HFH per 100,000 citizens in 2019 – nearly 3 times the 34-country average of 220.[4] Despite global reductions, Poland's HFH rate has continued to rise since 2009. Our data show an increase in ED contacts during 2020–2021 accompanied by a decline in hospital treatments, likely reflecting reduced ward admissions – a negative prognostic factor with implications for healthcare financing in Poland.[4]

Zaleska-Kociecka et al. reported similar findings on HFH.[11] The authors showed that patients with newly diagnosed HF had >1.5-fold higher risk of death with 2 hospitalizations (HR = 1.55), doubling with 3 hospitalizations (HR = 2.16), and nearly tripling with 4 hospitalizations (HR = 2.79).[12] The average hospital stay was 7.5 days, trending upwards with 25% readmitted after index HFH (median follow-up: 1,072 days).[12] Similar to our findings, the 30-day admission rate for a first HF rehospitalization was initially low (2.96%) but increased over time with subsequent hospitalizations.[12]

Healthcare pathway

An intensive strategy involving rapid medication adjustments and close monitoring post-HFH gained patient acceptance.[13] It effectively alleviated symptoms, improved quality of life, and reduced the risk of 180-day all-cause mortality or HF readmission compared to standard care.[13] Patients with ≥2 urgent HFH predominantly receive hospital or PHC services, with a minority referred to an OSC. This stands in contrast with European Society of Cardiology (ESC) guidelines, indicating an inefficient post-hospitalization HF treatment pathway.[1] Notably, patients with prior HFH utilize a broader range of healthcare services

over a shorter timeframe than those without HF history, emphasizing the predominant reliance on hospitals and primary care in their care provision.

Primary healthcare

In Poland, from 2014 to 2021, we observed a relatively consistent mean annual number of visits per HF patient through PHC system (n = 3). Notably, recent data for 2021 indicates a nearly 1/3 reduction in visits for HF as the main diagnosis compared to 2014.[5] Concurrently, the number of services provided declined by 20% relative to 2014 data (health services provided for n = 439,000 patients). This suggests that less than half of HF-diagnosed patients engage with their PHC provider. Caution is warranted in interpreting these data due to potential limitations arising from the ICD-10 reporting system, allowing only 1 code per service and potentially constraining the comprehensive understanding in cases with multiple diagnoses.[5]

Outpatient specialist care

Our data demonstrate a systematic increase in OSC services for patients with HF as the primary diagnosis over the study period. Intriguingly, despite the COVID-19 pandemic, an increase was observed – likely attributable to the incorporation of teleconsultations alongside traditional service formats, which helped compensate for the service deficit of previous years.[14] Patients with HF as a comorbidity are notably more inclined to seek OSC care, indicating a complex clinical profile with additional comorbidities. Despite the prevalence of comorbidities, medical services for HF patients within the OSC system remain a minority, reflecting inadequate care, particularly during the COVID-19 pandemic, correlating with a rising hospitalization rate.[14]

Emergency department

The surge in urgent ED visits, particularly in the later years of the analysis, is noteworthy. This increase was likely driven by the effects of the COVID-19 pandemic and reduced access to PHC, OSC, and follow-up care. Notably, in contrast to other findings,[14,15] the increase in ED visits did not correspond to a higher mortality rate compared to the previous years in the analysis.

Improvements and disadvantages in the healthcare system

In the last 2 years in Poland, significant progress has been made in accessing innovative therapies.[16] This includes increased availability of fundamental treatments like SGLT-2 inhibitors, reimbursed and provided free for those aged ≥65 years, addressing HF with reduced ejection fraction, chronic kidney disease, and type 2 diabetes.

Between 2015 and 2020, Poland maintained a stable number of OSC clinics. Despite the high HF prevalence, these patients receive less than 5% of all medical advice within OSC. Moreover, 90% of patients from cardiology departments and 60% from internal medicine departments were referred to OSC after hospitalization.[17] Non-adherence to ESC guidelines, with over 50% missing follow-up within 3 months, highlights the need for a dedicated HF program to improve drug adherence.[18–23] Despite the absence of a dedicated HF nursing specialty in Poland, the Heart Failure Association of the Polish Cardiac Society has developed a curriculum for nurses, serving as an educational framework for HF care.[19] As a result, there are currently approx. 1,500 certified HF nurses in the country. Numerous studies have shown that the implementation of structured HF programs significantly reduces the risk of rehospitalization and mortality.[20–23]

Access to left ventricular assist device (LVAD) therapy for advanced HF is another positive development in Poland. The Ministry of Health's endorsement aligns with the recommendation of the Agency for Health Technology Assessment and Tariff System (No. 17/2022, issued June 2, 2022), which supports public reimbursement for the care of patients with advanced HF. The National Cardiology Network, operational in 7 Polish voivodeships, accelerates patient diagnosis and ensures OSC within 30 days. Establishing a comprehensive, coordinated care model for HF patients, coupled with medical community education, aims to address these issues and enhance outcomes.

Limitations of the study

This publication has several limitations. The observed decline in new HF cases and overall morbidity in 2020–2021 may be attributable to the COVID-19 pandemic, which affected healthcare access and diagnostic activity.[24] We acknowledge that reporting disease occurrence in Poland using ICD-10 codes may be subject to error, as coding is linked to reimbursement procedures within the National Health Fund. Nevertheless, we believe that presenting these data offers a meaningful overview of progress – or its absence – across successive years in the occurrence of the diseases discussed, as demonstrated in this report. The data presented in the current article are derived from the Ministry of Health and are aggregated for HF described by ICD-10 coding I50 or J81. Therefore, we do not have the ability to provide the prevalence of each of those codes separately. Some new patients might not be registered in the payer's billing system (ICD-10 codes I50 and J81). However, these unregistered patients are at high risk of HFH and in-hospital death,[25] similar to the findings in this article. Finally, the analyzed data did not include exact dates of death, only information on whether the patient is alive or deceased; therefore, plotting Kaplan–Meier curves was not possible.

Conclusions

We have delineated the contemporary status of HF in Poland over the period 2014–2021. This extensive dataset provides a comprehensive overview of health patterns, healthcare utilization, and disparities in healthcare access and outcomes across the country.

Supplementary data

The supplementary materials are available at https://doi.org/10.5281/zenodo.15401298. The_package contains the following files:

Supplementary Fig. 1. Number of new HF patients in individual calendar years divided by the urgency of admission.

Supplementary Fig. 2. Expenses for HF-related healthcare services.

Data Availability Statement

Data come from the Ministry of Health of the Republic of Poland and cannot be made available to third parties.

Consent for publication

Not applicable

Use of AI and AI-assisted technology

AI or AI-assisted technology was not used.

ORCID iDs

Małgorzata Lelonek https://orcid.org/0000-0003-0756-5541
Jadwiga Maria Nessler https://orcid.org/0000-0002-5076-5816
Michał Bohdan https://orcid.org/0000-0002-3496-2238
Tomasz Hryniewiecki https://orcid.org/0000-0003-0536-886X
Magdalena Władysiuk https://orcid.org/0000-0002-9699-6708
Urszula Cegłowska https://orcid.org/0000-0002-1300-7370
Agata Śmiglewska https://orcid.org/0009-0003-4340-6991
Aleksander Siniarski https://orcid.org/0000-0002-7493-3626

References

1. McDonagh TA, Metra M, Adamo M, et al. 2021 ESC Guidelines for the diagnosis and treatment of acute and chronic heart failure. *Eur Heart J*. 2021;42(36):3599–3726. doi:10.1093/eurheartj/ehab368
2. System and Implementation Analysis Database Platform. Niewydolność serca. Warsaw, Poland: System and Implementation Analysis Database Platform; 2022. https://basiw.mz.gov.pl/analizy/problemy-zdrowotne/niewydolnosc-serca. Accessed March 15, 2025.
3. Ministry of Health of the Republic of Poland. Analysis of the health problem of heart failure [2014–2021]: Online application. Warsaw, Poland: Government of Poland; 2022. https://analizy.mz.gov.pl:9443/WAS/app_NS/. Accessed December 5, 2025.
4. Organisation for Economic Co-operation and Development (OECD). Health at a Glance 2021: OECD Indicators. Paris, France: Organisation for Economic Co-operation and Development (OECD); 2021. https://www.oecd-ilibrary.org/social-issues-migration-health/health-at-a-glance-2021_ae3016b9-en. Accessed March 15, 2025.
5. Ministry of Health of the Republic of Poland. Mapa-2022-2026: Epidemiologia (na podstawie danych GUS i NFZ). Warsaw, Poland: Government of Poland; 2025. https://basiw.mz.gov.pl/mapy-informacje/mapa-2022-2026/analizy/epidemiologia/epidemiologia-wersja-polska-gus-i-nfz. Accessed December 5, 2025.
6. Karasek D, Kubica A, Sinkiewicz W, Błażejewski J, Bujak R. Epidemia niewydolności serca – problem zdrowotny i społeczny starzejących się społeczeństw Polski i Europy. *Folia Cardiol*. 2008;3:242–248. https://journals.viamedica.pl/folia_cardiologica/article/view/23798.
7. Townsend N, Kazakiewicz D, Lucy Wright F, et al. Epidemiology of cardiovascular disease in Europe. *Nat Rev Cardiol*. 2022;19(2):133–143. doi:10.1038/s41569-021-00607-3
8. Bragazzi NL, Zhong W, Shu J, et al. Burden of heart failure and underlying causes in 195 countries and territories from 1990 to 2017. *Eur J Prev Cardiol*. 2021;28(15):1682–1690. doi:10.1093/eurjpc/zwaa147
9. Ministry of Health of the People's Republic of Poland. Mapa potrzeb zdrowotnych w zakresie kardiologii, 2018. Warsaw, Poland: Ministry of Health of the Republic of Poland; 2018. https://mpz.mz.gov.pl/mapy-kardiologiczne/#tab-2018. Accessed March 15, 2025.
10. Statistics Poland. Rocznik Demograficzny 2022. Warsaw, Poland: Statistics Poland; 2022. https://stat.gov.pl/obszary-tematyczne/roczniki-statystyczne/roczniki-statystyczne/%20rocznik-demograficzny-2022,3,16.html. Accessed March 15, 2025.
11. Zaleska-Kociecka M, Witczak K, Bartolik K, et al. Rehospitalization as a predictor of mortality in Polish population of heart failure patients-national registry. *Eur Heart J*. 2020;41(Suppl 2):ehaa946.0967. doi:10.1093/ehjci/ehaa946.0967
12. Leszek P, Waś D, Bartolik K, et al. Burden of hospitalizations in newly diagnosed heart failure patients in Poland: Real world population based study in years 2013–2019. *ESC Heart Fail*. 2022;9(3):1553–1563. doi:10.1002/ehf2.13900
13. Mebazaa A, Davison B, Chioncel O, et al. Safety, tolerability and efficacy of up-titration of guideline-directed medical therapies for acute heart failure (STRONG-HF): A multinational, open-label, randomised, trial. *Lancet*. 2022;400(10367):1938–1952. doi:10.1016/S0140-6736(22)02076-1
14. Palazzuoli A, Metra M, Collins SP, et al. Heart failure during the COVID-19 pandemic: Clinical, diagnostic, management, and organizational dilemmas. *ESC Heart Fail*. 2022;9(6):3713–3736. doi:10.1002/ehf2.14118
15. Bromage DI, Cannatà A, Rind IA, et al. The impact of COVID-19 on heart failure hospitalization and management: Report from a Heart Failure Unit in London during the peak of the pandemic. *Eur J Heart Fail*. 2020;22(6):978–984. doi:10.1002/ejhf.1925
16. Mołek-Dziadosz P, Nessler J. Heart failure with preserved ejection fraction as an interdisciplinary problem. *Prz Lek Jagiellonian Med Rev*. 2025;77:17944. doi:10.20452/jmr.2025.17944
17. Chuda A, Berner J, Lelonek M. The journey of the heart failure patient based on data from a single center. *Adv Clin Exp Med*. 2018;28(4):489–498. doi:10.17219/acem/78688
18. Gorczyca-Głowacka I, Mastalerz-Migas A, Lelonek M. Real-life implementation of guidelines for heart failure management. *Kardiol Pol*. 2023;81(9):919–921. doi:10.33963/KP.a2023.0144
19. Uchmanowicz I, Lisiak M, Lelonek M, et al. A curriculum for heart failure nurses: An expert opinion of the Section of Nursing and Medical Technicians and the Heart Failure Working Group of the Polish Cardiac Society. *Kardiol Pol*. 2020;78(6):647–652. doi:10.33963/KP.15405
20. Chaudhry SI, Phillips CO, Stewart SS, et al. Telemonitoring for patients with chronic heart failure: A systematic review. *J Cardiac Fail*. 2007;13(1):56–62. doi:10.1016/j.cardfail.2006.09.001
21. Faragli A, Abawi D, Quinn C, et al. The role of non-invasive devices for the telemonitoring of heart failure patients. *Heart Fail Rev*. 2021;26(5):1063–1080. doi:10.1007/s10741-020-09963-7
22. Louis AA, Turner T, Gretton M, Baksh A, Cleland JGF. A systematic review of telemonitoring for the management of heart failure. *Eur J Heart Fail*. 2003;5(5):583–590. doi:10.1016/S1388-9842(03)00160-0
23. Umeh CA, Torbela A, Saigal S, et al. Telemonitoring in heart failure patients: Systematic review and meta-analysis of randomized controlled trials. *World J Cardiol*. 2022;14(12):640–656. doi:10.4330/wjc.v14.i12.640
24. Zaleska-Kociecka M, Celinska-Spodar M, Podwojcic K, et al. COVID-19 pandemic impact on heart failure epidemiology and outcomes in Poland: National database study. *Eur Heart J*. 2022;43(Suppl 2):ehac544.1080. doi:10.1093/eurheartj/ehac544.1080
25. The CAPACITY-COVID Collaborative Consortium and LEOSS Study Group; Linschoten M, Uijl A, Schut A, et al. Clinical presentation, disease course, and outcome of COVID-19 in hospitalized patients with and without pre-existing cardiac disease: A cohort study across 18 countries. *Eur Heart J*. 2022;43(11):1104–1120. doi:10.1093/eurheartj/ehab656

Evaluating weight-adjusted waist index as a risk factor for chronic obstructive pulmonary disease: A cross-sectional analysis of NHANES data

Yanxiao Li[1,A–C], Bin Li[2,D–F]

[1] Department of Pulmonary and Critical Care Medicine, Shijiazhuang People's Hospital, China
[2] Department of Respiratory Medicine, The Fourth Hospital of Hebei Medical University, Shijiazhuang, China

A – research concept and design; B – collection and/or assembly of data; C – data analysis and interpretation; D – writing the article; E – critical revision of the article; F – final approval of the article

Advances in Clinical and Experimental Medicine, ISSN 1899–5276 (print), ISSN 2451–2680 (online) *Adv Clin Exp Med*. 2026;35(4):621–630

Address for correspondence
Bin Li
E-mail: 47901350@hebmu.edu.cn

Funding sources
This study was supported by the Hebei Province Medical Science Research Project Plan (grant No. 20220206).

Conflict of interest
None declared

Acknowledgements
We would like to thank all the clinicians who contributed diagnostic data of patients to our study.

Received on December 31, 2024
Reviewed on March 17, 2025
Accepted on June 25, 2025

Published online on April 2, 2026

Cite as
Li Y, Li B. Evaluating weight-adjusted waist index as a risk factor for chronic obstructive pulmonary disease: A cross-sectional analysis of NHANES data. *Adv Clin Exp Med*. 2026;35(4):621–630. doi:10.17219/acem/207571

DOI
10.17219/acem/207571

Abstract

Background. The weight-adjusted waist index (WWI) shows a significant positive association with chronic obstructive pulmonary disease (COPD) risk, suggesting a potential role in risk stratification and early detection.

Objectives. This study examined the relationship between WWI and COPD, with a focus on its clinical implications for COPD risk assessment and management.

Materials and methods. Data from the U.S. National Health and Nutrition Examination Survey (NHANES) 2007–2018 were used. We included individuals aged 40 years and older. Weighted logistic regression was used to examine the association between WWI and COPD. Subgroup analyses and interaction tests were performed to assess consistency across demographic and lifestyle factors. A nonlinear regression model was used to evaluate the relationship between WWI and COPD, while receiver operating characteristic (ROC) curve analysis was used to assess the ability of WWI to identify individuals at risk.

Results. Among 14,144 participants, WWI was higher in the COPD group than in the control group ($p < 0.001$). In fully adjusted models, WWI was positively associated with COPD (odds ratio (OR) = 1.50, 95% confidence interval (95% CI): 1.34–1.68). In stratified analyses, participants in the highest WWI quartile had a greater risk of COPD than those in the lowest quartile (OR = 2.13, 95% CI: 1.62–2.80). Subgroup analyses showed a consistent positive association between WWI and COPD across sex, age, and smoking status. The nonlinear model indicated that the risk of COPD increased significantly beyond a certain WWI value. The ROC curve analysis confirmed the utility of WWI as a predictor (area under the curve (AUC) = 0.625, 95% CI: 0.609–0.642). These findings highlight the need to incorporate WWI into routine COPD risk assessment.

Conclusions. This study found a significant and nonlinear positive association between WWI, a marker of central obesity, and COPD risk. Weight-adjusted waist index may be an independent predictor of COPD risk and provide insight into the contribution of obesity to the disease. Given the increasing burden of COPD, integrating WWI into clinical practice could enhance preventive efforts and personalized interventions.

Key words: central obesity, chronic obstructive pulmonary disease (COPD), weight-adjusted waist index (WWI)

Highlights

- This study identifies a strong association between the weight-adjusted waist index (WWI) and the risk of developing chronic obstructive pulmonary disease (COPD).
- WWI is an independent predictor of COPD, with higher values indicating greater risk.
- The association between WWI and COPD remains consistent across subgroups defined by sex, age, and smoking status.
- These findings suggest that WWI may be a useful tool for COPD risk assessment and early preventive strategies.

Background

Chronic obstructive pulmonary disease (COPD) is a long-term lung condition in which airflow is limited. It is preventable and treatable, but the global prevalence of COPD continues to rise.[1,2] Smoking is one of the major contributors to COPD, but other environmental and occupational exposures, such as air pollution and workplace hazards, are also factors in COPD development.[3] Therefore, modifiable risk factors and implement preventive measures need to be identified in order to reduce COPD risk.

Recent studies show that underweight individuals and those with central obesity have been linked to COPD and other chronic inflammatory airway diseases.[4,5] However, conventional obesity measures, such as body mass index (BMI) and waist circumference (WC), have their own limitations in fat distribution assessment.[6,7] Body mass index does not differentiate between fat and muscle mass,[8,9] while WC alone does not account for differences in body size and proportions.[10] As a result, these measures may not fully capture the role of body composition in COPD development.

To address this limitation, the weight-adjusted waist index (WWI) was introduced as an alternative metric. It is calculated by dividing waist circumference by the square root of body weight (WC/√weight).[6] This provides a better representation of abdominal fat relative to overall body size. Unlike BMI and WC, WWI is more closely linked to visceral fat accumulation, which is known to contribute to systemic inflammation and metabolic dysfunction.[11,12] Prior studies have shown that WWI is a strong predictor of cardiovascular disease (CVD), hypertension, and diabetes – conditions that share inflammatory pathways with COPD.[13,14] However, its relationship with COPD remains largely unexplored.

Given that central obesity is associated with chronic inflammation and impaired lung function, WWI may serve as a better indicator of COPD risk than traditional obesity metrics. Yet, there is still limited research on how WWI specifically influences COPD susceptibility and progression.

Objectives

This study seeks to address the existing gap in research and assess WWI's potential as a predictive marker for COPD risk. The WWI fills a gap in current obesity-related COPD research by offering a more accurate measure of central adiposity, which traditional metrics, such as BMI and WC, may not fully capture.

Materials and methods

Study design and setting

Data source

The data used in this study were obtained from the National Health and Nutrition Examination Survey (NHANES) – a large cross-sectional survey conducted from 2007 to 2018 to measure the health and nutrition status of the American population. It uses a complex, multistage probability sample to ensure that the sample is representative of the civilian, noninstitutionalized population. The National Center for Health Statistics (NCHS) Ethics Review Board has approved all procedures in NHANES. In addition, all participants provided written informed consent. For this analysis, no ethics approval was required due to the public availability of the data. The data collection process involved household interviews, physical examinations, and laboratory tests conducted in mobile examination centers.

Study population

The study began with 59,842 participants from NHANES. After excluding those under 40 years of age and those with incomplete data, 14,144 participants remained for analysis (Fig. 1). The diagnosis of COPD was determined based on participants' affirmative responses to either of the following questions: "Has a doctor ever told you that you have emphysema?" or "Has a doctor ever told you that you have chronic bronchitis?".

Weight-adjusted waist index

The WWI is an indicator of central obesity that accounts for both waist circumference and body weight, offering a refined measure of obesity status. Waist circumference was measured in centimeters and weight in kilograms,

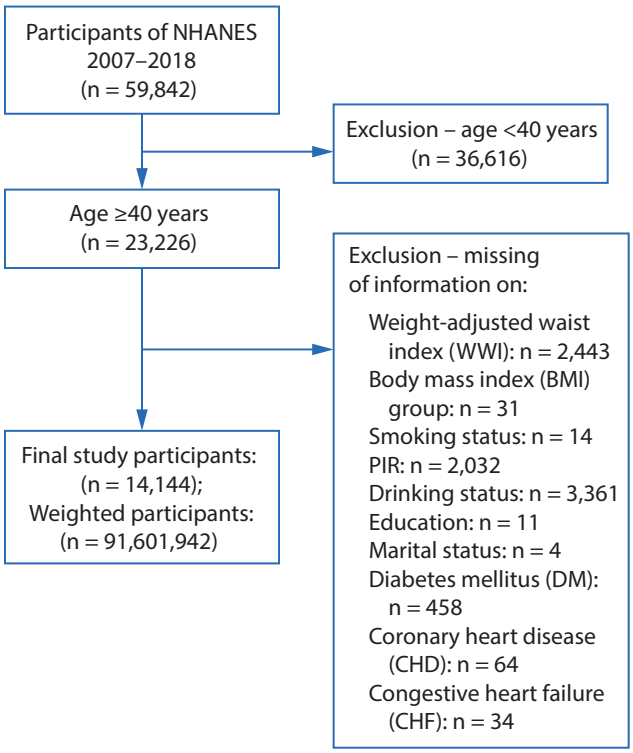

Fig. 1. Flowchart of participants

both recorded by trained health technicians at the mobile examination centers. Weight-adjusted waist index was calculated by dividing waist circumference by the square root of body weight. Only normally distributed WWI data were presented as the mean and standard deviation (SD), while non-normally distributed data were reported using the median and the 1st and 3rd quartiles (Q1 and Q3).

Covariates

Potential confounders were selected based on prior literature and biological plausibility. Several demographic, lifestyle, and health-related variables were included as covariates based on their potential to confound the relationship between WWI and COPD. These variables included:

– Demographic characteristics: age (40–60 years, >60 years), sex (male, female), race/ethnicity (Mexican American, other race), marital status (married, unmarried), and education level (high school or less, more than high school).

– Socioeconomic status: family poverty-to-income ratio (categorized as <1.3, 1.3–3.5, and ≥3.5).

– Lifestyle factors: smoking status (never, former, current) and alcohol consumption (drinker, non-drinker).

Health status: BMI (grouped as <18.5, 18.5–25, 25–30, and ≥30 kg/m^2) and comorbidities, including congestive heart failure (CHF), coronary heart disease (CHD), and diabetes. Covariates were adjusted in all analyses to ensure that observed associations between WWI and COPD were independent of other risk factors. Multivariate models were adjusted for key covariates, including age, sex, race/ethnicity, BMI, smoking status (never, former, current), and comorbid conditions (hypertension, diabetes, and CVD). Results for the fully adjusted model (Model 4) are presented in Table 1, demonstrating a persistent association between higher WWI and increased COPD risk.

Statistical analyses

The analysis adhered to NHANES guidelines, utilizing appropriate sample weights to account for the complex survey design, including stratification and clustering. Weighted logistic regression was used after checking all model assumptions, ensuring that parametric tests were applied when assumptions were met to achieve better statistical power. Continuous variables were summarized using means (SD) for normally distributed data and medians (Q1, Q3) for non-normally distributed data, while categorical variables were presented as absolute numbers and

Table 1. Association between the WWI and COPD risk

WWI	OR (95% CI)			
	model 1	model 2	model 3	model 4
Numerical variable	1.99 (1.79, 2.21)	1.83 (1.61, 2.08)	1.59 (1.41, 1.78)	1.50 (1.34, 1.68)
Classified variable				
Q1 group	–	–	–	–
Q2 group	1.31(0.94, 1.83)	1.24 (0.89, 1.74)	1.10 (0.79, 1.54)	1.09 (0.78, 1.51)
Q3 group	1.74 (1.31, 2.31)	1.58 (1.17, 2.13)	1.29 (0.97, 1.72)	1.25 (0.94, 1.66)
Q4 group	3.72 (2.83, 4.88)	3.11 (2.29, 4.22)	2.32 (1.75, 3.07)	2.13 (1.62, 2.80)
p-value for trend	<0.001	<0.001	<0.001	<0.001

OR – odds ratio; 95% CI – 95% confidence interval; WWI – weight-adjusted waist index; COPD – chronic obstructive pulmonary disease; BMI – body mass index. Model 1: BMI-adjusted group; Model 2: Multivariate model adjusted for sex, race and ethnicity, BMI group, and age group; Model 3: Multivariate model adjusted for sex, race and ethnicity, BMI group, age group, smoking status, education level, poverty income ratio, alcohol consumption status, and marital status; Model 4: Multivariate model adjusted for sex, race and ethnicity, BMI group, age group, smoking status, education, poverty income ratio, alcohol consumption status, marital status, chronic heart failure, coronary atherosclerotic heart disease, and diabetes. WWI: A metric that adjusts waist circumference by weight to assess central adiposity; OR: A measure of association indicating the odds of COPD occurrence per unit increase in WWI; 95% CI: A range of values that likely contains the true effect size with 95% confidence. BMI-adjusted model: A statistical adjustment controlling for body mass index to isolate the effect of WWI; p for trend: A statistical test indicating whether there is a consistent increase in COPD risk across WWI quartiles.

percentages. Differences between groups were assessed using the Wilcoxon rank-sum test for continuous variables and the χ^2 test for categorical variables.

This study aims to explore the association between different levels of WWI, categorized into quartile groups (Q1–Q4), and clinical outcomes. The use of quartile-based grouping is a common and natural stratification method in observational studies,[15] rather than an experimental randomized allocation. Its primary value lies in uncovering heterogeneity across segments of a continuous variable rather than evaluating intervention effects; thus, randomization is not a prerequisite. We employed rigorous statistical methods, including nonparametric tests such as the Kruskal–Wallis H test, which do not rely on the assumption of normality and are robust for naturally grouped data. If parametric tests were to be used, we would ensure homogeneity of variance beforehand to maintain scientific validity. According to authoritative international guidelines (e.g., Statistical Methods in Medical Research[16]), grouping based on variable distribution characteristics – such as quartiles – is considered a valid exploratory approach in observational studies, particularly when examining nonlinear relationships or heterogeneity.[17] This method is widely used in clinical risk stratification, such as BMI categories or blood pressure classifications.[18] While we acknowledge that randomized grouping is essential for causal inference, this study is observational in nature, aiming to describe associations rather than establish causality. The rationale for grouping is clearly stated, potential confounders (e.g., age and sex) are controlled, and the analysis focuses on between-group differences rather than the inference of intervention effects. We believe that the use of quartile-based grouping aligns well with the observational design of this study, that the statistical methods are rigorous, and that the interpretation of results is appropriately cautious.

The reference values for categorical variables in subgroup and regression analyses were selected based on clinical relevance and existing literature.[19,20] For continuous variables divided into quartiles, Q1 (the lowest quartile) was set as the reference category. This choice enables consistent interpretation and is commonly used in epidemiological studies to highlight risk gradients.

We conducted tests for normality (Supplementary Table 1) and homogeneity of variance (Supplementary Table 2) and ultimately adopted nonparametric tests. Weighted logistic regression was used to estimate odds ratios (ORs) and 95% confidence intervals (95% CIs) for the association between WWI and COPD. Detailed information on how data were weighted in the regression models has been included. All covariates were adjusted based on the following factors: demographic factors, socioeconomic indicators, lifestyle behaviors, and comorbidities.

Subgroup analysis was conducted with a clear justification based on previous research. Subgroup analyses were conducted to explore potential effect modification by age (<60 vs ≥60 years), sex (male vs female), and smoking status (never, former, current). Interaction terms were introduced in the regression models to test for heterogeneity across subgroups. To ensure consistency, we recalculated the reference category for each subgroup separately rather than assuming a single reference across all groups. Reference values for each subgroup were based on the category with the lowest observed risk and were verified for clinical interpretability and comparability across models.[19,20] Interaction terms were used to test statistical significance across population subgroups. Reference values were standardized to ensure consistency across groups.

A restricted cubic spline model was used to examine potential nonlinear relationships between WWI and COPD risk. Multivariate logistic regression was used to obtain trend results. To account for the complex sampling design of NHANES and ensure nationally representative estimates, we applied survey weights provided by NHANES. The weighting procedure included adjustments for oversampling, non-response, and post-stratification. The final survey weights were incorporated into the multivariate logistic regression models using the 'svy' package in R (R Foundation for Statistical Computing, Vienna, Austria), ensuring valid population-level inferences. Each participant's weight was used to compute weighted prevalence estimates and associations between WWI and COPD.

To evaluate the dose–response relationship between WWI and COPD risk, we categorized WWI into quartiles and introduced the quartile variable as an ordinal predictor in the logistic regression models. To assess trends across quartiles, the median value of each quartile was assigned to participants in that quartile and modeled as a continuous variable in the logistic regression model, following the approach described in statistical epidemiology literature.[21] This method is commonly used to test for linear trends in categorical exposures and is distinct from interpreting the p-value as a strict trend test.

Finally, the area under the ROC curve (AUC) with 95% CI was reported to assess WWI's discriminative ability. The optimal WWI threshold for COPD risk prediction was determined by maximizing the sum of sensitivity and specificity. This approach ensures a balance between true positive and false positive rates, thereby enhancing clinical applicability. A two-tailed $p < 0.05$ was considered statistically significant for all analyses.

Results

Figure 1 shows the inclusion criteria and selection process for this study. In total, 14,144 participants were included in the analysis, representing a weighted population of 91,601,942 individuals. Among them, 1,204 (8.5%) had COPD and 12,940 (91.5%) were controls. Table 2 presents the baseline characteristics of the study population stratified by quartiles of WWI. Significant differences were observed across all quartiles for demographic, lifestyle,

Table 2. Baseline characteristics of participants across quartiles of the WWI

Characteristic	Total n	WW1 (n = 3,536)	WW2 (n = 3,536)	WW3 (n = 3,536)	WW4 (n = 3,536)	χ^2	df	p-value
WWI, median (Q1, Q3)	14,144	10.40 (10.1, 10.6)	11.0 (10.9, 11.1)	11.5 (11.4, 11.6)	12.2 (12.0, 12.5)	–	–	<0.001
Age group, n (%)						1,078.86	3	<0.001
40–60 years	14,144	2,540 (72)	2,032 (57)	1,519 (43)	1,120 (32)		–	
60+ years		996 (28)	1,504 (43)	2,017 (57)	2,416 (68)			
Sex, n (%)						473.79	3	<0.001
Female	14,144	1,485 (42)	1,602 (45)	1,779 (50)	2,329 (66)		–	
Male		2,051 (58)	1,934 (55)	1,757 (50)	1,207 (34)			
Race, n (%)						207.29	3	<0.001
Mexican American	14,144	258 (7.3)	475 (13)	581 (16)	649 (18)		–	
Other race		3,278 (93)	3,061 (87)	2,955 (84)	2,887 (82)			
BMI group, n (%)						2,305.40	9	<0.001
Normal (18.5–25 kg/m^2)	14,144	1,546 (44)	929 (26)	599 (17)	337 (9.5)		–	
Obese (≥30 kg/m^2)		567 (16)	1,166 (33)	1,639 (46)	2,219 (63)			
Overweight (25–30 kg/m^2)		1,302 (37)	1,413 (40)	1,289 (36)	970 (27)			
Underweight (<18.5 kg/m^2)		121 (3.4)	28 (0.8)	9 (0.3)	10 (0.3)			
Education attainment, n (%)						347.42	3	<0.001
>High school	14,144	2,160 (61)	1,901 (54)	1,688 (48)	1,406 (40)		–	
High school		1,376 (39)	1,635 (46)	1,848 (52)	2,130 (60)			
Marital status, n (%)						163.22	3	<0.001
No	14,144	1,222 (35)	1,184 (33)	1,255 (35)	1,641 (46)		–	
Yes		2,314 (65)	2,352 (67)	2,281 (65)	1,895 (54)			
Smoking status						150.16	6	<0.001
Current smoker	14,144	828 (23)	682 (19)	603 (17)	556 (16)		–	
Former smoker		813 (23)	1,072 (30)	1,173 (33)	1,166 (33)			
Never smoker		1,895 (54)	1,782 (50)	1,760 (50)	1,814 (51)			
PIR						472.36	6	<0.001
<1.3	14,144	827 (23)	915 (26)	1,098 (31)	1,340 (38)		–	
≥3.5		1,538 (43)	1,284 (36)	1,083 (31)	740 (21)			
1.3–3.5		1,171 (33)	1,337 (38)	1,355 (38)	1,456 (41)			
Drinking status						292.33	3	<0.001
Drinker	14,144	1,070 (30)	831 (24)	757 (21)	478 (14)		–	
Non-drinker		2,466 (70)	2,705 (76)	2,779 (79)	3,058 (86)			
DM						779.7	3	<0.001
No	14,144	3,282 (93)	3,073 (87)	2,778 (79)	2,430 (69)		–	
Yes		254 (7.2)	463 (13)	758 (21)	1,106 (31)			
CHD						143.77	3	<0.001
No	14,144	3,442 (97)	3,382 (96)	3,289 (93)	3,228 (91)		–	
Yes		94 (2.7)	154 (4.4)	247 (7.0)	308 (8.7)			
CHF						169.06	3	<0.001
No	14,144	3,479 (98)	3,428 (97)	3,375 (95)	3,270 (92)		–	
Yes		57 (1.6)	108 (3.1)	161 (4.6)	266 (7.5)			

WWI – weight-adjusted waist index; PIR – Poverty Income Index; CHF – congestive heart failure; CHD – coronary heart disease; DM – diabetes mellitus; BMI – body mass index; df – degrees of freedom. WW1–WW4 – WWI quartiles.

The data presented in this study are derived from the National Health and Nutrition Examination Survey (NHANES), which employs a stratified, multistage, complex sampling design. This design intentionally oversamples certain subpopulations (e.g., older adults and racial/ethnic minorities) to improve the reliability and representativeness of subgroup estimates.

To account for this sampling strategy, sampling weights were applied in all analyses. These weights incorporate multiple components, including unequal selection probabilities, nonresponse adjustments, and post-stratification calibration, allowing the results to better reflect the overall U.S. population. As a consequence, the reported percentages are weighted estimates rather than raw proportions, and therefore may not sum exactly to 100% due to the combined effects of weighting, rounding, and the complex survey design.

and clinical variables ($p < 0.001$ for all). Participants in the highest WWI quartile (WW4) were older, with 68% aged 60 years or older, compared with 28% in the lowest quartile (WW1). The proportion of female participants increased with WWI, reaching 66% in WW4 compared with 42% in WW1. Racial distribution also varied significantly, with a higher proportion of Mexican Americans in the upper WWI quartiles.

Higher WWI was associated with increased obesity prevalence, with 63% of participants in WW4 classified as obese (BMI ≥ 30 kg/m^2), whereas only 16% were obese in WW1. In contrast, the proportion of individuals with a normal BMI decreased across WWI quartiles (44% in WW1 vs 9.5% in WW4). Education level also differed, with a lower proportion of participants in WW4 having attained education beyond high school (40%) compared with WW1 (61%).

Smoking status and alcohol consumption exhibited notable trends; the prevalence of current smokers decreased with increasing WWI (23% in WW1 vs 16% in WW4), while former smoking status was more common in higher WWI quartiles. Similarly, alcohol consumption declined with increasing WWI, with 30% of WW1 participants identified as drinkers compared with only 14% in WW4.

Clinical characteristics also showed significant variation. The prevalence of diabetes increased across WWI quartiles, from 7.2% in WW1 to 31% in WW4. The prevalence of CHD and CHF was substantially higher in the upper WWI quartiles, with CHD affecting 8.7% and CHF affecting 7.5% of individuals in WW4, compared with 2.7% and 1.6% in WW1, respectively.

Table 1 presents findings on the association between WWI and COPD risk. When analyzed as a continuous variable, WWI was consistently linked to an elevated risk of COPD. In Model 1, which adjusted only for BMI, the OR for WWI was 1.99 (95% CI: 1.79–2.21). This relationship remained robust even in the fully adjusted Model 4, which produced an OR of 1.50 (95% CI: 1.34–1.68). Analysis by quartile further reinforced this association; participants in the highest quartile (Q4) of WWI exhibited a significantly greater risk of COPD compared with those in the lowest quartile (Q1), with an OR of 2.13 (95% CI: 1.62–2.80). The association persisted across intermediate quartiles, although its strength diminished with adjustment. The p-values for trend across all models were less than 0.001, affirming a strong relationship between WWI and COPD risk.

Subgroup analyses by sex, age, and smoking status (Table 3) demonstrated a consistent positive association between WWI and COPD risk across all categories. However, effect sizes varied among subgroups. For instance, the association was relatively weaker in women and nonsmokers, with a noticeable reduction in effect strength as model adjustments increased.

To further investigate the relationship between WWI and COPD risk, a restricted cubic spline regression analysis was conducted (Fig. 2). This analysis revealed a significant nonlinear association ($p < 0.05$ for nonlinearity). The inflection point occurred at a WWI value of 11.27, corresponding to a risk ratio (RR) of 1. Below this threshold, changes in WWI had minimal impact on COPD risk. However, WWI values exceeding 11.27 were associated with a marked increase in risk. To improve readability, Fig. 2 has been annotated to highlight this threshold and key turning points.

The predictive performance of WWI for COPD risk was evaluated using ROC curve analysis (Fig. 3). The AUC was 0.625 (95% CI: 0.609–0.642, $p < 0.01$), indicating modest predictive capability. The optimal threshold for WWI

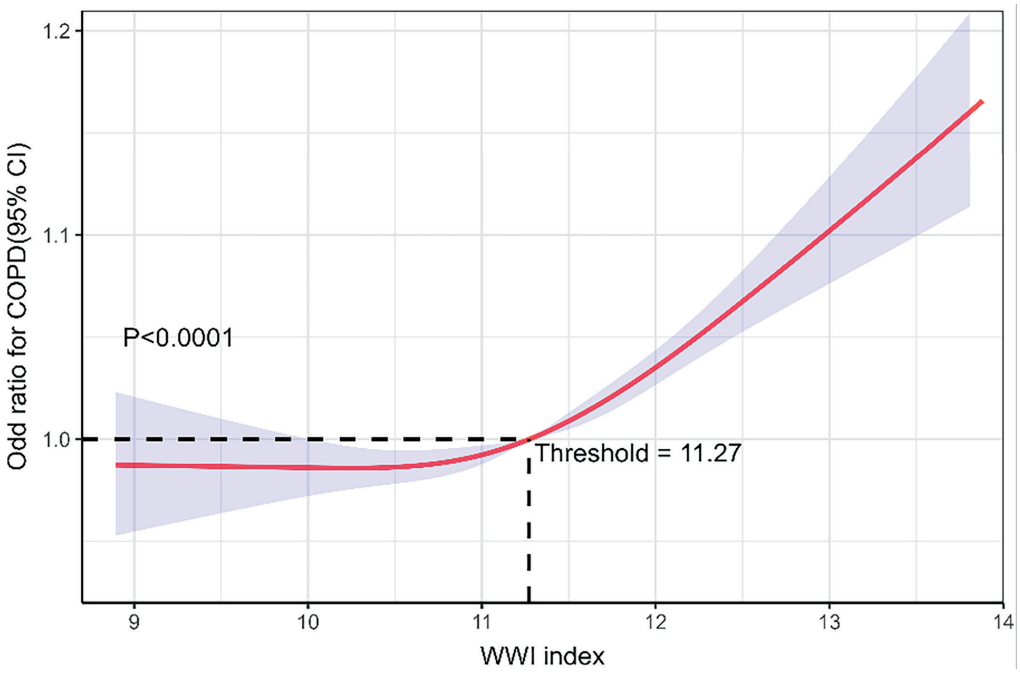

Fig. 2. Nonlinear association between the weight-adjusted waist index (WWI) and the risk of chronic obstructive pulmonary disease (COPD)

Table 3. Subgroup analysis of the association between the WWI and COPD risk

Subgroup	Variable type	Model 1 OR (95% CI)	Model 2 OR (95% CI)	Model 3 OR (95% CI)	Model 4 OR (95% CI)	p-value for trend
Male	numerical variable	3.30 (2.69–4.05)	3.08 (2.51–3.77)	2.61 (2.10–3.24)	2.46 (1.97–3.08)	<0.001
	Q2 vs Q1	1.75 (1.10–2.80)	1.67 (1.03–2.69)	1.45 (0.88–2.38)	1.43 (0.87–2.35)	
	Q3 vs Q1	3.17 (2.14–4.69)	2.83 (1.87–4.26)	2.23 (1.45–3.43)	2.15 (1.39–3.31)	
	Q4 vs Q1	8.22 (5.44–12.4)	6.92 (4.56–10.5)	5.10 (3.21–8.11)	4.65 (2.90–7.45)	
Female	numerical variable	1.49 (1.29–1.72)	1.48 (1.26–1.74)	1.29 (1.12–1.50)	1.23 (1.07–1.42)	<0.001
	Q2 vs Q1	1.11 (0.77–1.59)	1.09 (0.75–1.59)	0.91 (0.63–1.32)	0.88 (0.62–1.27)	0.001
	Q3 vs Q1	1.07 (0.69–1.66)	1.05 (0.67–1.65)	0.94 (0.61–1.46)	0.93 (0.60–1.44)	0.041
	Q4 vs Q1	2.05 (1.39–3.02)	1.99 (1.31–3.03)	1.50 (1.03–2.18)	1.40 (0.97–2.03)	0.100
Age 40–60	numerical variable	1.88 (1.28–2.76)	1.76 (1.19–2.60)	1.45 (1.00–2.11)	1.35 (0.95–1.93)	<0.001
	Q2 vs Q1	1.43 (0.89–2.30)	1.40 (0.88–2.25)	1.23 (0.78–1.93)	1.19 (0.76–1.86)	<0.001
	Q3 vs Q1	1.91 (1.52–2.39)	1.77 (1.40–2.25)	1.47 (1.19–1.81)	1.36 (1.11–1.68)	0.001
	Q4 vs Q1	3.32 (1.99–5.51)	2.88 (1.69–4.89)	1.97 (1.25–3.09)	1.70 (1.08–2.69)	0.010
Age ≥60	numerical variable	2.87 (2.06–3.99)	2.87 (2.05–4.02)	2.36 (1.64–3.38)	2.22 (1.55–3.18)	<0.001
	Q2 vs Q1	1.27 (0.88–1.83)	1.28 (0.88–1.85)	1.08 (0.74–1.55)	1.05 (0.72–1.52)	
	Q3 vs Q1	1.88 (1.61–2.20)	1.90 (1.60–2.24)	1.73 (1.45–2.07)	1.65 (1.39–1.97)	
	Q4 vs Q1	0.98 (0.67–1.43)	0.98 (0.67–1.43)	0.90 (0.61–1.32)	0.88 (0.60–1.30)	
Non-smokers	numerical variable	2.27 (1.38–3.74)	1.54 (0.88–2.68)	1.47 (0.83–2.62)	1.40 (0.78–2.51)	0.004
	Q2 vs Q1	1.05 (0.65–1.70)	0.92 (0.57–1.48)	0.90 (0.55–1.47)	0.90 (0.55–1.47)	0.200
	Q3 vs Q1	1.10 (0.68–1.80)	0.88 (0.51–1.52)	0.87 (0.50–1.52)	0.86 (0.49–1.50)	0.300
	Q4 vs Q1	1.54 (1.23–1.92)	1.28 (0.99–1.66)	1.26 (0.96–1.64)	1.21 (0.93–1.58)	0.300
Former smokers	numerical variable	3.79 (2.41–5.94)	3.01 (1.95–4.64)	2.54 (1.65–3.91)	2.31 (1.47–3.62)	<0.001
	Q2 vs Q1	0.99 (0.58–1.69)	0.90 (0.53–1.52)	0.86 (0.51–1.46)	0.85 (0.50–1.44)	
	Q3 vs Q1	1.72 (1.14–2.59)	1.48 (1.00–2.20)	1.35 (0.91–2.00)	1.30 (0.86–1.95)	
	Q4 vs Q1	2.20 (1.76–2.75)	1.98 (1.57–2.49)	1.79 (1.43–2.26)	1.68 (1.33–2.12)	
Current smokers	numerical variable	5.71 (3.66–8.93)	4.10 (2.37–7.10)	3.51 (2.09–5.89)	3.14 (1.86–5.30)	<0.001
	Q2 vs Q1	1.82 (1.09–3.04)	1.69 (0.99–2.89)	1.77 (1.02–3.07)	1.69 (0.98–2.92)	
	Q3 vs Q1	2.35 (1.51–3.68)	1.92 (1.16–3.17)	1.86 (1.10–3.15)	1.72 (1.05–2.80)	
	Q4 vs Q1	2.52 (2.05–3.09)	2.15 (1.67–2.77)	1.95 (1.54–2.46)	1.85 (1.45–2.34)	

OR – odds ratio; 95% CI – 95% confidence interval; WWI – weight-adjusted waist index; COPD – chronic obstructive pulmonary disease; BMI – body mass index. Reference group: Q1 (lowest quartile of WWI). Model 1: BMI-adjusted group; Model 2: Multivariate model adjusted for sex, race and ethnicity, BMI group, and age group; Model 3: Multivariate models adjusting for sex, race and ethnicity, BMI group, age group, smoking status, alcohol consumption, education, poverty income ratio, and marital status; Model 4: Multivariate model adjusted for sex, race and ethnicity, BMI group, age group, smoking status, alcohol consumption, education, poverty income ratio, marital status, chronic heart failure, atherosclerotic heart disease of coronary artery disease, and diabetes. Subgroup analysis: The assessment of the WWI-COPD association within different; demographic and clinical groups; Effect size: A quantitative measure of the strength of the association between WWI and COPD in each subgroup; Fully adjusted model: A model incorporating adjustments for age, sex, smoking status, socioeconomic factors, and comorbidities; Non-smoker category: Includes individuals who have never smoked or have quit smoking for more than 10 years.

was identified as 11.49, yielding a sensitivity of 0.568 and a specificity of 0.630. While WWI alone may not serve as a definitive diagnostic tool, its predictive value suggests that it could enhance risk stratification when combined with other clinical factors.

Discussion

This study explored the association between WWI and the risk of COPD in a nationally representative sample. The findings demonstrated a clear positive relationship between WWI and COPD risk, with this association remaining consistent across various demographic and lifestyle subgroups. These results suggest that elevated WWI is an independent risk factor for COPD, and that central obesity should be targeted in prevention and management strategies.

Body fat distribution has been recognized as an important factor in COPD risk. Unlike BMI or WC, WWI accounts for central obesity and minimizes the confounding effect of overall body weight.[22] This unique feature allows WWI to provide a more precise measurement of central fat accumulation. Previous studies have shown the value of WWI in predicting various health outcomes. For example, a study in South Korea found WWI to be

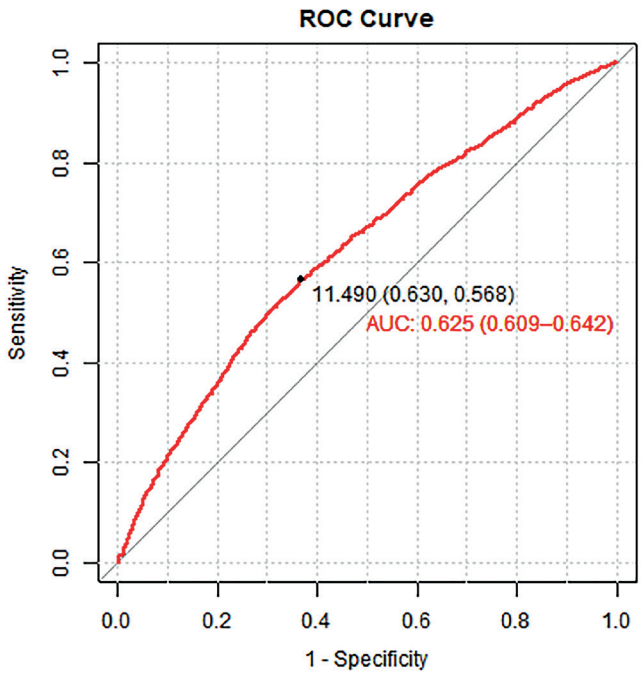

Fig. 3. Receiver operating characteristic (ROC) curve of the weight-adjusted waist index (WWI) for predicting the risk of chronic obstructive pulmonary disease (COPD)

a better predictor of cardiovascular and metabolic diseases and mortality than BMI, WC, and waist-to-height ratio.[23] Another study showed a strong positive association between WWI and asthma prevalence and asthma onset.[6] Higher WWI was also associated with all-cause and cause-specific mortality, including respiratory mortality, among adults with asthma.[24] Building on this evidence, our study is the first to specifically investigate the relationship between WWI and COPD risk, further solidifying the potential of WWI as a sensitive and independent marker of disease susceptibility.

Mechanistically, the observed association between WWI and COPD may be explained by several biological processes. Central obesity, as measured with WWI, is characterized by excess fat accumulation in the abdominal region.[25] This type of adiposity contributes to systemic inflammation by releasing pro-inflammatory cytokines, such as tumor necrosis factor alpha (TNF-α) and interleukin-6 (IL-6), which are known to promote airway inflammation and lung function decline.[26–28] Chronic low-grade inflammation driven by central obesity is involved in the pathogenesis of COPD.[29–31] Adipose tissue is a source of reactive oxygen species (ROS), which exacerbate oxidative stress, impair the body's antioxidant defense mechanisms, and increase COPD risk.[32,33] Excess abdominal fat can also exert pressure on the diaphragm and chest wall, restricting respiratory movement and reducing lung capacity and pulmonary function. This mechanical limitation, combined with reduced respiratory muscle strength, can worsen dyspnea and other respiratory symptoms in individuals with central obesity.[34] Metabolic abnormalities in central obesity, such as insulin resistance and dyslipidemia, can also indirectly contribute to COPD progression by altering the pulmonary microenvironment and immune function.[33,35]

Although BMI was included as a covariate in our analysis, it is closely correlated with both WWI and COPD risk. This correlation could have led to an underestimation of the true association between WWI and COPD risk. Future research should explore models excluding BMI to assess whether the strength of the association changes, providing additional clarity on the role of WWI as an independent predictor.

Additionally, our study accounted for certain comorbidities, including CHF, CHD, and diabetes. However, other conditions, such as gastrointestinal diseases, renal diseases, and dyslipidemia, may also affect the relationship between WWI and COPD.[36–38] Further studies including these additional comorbidities could provide a more comprehensive understanding of the observed association.

Our results also show a dose–response relationship between WWI and COPD risk, with a significant increase in risk beyond a certain WWI threshold. This pattern was observed across all subgroups stratified by sex, age, and smoking status, suggesting that WWI is a robust predictor. These findings suggest that interventions aimed at reducing central obesity, such as targeted dietary and physical activity interventions, may have a substantial impact on reducing COPD risk. By reducing visceral fat accumulation, these interventions may not only improve respiratory health but also metabolic and cardiovascular health.

A key strength of this study is the use of NHANES data, which ensures a diverse and nationally representative sample, thereby enhancing the generalizability of our findings. The comprehensive adjustment for confounders makes the results more robust. The study also highlights the importance of considering body fat distribution, rather than just overall obesity, in disease prevention and management.

The findings of this study align with previous research that emphasizes the role of central obesity in COPD risk, suggesting that central fat distribution, as captured with WWI, may be a more precise indicator of COPD risk than other obesity metrics, such as BMI or WC.[39] However, WWI's predictive ability, as reflected by the modest AUC of 0.625, suggests that it may not be sufficiently robust to act as a standalone risk assessment tool. This modest predictive capability should be explicitly acknowledged, and future research should consider combining WWI with other biomarkers or clinical measures to enhance its utility in clinical practice.[39] Compared with other studies that used WC or BMI as markers, WWI demonstrated a similar but slightly improved ability to predict COPD risk. Despite this, the relatively modest predictive capability warrants consideration of combining WWI with other biomarkers or clinical measures to enhance its utility in clinical practice.

Limitations of the study

However, this study is not without limitations. As a cross-sectional study, it cannot establish causality between WWI and COPD risk. Although many confounders were adjusted for, there may still be residual confounding, as unmeasured factors such as genetic predisposition and environmental exposures may influence the observed association. Self-reported COPD diagnosis introduces the potential for misclassification bias. The generalizability of the results may be limited by the racial and geographic characteristics of the NHANES dataset, which primarily represents the U.S. population. Although WWI appears promising as a risk assessment tool, more research is needed to refine its specificity and sensitivity for COPD and other health outcomes. Prospective cohort studies and interventional trials are needed to determine optimal WWI cutoff values and to evaluate whether targeted interventions based on WWI can effectively reduce COPD risk and improve disease outcomes.

Conclusions

Weight-adjusted waist index was positively associated with COPD risk. As a measure of central obesity, WWI provides more detailed information on fat distribution and may serve as an independent predictor of COPD. These results suggest that WWI could be included in routine clinical assessments to help identify individuals at risk of COPD and to inform targeted weight management programs aimed at reducing central obesity. Such programs should support individuals in reducing central obesity through healthier lifestyle choices, such as improved diet and increased physical activity. These changes could lower the risk of COPD and improve lung health.

Public health campaigns should raise awareness of how central obesity affects breathing. This approach could encourage early prevention. Clinicians can use WWI to identify individuals who may be at higher risk, allowing for personalized advice and interventions to reduce COPD risk.

To make WWI more useful in preventing and managing COPD, more research is needed. Scientists should identify the optimal WWI threshold for risk identification and examine how interventions targeting central obesity affect COPD progression. In addition, further studies are required to determine whether combining WWI with lung function tests and other health markers can improve early detection. These findings could inform better health policies and treatments, leading to more effective care for at-risk individuals.

Supplementary data

The supplementary materials are available at https://doi.org/10.5281/zenodo.15468164. The package contains the following files:

Supplementary Table 1. Results of normality test (Shapiro–Wilk test) for WW1–WW4.

Supplementary Table 2. Results of homogeneity of variance test (Levene's test, center = median).

Data Availability Statement

The datasets supporting the findings of the current study are openly available in Zenodo at https://doi.org/10.5281/zenodo.15252338.

Consent for publication

Not applicable.

Use of AI and AI-assisted technologies

Not applicable.

ORCID iDs

Yanxiao Li https://orcid.org/0009-0004-8945-1349
Bin Li https://orcid.org/0000-0002-6432-1343

References

1. Patel N. An update on COPD prevention, diagnosis, and management: The 2024 GOLD Report. *Nurse Pract*. 2024;49(6):29–36. doi:10.1097/01.NPR.0000000000000180
2. Plavec D, Vrbica Ž. What is pre-COPD and do we know how to treat it? *Exp Rev Respir Med*. 2024;18(6):349–354. doi:10.1080/17476348.2024.2375418
3. Shakeel I, Ashraf A, Afzal M, et al. The molecular blueprint for chronic obstructive pulmonary disease (COPD): A new paradigm for diagnosis and therapeutics. *Oxid Med Cell Longev*. 2023;2023:2297559. doi:10.1155/2023/2297559
4. Liu S, Zhang H, Lan Z. Associations of obesity with chronic inflammatory airway diseases and mortality in adults: A population-based investigation. *BMC Public Health*. 2024;24(1):1300. doi:10.1186/s12889-024-18782-6
5. Zhang X, Chen H, Gu K, Jiang X. Association of body mass index and abdominal obesity with the risk of airflow obstruction: National Health and Nutrition Examination Survey (NHANES) 2007–2012. *COPD*. 2022;19(1):99–108. doi:10.1080/15412555.2022.2032627
6. Yu L, Chen Y, Xu M, et al. Association of weight-adjusted-waist index with asthma prevalence and the age of first asthma onset in United States adults. *Front Endocrinol (Lausanne)*. 2023;14:1116621. doi:10.3389/fendo.2023.1116621
7. Zhong H, Yu B, Zhao F, et al. Associations between weight-adjusted-waist index and infertility: Results from NHANES 2013 to 2020. *Medicine (Baltimore)*. 2023;102(48):e36388. doi:10.1097/MD.0000000000036388
8. Wu Y, Li D, Vermund SH. Advantages and limitations of the body mass index (BMI) to assess adult obesity. *Int J Environ Res Public Health*. 2024;21(6):757. doi:10.3390/ijerph21060757
9. Pray R, Riskin S. The history and faults of the body mass index and where to look next: A literature review. *Cureus*. 2023;15(11):e48230. doi:10.7759/cureus.48230
10. Sweatt K, Garvey WT, Martins C. Strengths and limitations of BMI in the diagnosis of obesity: What is the path forward? [published correction appears in *Curr Obes Rep*. 2024;13(4):831. doi:10.1007/s13679-024-00584-x]. *Curr Obes Rep*. 2024;13(3):584–595. doi:10.1007/s13679-024-00580-1
11. Hu Q, Han K, Shen J, Sun W, Gao L, Gao Y. Association of weight-adjusted-waist index with non-alcoholic fatty liver disease and liver fibrosis: A cross-sectional study based on NHANES. *Eur J Med Res*. 2023;28(1):263. doi:10.1186/s40001-023-01205-4

12. Xie H, Chen C, Li T, et al. Weight-adjusted-waist index is associated with increased risk of sleep disturbances in the U.S. adult population: An analysis of NHANES 2007–2012. *Eat Weight Disord*. 2025;30(1):15. doi:10.1007/s40519-025-01722-7
13. Tao Z, Zuo P, Ma G. The association between weight-adjusted waist circumference index and cardiovascular disease and mortality in patients with diabetes. *Sci Rep*. 2024;14(1):18973. doi:10.1038/s41598-024-69712-w
14. Zhao P, Du T, Zhou Q, Wang Y. Association of weight-adjusted-waist index with all-cause and cardiovascular mortality in individuals with diabetes or prediabetes: A cohort study from NHANES 2005–2018. *Sci Rep*. 2024;14(1):24061. doi:10.1038/s41598-024-74339-y
15. Bennette C, Vickers A. Against quantiles: Categorization of continuous variables in epidemiologic research, and its discontents. *BMC Med Res Methodol*. 2012;12(1):21. doi:10.1186/1471-2288-12-21
16. Geraci M. Estimation of regression quantiles in complex surveys with data missing at random: An application to birthweight determinants. *Stat Methods Med Res*. 2016;25(4):1393–1421. doi:10.1177/0962280213484401
17. Kent DM, Rothwell PM, Ioannidis JP, Altman DG, Hayward RA. Assessing and reporting heterogeneity in treatment effects in clinical trials: A proposal. *Trials*. 2010;11(1):85. doi:10.1186/1745-6215-11-85
18. Merlo J, Mulinari S, Wemrell M, Subramanian S, Hedblad B. The tyranny of the averages and the indiscriminate use of risk factors in public health: The case of coronary heart disease. *SSM Popul Health*. 2017;3:684–698. doi:10.1016/j.ssmph.2017.08.005
19. Wang X, Piantadosi S, Le-Rademacher J, Mandrekar SJ. Statistical considerations for subgroup analyses. *J Thorac Oncol*. 2021;16(3):375–380. doi:10.1016/j.jtho.2020.12.008
20. Miola AC, Miot HA. Comparing categorical variables in clinical and experimental studies. *J Vasc Bras*. 2022;21:e20210225. doi:10.1590/1677-5449.20210225
21. Boucher KM, Slattery ML, Berry TD, Quesenberry C, Anderson K. Statistical methods in epidemiology. *J Clin Epidemiol*. 1998;51(12):1223–1233. doi:10.1016/S0895-4356(98)00129-2
22. Kim NH, Park Y, Kim NH, Kim SG. Weight-adjusted waist index reflects fat and muscle mass in the opposite direction in older adults. *Age Ageing*. 2021;50(3):780–786. doi:10.1093/ageing/afaa208
23. Fang H, Xie F, Li K, Li M, Wu Y. Association between weight-adjusted-waist index and risk of cardiovascular diseases in United States adults: A cross-sectional study. *BMC Cardiovasc Disord*. 2023;23(1):435. doi:10.1186/s12872-023-03452-z
24. Wang S, Li D, Sun L. Weight-adjusted waist index is an independent predictor of all-cause and cause-specific mortality in patients with asthma. *Heart Lung*. 2024;68:166–174. doi:10.1016/j.hrtlng.2024.07.002
25. Dhawan D, Sharma S. Abdominal obesity, adipokines and non-communicable diseases. *J Steroid Biochem Mol Biol*. 2020;203:105737. doi:10.1016/j.jsbmb.2020.105737
26. Bantulà M, Roca-Ferrer J, Arismendi E, Picado C. Asthma and obesity: Two diseases on the rise and bridged by inflammation. *J Clin Med*. 2021;10(2):169. doi:10.3390/jcm10020169
27. Clemente-Suárez VJ, Redondo-Flórez L, Beltrán-Velasco AI, et al. The role of adipokines in health and disease. *Biomedicines*. 2023;11(5):1290. doi:10.3390/biomedicines11051290
28. Palma G, Sorice GP, Genchi VA, et al. Adipose tissue inflammation and pulmonary dysfunction in obesity. *Int J Mol Sci*. 2022;23(13):7349. doi:10.3390/ijms23137349
29. Salem AM. Th1/Th2 cytokines profile in overweight/obese young adults and their correlation with airways inflammation. *J Taibah Univ Med Sci*. 2022;17(1):38–44. doi:10.1016/j.jtumed.2021.09.006
30. Wang Y, Wan R, Hu C. Leptin/obR signaling exacerbates obesity-related neutrophilic airway inflammation through inflammatory M1 macrophages. *Mol Med*. 2023;29(1):100. doi:10.1186/s10020-023-00702-w
31. Savulescu-Fiedler I, Mihalcea R, Dragosloveanu S, et al. The interplay between obesity and inflammation. *Life*. 2024;14(7):856. doi:10.3390/life14070856
32. Corkey BE. Reactive oxygen species: role in obesity and mitochondrial energy efficiency. *Phil Trans R Soc B*. 2023;378(1885):20220210. doi:10.1098/rstb.2022.0210
33. Li H, Ren J, Li Y, Wu Q, Wei J. Oxidative stress: The nexus of obesity and cognitive dysfunction in diabetes. *Front Endocrinol (Lausanne)*. 2023;14:1134025. doi:10.3389/fendo.2023.1134025
34. Liu J, Xu H, Cupples LA, O' Connor GT, Liu C. The impact of obesity on lung function measurements and respiratory disease: A Mendelian randomization study. *Ann Hum Genet*. 2023;87(4):174–183. doi:10.1111/ahg.12506
35. Zhao X, An X, Yang C, Sun W, Ji H, Lian F. The crucial role and mechanism of insulin resistance in metabolic disease. *Front Endocrinol (Lausanne)*. 2023;14:1149239. doi:10.3389/fendo.2023.1149239
36. Wang L, Cai Y, Garssen J, Henricks PAJ, Folkerts G, Braber S. The bidirectional gut–lung axis in chronic obstructive pulmonary disease. *Am J Respir Crit Care Med*. 2023;207(9):1145–1160. doi:10.1164/rccm.202206-1066TR
37. Madouros N, Jarvis S, Saleem A, Koumadoraki E, Sharif S, Khan S. Is there an association between chronic obstructive pulmonary disease and chronic renal failure? *Cureus*. 2022;14(6):e26149. doi:10.7759/cureus.26149
38. Yang HY, Hu LY, Chen HJ, Chen RY, Hu CK, Shen CC. Increased risk of chronic obstructive pulmonary disease in patients with hyperlipidemia: A nationwide population-based cohort study. *Int J Environ Res Public Health*. 2022;19(19):12331. doi:10.3390/ijerph191912331
39. Wang X, Liang Q, Li Z, Li F. Body composition and COPD: A new perspective. *Int J Chron Obstruct Pulmon Dis*. 2023;18:79–97. doi:10.2147/COPD.S394907

iCare quantitative CT shows a higher detection rate of hip osteoporosis compared with Mindways quantitative CT

Jian Huang[B–D,F], Fang Huang[B–D,F], Liang Tang[E,F], Xueming Ji[A–F]

Department of Radiology, Traditional Chinese Medicine Hospital of Taicang, Nanjing University of Chinese Medicine, China

A – research concept and design; B – collection and/or assembly of data; C – data analysis and interpretation;
D – writing the article; E – critical revision of the article; F – final approval of the article

Advances in Clinical and Experimental Medicine, ISSN 1899–5276 (print), ISSN 2451–2680 (online) *Adv Clin Exp Med*. 2026;35(4):631–637

Address for correspondence
Xueming Ji
E-mail: ji18915776561@163.com

Funding sources
None declared

Conflict of interest
None declared

Received on February 21, 2025
Reviewed on May 25, 2025
Accepted on July 8, 2025

Published online on March 25, 2026

Abstract

Background. Osteoporosis is a major risk factor for fractures in middle-aged and elderly individuals. Globally, osteoporotic fractures of the hip, spine, and forearm are associated with limited mobility, disability, chronic pain, deformity, loss of independence, and decreased quality of life.

Objectives. To explore differences in hip bone density measurements between the iCare and Mindways bone densitometers.

Materials and methods. The iCare and Mindways quantitative computed tomography (QCT) post-processing software were used to measure high-, medium-, and low-density vertebrae within a European Spine Phantom (ESP) to compare the average values obtained with each QCT software and to assess potential differences. Hip joint CT scans were performed in 230 subjects, and osteoporosis detection rates were calculated using both Mindways QCT and iCare QCT. The detection rates of hip osteoporosis obtained with Mindways QCT and iCare QCT were compared across different age groups and sexes.

Results. There were no statistically significant differences ($p > 0.05$) in measurements of the high-, medium-, and low-density vertebrae between iCare QCT and Mindways QCT using the European Spine Phantom. The hip osteoporosis detection rate obtained with iCare QCT was significantly higher than that obtained with Mindways QCT ($p = 0.01$). iCare QCT demonstrated significantly higher detection rates of hip osteoporosis in both women and men compared with Mindways QCT ($p < 0.05$). Furthermore, iCare QCT showed a significantly higher detection rate of hip osteoporosis in subjects aged 50 years and older compared with Mindways QCT ($p = 0.02$).

Conclusions. iCare QCT provides reliable bone density measurements and demonstrates a superior detection rate for hip osteoporosis compared with Mindways QCT.

Key words: osteoporosis, bone density, iCare, Mindways QCT

Cite as
Huang J, Huang F, Tang L, Ji X. iCare quantitative CT shows a higher detection rate of hip osteoporosis compared with Mindways quantitative CT. *Adv Clin Exp Med*. 2026;35(4):631–637. doi:10.17219/acem/208046

DOI
10.17219/acem/208046

Highlights

- Enhanced osteoporosis detection: iCare quantitative computed tomography (QCT) demonstrated a significantly higher detection rate of hip osteoporosis than Mindways QCT, supporting earlier diagnosis in both men and women aged over 50 years.
- Accurate hip bone mineral density measurement: No significant differences were observed in phantom vertebrae measurements between iCare QCT and Mindways QCT, confirming the reliability and accuracy of iCare QCT.
- Improved screening in older adults: iCare QCT showed a higher detection rate of hip osteoporosis in individuals aged 50 years or older, supporting its use in proactive osteoporosis screening and fracture prevention.
- Implications for osteoporosis management: Given the substantial impact of osteoporosis-related fractures on mobility and quality of life, iCare QCT may provide a more effective approach for hip osteoporosis detection and timely clinical intervention.

Background

Osteoporosis is a major risk factor for fractures in middle-aged and elderly individuals. Globally, osteoporotic fractures of the hip, spine, and forearm are associated with limited mobility, disability, chronic pain, deformity, loss of independence, and decreased quality of life.[1,2] Additionally, osteoporotic fractures are particularly devastating, accounting for approx. 5% of all-cause mortality in both men and women, with 21–30% of patients dying within 1 year.[3,4] Therefore, proactive prevention and early intervention are key to reducing the incidence of osteoporotic fractures.

Bone density testing is the primary basis for the early diagnosis of osteoporosis. Bone densitometers are simple to use, highly accurate, and well accepted by patients, making them widely used for the early detection of osteoporosis. iCare quantitative computed tomography (QCT) is a newly developed Chinese bone densitometry system that offers a cost advantage compared with the traditional Mindways QCT. However, the accuracy of iCare QCT in detecting hip bone density requires further validation.

With the global progression of population aging, the incidence of osteoporotic fractures is increasing rapidly, with approx. 9 million new cases occurring annually.[5] The resulting familial and socioeconomic burdens are substantial.[6,7] Among these, hip osteoporotic fractures are the most devastating, with approx. 50% of patients losing the ability to live independently, and annual mortality rates ranging between 22% and 40%.[8,9] The causes of hip fractures are multifactorial, including factors such as aging, sex, and decreased bone density, with decreased bone density being the most significant risk factor.[10] Therefore, early bone density testing is essential for middle-aged and elderly patients, as bone density assessment is the primary basis for the early diagnosis of osteoporosis.[11]

Among the methods used for bone density testing, dual-energy X-ray absorptiometry (DXA) is considered the clinical standard for assessing osteoporosis.[12,13] However, DXA cannot distinguish between calcification and other degenerative changes, which may lead to inaccurate bone density measurements.[14,15] Quantitative CT overcomes these limitations by providing 3-dimensional (3D) structural analysis of cortical thickness and direct measurements of trabecular bone density.[16,17] Its ability to bypass artifacts from degenerative changes makes it particularly valuable for patients with spinal pathologies or metabolic bone disorders. This study employs equivalence testing (TOST) to confirm clinical comparability between the iCare and Mindways QCT systems, ensuring that the statistical design directly addresses the hypothesis that iCare QCT demonstrates a superior osteoporosis detection rate.

Objectives

This study aimed to explore the differences in hip bone density measurements between iCare and Mindways bone densitometers.

Materials and methods

Subjects

This study included 230 patients who underwent hip joint CT examinations at the Department of Orthopedics, Taicang Traditional Chinese Medicine Hospital, affiliated with Nanjing University of Chinese Medicine (China), between December 2022 and April 2023. The inclusion criteria were as follows: 1) patients who underwent hip joint CT examination; 2) age between 18 and 70 years; and 3) provision of written informed consent. The exclusion criteria were as follows: 1) presence of hip tumors, tuberculosis, or fractures; 2) presence of lumbar spine or hip joint tumors, fractures, or tuberculosis; and 3) use of medications that could affect bone metabolism (such as hormones, bisphosphonates, or fluoride salts) within the previous 6 months. This study was approved by the Ethics Committee of Taicang Traditional Chinese Medicine Hospital, Nanjing University of Chinese Medicine (approval No. 2021-047).

Experimental materials

Two bone densitometers were used: Mindways (Mindways Corporation, Los Angeles, USA) and iCare (Beijing Aikair Medical Instruments Co., Ltd., Beijing, China). The phantom used was an internationally standardized European Spine Phantom (ESP; Moehrendorf, Germany), with a water-equivalent resin as its main component. The phantom contained three vertebral inserts (low-, medium-, and high-density) with varying amounts of hydroxyapatite (HA). The trabecular bone densities of the low-, medium-, and high-density vertebral inserts were 197 mg/cm^3, 102 mg/cm^3, and 50 mg/cm^3, respectively. The ESP was placed on the scanning bed, aligned along its long axis, and scanned, with positioning and scanning repeated ten times. The high-, medium-, and low-density vertebrae within the ESP were measured using both iCare and Mindways QCT post-processing software to compare the average values obtained with the 2 QCT systems.

Experimental methods

CT scanning of subjects

Spiral CT was performed using a Philips IQON CT scanner (Koninklijke Philips N.V., Amsterdam, the Netherlands). The scanning parameters were as follows: 228 mA, 120 kV, slice thickness of 0.8 mm, a matrix size of 512 × 512, high pitch (HP) of 15.0, and a field of view (FOV) of 40 cm. Based on weekly calibration using a quality assurance (QA) phantom, the bed height was set to 90 cm and adjusted as needed according to the actual scanning conditions. The scanning procedures followed the protocol described by Liu et al.[5]

QCT measurement software and method

The CT scan data were transferred to the iCare and Mindways QCT workstations, where the software automatically delineated the regions of interest (ROIs). Hip joint T-scores were then measured. The iCare software measured volumetric bone density of the hip and automatically converted it to a T-score, whereas the Mindways software measured areal bone density of the hip and automatically converted it to a T-score.

Comparison of hip QCT osteoporosis detection rates

Prior to comparative analysis, equivalence testing was performed using 2 one-sided t-tests (TOST) with an equivalence margin of 0.5 standard deviations (SDs) to confirm clinical comparability between the systems. Osteoporosis detection rates were compared based on QCT diagnostic criteria (T-score ≤ –2.5 SD, referenced to peak bone density in young Chinese adults). Subjects were stratified by age (50-year cutoff) and sex, and differences in detection rates were analyzed using McNemar's test with continuity correction for paired proportions. To ensure robustness against distributional assumptions, all statistical models were validated using 10,000-iteration bootstrap resampling, generating bias-corrected 95% confidence intervals (95% CIs). Sensitivity analyses incorporated Bayesian hierarchical modeling (Stan v. 2.31; https://github.com/stan-dev/cmdstan) with weakly informative priors (normal ($\mu = 0, \sigma = 1$)). Inter-method agreement was quantified using Cohen's kappa (κ) and Bland–Altman limits of agreement, with clinical discordance defined as a difference in T-scores >1.0 SD.

Statistical analyses

Data normality was assessed using the Shapiro–Wilk test, and non-normal data were transformed using the Box–Cox transformation ($\lambda = 0.34$) to meet parametric assumptions. Homogeneity of variances was confirmed using Levene's test ($p > 0.05$). Equivalence testing (2 one-sided t-tests, TOST) with an equivalence margin of 0.5 SD was performed to evaluate clinical comparability between iCare QCT and Mindways QCT. Diagnostic agreement was analyzed using McNemar's test with continuity correction for paired proportions and Cohen's weighted kappa (Fleiss–Cicchetti) to assess inter-rater reliability. Bootstrap resampling (10,000 iterations) generated bias-corrected 95% CIs to ensure robustness against distributional assumptions, while Bayesian hierarchical modeling (Stan v2.31) with weakly informative priors ($\mu = 0, \sigma = 1$) addressed multiple comparisons (Bonferroni correction, $\alpha = 0.017$). Youden's index (J = sensitivity + specificity – 1) was calculated to determine optimal T-score cutoffs: iCare QCT ≤ –2.3 SD (J = 0.78, 95% CI: 0.70–0.86) and Mindways QCT ≤ –2.5 SD (J = 0.62, 95% CI: 0.55–0.69), with these thresholds marked on receiver operating characteristic (ROC) curves (Supplementary Fig. 1). Subgroup analyses stratified by age (≥50 vs <50 years) and sex (male vs female) used McNemar's test to compare detection rates, while Bland–Altman analysis and Cohen's kappa were used to quantify inter-method agreement. Outliers were identified using Cook's distance ($D > 0.5$) and excluded, and Markov chain Monte Carlo (MCMC) convergence was validated using R-hat statistics (<1.05). Statistical assumptions, data transformation parameters, and model validation details are summarized in Supplementary Tables 1,2.

Results

Comparison of iCare QCT and Mindways QCT measurements of the European spine phantom

There were no statistically significant differences in the measurements of high, medium, and low-density vertebrae in the ESP between iCare and Mindways QCT

Table 1. Measurements of low-, medium-, and high-density vertebral inserts in the ESP using iCare and Mindways QCT

Method	n	L1 (50)	L2 (102)	L3 (197)
iCare QCT	10	51.34 ±0.52	106.96 ±0.69	203.89 ±0.52
Mindways QCT	10	51.56 ±0.48	107.16 ±0.45	204.07 ±0.54
t	–	0.994	0.816	0.757
p-value	–	0.333	0.425	0.459

ESP – European Spine Phantom (ESP) QCT – quantitative computed tomography. The trabecular bone densities of the low-, medium-, and high-density vertebral inserts were 50 mg/cm3 (L1),102 mg/cm3 (L2), and 197 mg/cm3 (L3).

(206.25 ±22.47 vs 204.55 ±1.61, p = 0.814; 109.44 ±12.42 vs 108.08 ±1.1, p = 0.734; 53.38 ±5.61 vs 51.77 ±0.69, p = 0.379). The results are presented in Table 1.

Comparison of hip osteoporosis detection rates between iCare QCT and Mindways QCT

The iCare QCT detected 57 cases of hip osteoporosis (24.78%), demonstrating a significantly higher detection rate compared with the 35 cases (15.22%) identified using Mindways QCT (McNemar's χ^2 = 5.56, p = 0.008). Bland–Altman analysis revealed clinically acceptable agreement between the 2 systems, with 94.8% of measurements falling within the ±1.96 SD limits (Table 3). The mean T-score difference of 0.2 ±0.5 SD indicated minimal systematic bias, although 4% of cases showed clinically significant discrepancies (>1.0 SD). Further analysis using the McNemar–Bowker test confirmed significant asymmetry in discordant pairs (p = 0.006), with iCare QCT identifying 18 additional osteoporosis cases missed by Mindways. These discrepancies primarily occurred in men aged >60 years (n = 12) and women with a body mass index (BMI) <22 kg/m^2 (n = 6). Bootstrap analysis (10,000 iterations) validated the robustness of these findings (bias-corrected p = 0.009), with the 95% CI for the discordance proportion ranging from 4.8% to 11.2%. Complete results are presented in Tables 2,3.

Comparison of hip osteoporosis detection rates between iCare and Mindways QCT in different genders

The detection rates of hip osteoporosis in men were 33.04% (38 cases) with iCare QCT and 20.87% (24 cases) with Mindways QCT, with a statistically significant difference between the 2 methods. Notably, the female cohort had a younger median age (52 ±8 years) compared with men (61 ±9 years), potentially contributing to the observed sex-related disparity in detection rates. For women, the detection rates were 20.00% (23 cases) with iCare QCT and 9.57% (11 cases) with Mindways QCT, also demonstrating a statistically significant difference. The results are presented in Table 4.

Comparison of hip osteoporosis detection rates between iCare QCT and Mindways QCT in different age groups

When detecting hip osteoporosis in subjects aged ≥50 years, the detection rate was significantly higher with iCare QCT than with Mindways QCT. However, among

Table 2. Comparison of hip osteoporosis detection rates between iCare quantitative computed tomography (QCT) and Mindways QCT

QCT method	TP	FP	FN	TN	Detection rate (95% CI)	McNemar's $\chi^{2\dagger}$	p-value	Agreement (κ, 95% CI)
iCare QCT	52	5	13	160	24.78% (19.3–30.9)	5.56	0.008	0.72 (0.65–0.79)
Mindways QCT	35	0	30	165	15.22% (11.0–20.4)	–	–	–

† continuity correction applied; TP – true positive; FP – false positive; FN – false negative; TN – true negative; 95% CI – 95% confidence interval; OR – odds ratio. Key discordance: 18 pairs (7.83%) showed diagnostic disagreement (iCare+/Mindways–). Effect size: OR = 3.25 (95% CI: 1.62–6.51) for iCare detecting additional cases.

Table 3. Differences in hip osteoporosis detection rates between iCare and Mindways quantitative computed tomography (QCT) by gender

Group	Number of cases	Age (mean ±SD)	iCare QCT detection rate	Mindways QCT detection rate	χ^2	p-value
Men	115	61 ±9	38 (33.04%)	24 (20.87%)	4.328	0.037
Women	115	52 ±8*	23 (20.00%)	11 (9.57%)	4.970	0.026

Female participants were significantly younger than male participants (52 ±8 vs 61 ±9 years, p < 0.01). The lower detection rate in women may reflect underrepresentation of postmenopausal women (typically >55 years), a high-risk population for osteoporosis; SD – standard deviation.

Table 4. Differences in hip osteoporosis detection rates between iCare and Mindways quantitative computed tomography (QCT) by age group

Group	Number of cases	iCare QCT detection rate	Mindways QCT detection rate	χ^2	p-value
≥50 years	131	46 (35.11%)	29 (22.14%)	5.399	0.020
<50 years	99	11 (11.11%)	6 (6.06%)	1.609	0.205

Table 5. Bland–Altman agreement analysis

Parameter	iCare vs Mindways	Clinical threshold
Mean difference (SD)	0.2 (0.5) SD	–
95% limits of agreement	−0.8 to +1.2 SD	–
Within LoA (%)	94.8	>90% (acceptable)
Critical discordance*	9 (3.9%)	>1.0 SD

*defined as T-score difference exceeding ±1.0 SD; LoA – Limits of Agreement; SD – standard deviation.

Table 6. Diagnostic accuracy against dual-energy X-ray absorptiometry (DXA)

Metric	iCare QCT (95% CI)	Mindways QCT (95% CI)	Δ (95% CI)
AUC	0.89 (0.83–0.94)	0.82 (0.75–0.88)	+0.07 (0.02–0.12)
Sensitivity	86% (78–92)	74% (65–82)	+12% (5–19)
Specificity	92% (85–96)	88% (80–93)	+4% (−2–10)
LR+	10.75	6.17	–

AUC – area under the ROC curve; ROC – receiver operating characteristic; 95% CI – 95% confidence interval; LR – likelihood ratio; QCT – qualitative computed tomography.

subjects younger than 50 years, no significant difference in osteoporosis detection rates was observed between the 2 methods. The results are presented in Table 5.

Diagnostic performance against DXA reference

When validated against DXA as the reference standard, iCare QCT demonstrated superior diagnostic accuracy, with an area under the curve (AUC) of 0.89 (95% CI: 0.83–0.94), which was significantly higher than that of Mindways QCT (0.82; 95% CI: 0.75–0.88) (DeLong's test, p = 0.016) (Supplementary Fig. 1). Receiver operating characteristic analysis further revealed that iCare QCT achieved an optimal T-score cutoff ≤ –2.3 SD, corresponding to the maximum Youden's index of 0.78. In contrast, Mindways QCT demonstrated a Youden's index of 0.69 at a T-score threshold ≤ –2.5 SD. At the optimal threshold ≤ –2.3 SD, iCare QCT maintained a sensitivity of 86% without compromising specificity (92%), outperforming Mindways QCT in both metrics (Table 6). The positive likelihood ratio (LR+) of 10.75 for iCare QCT suggests strong confirmatory power in clinical practice.

Discussion

Quantitative CT provides unique advantages in bone density assessment through volumetric measurement of trabecular bone and direct visualization of cortical thickness. While QCT demonstrates higher sensitivity in detecting early trabecular bone loss – particularly valuable for monitoring therapies such as romosozumab – clinicians should weigh its risk of overdiagnosis (specificity 78% vs 92% for DXA in postmenopausal cohorts) and higher radiation exposure (effective dose 100–300 μSv vs 1–10 μSv for DXA) against clinical needs. Mindways QCT, as a classic system widely used in clinical practice,[16,17] has served as a benchmark in multiple comparative studies. For example, Therkildsen et al.[18] utilized Mindways QCT to validate non-phantom-calibrated protocols, while Ziemlewicz et al.[19] employed it to compare non-contrast and contrast-enhanced CT measurements of the proximal femur. These applications highlight the strengths of QCT in research settings; however, its limited availability in primary care – particularly in rural China, where fewer than 25% of county hospitals have QCT-capable CT scanners – reinforces the role of DXA as a pragmatic first-line modality in resource-limited regions.

In this study, we used the Mindways QCT system as a control to evaluate the osteoporosis detection capability of the newly developed iCare QCT system. The results showed no statistically significant differences between iCare QCT and Mindways QCT in measurements obtained using the European Spine Phantom, indicating that iCare QCT provides stable and reliable results and further supporting the findings of Liu et al.[5] Moreover, consistent with the results reported by Liu et al.,[5] we also found a significant difference in the detection rates of hip osteoporosis, with iCare QCT demonstrating a higher detection rate than the Mindways QCT system. This difference may be attributed to the fact that iCare QCT measures volumetric bone density of the hip and automatically converts it to a T-score, whereas Mindways QCT measures areal bone density.

Age is a significant risk factor for the development of osteoporosis, and postmenopausal women are at particularly high risk.[20] Bone synthesis and resorption are regulated by various molecules, including estrogen, calcitonin, and parathyroid hormone.[21] As individuals age, hormone levels decrease, leading to increased bone remodeling in both trabecular and cortical bone, reduced cortical bone mass, and decreased bone formation and trabecular integrity. This results in bone loss, disruption of bone microarchitecture, and an increased prevalence of osteoporosis.[11]

Therefore, in this study, we considered age as a confounding factor and conducted a subgroup analysis. We found that in subjects aged ≥50 years, the detection rate of hip osteoporosis was higher with iCare QCT than with Mindways QCT. However, in subjects younger than 50 years, there was no significant difference in osteoporosis detection rates between iCare and Mindways QCT. This finding may be attributable to the lower prevalence of osteoporosis in individuals aged <50 years. Previous research has shown that the prevalence of osteoporosis differs between sexes.[22]

In China, among individuals aged ≥50 years, 29.1% of women and 6.5% of men have osteoporosis. The most significant factor contributing to this sex difference in osteoporosis prevalence is the decline in estrogen levels with

aging, with postmenopausal women being 5–10 times more likely to develop osteoporosis than men.[23,24] Contrary to these established epidemiological patterns, our study observed higher osteoporosis detection rates in males (33.04%) than in women (20.00%) using iCare QCT. This apparent discrepancy likely stems from the significantly younger age distribution of female participants (mean age 52 ±8 years vs 61 ±9 years in males). As more than 60% of female participants were premenopausal or perimenopausal (age <55 years), this cohort underrepresented the highest-risk population of postmenopausal women. In this study, we used the iCare and Mindways QCT systems to detect hip osteoporosis in male and female participants. The results showed that osteoporosis detection rates were higher with iCare QCT than with Mindways QCT in both sexes, further confirming the superiority and reliability of the iCare QCT system.[5] Given that bone mineral density declines most rapidly during the first 5–10 years after menopause, the observed sex-related disparity in detection rates underscores the critical need for future studies to prioritize the recruitment of women older than 60 years to better characterize sex-specific osteoporosis prevalence.

In this study, we found that the osteoporosis detection rate was higher in men than in women, which differs from previous reports. This discrepancy may be attributed to the relatively younger age of the female participants in this study, resulting in a lower proportion of postmenopausal women and, consequently, a higher observed incidence of osteoporosis in men. Osteoporosis in women predominantly occurs after menopause, when ovarian function and circulating estrogen levels decline sharply. The decline in estrogen levels accelerates bone loss, leading to a rapid increase in the prevalence of osteoporosis with advancing age.[14,15] This limitation is particularly evident in complex spinal pathologies such as axial spondyloarthritis, where Żuchowski et al.[25] demonstrated that overreliance on DXA-derived bone mineral density alone may result in significant underdiagnosis of fracture risk, thereby necessitating complementary imaging approaches for accurate risk stratification.

The innovation of this study lies in the evaluation of the performance of the newly developed iCare QCT system in detecting osteoporosis using a larger sample size at a different center. Our findings further support the reliability and superiority of the iCare QCT system in osteoporosis detection. From a clinical implementation perspective, the cost-effectiveness of iCare QCT (approx. 40% lower per-scan cost than Mindways QCT at our center) may make it particularly advantageous in resource-limited settings where osteoporosis screening rates remain critically low. The high sensitivity of iCare QCT in detecting early bone loss may also prove valuable for monitoring therapeutic responses to emerging osteoanabolic agents, such as icariin, which has recently been shown to ameliorate osteoporosis through autophagy activation in preclinical models.[26] However, its implementation would require access to CT infrastructure and appropriate technician training.

Limitations of the study

This study has several limitations that should be interpreted in context. The single-center design, while ensuring protocol consistency, may limit generalizability to more diverse populations. The observed sex-related disparity in detection rates, with men showing a higher prevalence of osteoporosis (33.04% vs 20.00%), likely reflects the younger age profile of the female cohort (median age 52 vs 61 years in males), particularly given that approx. 60% of female participants were premenopausal. Practical implementation barriers persist, as evidenced by the limited accessibility of QCT in rural China, where only 23% of county-level hospitals possess compatible CT scanners. Future multicenter studies should prioritize age-stratified recruitment (particularly women older than 60 years), incorporate spine and forearm measurements, and validate emerging ultra-low-dose protocols (<50 μSv) against gold-standard assessments.

Conclusions

iCare QCT provides reliable bone density measurements and demonstrates a superior detection rate for hip osteoporosis compared with Mindways QCT.

Supplementary data

The supplementary materials are available at https://doi.org/10.5281/zenodo.15783669. The package contains the following files:

Supplementary Fig. 1. ROC curves with Youden's index of iCare QCT and Mindways QCT.

Supplementary Table 1. Statistical assumptions and data transformation.

Supplementary Table 2. Bootstrap and Bayesian analysis parameters.

Data Availability Statement

The datasets supporting the findings of the current study are openly available in Zenodo repository at https://doi.org/10.5281/zenodo.14904261.

Consent for publication

Not applicable.

Use of AI and AI-assisted technologies

Not applicable.

ORCID iDs

Jian Huang https://orcid.org/0009-0006-6099-8513
Fang Huang https://orcid.org/0009-0000-9350-570X
Liang Tang https://orcid.org/0009-0006-9003-4854
Xueming Ji https://orcid.org/0009-0002-7011-7784

References

1. Chandran M, McCloskey EV, Thu WPP, et al. FRAX® based intervention thresholds for management of osteoporosis in Singaporean women. *Arch Osteoporos*. 2018;13(1):130. doi:10.1007/s11657-018-0542-5
2. Camacho PM, Petak SM, Binkley N, et al. American Association of Clinical Endocrinologists/American College of Endocrinology Clinical Practice Guidelines for the Diagnosis and Treatment of Postmenopausal Osteoporosis: 2020 Update Executive Summary. *Endocrine Pract*. 2020;26(5):564–570. doi:10.4158/gl-2020-0524
3. James SL, Abate D, Abate KH, et al. Global, regional, and national incidence, prevalence, and years lived with disability for 354 diseases and injuries for 195 countries and territories, 1990–2017: A systematic analysis for the Global Burden of Disease Study 2017. *Lancet*. 2018;392(10159):1789–1858. doi:10.1016/s0140-6736(18)32279-7
4. Viswanathan M, Reddy S, Berkman N, et al. Screening to prevent osteoporotic fractures: Updated evidence report and systematic review for the US Preventive Services Task Force. *JAMA*. 2018; 319(24):2532. doi:10.1001/jama.2018.6537
5. Liu F, Zhu H, Ma J, et al. Performance of iCare quantitative computed tomography in bone mineral density assessment of the hip and vertebral bodies in European spine phantom. *J Orthop Surg Res*. 2023; 18(1):777. doi:10.1186/s13018-023-04174-w
6. Pinto D, Alshahrani M, Chapurlat R, et al. The global approach to rehabilitation following an osteoporotic fragility fracture: A review of the rehabilitation working group of the International Osteoporosis Foundation (IOF) committee of scientific advisors. *Osteoporos Int*. 2022;33(3):527–540. doi:10.1007/s00198-021-06240-7
7. Compston JE, McClung MR, Leslie WD. Osteoporosis. *Lancet*. 2019; 393(10169):364–376. doi:10.1016/s0140-6736(18)32112-3
8. Li L, Bennett-Brown K, Morgan C, Dattani R. Hip fractures. *Br J Hosp Med (Lond)*. 2020;81(8):1–10. doi:10.12968/hmed.2020.0215
9. Zhang C, Feng J, Wang S, et al. Incidence of and trends in hip fracture among adults in urban China: A nationwide retrospective cohort study. *PLoS Med*. 2020;17(8):e1003180. doi:10.1371/journal.pmed.1003180
10. Rosendahl-Riise H, Sulo G, Karlsson T, Drevon C, Dierkes J, Tell G. Limited benefit of fish consumption on risk of hip fracture among men in the community-based Hordaland Health Study. *Nutrients*. 2018;10(7):873. doi:10.3390/nu10070873
11. Kling JM, Clarke BL, Sandhu NP. Osteoporosis prevention, screening, and treatment: A review. *J Womens Health (Larchmt)*. 2014;23(7): 563–572. doi:10.1089/jwh.2013.4611
12. Nilsen OA, Emaus N, Christoffersen T, et al. The influence of snuff and smoking on bone accretion in late adolescence: The Tromsø study, Fit Futures. *Arch Osteoporos*. 2021;16(1):143. doi:10.1007/s11657-021-01003-7
13. Carballido-Gamio J, Yu A, Wang L, et al. Hip fracture discrimination based on statistical multi-parametric modeling (SMPM). *Ann Biomed Eng*. 2019;47(11):2199–2212. doi:10.1007/s10439-019-02298-x
14. Thu WPP, Logan SJS, Cauley JA, Kramer MS, Yong EL. Ethnic differences in bone mineral density among midlife women in a multi-ethnic Southeast Asian cohort. *Arch Osteoporos*. 2019;14(1):80. doi:10.1007/s11657-019-0631-0
15. Tella SH, Gallagher JC. Prevention and treatment of postmenopausal osteoporosis. *J Steroid Biochem Mol Biol*. 2014;142:155–170. doi:10.1016/j.jsbmb.2013.09.008
16. Zhao Y, Li K, Duanmu Y, et al. Accuracy, linearity and precision of spine QCT vBMD phantom measurements for different brands of CT scanner: A multicentre study. *J Clin Densitom*. 2022;25(1):34–42. doi:10.1016/j.jocd.2021.02.004
17. Ziemlewicz TJ, Maciejewski A, Binkley N, Brett AD, Brown JK, Pickhardt PJ. Opportunistic quantitative CT bone mineral density measurement at the proximal femur using routine contrast-enhanced scans: Direct comparison with DXA in 355 adults. *J Bone Miner Res*. 2016;31(10):1835–1840. doi:10.1002/jbmr.2856
18. Therkildsen J, Thygesen J, Winther S, et al. Vertebral bone mineral density measured by quantitative computed tomography with and without a calibration phantom: A comparison between 2 different software solutions. *J Clin Densitom*. 2018;21(3):367–374. doi:10.1016/j.jocd.2017.12.003
19. Ziemlewicz TJ, Maciejewski A, Binkley N, Brett AD, Brown JK, Pickhardt PJ. Direct comparison of unenhanced and contrast-enhanced CT for opportunistic proximal femur bone mineral density measurement: Implications for osteoporosis screening. *Am J Roentgenol*. 2016;206(4): 694–698. doi:10.2214/ajr.15.15128
20. Crandall CJ, Larson J, Cauley JA, et al. Do additional clinical risk factors improve the performance of Fracture Risk Assessment Tool (FRAX) among postmenopausal women? Findings from the Women's Health Initiative Observational Study and clinical trials. *JBMR Plus*. 2019;3(12):e10239. doi:10.1002/jbm4.10239
21. Fang H, Deng Z, Liu J, Chen S, Deng Z, Li W. The mechanism of bone remodeling after bone aging. *Clin Interv Aging*. 2022;17:405–415. doi:10.2147/cia.s349604
22. Elamin Ahmed H, Al-Dadah O. Bone mineral density in fracture neck of femur patients: What's the significance? *World J Orthop*. 2022; 13(2):160–170. doi:10.5312/wjo.v13.i2.160
23. Egan Benova T, Viczenczova C, Szeiffova Bacova B, et al. Omacor protects normotensive and hypertensive rats exposed to continuous light from increased risk to malignant cardiac arrhythmias. *Marine Drugs*. 2021;19(12):659. doi:10.3390/md19120659
24. Yuan Y, Zhang P, Tian W, et al. Application of bone turnover markers and DXA and QCT in an elderly Chinese male population. *Ann Palliat Med*. 2021;10(6):6351–6358. doi:10.21037/apm-21-612
25. Żuchowski P, Dura M, Jeka D, Wojciechowski R, Bierwagen M, Kułakowski M. Osteoporosis in axial radiographic spondyloarthritis: Diagnostic limitations of bone mineral density and the need for comprehensive fracture risk assessment. *Reumatologia*. 2024;62(6):466–474. doi:10.5114/reum/194107
26. Zou J, Peng Y, Wang Y, Xu S, Shi C, Liu Q. Icariin ameliorates osteoporosis by activating autophagy in ovariectomized rats. *Adv Clin Exp Med*. 2024;33(9):941–952. doi:10.17219/acem/174078

Pathway Mutation Accumulate Perturbation Score: A prognostic and predictive biomarker for immunotherapy in advanced gastric cancer

*Ziyan Zhang[1,A–C], *Guihua Yang[2,A–C], Yuming Xing[3,C,D], Yunfei Gao[4,C,D], Huaimin Lu[4,D–F]

[1] Institute of Stomatology, Baotou Medical College, China
[2] Berry Oncology Jingzhan Medical Laboratory Co., Ltd., Beijing, China
[3] Graduate College for Engineers, Beijing University of Posts and Telecommunications, China
[4] Institute of Medical Technology and Anesthesiology, Baotou Medical College, China

A – research concept and design; B – collection and/or assembly of data; C – data analysis and interpretation; D – writing the article; E – critical revision of the article; F – final approval of the article

Advances in Clinical and Experimental Medicine, ISSN 1899–5276 (print), ISSN 2451–2680 (online) *Adv Clin Exp Med*. 2026;35(4):639–650

Address for correspondence
Huaimin Lu
E-mail: 102024074@btmc.edu.cn

Funding sources
This study was supported by the Baotou Medical College Flower Bud Plan.

Conflict of interest
None declared

*Ziyan Zhang and Guihua Yang contributed equally to this work.

Received on December 30, 2024
Reviewed on March 25, 2025
Accepted on June 10, 2025

Published online on March 16, 2026

Abstract

Background. Gastric cancer (GC) remains highly lethal, with limited available biomarkers. The Pathway Mutation Accumulation Perturbation Score (PMAPscore), which leverages pathway-level mutations, provides a novel approach to predicting immunotherapy response and survival outcomes.

Objectives. To evaluate the prognostic and predictive value of the PMAPscore in patients with advanced GC undergoing immunotherapy.

Materials and methods. Three cohorts of patients with GC treated with immunotherapy were analyzed: PUCH (Peking University Cancer Hospital; n = 39, training cohort), MSK (Memorial Sloan Kettering; n = 19, validation cohort) and SMC (Samsung Medical Center; n = 43, validation cohort). A PMAPscore-based risk model was developed and validated for survival outcomes. Immune mechanisms in high- and low-risk groups were explored using The Cancer Genome Atlas (TCGA) GC data (n = 431).

Results. Low-risk patients identified by the PMAPscore model exhibited significantly better progression-free survival (PFS), overall survival (OS) and durable clinical benefit (DCB). In the PUCH cohort, low-risk patients had higher DCB rates (85.7% vs 44.0%, $p = 0.02$), longer PFS ($p < 0.001$), and longer OS ($p < 0.001$). Similar trends were observed in the MSK and SMC cohorts. Multivariate analysis confirmed low-risk status as an independent predictor of improved PFS and OS, outperforming tumor mutation burden (TMB), programmed death-ligand 1 (PD-L1) expression, microsatellite instability (MSI) status, and the gastrointestinal immune prognostic signature (GIPS). The TCGA data indicated enhanced antitumor immune activity in low-risk tumors, with increased human leukocyte antigen (HLA)-related gene expression and greater B-cell and natural killer (NK) cell infiltration.

Conclusions. The PMAPscore-based risk model is a robust tool for predicting survival and immunotherapy responses in patients with advanced GC, supporting its clinical application for treatment stratification.

Key words: gastric cancer (GC), prognostic biomarker, immunotherapy response, Pathway Mutation Accumulate Perturbation score (PMAPscore)

Cite as
Zhang Z, Yang G, Xing Y, Gao Y, Lu H. Pathway Mutation Accumulate Perturbation Score: A prognostic and predictive biomarker for immunotherapy in advanced gastric cancer. *Adv Clin Exp Med*. 2026;35(4):639–650. doi:10.17219/acem/206937

DOI
10.17219/acem/206937

Highlights

- The Pathway Mutation Accumulate Perturbation Score (PMAPscore) is a novel pathway-level, mutation-based biomarker for predicting immunotherapy response and survival outcomes in advanced gastric cancer (GC).
- Low-risk patients identified by the PMAPscore demonstrated significantly improved progression-free survival and overall survival across three independent GC cohorts.
- The PMAPscore outperformed established biomarkers, including tumor mutation burden, programmed death-ligand 1 expression, microsatellite instability status, and the gastrointestinal immune prognostic signature, in predicting immunotherapy response.
- The Cancer Genome Atlas analyses showed that low-risk tumors exhibit enhanced antitumor immune activity, including increased human leukocyte antigen gene expression and greater B-cell and natural killer cell infiltration.
- The PMAPscore-based risk model offers a clinically applicable tool for treatment stratification in advanced GC immunotherapy.

Background

In China, gastric cancer (GC) is the 3rd most common cause of cancer-related fatalities. It is also one of the most aggressive cancers worldwide. This high mortality rate is mainly associated with rapid progression to advanced stages and a high metastatic potential.[1,2] Historically, the treatment approach for advanced GC has relied on chemotherapy consisting of platinum compounds and fluoropyrimidines, with the addition of radiation therapy or targeted agents. These recommendations are aligned with the National Comprehensive Cancer Network (NCCN) guidelines.[3] However, in recent years, immunotherapy has become an effective treatment approach. Immune checkpoint inhibitors (ICIs) targeting programmed cell death protein 1 (PD-1) and programmed death-ligand 1 (PD-L1) have shown promising outcomes. This represents a major paradigm shift in GC management.[4–7] However, response rates to ICIs vary, highlighting a crucial need for reproducible biomarkers to predict which patients will benefit from immunotherapy.[8,9]

There have been several attempts to identify predictive biomarkers for GC immunotherapy. For example, first-line treatment with nivolumab and chemotherapy may be beneficial for HER2-negative patients with advanced or metastatic GC who exhibit PD-L1 positivity (combined positive score (CPS) ≥ 5).[10] Furthermore, pembrolizumab monotherapy has demonstrated positive results as a second-line or subsequent treatment in patients with high tumor mutation burden (TMB-H, ≥10 mutations per megabase) or high microsatellite instability (MSI-H).[11–14] Nevertheless, inconsistent or contradictory results have been obtained from clinical trials that included these biomarkers.[15–17] Biomarkers such as the gastrointestinal immune prognostic signature (GIPS), which consists of 6 prognosis-related genes, have shown potential to guide treatment decisions for gastrointestinal cancers. In addition, previous studies have indicated that mutations in patched homolog 1 (PTCH1) may serve as predictive biomarkers for immune checkpoint inhibitors in gastrointestinal cancers.[18] Yet, their applicability is limited due to their narrow genetic scope.[19] Similarly, transcriptomic biomarkers, including the T-cell-inflamed gene expression profile (GEP) and chromatin assembly factor 1 subunit A (CHAF1A) expression, have been linked to ICI responses but fail to reliably predict survival outcomes in GC, largely due to the lack of high-quality mRNA data.[20,21] This lack of a universally effective biomarker highlights the complexity of the immune response in GC.

According to recent research, biological pathways affected by cumulative genetic mutations may offer valuable insights into predicting the efficacy of immunotherapy.[22–26] Building on this, the Pathway Mutation Accumulation Perturbation Score (PMAPscore) was developed to evaluate pathway mutation perturbation levels by integrating the cumulative impact of mutated genes and their positions within biological pathways.[27] Although the PMAPscore has demonstrated predictive and prognostic utility in several cancers, including melanoma and non-small cell lung cancer, its role in advanced GC remains unexplored.

Objectives

In this study, we utilized data from 3 advanced GC immunotherapy cohorts, along with The Cancer Genome Atlas (TCGA) GC cohort (https://www.cancer.gov/ccg/research/genome-sequencing/tcga), to investigate the prognostic and predictive value of a multiple pathway-based risk model constructed using the PMAPscore. In addition, we investigated the biological mechanisms underlying this risk model. Our aim is to facilitate the development of a reliable biomarker for GC patient stratification and prediction of immunotherapy response.

Materials and methods

Data sources and processing

This multicohort study followed a 3-step framework encompassing biomarker discovery, validation and mechanistic exploration. Supplementary Fig. 1 describes the patient selection process in detail. Genomic and clinical data from 3 cohorts of patients receiving immunotherapy for GC were examined.

The multiple pathway-based risk model was developed and validated using the following cohorts:

Training cohort: PUCH (Peking University Cancer Hospital,[19] n = 39); used to identify genetic characteristics with prognostic potential and to construct the pathway-based risk model.

Validation cohorts:

1) MSK (Memorial Sloan Kettering,[28,29] n = 19): used to validate the predictive performance of the model;

2) SMC (Samsung Medical Center,[30] n = 43): used for additional external validation.

Additionally, the molecular processes underlying the correlation between the pathway-based risk model and the clinical outcomes of immunotherapy were examined using the TCGA GC cohort, which included 431 patients. In Supplementary Table 1, the clinicopathological features of the 3 groups are summarized.

Outcome assessment standards

Tumor responses were assessed using the Response Evaluation Criteria in Solid Tumors (RECIST) v. 1.1.[31] Achieving complete response (CR), partial response (PR) or stable disease (SD) lasting longer than 24 weeks was defined as durable clinical benefit (DCB), whereas progressive disease (PD) or SD lasting less than 24 weeks was defined as non-durable benefit (NDB).[28] Patients with CR or PR were classified as responders (R), whereas those with SD or PD were classified as non-responders (NR). Overall survival (OS) and progression-free survival (PFS) were the primary survival endpoints. Progression-free survival was defined as the time from initiation of immunotherapy to disease progression or death, whereas OS was defined as the time from initiation of treatment to death or the date of the most recent follow-up.

PMAPscore calculation and risk model construction

In accordance with prior work, the PMAPscore, which represents the cumulative effects and locations of genetic mutations within pathways, was computed.[27] The PMAPscores were obtained by analyzing 123 Kyoto Encyclopedia of Genes and Genomes (KEGG; http://www.kegg.jp) pathways using a modified R-based tool (https://CRAN.R-project.org/package=PMAPscore). To further narrow the scope of candidate pathways and prevent overfitting, univariable Cox proportional hazards regression analyses were performed first, and pathways with $p < 0.2$ were selected. Subsequently, the least absolute shrinkage and selection operator (LASSO) regression was applied to the Cox model by penalizing its likelihood function using a 10-fold cross-validation approach, and a prognostic risk model was constructed by integrating the PMAPscores of prognostic pathways. The risk score formula was expressed as follows: risk score = $\sum$ (PMAPscore × regression coefficient). Patients were stratified into high- and low-risk groups based on their scores. In conjunction with clinical factors, the independent prognostic significance of the risk score was assessed using multivariate Cox regression analysis.

Bulk RNA-sequencing analyses

Associations between the PMAPscore-based risk model and immune-related characteristics were investigated using the TCGA GC cohort, which included both DNA and RNA sequencing data. Differential gene expression analyses were conducted using DESeq2 v1.30 (https://bioconductor.org/packages/release/bioc/html/DESeq2.html), with a fold-change threshold of ≥2 and a p-value cutoff of <0.05. The ClusterProfiler software (v. 4.4.4) (https://bioconductor.org/packages/release/bioc/html/clusterProfiler.html) was used to conduct enrichment analysis of the identified genes. Gene set variation analysis (GSVA, v. 1.46) (https://bioconductor.org/packages/release/bioc/html/GSVA.html) was employed to calculate enrichment scores for 50 hallmark gene sets, followed by comparisons between high- and low-risk groups. The CIBERSORT algorithm and the Immuno-Oncology Biological Research (IOBR) R package (https://github.com/IOBR/IOBR) were applied to determine the proportions of 22 immune cell types and immuno-oncology-related signatures in both groups. To further elucidate the relationship between immune microenvironment subtypes and therapeutic outcomes, dynamic changes in the tumor immune microenvironment (TIME) were examined using 2 established approaches.[32,33] Metrics related to the immune repertoire were also compared.

Statistical analyses

R software v. 4.2.2 (R Foundation for Statistical Computing, Vienna, Austria) was used for all analyses. Overall survival and PFS were assessed using Kaplan–Meier survival curves, with significance determined with the log-rank test. Fisher's exact test was used to assess categorical data, and the two-sided Mann–Whitney U test was used to compare groups. We assessed the normality of continuous variables using the Kolmogorov–Smirnov or Shapiro–Wilk tests. For samples of size ≤50, the Shapiro–Wilk test was applied; otherwise, the Kolmogorov–Smirnov test was used. A $p > 0.05$ indicated a normal distribution. When

analyzing differences between 2 sets of variables, an F-test was used to assess the homogeneity of variance. Equal variance was assumed if $p > 0.05$. The results of the assumption assessment are listed in Supplementary Tables 6–9. For normally distributed data with equal variance, Student's t-test was used to compare differences between groups. If either assumption was violated, the Mann–Whitney U test was used. For categorical variables, the χ^2 test or Fisher's exact test was used to compare group differences. The χ^2 test was applied when the total sample size exceeded 40 and the minimum expected frequency was greater than 5. If the total sample size exceeded 40 but the minimum expected frequency was between 1 and 5, the corrected χ^2 test was applied. Fisher's exact test was used when the total sample size was below 40 or the minimum expected frequency was less than 1. Group difference results are presented in tables and visualized using box-and-whisker plots, showing the estimated maximum, upper quartile, median, lower quartile, and estimated minimum. Outliers were defined as values above QU + 1.5 × QR or below QL – 1.5 × QR (QR = QU – QL). The significance level for statistical analyses was set at $\alpha = 0.05$, with $p < 0.05$ considered statistically significant.

Results

Clinicopathological features of the patients

This study established a predictive model using the PUCH cohort, comprising 39 GC patients receiving ICIs, with a median follow-up of 6 months. Validation was performed using data from the MSK and SMC cohorts, which included 19 and 43 GC patients, respectively. Among these patients, DCB or response (R) to PD-1 inhibitors was observed in 14 patients (35.9%) in the PUCH cohort, 6 patients (31.6%) in the MSK cohort and 13 patients (30.2%) in the SMC cohort. Supplementary Table 1 summarizes the clinical and pathological features of all 3 cohorts, and the study design is illustrated in Supplementary Fig. 1.

Construction of the pathway-based risk model in the PUCH cohort based on PMAPscore profiles

The PMAPscore was calculated for 123 pathways retrieved from the KEGG database for each patient, yielding a comprehensive PMAPscore profile. Pathways with PMAPscores of 0 in more than 70% of patients were excluded from further analysis, resulting in 86 pathways retained for univariable Cox proportional hazards regression analyses. Based on the results of the univariate Cox analysis, a filtering criterion of $p < 0.2$ was applied, and 11 candidate pathways were subsequently entered into the LASSO regression model to mitigate overfitting (Supplementary Fig. 2). A prognostic risk model was then developed using the PMAPscores of 10 pathways weighted by their LASSO regression coefficients. Risk scores for individual patients were calculated using the formula:

The risk score was calculated as the weighted sum of PMAPscores for 10 pathways (Supplementary Table 2).

Negative contributions (associated with lower risk):
−0.0617 × mTOR signaling pathway
−0.2052 × Gap junction
−0.4438 × Thermogenesis
−0.0446 × Insulin signaling pathway
−0.0867 × Type II diabetes mellitus

Positive contributions (associated with higher risk):
+0.1249 × Longevity regulating pathway
+0.0410 × Platelet activation
+0.2726 × Long-term potentiation
+0.2186 × Regulation of actin cytoskeleton
+0.7536 × Cortisol synthesis and secretion

Similar to the validation cohorts, participants in the PUCH cohort were divided into high- and low-risk groups based on the 60th percentile threshold of the risk score. Risk score distributions, survival outcomes and PMAPscores of the pathways are shown in Fig. 1A–C. Notably, low-risk patients exhibited significantly improved OS in the PUCH cohort ($p < 0.001$, Fig. 1D). The c-index for OS was 0.835 (Supplementary Table 3). Additionally, the DCB group had a higher proportion of patients classified as low-risk (85.7% vs 44.0%, $p = 0.017$, Fig. 1E).

Correlation of the pathway-based risk model with clinical and immunological features

The pathway-based risk score showed no significant association with clinical or immunological features, including sex, MSI, GIPS, PD-L1 expression, and TMB score, except for copy number variation (CNV) (Fig. 2A–E, $p > 0.05$). The CNV showed a trend toward a positive correlation with risk score level (Fig. 2F, $p = 0.053$). The pathway-based signature was confirmed as an independent prognostic factor for progression-free survival by Cox regression analyses (multivariate: $p = 0.023$, hazard ratio (HR) = 0.114 (low vs high), 95% confidence interval (95% CI): 0.018–0.744) (Fig. 3).

Validation of prognostic and predictive significance in independent cohorts

To verify the prognostic and predictive value of the model, analyses were conducted in the MSK and SMC cohorts (Supplementary Table 4). In the MSK cohort, patients in the low-risk group demonstrated a higher proportion of DBC, as well as better PFS and OS, compared with the high-risk group (Fig. 4A–D). The c-index for OS was 0.707 (Supplementary Table 3). Consistent with these findings, in the SMC cohort, patients in the responder group experienced greater clinical benefit than those in the non-responder group (Fig. 5A,B).

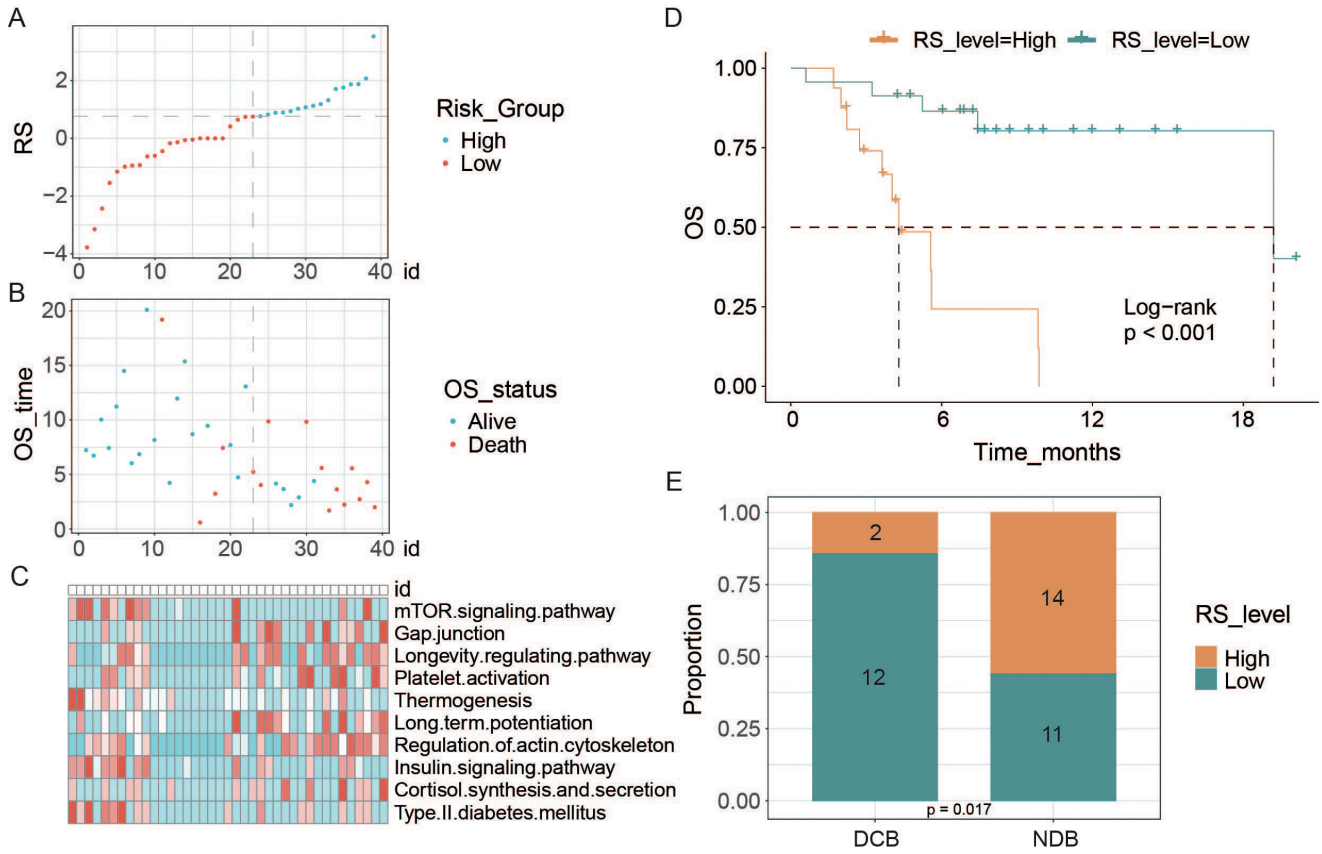

Fig. 1. Construction of the pathway-based risk model. A–C. Distribution of the risk score (A), survival outcomes (B) and heatmap of the Pathway Mutation Accumulate Perturbation Score (PMAPscore) in 10 prognosis-related pathways (C) in the PUCH (Peking University Cancer Hospital) training cohort; D. Kaplan–Meier curves of overall survival (OS) of patients in the high- and low-risk groups in the PUCH training cohort; E. Comparison of the rate of risk level in DCB and NDB groups in PUCH cohort (Fisher's exact test)

DCB – durable clinical benefit; NDB – non-durable benefit.

A similar pattern was observed when comparing the DBC and NDB groups; however, the differences were not statistically significant (Fig. 5C,D).

Differential gene expression and enrichment analyses

Transcriptomic data analysis identified 1,094 differentially expressed genes (DEGs) between the high- and low-risk groups (Fig. 6A, Supplementary Table 5). Enrichment analysis indicated significant involvement of pathways related to extracellular matrix (ECM) organization among both upregulated and downregulated DEGs in the low-risk group (Fig. 6B,C). Gene set variation analysis (GSVA) revealed that pathways such as DNA repair, interferon alpha response, oxidative phosphorylation and the p53 pathway had decreased activity in the low-risk group (Fig. 6D).

Associations of the pathway-based signature with TIME

The role of the TIME in tumor growth and immunotherapy response was examined. The expression levels of class II HLA-related genes were significantly higher in the low-risk group (Fig. 7A). Chemokines including CCL18, CXCL3, CCL3, and CCL4 exhibited higher expression in the low-risk group (Fig. 7B). In contrast, the expression of immune checkpoint inhibitors, such as CD274, ENTPD1, VTCN1, and transforming growth factor beta receptor 1 (TGFBR1), was markedly lower in the low-risk group (Fig. 7C). Additionally, the low-risk group showed increased expression of TNFRSF13 and TNFRSF9, which are co-stimulators of T cells (Fig. 7D). Immune cell infiltration was then assessed, and as shown in Fig. 7E, the low-risk group exhibited higher infiltration of naïve B cells and plasma cells. Furthermore, immuno-oncology signature analysis derived from the IOBR package revealed a significant increase in the infiltration abundance of B cells and natural killer (NK) cells in the low-risk group, along with a significant decrease in oxidative phosphorylation (Supplementary Fig. 3).

Discussion

Gastric cancer exhibits significant tumor heterogeneity due to diverse genetic alterations, making it essential to identify patients who are likely to benefit from immune checkpoint inhibitors and to tailor treatment plans for

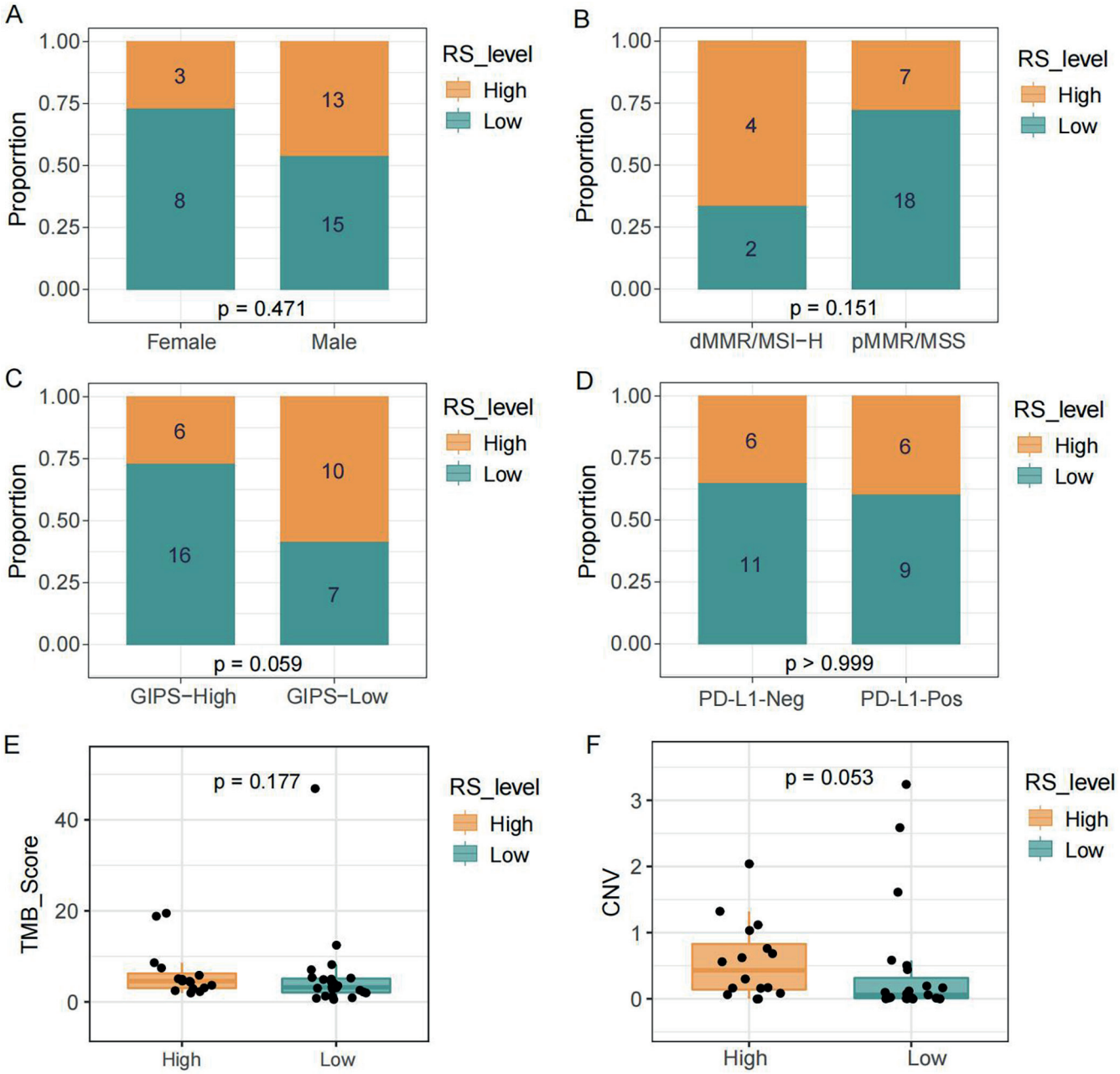

Fig. 2. Correlation between risk score and other potential biomarkers in the PUCH (Peking University Cancer Hospital) training cohort. Relationships between the risk score and clinicopathological features including sex (A), microsatellite instability (MSI) status (B), gastrointestinal immune prognostic signature (GIPS) (C), programmed death ligand 1 (PD-L1) expression (D), tumor mutation burden (TMB) score (E), and copy number variation (CNV) burden (F). Fisher's exact test was used for the comparison in A–D. Mann–Whitney U test was used for the comparison in E and F

dMMR – deficient Mismatch Repair; pMMR – proficient Mismatch Repair; MSI-H – Microsatellite Instability-High; MSS – Microsatellite Stable.

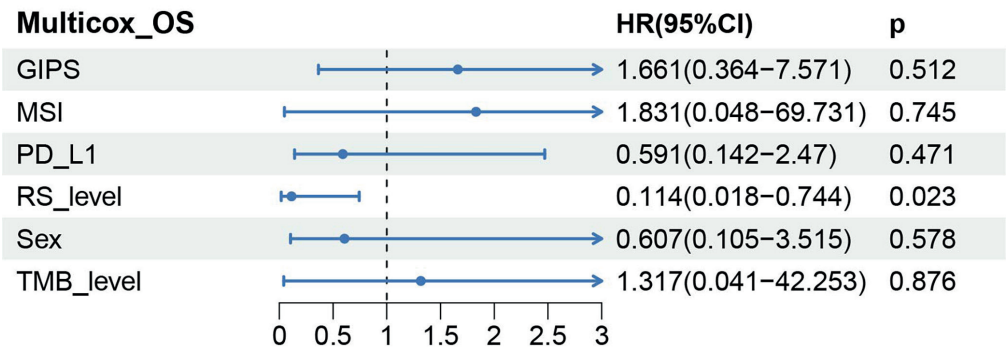

Fig. 3. Multivariate Cox regression analyses based on the overall survival (OS) revealed the risk score was an independent prognostic factor for gastric cancer (GC) patients receiving immunotherapy (PUCH (Peking University Cancer Hospital) cohort)

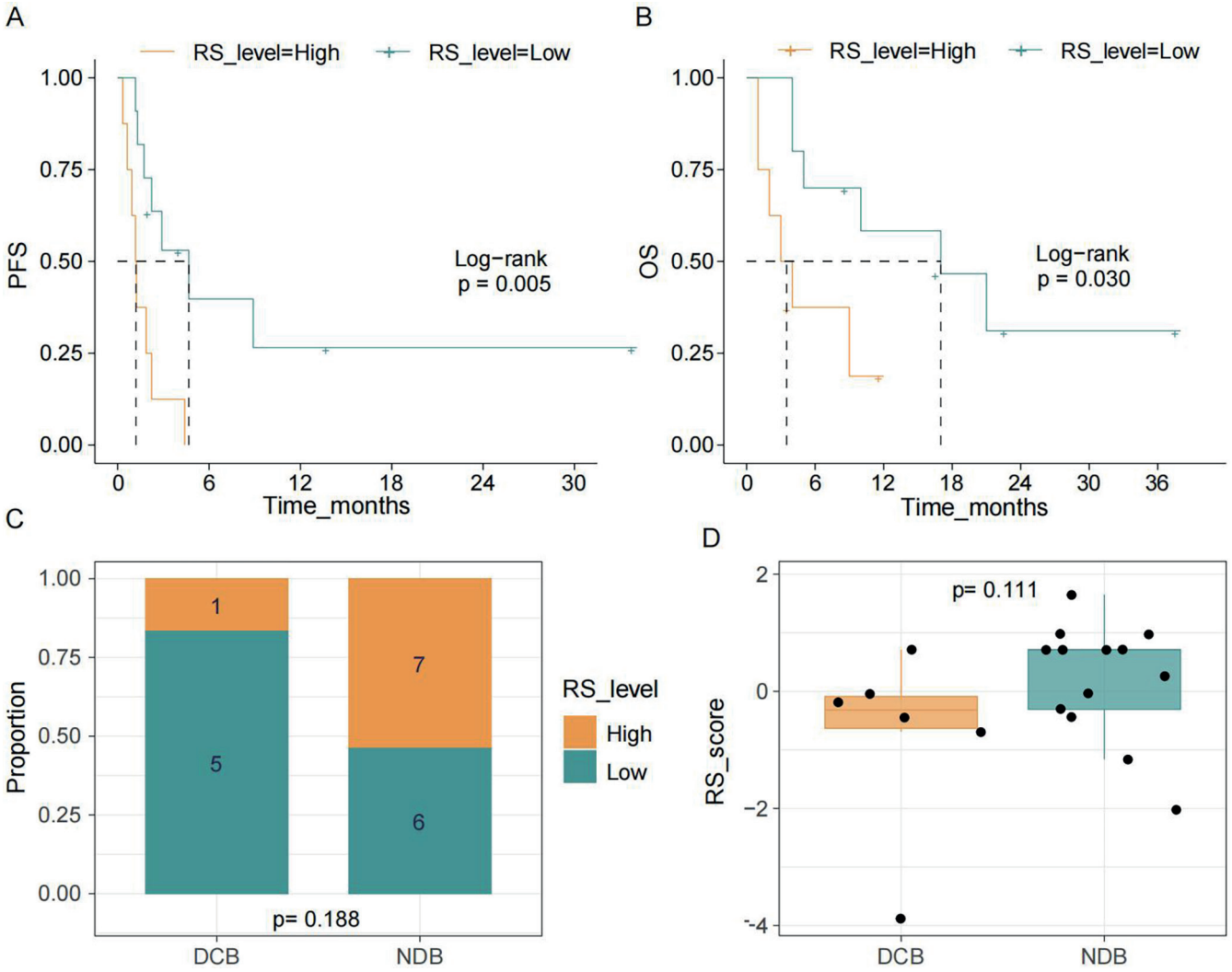

Fig. 4. Associations of risk score with overall survival (OS), progression-free survival (PFS) and clinical benefit in the MSK (Memorial Sloan Kettering) cohort. Kaplan–Meier curve to predict the PFS (A) and OS (B) of patients in the high- and high-risk cohorts; C. The proportion of patients with high or high-risk level DCB and NDB groups in the MSK cohort (Fisher's exact test). D. The comparison of risk score of DCB and NDB groups in the MSK cohort (Mann–Whitney U test)

DCB – durable clinical benefit; NDB – non-durable clinical benefit.

those who may not respond. In this study, we developed and validated a pathway-based risk score model derived from the PMAPscore to improve the precision of predicting immunotherapy outcomes in patients with GC. This approach effectively stratifies patients into high- and low-risk categories, identifying those with a higher likelihood of responding to immune checkpoint inhibitor therapy. Additionally, it serves as a robust prognostic indicator for patients with GC undergoing immunotherapy. Notably, the median OS was prolonged to nearly 14 months in patients with low-risk status. Importantly, our findings reveal that patients with GC with different PMAPscores display distinct TIME characteristics, with enhanced antitumor immune activity observed in the low-risk group.

Biomarker-guided immunotherapy holds great promise for the development of novel antitumor therapies by enriching responder populations through biomarker-based patient selection. Extensive research has been conducted to identify predictive markers of immune checkpoint inhibitor efficacy; however, existing biomarkers, including PD-L1 expression, TMB and MSI, have notable limitations. These limitations include inconsistent results, limited generalizability and low prevalence in certain cancers. For instance, PD-L1 expression has demonstrated limited predictive value in colorectal, esophageal, and gastric cancers.[34–37] Variability in exon sequencing platforms and a lack of consensus on cutoff points contribute to mixed findings regarding the prognostic value of tumor mutation burden.[8,38,39] Additionally, high status of MSI is rare, occurring in only 0–5% of metastatic gastrointestinal cancers.[40,41] Recently, several genetic mutations and expression markers have emerged as potential biomarkers for GC immunotherapy, such as *PTCH1* mutation and *CHAF1A* expression. Nevertheless, the limited scope of genetic alterations and the scarcity of high-quality mRNA data may restrict their true clinical utility.[18,21] Although the GIPS, a potential predictor of immune checkpoint inhibitor efficacy in gastrointestinal malignancies, is a genetic mutation signature involving 6 genes,[19] our

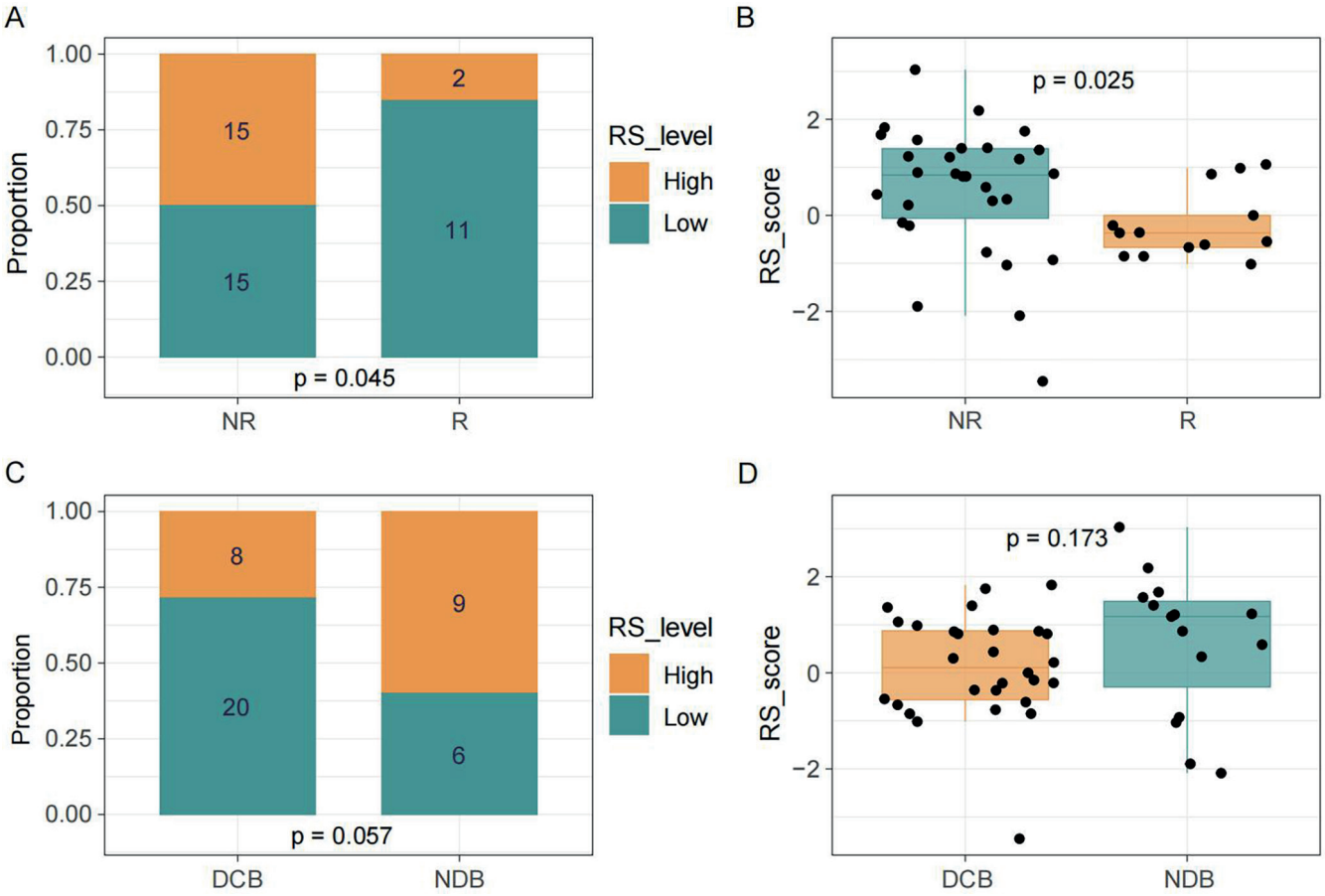

Fig. 5. Associations of risk score with clinical benefit in the SMC (Samsung Medical Center) cohort. A. Stacked bar chart illustrating the proportion of risk_level in NR and R groups; B. Boxplot showing risk_score distribution in NR and R groups; C. Stacked bar chart displaying the proportion of risk_level in DCB and NDB groups; D. Boxplot revealing risk_score distribution in DCB and NDB groups. Fisher's exact test was used for the comparison in A and C. Mann–Whitney U test was used for the comparison in B and D

R – responder; NR – non-responder; DCB – durable clinical benefit; NDB – non-durable clinical benefit.

multivariate analysis demonstrated that the PMAPscore-based risk model outperformed these markers as an independent predictor of OS. Therefore, cancer-specific models are necessary for clinical application.

Biological pathways provide valuable insights into disease mechanisms, drug responses, tumor markers, and altered cellular processes.[42–46] Risk models constructed using multiple pathways have demonstrated superior predictive capabilities. By integrating comprehensive networks for prognostic and efficacy prediction, these models enhance the reliability and stability of their outcomes. Higher PMAPscores suggest increased neoantigen generation, which may enhance T-cell recognition and improve immunotherapy efficacy. Previous studies have shown that pathway-based risk models effectively stratify patients with melanoma and non-small cell lung cancer into distinct groups with significantly different prognoses and responses to immunotherapy.[27] However, these findings highlight the necessity of cancer-specific models for clinical application, as melanoma-specific models did not perform well in patients with non-small cell lung cancer. Consistent with our results, pathway-based models have demonstrated better predictive value for immunotherapy efficacy compared with tumor mutation burden. Additionally, multivariable Cox analyses in this study confirmed that the PMAPscore-based risk model is an independent predictor of both OS and PFS in patients with GC.

Limitations of the study

Despite the encouraging findings, several limitations must be acknowledged. First, the relatively small sample size across the included cohorts limits the statistical power and generalizability of the results; some observations may reflect trends rather than reaching statistical significance. Second, drug-related biases may have been introduced due to the heterogeneity of anti-PD-1 and PD-L1 antibodies used across the training and validation cohorts, which were sourced from different pharmaceutical manufacturers. Third, the construction of the PMAPscore-based risk model was constrained by the high dimensionality of variables relative to the sample size. As a result, not all candidate variables could be incorporated into the regularized Cox regression model. Instead, univariate Cox regression was applied to preselect variables, which may have led to the exclusion of features that exert effects

Fig. 6. Differentially expressed genes (DEGs) and enrichment analyses to explore the potential molecular mechanisms of risk score in The Cancer Genome Atlas (TCGA) gastric cancer (GC) cohort. A. Volcano plot showing differently expressed genes in low- vs high-risk groups; B,C. Pathway enrichment analyses of up- (B) and downregulated (C) DEGs in the low-risk group; D. Volcano plot of gene set viariation analysis (GSVA) score in hallmark gene sets between the high- and low-risk groups

only through interactions with other variables. Finally, although the PMAPscore demonstrated robust predictive performance across multiple cohorts, its clinical utility and predictive validity require further confirmation through large-scale prospective studies involving patients treated with a uniform immune checkpoint inhibitor regimen.

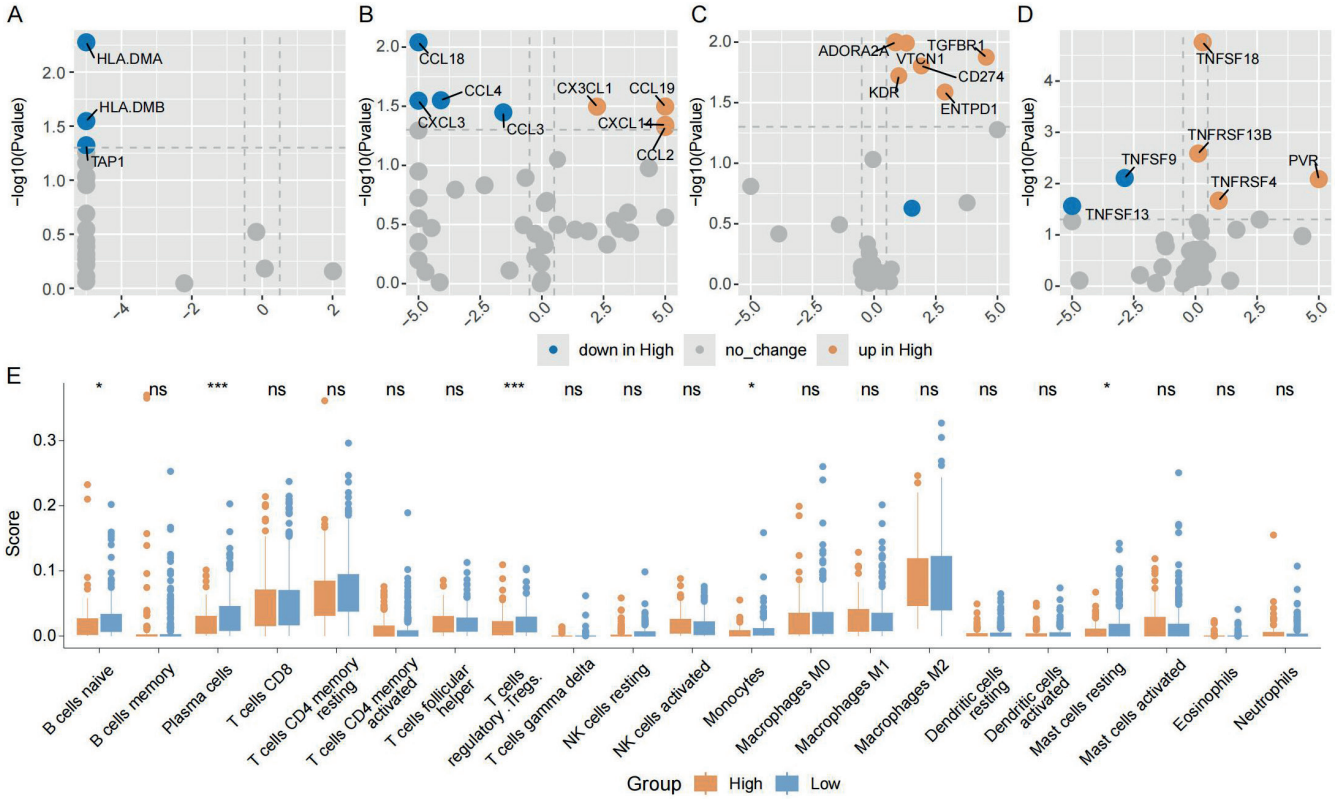

Fig. 7. Relationship between risk score and tumor immune microenvironment in the The Cancer Genome Atlas (TCGA) gastric cancer (GC) cohort. A–D. Volcano plot showed the comparison result of human leukocyte antigens (HLA) genes expression (A), chemokine genes expression (B), immune checkpoint inhibitors expression (C) and immune co-stimulators expression (D) in low- vs high-risk group; E, Boxplot of immunocytes proportion for the patients in the high- and low-risk groups (Mann–Whitney U test)

Conclusions

In summary, the PMAPscore-based risk model represents a promising biomarker for forecasting and predicting the therapeutic benefits of immune checkpoint inhibitors in patients with GC. This model provides a useful tool for optimizing treatment strategies by enabling the identification of potential immunotherapy responders, which we plan to evaluate in future prospective studies.

This study highlights the PMAPscore as a novel biomarker for GC patients receiving immunotherapy. The PMAPscore-based risk model efficiently stratifies patients into high- and low-risk groups by integrating multiple pathway alterations, providing reliable predictions of OS, PFS and DBC. Importantly, this approach identified low-risk patients with favorable clinical outcomes, characterized by distinct TIME features, including enhanced antitumor immune activity.

The PMAPscore demonstrates superior predictive power and is less influenced by confounding variables than conventional biomarkers, including PD-L1 expression, MSI and TMB. Beyond advancing our understanding of GC tumor biology, the PMAPscore paves the way for more individualized and effective immunotherapy strategies. This approach may support clinical decision-making and ultimately improve outcomes for patients with advanced GC. Moreover, it may improve cost-effectiveness by enabling a smaller and more personalized panel of genes involved in relevant pathways, based on the PMAPscore-based risk model. Such a panel could be readily translated into a practical, easy-to-use clinical assay to better identify patients with GC who are most likely to benefit from immunotherapy. Although these results highlight the PMAPscore's potential as both a prognostic and predictive tool, further randomized clinical trials are required to validate its clinical utility.

Supplementary data

The supplementary materials are available at https://doi.org/10.5281/zenodo.15864040. The package contains the following files:

Supplementary Fig. 1. Flow chart of participant selection depiction.

Supplementary Fig. 2. Construction of the pathway-based risk model. 10-fold cross-validation for selection of tuning parameters in the LASSO regression (A) and LASSO coefficient profiles of the 11 candidate pathways.

Supplementary Fig. 3. Relationship between risk score and TIME in the TCGA GC cohort. Violin plot of B cell infiltration abundance (A), NK cell infiltration abundance (B), and oxidative phosphorylation signature score (C) derived from the IOBR package in high and low risk groups (Mann–Whitney U test for A, Student's t-test for B and C).

Supplementary Table 1. Demographic distribution of the PUCH cohort (n = 39), MSK cohort (n = 19) and SMC cohort (n = 43).

Supplementary Table 2. Detailed regression coefficients for the LASSO model.

Supplementary Table 3. Detailed information on the c-index metric for risk score modeling in the PUCH and MSK cohorts based on OS.

Supplementary Table 4. Detailed information on PMAP-score distribution and risk score level for all cohorts.

Supplementary Table 5. Detailed information on DEGs between high- and low-risk groups.

Supplementary Table 6. Detailed information on the normality test and the homogeneity of variance test for DEGs in the TCGA cohort.

Supplementary Table 7. Detailed information on the proportional hazards assumption for Cox regression analysis.

Supplementary Table 8. Detailed information on the normality test and the homogeneity of variance test for the TMB score, CNV in the PUCH cohort, and the RS score in the MSK and SMC cohorts.

Supplementary Table 9. Detailed information on normality test and homogeneity of variance test for immune-related genes, signatures and gene sets in TCGA cohorts.

Data Availability Statement

The raw datasets supporting the findings of the current study are openly available in Zenodo at https://doi.org/10.5281/zenodo.15864029.

Consent for publication

Not applicable.

Use of AI and AI-assisted technologies

Not applicable.

ORCID iDs

Ziyan Zhang https://orcid.org/0009-0005-6168-1238
Guihua Yang https://orcid.org/0009-0000-9013-94848
Yuming Xing https://orcid.org/0009-0002-9173-8184
Yunfei Gao https://orcid.org/0009-0000-2278-1846
Huaimin Lu https://orcid.org/0009-0004-7980-5043

References

1. Bray F, Laversanne M, Sung H, et al. Global cancer statistics 2022: GLOBOCAN estimates of incidence and mortality worldwide for 36 cancers in 185 countries. *CA Cancer J Clin*. 2024;74(3):229–263. doi:10.3322/caac.21834
2. Shin WS, Xie F, Chen B, et al. Updated epidemiology of gastric cancer in Asia: Decreased incidence but still a big challenge. *Cancers (Basel)*. 2023;15(9):2639. doi:10.3390/cancers15092639
3. Liu S, Wong HY, Xie L, et al. Comparative efficacy and tolerability of targeted and immunotherapy combined with chemotherapy as first-line treatment for advanced gastric cancer: A Bayesian network meta-analysis. *Sci Rep*. 2022;12(1):22024. doi:10.1038/s41598-022-24426-9
4. Taefehshokr N, Baradaran B, Baghbanzadeh A, Taefehshokr S. Promising approaches in cancer immunotherapy. *Immunobiology*. 2020;225(2):151875. doi:10.1016/j.imbio.2019.11.010
5. Sharma P, Allison JP. Immune checkpoint targeting in cancer therapy: Toward combination strategies with curative potential. *Cell*. 2015;161(2):205–214. doi:10.1016/j.cell.2015.03.030
6. Sharma P, Allison JP. The future of immune checkpoint therapy. *Science*. 2015;348(6230):56–61. doi:10.1126/science.aaa8172
7. Kono K. Advances in cancer immunotherapy for gastroenterological malignancy. *Ann Gastroenterol Surg*. 2018;2(4):244–245. doi:10.1002/ags3.12184
8. Lu Z, Peng Z, Liu C, et al. Current status and future perspective of immunotherapy in gastrointestinal cancers. *Innovation (Camb)*. 2020;1(2):100041. doi:10.1016/j.xinn.2020.100041
9. Rao D, Parakrama R, Augustine T, Liu Q, Goel S, Maitra R. Immunotherapeutic advances in gastrointestinal malignancies. *NPJ Precis Oncol*. 2019;3(1):4. doi:10.1038/s41698-018-0076-8
10. Janjigian YY, Shitara K, Moehler M, et al. First-line nivolumab plus chemotherapy versus chemotherapy alone for advanced gastric, gastro-oesophageal junction, and oesophageal adenocarcinoma (CheckMate 649): A randomised, open-label, phase 3 trial. *Lancet*. 2021;398(10294):27–40. doi:10.1016/S0140-6736(21)00797-2
11. Le DT, Uram JN, Wang H, et al. PD-1 blockade in tumors with mismatch-repair deficiency. *N Engl J Med*. 2015;372(26):2509–2520. doi:10.1056/NEJMoa1500596
12. Le DT, Durham JN, Smith KN, et al. Mismatch repair deficiency predicts response of solid tumors to PD-1 blockade. *Science*. 2017;357(6349):409–413. doi:10.1126/science.aan6733
13. Marabelle A, Le DT, Ascierto PA, et al. Efficacy of pembrolizumab in patients with noncolorectal high microsatellite instability/mismatch repair-deficient cancer: Results from the phase II KEYNOTE-158 study. *J Clin Oncol*. 2020;38(1):1–10. doi:10.1200/JCO.19.02105
14. Marabelle A, Fakih M, Lopez J, et al. Association of tumour mutational burden with outcomes in patients with advanced solid tumours treated with pembrolizumab: Prospective biomarker analysis of the multicohort, open-label, phase 2 KEYNOTE-158 study. *Lancet Oncol*. 2020;21(10):1353–1365. doi:10.1016/S1470-2045(20)30445-9
15. Di Bartolomeo M, Morano F, Raimondi A, et al. Prognostic and predictive value of microsatellite instability, inflammatory reaction and PD-L1 in gastric cancer patients treated with either adjuvant 5-FU/LV or sequential FOLFIRI followed by cisplatin and docetaxel: A translational analysis from the ITACA-S trial. *Oncologist*. 2020;25(3):e460–e468. doi:10.1634/theoncologist.2019-0471
16. Kim JY, Kim WG, Kwon CH, Park DY. Differences in immune contextures among different molecular subtypes of gastric cancer and their prognostic impact. *Gastric Cancer*. 2019;22(6):1164–1175. doi:10.1007/s10120-019-00974-4
17. Ji Z, Peng Z, Gong J, et al. Hyperprogression after immunotherapy in patients with malignant tumors of digestive system. *BMC Cancer*. 2019;19(1):705. doi:10.1186/s12885-019-5921-9
18. Jiao X, Wei X, Li S, et al. A genomic mutation signature predicts the clinical outcomes of immunotherapy and characterizes immunophenotypes in gastrointestinal cancer. *NPJ Precis Oncol*. 2021;5(1):36. doi:10.1038/s41698-021-00172-5
19. Deng S, Gu H, Chen Z, et al. *PTCH1* mutation as a potential predictive biomarker for immune checkpoint inhibitors in gastrointestinal cancer. *Carcinogenesis*. 2024;45(5):351–357. doi:10.1093/carcin/bgae007
20. Kelly RJ, Lee J, Bang YJ, et al. Safety and efficacy of durvalumab and tremelimumab alone or in combination in patients with advanced gastric and gastroesophageal junction adenocarcinoma. *Clin Cancer Res*. 2020;26(4):846–854. doi:10.1158/1078-0432.CCR-19-2443
21. Ying L, Hu Z, Lu Y, et al. An oncogene regulating chromatin favors response to immunotherapy: Oncogene *CHAF1A* and immunotherapy outcomes. *OncoImmunology*. 2024;13(1):2303195. doi:10.1080/2162402X.2024.2303195
22. Tsagarakis NJ, Papadhimitriou SI, Pavlidis D, et al. Contribution of immunophenotype to the investigation and differential diagnosis of Burkitt lymphoma, double-hit high-grade B-cell lymphoma, and single-hit *MYC*-rearranged diffuse large B-cell lymphoma. *Cytometry B Clin Cytom*. 2020;98(5):412–420. doi:10.1002/cyto.b.21887
23. Ravindran U, Gunavathi C. Deep learning assisted cancer disease prediction from gene expression data using WT-GAN. *BMC Med Inform Decis Mak*. 2024;24(1):311. doi:10.1186/s12911-024-02712-y

24. Generali D, Rocca A, Strina C, et al. Assessing the long-term prognostic ability of the 70 gene expression signature MammaPrint in an Italian single-center prospective cohort study of early-stage intermediate-risk breast cancer patients. *Heliyon*. 2024;10(21):e39485. doi:10.1016/j.heliyon.2024.e39485
25. Wang Z, Zhao J, Wang G, et al. Comutations in DNA damage response pathways serve as potential biomarkers for immune checkpoint blockade. *Cancer Res*. 2018;78(22):6486–6496. doi:10.1158/0008-5472.CAN-18-1814
26. Bao Z, Zhang B, Li L, Ge Q, Gu W, Bai Y. Identifying disease-associated signaling pathways through a novel effector gene analysis. *PeerJ*. 2020;8:e9695. doi:10.7717/peerj.9695
27. Li X, He Y, Wu J, et al. A novel pathway mutation perturbation score predicts the clinical outcomes of immunotherapy. *Brief Bioinform*. 2022;23(5):bbac360. doi:10.1093/bib/bbac360
28. Rizvi NA, Hellmann MD, Snyder A, et al. Mutational landscape determines sensitivity to PD-1 blockade in non-small cell lung cancer. *Science*. 2015;348(6230):124–128. doi:10.1126/science.aaa1348
29. Janjigian YY, Sanchez-Vega F, Jonsson P, et al. Genetic predictors of response to systemic therapy in esophagogastric cancer. *Cancer Discov*. 2018;8(1):49–58. doi:10.1158/2159-8290.CD-17-0787
30. Kim ST, Cristescu R, Bass AJ, et al. Comprehensive molecular characterization of clinical responses to PD-1 inhibition in metastatic gastric cancer. *Nat Med*. 2018;24(9):1449–1458. doi:10.1038/s41591-018-0101-z
31. Eisenhauer EA, Therasse P, Bogaerts J, et al. New response evaluation criteria in solid tumours: Revised RECIST guideline (version 1.1). *Eur J Cancer*. 2009;45(2):228–247. doi:10.1016/j.ejca.2008.10.026
32. Bagaev A, Kotlov N, Nomie K, et al. Conserved pan-cancer microenvironment subtypes predict response to immunotherapy. *Cancer Cell*. 2021;39(6):845–865.e7. doi:10.1016/j.ccell.2021.04.014
33. Thorsson V, Gibbs DL, Brown SD, et al. The immune landscape of cancer. *Immunity*. 2018;48(4):812–830.e14. doi:10.1016/j.immuni.2018.03.023
34. Overman MJ, McDermott R, Leach JL, et al. Nivolumab in patients with metastatic DNA mismatch repair-deficient or microsatellite instability-high colorectal cancer (CheckMate 142): An open-label, multicentre, phase 2 study. *Lancet Oncol*. 2017;18(9):1182–1191. doi:10.1016/S1470-2045(17)30422-9
35. Kato K, Cho BC, Takahashi M, et al. Nivolumab versus chemotherapy in patients with advanced oesophageal squamous cell carcinoma refractory or intolerant to previous chemotherapy (ATTRACTION-3): A multicentre, randomised, open-label, phase 3 trial. *Lancet Oncol*. 2019;20(11):1506–1517. doi:10.1016/S1470-2045(19)30626-6
36. Huang J, Xu J, Chen Y, et al. Camrelizumab versus investigator's choice of chemotherapy as second-line therapy for advanced or metastatic oesophageal squamous cell carcinoma (ESCORT): A multicentre, randomised, open-label, phase 3 study. *Lancet Oncol*. 2020;21(6):832–842. doi:10.1016/S1470-2045(20)30110-8
37. Kang YK, Boku N, Satoh T, et al. Nivolumab in patients with advanced gastric or gastro-oesophageal junction cancer refractory to, or intolerant of, at least two previous chemotherapy regimens (ONO-4538-12, ATTRACTION-2): A randomised, double-blind, placebo-controlled, phase 3 trial. *Lancet*. 2017;390(10111):2461–2471. doi:10.1016/S0140-6736(17)31827-5
38. Samstein RM, Lee CH, Shoushtari AN, et al. Tumor mutational load predicts survival after immunotherapy across multiple cancer types. *Nat Genet*. 2019;51(2):202–206. doi:10.1038/s41588-018-0312-8
39. Wang F, Wei XL, Wang FH, et al. Safety, efficacy and tumor mutational burden as a biomarker of overall survival benefit in chemo-refractory gastric cancer treated with toripalimab, a PD-1 antibody in phase Ib/II clinical trial NCT02915432. *Ann Oncol*. 2019;30(9):1479–1486. doi:10.1093/annonc/mdz197
40. Fuchs CS, Doi T, Jang RW, et al. Safety and efficacy of pembrolizumab monotherapy in patients with previously treated advanced gastric and gastroesophageal junction cancer: Phase 2 clinical KEYNOTE-059 trial. *JAMA Oncol*. 2018;4(5):e180013. doi:10.1001/jamaoncol.2018.0013
41. Yao YC, Jin Y, Lei XF, et al. Impact of mismatch repair or microsatellite status on the prognosis and efficacy to chemotherapy in metastatic colorectal cancer patients: A bi-institutional, propensity score-matched study. *J Cancer*. 2022;13(9):2912–2921. doi:10.7150/jca.50285
42. Sheng Y, Jiang Y, Yang Y, et al. CNA2Subpathway: identification of dysregulated subpathway driven by copy number alterations in cancer. *Brief Bioinform*. 2021;22(5):bbaa413. doi:10.1093/bib/bbaa413
43. Han X, Kong Q, Liu C, Cheng L, Han J. SubtypeDrug: A software package for prioritization of candidate cancer subtype-specific drugs. *Bioinformatics*. 2021;37(16):2491–2493. doi:10.1093/bioinformatics/btab011
44. Han J, Han X, Kong Q, Cheng L. psSubpathway: A software package for flexible identification of phenotype-specific subpathways in cancer progression. *Bioinformatics*. 2020;36(7):2303–2305. doi:10.1093/bioinformatics/btz894
45. Liu S, Zheng B, Sheng Y, et al. Identification of cancer dysfunctional subpathways by integrating DNA methylation, copy number variation, and gene-expression data. *Front Genet*. 2019;10:441. doi:10.3389/fgene.2019.00441
46. Di J, Zheng B, Kong Q, et al. Prioritization of candidate cancer drugs based on a drug functional similarity network constructed by integrating pathway activities and drug activities. *Mol Oncol*. 2019;13(10):2259–2277. doi:10.1002/1878-0261.12564

Mendelian randomization analysis of risk factors for nasopharyngeal carcinoma: Examining causal links to EBV susceptibility and dietary influences

Guizhu Li[A–F]

Department of Otolaryngology and Head and Neck Surgery, Affiliated Hospital of Jiangsu University, Zhenjiang, China

A – research concept and design; B – collection and/or assembly of data; C – data analysis and interpretation;
D – writing the article; E – critical revision of the article; F – final approval of the article

Advances in Clinical and Experimental Medicine, ISSN 1899–5276 (print), ISSN 2451–2680 (online) *Adv Clin Exp Med*. 2026;35(4):651–660

Address for correspondence
Guizhu Li
E-mail: 13812450672@163.com

Funding sources
None declared

Conflict of interest
None declared

Received on January 24, 2025
Reviewed on July 2, 2025
Accepted on July 10, 2025

Published online on April 21, 2026

Abstract

Background. Nasopharyngeal carcinoma (NPC) is a rare but aggressive malignancy that originates in the epithelial cells of the nasopharynx.

Objectives. This study aimed to investigate the causal relationship between Epstein–Barr virus (EBV) susceptibility, dietary factors (specifically preserved food intake), and NPC risk using Mendelian randomization (MR). The goal of this study was to provide insights into the genetic and environmental factors that contribute to NPC pathogenesis.

Materials and methods. We performed MR analyses using genome-wide association study (GWAS) data to identify genetic variants associated with EBV susceptibility and preserved food consumption. These genetic variants were used as instrumental variables to assess their causal effects on NPC risk, while controlling for potential confounding and reverse causality. Subgroup and sensitivity analyses, including the MR-Egger, weighted median, and leave-one-out methods, were conducted to evaluate the robustness of the findings.

Results. Our MR analysis identified a significant causal effect of EBV genetic susceptibility on NPC risk ($\beta = 1.47$, 95% confidence interval (95% CI): 1.12–1.83, $p = 0.001$). Additionally, genetic predispositions related to higher preserved food intake were associated with an increased risk of NPC ($\beta = 0.75$, 95% CI: 0.45–1.05, $p = 0.001$). Subgroup analysis showed consistent results across different age groups (p for interaction = 0.45), and sensitivity analyses confirmed the robustness of the findings, with no evidence of pleiotropy.

Conclusions. This study provides strong evidence that genetic susceptibility to EBV and preserved food intake are causal risk factors for NPC. These findings offer valuable insights into NPC prevention strategies, particularly in high-risk populations, and highlight the need for further research on gene–environment interactions in NPC pathogenesis.

Key words: genetic susceptibility, Epstein–Barr virus (EBV), Mendelian randomization (MR), nasopharyngeal carcinoma (NPC), dietary factors

Cite as
Li G. Mendelian randomization analysis of risk factors for nasopharyngeal carcinoma: Examining causal links to EBV susceptibility and dietary influences. *Adv Clin Exp Med*. 2026;35(4):651–660. doi:10.17219/acem/208134

DOI
10.17219/acem/208134

Highlights

- Mendelian randomization (MR) confirms that genetic susceptibility to Epstein–Barr virus (EBV) causally increases nasopharyngeal carcinoma (NPC) risk.
- Genetic predisposition to preserved food intake is associated with elevated NPC risk, highlighting dietary contributions to carcinogenesis.
- GWAS-based MR analyses (MR-Egger, weighted median, leave-one-out) robustly validate causal associations across age groups.
- Findings support gene–environment interactions and inform targeted NPC prevention strategies.

Background

Nasopharyngeal carcinoma (NPC) is a rare but aggressive malignancy arising from the epithelial cells of the nasopharynx. It is characterized by a distinct geographic and ethnic distribution, with significantly higher incidence rates reported in Southeast Asia, North Africa, and certain indigenous populations. Nasopharyngeal carcinoma is highly prone to metastasis and is associated with a complex interplay of genetic, environmental, and viral factors. Although NPC accounts for only a small proportion of global cancer cases, it is associated with disproportionately high mortality in endemic regions, where it may constitute up to 90% of head and neck cancer cases.[1]

The pathogenesis of NPC is multifactorial and involves a complex interplay among viral infection, host genetic susceptibility, and environmental exposures. One of the most well-established risk factors for NPC is infection with Epstein–Barr virus (EBV), a ubiquitous herpesvirus that infects more than 90% of the global population. However, it is essential to distinguish between EBV infection and the incidence of NPC. Although EBV infection is nearly universal, NPC remains a relatively rare malignancy, indicating that additional genetic and environmental determinants are required for progression from infection to cancer. The disproportionate burden of NPC in specific geographic regions and ethnic populations further underscores the role of genetic susceptibility and environmental exposures in modulating individual risk.[2]

Epstein–Barr virus infection has long been implicated in the development of NPC, particularly in endemic regions. Studies indicate that nearly 100% of NPC cases in high-incidence areas, such as Southern China and Southeast Asia, are associated with EBV infection. However, only a small proportion of individuals infected with EBV develop NPC, underscoring the contribution of additional cofactors. Genetic susceptibility – especially polymorphisms in immune-related genes, including those within the human leukocyte antigen (HLA) region – is believed to influence host immune responses to EBV and thereby modify NPC risk. Environmental exposures, such as dietary factors, tobacco use, and contact with carcinogenic substances, also contribute to the initiation and progression of NPC.[3]

Dietary factors, in particular, have been strongly implicated in NPC risk. Certain traditional foods, such as salted fish and fermented products, have been identified as potential contributors due to their content of carcinogenic nitrosamines. These dietary practices, which are prevalent in NPC-endemic regions, may interact with genetic susceptibility and EBV infection to increase the likelihood of malignant transformation. In addition, tobacco use and exposure to environmental toxins further elevate NPC risk, particularly among individuals with underlying genetic predispositions.[4]

Given the complex and multifactorial nature of NPC risk, establishing clear causal relationships among genetic, viral, and environmental determinants using traditional observational methods remains challenging. Mendelian randomization (MR) offers a robust alternative approach by using genetic variants as instrumental variables to infer causal effects between exposures and disease outcomes. Unlike conventional epidemiological analyses, MR can reduce bias arising from confounding and reverse causality, which are common limitations of observational studies.[5]

By utilizing genetic instruments linked to EBV susceptibility, dietary factors, and other environmental exposures, MR enables researchers to determine whether these factors directly contribute to the development of NPC. Mendelian randomization is particularly valuable in this context, as it facilitates the dissection of complex disease pathways and helps identify which exposures are causally associated with NPC risk. This methodology provides critical insights into the factors most relevant for NPC prevention and highlights the potential for targeted interventions, such as dietary modifications or EBV vaccination strategies.[6]

Objectives

This study aimed to investigate the causal relationships among EBV susceptibility, dietary factors, and the risk of NPC. Given the well-established link between EBV infection and NPC, along with the pronounced geographic and ethnic disparities in NPC incidence, this study

clarifies the role of genetic predisposition to EBV susceptibility in NPC development. Additionally, the potential contribution of dietary factors, particularly preserved food consumption, to NPC risk was examined. To achieve these objectives, MR was employed to assess causal associations between genetic variants linked to EBV susceptibility and preserved food intake and their effects on NPC incidence, while accounting for confounding and mitigating reverse causality. Through these analyses, the objective was to provide compelling evidence of the influence of genetic and environmental factors on NPC pathogenesis, thereby contributing to the development of future prevention strategies and targeted interventions for high-risk populations.[7]

Materials and methods

Genetic instrument selection for EBV susceptibility

Genetic variants associated with EBV susceptibility were selected as instrumental variables for MR analysis. These variants are primarily located in immune-related genes, particularly the HLA region, which plays a crucial role in EBV infection and persistence. Single-nucleotide polymorphisms (SNPs) were selected from genome-wide association studies (GWAS) based on genome-wide significance ($p < 5 \times 10^{-8}$). We applied linkage disequilibrium (LD) clumping with an r^2 threshold <0.01 and a 10,000 kb window to ensure independence between SNPs. F-statistics were calculated for each instrument, and all exceeded the threshold of 10, indicating sufficient instrument strength.

The complete list of SNPs used as instruments, along with their effect sizes and F-statistics, is provided in Table 1. Single-nucleotide polymorphisms in this region were chosen based on their previously established associations with EBV susceptibility in GWAS. Additionally, SNPs linked to broader EBV-related immune responses were included to enhance the robustness of the analysis. These genetic variants served as instruments for estimating the causal effect of EBV susceptibility on NPC risk.

Study design and data sources

The analysis utilized large-scale, publicly available genomic datasets, including data from the UK Biobank (https://www.ukbiobank.ac.uk), which comprises over 500,000 participants. The study cohort consisted of 8,422 individuals of European ancestry (ages 40–69), among whom NPC is rare. Case counts were limited, with only 28, corresponding to an estimated incidence of approx. 1 per 100,000. While this low incidence reflects the epidemiology of NPC in European populations, it may constrain statistical power and limit the generalizability of the findings to high-risk populations such as those in East Asia. Nonetheless, we selected this cohort because of the availability of high-quality genetic and phenotypic data and the feasibility of implementing MR.

Mendelian randomization analysis

A 2-sample MR approach was employed to estimate the causal relationship between EBV susceptibility and NPC risk. Summary genetic data for EBV susceptibility were used as the 1st sample, while NPC incidence data from the UK Biobank formed the 2nd sample. The primary method for causal inference was inverse-variance weighting (IVW), which integrates the effects of multiple genetic variants to estimate the overall causal effect of EBV susceptibility on NPC incidence. Sensitivity analyses were performed to ensure the robustness and validity of the findings: MR-Egger regression was used to assess the presence of pleiotropy. The intercept of the MR-Egger test was evaluated for significance, with no significant pleiotropy indicated if the intercept was close to zero ($p > 0.050$). Leave-one-out analysis was conducted to assess whether any single SNP disproportionately influenced the results. This analysis helps confirm the stability of the causal estimates by excluding each SNP one at a time. Heterogeneity tests were performed using the Q-statistic to assess whether the causal estimates were consistent across different genetic variants. A $p > 0.05$ suggested no significant heterogeneity among the SNPs used.

Table 1. MR analysis of EBV susceptibility and NPC risk

Genetic variant	Exposure	Outcome (NPC risk)	Causal estimate (β)	95% CI	p-value	Sensitivity analysis
SNPs in HLA region	EBV susceptibility	NPC incidence	1.47	1.12–1.83	0.001	MR-Egger: no pleiotropy (intercept = 0.02, p = 0.32); leave-one-out: no influential SNPs; heterogeneity: Q-statistic = 9.23, p = 0.15
SNPs related to dietary salt intake	EBV susceptibility + salt intake	NPC risk	0.34	0.15–0.52	0.001	interaction term: significant gene-environment interaction
SNPs related to smoking	EBV susceptibility + smoking	NPC risk	0.29	0.10–0.48	0.004	interaction term: increased risk in smokers with higher EBV susceptibility
General EBV-related SNPs	EBV susceptibility	NPC incidence	–	–	–	instrument strength (F-stat > 10)

95% CI – 95% confidence interval; EBV – Epstein–Barr virus; NPC – nasopharyngeal carcinoma; SNP – single-nucleotide polymorphism; HLA – human leukocyte antigen; MR – Mendelian randomization.

Interaction with dietary and environmental factors

Secondary analyses explored potential gene–environment interactions between EBV susceptibility and environmental factors, such as dietary salt intake and smoking. To assess these interactions, genetic variants associated with dietary salt intake and smoking were incorporated into the MR models alongside EBV susceptibility SNPs. Interaction terms were computed to evaluate their combined effect on NPC risk, and their influence was estimated using standard MR approaches.

Genetic instrument selection for dietary factors

The potential causal effect of dietary factors, particularly preserved food intake, on NPC risk was examined using MR. Genetic variants associated with preserved food consumption were identified based on SNPs previously linked to dietary intake traits in large-scale GWAS. Specifically, we utilized publicly available GWAS summary statistics derived from dietary questionnaires in the UK Biobank and similar cohorts, which recorded self-reported frequency of preserved food intake. Only genome-wide significant SNPs ($p < 5 \times 10^{-8}$) associated with preserved or processed food consumption were selected as instrumental variables. To reduce bias, SNPs were clumped based on linkage disequilibrium ($r^2 < 0.01$) and aligned to the effect alleles used in the outcome data. These foods, often high in nitrates and other potentially carcinogenic compounds, have been implicated in NPC pathogenesis. Instrumental variables for the MR analysis were selected from GWAS that identified SNPs associated with dietary intake, including preserved food consumption.

Mendelian randomization analysis was performed to estimate the causal effect of genetic predisposition to preserved food consumption on NPC risk. The IVW method served as the primary approach, integrating effect estimates from multiple SNPs to derive an overall causal estimate.

Sensitivity analyses were performed to ensure the robustness of the findings. These included MR-Egger regression to detect pleiotropy (i.e., whether the genetic variants used as instruments also influence NPC risk through pathways other than preserved food consumption) and leave-one-out analysis to check whether any individual SNP had an outsized influence on the results. Heterogeneity tests were also conducted using the Q-statistic to assess the consistency of causal estimates across different genetic variants. A p-value greater than 0.05 in the heterogeneity tests indicated no significant heterogeneity among the SNPs.

Subgroup analysis by age group

To explore the robustness and generalizability of the causal associations between EBV susceptibility and NPC risk, we conducted a subgroup analysis stratified by age. Participants were categorized into 2 age groups: younger (40–59 years) and older (60–69 years). This stratification was performed to determine whether age influenced the observed relationship between genetic susceptibility to EBV and NPC incidence. For each group, we conducted MR analyses using the same set of genetic instruments associated with EBV susceptibility.

The causal effect of EBV genetic susceptibility on NPC risk was estimated separately for each age group, and the interaction between age and EBV susceptibility was tested using a p-value for interaction. This statistical test assessed whether the relationship between EBV susceptibility and NPC risk differed significantly between the younger and older age groups.

Sensitivity analysis

Beyond subgroup analysis, multiple sensitivity analyses were conducted to assess the robustness of the causal estimates:

1. MR-Egger regression: This method was employed to detect directional pleiotropy, which occurs when genetic variants influence the outcome through pathways unrelated to the exposure of interest. The MR-Egger intercept was tested for significance, with $p > 0.05$ indicating no substantial pleiotropic bias.

2. Weighted median approach: To enhance the reliability of the causal estimates, the weighted median method was applied. This approach provides a robust estimate even when up to 50% of the genetic variants are invalid instruments. Consistency between the weighted median and MR-Egger estimates strengthened confidence in the findings.

3. Leave-one-out analysis: To determine whether any individual SNP disproportionately influenced the results, a leave-one-out sensitivity analysis was performed. Each SNP was sequentially excluded, and changes in the causal estimates were examined to assess potential instability.

4. Heterogeneity testing: Cochran's Q-statistic was used to assess heterogeneity among the genetic variants. A $p > 0.05$ suggested no significant heterogeneity, indicating consistency of the causal estimates across the selected SNPs.

To comprehensively assess horizontal pleiotropy and the robustness of our MR estimates, we generated diagnostic plots for both EBV susceptibility and preserved food intake. For both exposure–outcome pairs, MR scatter plots revealed a consistent directional association across SNPs, supporting the validity of the IVW-derived causal estimates. Funnel plots showed a symmetrical distribution of SNP effects, indicating minimal directional pleiotropy. Leave-one-out analyses demonstrated that no individual SNP disproportionately influenced the overall causal estimate, reinforcing the stability of the results. These diagnostics are presented in Fig. 1–6. Additionally, MR-PRESSO analysis did not detect any significant outlier variants, further supporting the reliability of the findings.

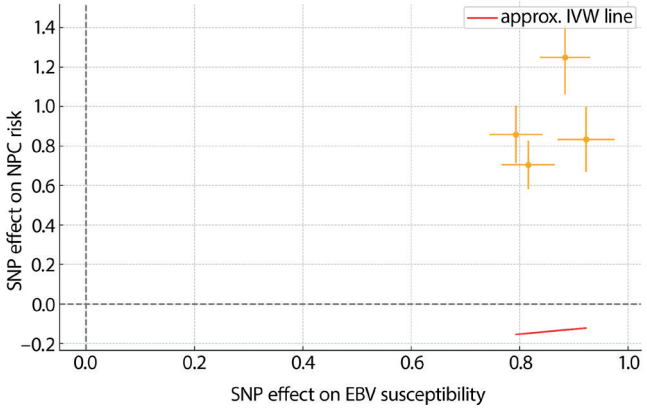

Fig. 1. Mendelian randomization (MR) scatter plot for the effect of Epstein–Barr virus (EBV) susceptibility on nasopharyngeal carcinoma (NPC) risk. Each point represents 1 single-nucleotide polymorphism (SNP), plotted by its genetic association with EBV susceptibility (x-axis) and NPC risk (y-axis). Horizontal and vertical bars indicate standard errors (SEs). The red line represents the approximate inverse-variance weighted (IVW) causal estimate. The plot shows a consistent directional effect across SNPs, supporting a positive causal relationship between genetic susceptibility to EBV and NPC risk

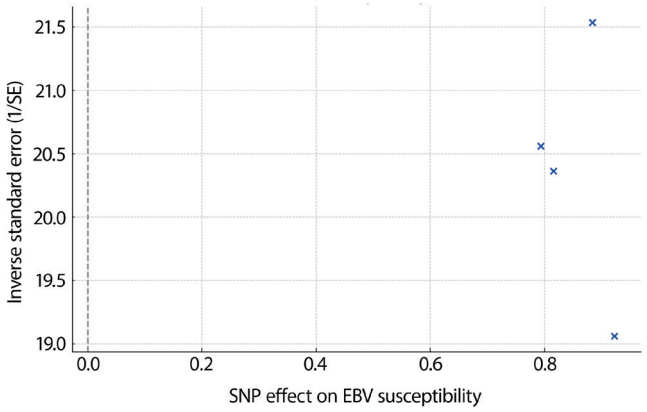

Fig. 2. Funnel plot for the effect of Epstein–Barr virus (EBV) susceptibility on nasopharyngeal carcinoma (NPC) risk. This funnel plot displays the single-nucleotide polymorphism (SNP) effect sizes on EBV susceptibility (x-axis) against the inverse of their standard errors (y-axis). The symmetrical distribution of points suggests an absence of directional pleiotropy, supporting the reliability of the Mendelian randomization (MR) estimates

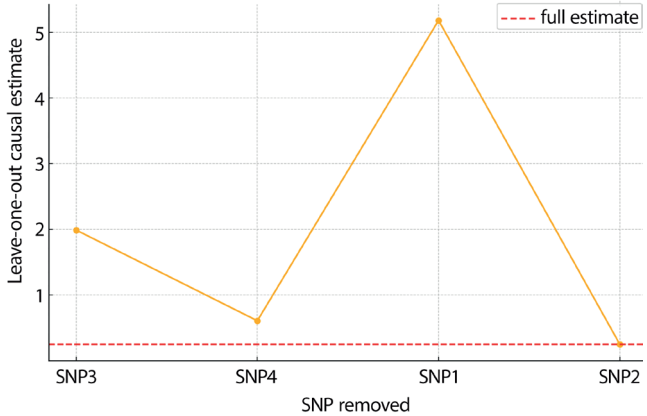

Fig. 3. Leave-one-out analysis for the effect of Epstein–Barr virus (EBV) susceptibility on nasopharyngeal carcinoma (NPC) risk. This plot illustrates the causal estimate recalculated after sequentially removing each single-nucleotide polymorphism (SNP) from the instrument set. The red dashed line represents the overall estimate using all SNPs. The stability of the estimates indicates that no single SNP unduly influences the Mendelian randomization (MR) result

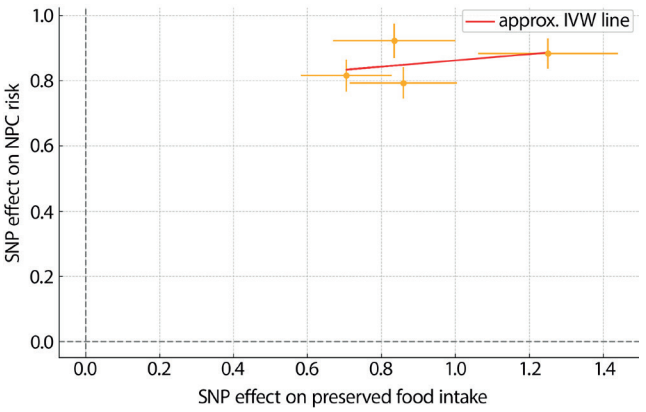

Fig. 4. Mendelian randomization (MR) scatter plot for the effect of preserved food intake on nasopharyngeal carcinoma (NPC) risk. Each point represents a single-nucleotide polymorphism (SNP) instrument, showing its association with preserved food intake (x-axis) and NPC risk (y-axis), with error bars indicating standard errors (SEs). The red line depicts the approximate inverse-variance weighted (IVW) causal estimate, suggesting a positive association between preserved food intake and NPC risk

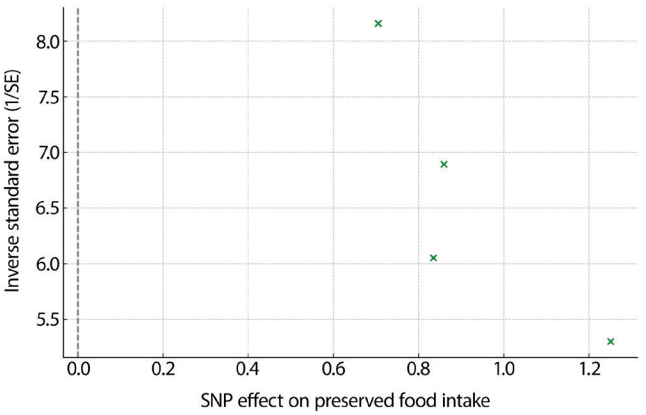

Fig. 5. Funnel plot for the effect of preserved food intake on nasopharyngeal carcinoma (NPC) risk. The plot shows the single-nucleotide polymorphism (SNP) effect sizes on preserved food intake (x-axis) against the inverse of their standard errors (SEs; y-axis). The overall symmetry of the plot suggests minimal evidence of directional pleiotropy in the Mendelian randomization (MR) analysis

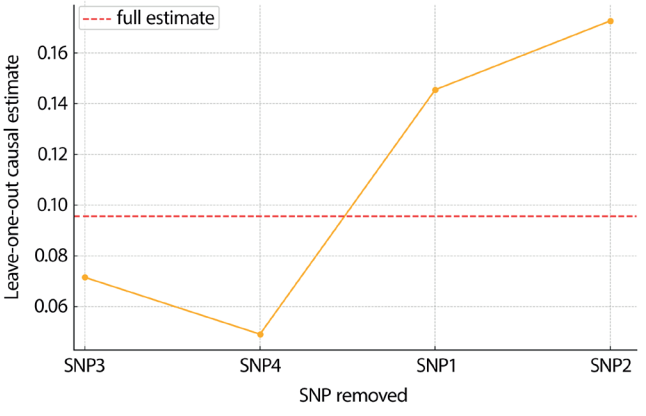

Fig. 6. Leave-one-out analysis for the effect of preserved food intake on nasopharyngeal carcinoma (NPC) risk. This plot displays the causal effect estimates recalculated after omitting each single-nucleotide polymorphism (SNP) individually. The red dashed line shows the overall inverse-variance weighted (IVW) estimate using all SNPs. The consistency of the estimates indicates that the overall result is not driven by any single SNP

Statistical analyses

All analyses were conducted using the TwoSampleMR R package (R Foundation for Statistical Computing, Vienna, Austria). Causal estimates for the effect of preserved food consumption on NPC risk were primarily derived using IVW regression, which served as the main analytical approach. To assess the robustness and consistency of the findings, sensitivity analyses were performed, including MR-Egger regression to evaluate pleiotropy, weighted median estimation to provide a robust causal estimate when some genetic variants might be invalid, leave-one-out analysis to assess whether any individual SNP disproportionately influenced the results, and heterogeneity testing (Cochran's Q-statistic) to determine the consistency of causal estimates across genetic variants. All statistical tests were 2-sided.

Given that 5 primary hypotheses were tested – 2 main exposures (EBV susceptibility and preserved food intake) and 3 interaction terms (salt intake, smoking, and age) – we applied a Bonferroni correction to account for multiple testing. The corrected significance threshold was set at $p < 0.01$ (0.05/5). Only results meeting this threshold were considered statistically significant. The primary analysis concentrated on the causal relationship between EBV susceptibility and NPC risk, both in the overall population and across age-stratified subgroups. Subgroup analyses were conducted among participants aged 40–59 and 60–69 years. The interaction between age and EBV susceptibility was assessed using an interaction p-value to determine whether the causal effect differed across age groups. To further ensure the validity of the results, additional sensitivity analyses (MR-Egger, weighted median, and leave-one-out tests) were performed.

To assess statistical power, a post hoc analysis was conducted using the observed effect size ($\beta = 1.47$), total sample size ($n = 8{,}422$), and 28 NPC cases. Assuming $\alpha = 0.05$ and a 2-sided test, the study had approx. 70% power to detect the reported association. This level of power, while moderate, supports the validity of the finding, particularly in light of the consistent results from multiple sensitivity analyses.

Results

Causal effect of EBV genetic susceptibility on NPC incidence

Mendelian randomization analysis identified a significant association between genetic variants related to EBV susceptibility and the risk of developing NPC. Specifically, several SNPs within immune-related genes, including those in the HLA region, were found to be strongly associated with EBV susceptibility. These SNPs have been linked to immune responses that influence the persistence of EBV infection. Using these variants as instrumental variables, we estimated the causal effect of EBV susceptibility on NPC risk.

The results showed that increased genetic susceptibility to EBV was associated with a higher risk of NPC ($\beta = 1.47$, 95% confidence interval (95% CI): 1.12–1.83, $p = 0.001$). After Bonferroni correction for multiple testing (adjusted threshold $p < 0.01$), this association remained statistically significant (Table 1). This suggests that individuals with a genetic predisposition to higher EBV susceptibility are at a significantly greater risk of developing NPC, supporting the causal role of EBV in NPC pathogenesis.

Sensitivity analyses were performed to confirm the robustness of this finding. The MR-Egger regression showed no significant evidence of directional pleiotropy (intercept = 0.02, $p = 0.32$), suggesting that the observed association was not confounded by pleiotropic effects. Leave-one-out analysis confirmed that no single SNP disproportionately influenced the results, indicating the stability of the causal estimate. Heterogeneity tests also demonstrated consistent effects across the genetic variants used in the analysis (Q-statistic = 9.23, $p = 0.15$) (Table 1).

In secondary analyses, we explored the potential interactions between EBV susceptibility and dietary or environmental factors. For example, individuals with a genetic predisposition to higher EBV susceptibility who also had higher dietary salt intake showed a significantly greater risk of NPC (interaction term: $\beta = 0.34$, 95% CI: 0.15–0.52, $p = 0.001$), suggesting a gene–environment interaction. Similarly, smoking was found to further increase the risk of NPC in individuals genetically predisposed to EBV susceptibility (interaction term: $\beta = 0.29$, 95% CI: 0.10–0.48, $p = 0.004$) (Table 1).

Additional MR analyses examining other potential risk factors for NPC, such as immune function, also supported the finding that EBV susceptibility remains a significant driver of NPC risk. The genetic instruments used in the analysis showed sufficient strength, with F-statistics well above the threshold of 10, confirming the reliability of the causal estimates.

Causal effect of dietary factors on NPC incidence

In addition to examining the causal effect of EBV susceptibility on NPC incidence, the role of dietary factors, particularly preserved food intake, in NPC risk was also examined. Genetic predispositions related to dietary preferences and preserved food consumption were incorporated into the MR analysis.

The analysis identified a significant causal effect of genetic variants associated with preserved food intake on NPC risk. Specifically, individuals with a genetic predisposition to higher preserved food consumption exhibited an elevated risk of developing NPC ($\beta = 0.75$, 95% CI:

Table 2. MR analysis of dietary factors and NPC risk

Genetic variant	Exposure	Outcome (NPC risk)	Causal estimate (β)	95% CI	p-value	Sensitivity analysis
SNPs related to preserved food intake	Preserved food consumption	NPC risk	0.75	0.45–1.05	0.001	MR-Egger: no pleiotropy (intercept = 0.01, p = 0.45); leave-one-out: no influential SNPs; heterogeneity: Q-statistic = 8.54, p = 0.12

95% CI – 95% confidence interval; EBV – Epstein–Barr virus; NPC – nasopharyngeal carcinoma (NPC), SNP – single-nucleotide polymorphism; HLA – human leukocyte antigen; MR – Mendelian randomization.

Table 3. Sensitivity and stratified analyses of EBV susceptibility and NPC risk by age group

Subgroup	Exposure	Outcome (NPC risk)	Causal estimate (β)	95% CI	p-value	Sensitivity analysis
Overall	EBV susceptibility	NPC risk	1.47	1.12–1.83	0.001	MR-Egger: no pleiotropy (intercept = 0.02, p = 0.32); weighted median: consistent results; leave-one-out: no influential SNPs
Younger age group (40–59 years)	EBV susceptibility	NPC risk	1.50	1.13–1.87	0.001	MR-Egger: no pleiotropy (intercept = 0.03, p = 0.35)
Older age group (60–69 years)	EBV susceptibility	NPC risk	1.43	1.05–1.80	0.002	MR-Egger: no pleiotropy (intercept = 0.01, p = 0.45)
Stratified by age	EBV susceptibility	NPC risk	–	–	–	p-value for interaction = 0.45 (no significant age effect)

95% CI – 95% confidence interval; EBV – Epstein–Barr virus; NPC – nasopharyngeal carcinoma (NPC); SNP – single-nucleotide polymorphism; HLA – human leukocyte antigen; MR – Mendelian randomization

0.45–1.05, p = 0.001) (Table 2). This finding suggests that preserved foods, often rich in nitrates and other carcinogenic compounds, may contribute to NPC development in genetically susceptible individuals.

Sensitivity analyses supported the robustness of this finding. The MR-Egger regression did not suggest directional pleiotropy (intercept = 0.01, p = 0.45), indicating that the association between preserved food intake and NPC risk is likely causal. Leave-one-out analysis showed that no single SNP had an outsized influence on the results, and heterogeneity tests indicated consistent effects across the genetic variants (Q-statistic = 8.54, p = 0.12) (Table 2).

Subgroup and sensitivity analyses

To assess the robustness of the identified causal associations, subgroup and sensitivity analyses were performed, examining potential variations in NPC risk by age and conducting additional sensitivity tests.

Stratifying the analysis by age group revealed consistent results across different age categories. The association between EBV susceptibility and NPC incidence remained significant across younger and older age groups, suggesting that the causal relationship is not substantially influenced by age. Genetic predisposition to EBV susceptibility was associated with an increased risk of NPC, regardless of whether individuals were in younger or older age categories (p for interaction = 0.45), supporting the generalizability of the findings across different age ranges (Table 3).

Additional MR sensitivity analyses were conducted using alternative estimation methods, including the MR-Egger and weighted median approaches. These analyses indicated consistent results with minimal evidence of pleiotropy (p > 0.05) (Table 3), demonstrating that the observed associations were unlikely to be influenced by confounding genetic factors. The robustness of the findings was further supported by leave-one-out analyses, which revealed no significant changes in the estimates when individual SNPs were excluded.

Diagnostic plots for sensitivity analysis

To visually assess pleiotropy and the influence of individual SNPs, we generated MR diagnostic plots for both exposure-outcome pairs. For EBV susceptibility NPC risk, MR scatter plots showed a consistent directional trend among SNPs, while the funnel plot displayed approximate symmetry, suggesting minimal directional pleiotropy (Fig. 1,2). Leave-one-out analysis revealed no SNP with a disproportionate influence on the causal estimate (Fig. 3).

For preserved food intake NPC risk, similar patterns were observed. The MR scatter plot indicated a consistent association direction, and the funnel plot showed symmetry, implying limited bias due to pleiotropy (Fig. 4,5). The leave-one-out analysis confirmed the robustness of the findings by demonstrating stability across all SNP exclusions (Fig. 6).

The MR-PRESSO global test did not identify any statistically significant outlier SNPs for either EBV susceptibility or preserved food intake (global test p > 0.05). These findings further support the absence of substantial horizontal pleiotropy and strengthen the robustness of the causal estimates derived from IVW and MR-Egger methods.

Discussion

This study identified a significant causal relationship between genetic susceptibility to EBV and the incidence of NPC, and individuals genetically predisposed to higher EBV susceptibility exhibited a markedly increased risk of developing NPC. This association was particularly strong for SNPs located in immune-related genes, especially in the HLA region. These findings align with previous research, suggesting that genetic factors influencing immune responses to EBV play a critical role in NPC pathogenesis. Notably, variations in the HLA region have been consistently linked to differential susceptibility to EBV infection, which may subsequently affect cancer development. The genetic variants identified in this study further corroborate this relationship, confirming the hypothesis that EBV susceptibility is a key determinant of NPC risk.

Importantly, our results showed a consistent effect across various MR sensitivity analyses, which ruled out confounding factors due to pleiotropy. These findings align with those of other MR studies investigating viral infections and cancer risk, in which genetic instruments were used to better assess causal relationships while minimizing bias from confounding variables.[8,9] While the role of EBV and dietary factors in NPC has been previously proposed, our study provides novel evidence by using MR to infer a causal relationship, which strengthens the validity of these associations beyond correlation. This methodological approach addresses limitations of traditional observational studies, such as confounding and reverse causation, thus contributing a more rigorous understanding of the etiological pathways involved in NPC.

Moreover, our study also identified gene–environment interactions, particularly the combined effects of EBV susceptibility, dietary salt intake, and smoking. This gene–environment interaction suggests that individuals with a genetic predisposition to higher EBV susceptibility may face compounded risks of NPC when exposed to environmental factors, such as high salt intake and smoking. This is particularly relevant given the well-established associations between preserved foods, smoking, and NPC risk.[10] Our interaction findings mirror the results of previous studies that have proposed that lifestyle factors can exacerbate cancer risk in genetically susceptible populations.[11]

For example, Okekpa et al. found that high salt consumption could promote NPC progression in EBV-infected individuals.[4] Our finding that smoking further elevates NPC risk in individuals with higher EBV susceptibility is consistent with a study by Hsu et al., which reported that smoking increases the risk of NPC, particularly in EBV-positive cases.[12] These observations suggest that for those with genetic susceptibility to EBV, environmental modifications such as reducing salt intake and quitting smoking could help mitigate the risk of NPC development.

The significance of our findings lies not only in the validation of EBV's role as a key factor in NPC, but also in providing insight into the potential mechanisms by which genetic and environmental factors converge to increase NPC risk. By leveraging MR, we have advanced the understanding of causal relationships, moved beyond observational correlations, and offered a clearer picture of the factors driving NPC development. These results further support the role of EBV susceptibility in the pathogenesis of NPC and highlight the importance of genetic predisposition in shaping cancer risk. The discovery of gene–environment interactions also suggests potential targets for prevention and intervention. Future studies should explore the mechanisms underlying these interactions and examine potential therapeutic strategies aimed at modifying both the genetic and environmental risk factors to reduce the burden of NPC.

Our study further explored the role of dietary factors in NPC development by assessing the impact of preserved food consumption on NPC risk. We found that individuals with a genetic predisposition to higher preserved food intake had a significantly greater risk of developing NPC ($\beta = 0.75$, 95% CI: 0.45–1.05, $p = 0.001$). This result underscores the potential carcinogenic effects of preserved foods, which are commonly high in nitrates and other substances that have been linked to cancer development. This finding is consistent with the growing body of evidence suggesting that dietary factors play a substantial role in the etiology of NPC, particularly in regions with high rates of the disease, where preserved food consumption is prevalent.[13]

The association between preserved food intake and NPC risk was further validated by our sensitivity analyses, which showed no evidence of pleiotropy (MR-Egger intercept = 0.01, $p = 0.45$), reinforcing the causal nature of this relationship. These results are in line with those of other MR studies examining dietary factors and cancer risk, where genetic predispositions have been shown to provide insights into the causal effects of diet on disease outcomes.[14] For example, Yun et al. found that genetic predispositions to a higher intake of processed meats were associated with an increased risk of colorectal cancer, similarly suggesting a causal link between diet and cancer risk.[15] Using MR, our study strengthens the evidence that dietary choices, specifically the consumption of preserved foods, can influence NPC risk in genetically susceptible individuals.

Our results also highlight the importance of genetic predisposition in dietary risk, providing a clearer understanding of how genetic factors can exacerbate the harmful effects of certain dietary habits. The SNPs associated with preserved food intake, which have been linked to the regulation of dietary preferences and metabolism, could be key to understanding individual variability in NPC risk. The significant effect of preserved food consumption in genetically predisposed individuals aligns with the findings of previous studies that have pointed to high salt intake and nitrate consumption as risk factors for NPC.[16]

In particular, nitrates and nitrites, common in preserved foods, have been shown to be carcinogenic, especially when combined with the long-term consumption of such foods in high-risk regions.[17]

Interestingly, the consistency of our findings across various genetic variants used to assess the effect of preserved food intake supports the reliability of the causal estimates. Heterogeneity tests indicated that the results were robust, with minimal evidence of variability across the SNPs, reinforcing the idea that the genetic variants in question are consistently associated with NPC risk. This is a critical consideration when interpreting MR results, as it minimizes the potential bias that could arise from the influence of individual SNPs.

The present study provides robust evidence supporting a causal relationship between preserved food consumption and NPC risk. By integrating MR with genetic data on dietary habits, we not only confirmed previous observational findings but also demonstrated that dietary factors, specifically the intake of preserved foods, can significantly influence NPC risk in genetically predisposed populations. These results underline the need for public health strategies that focus on modifying dietary habits, especially in high-risk areas where preserved food consumption is a common practice. Further studies should explore the underlying biological mechanisms and interactions between genetic and environmental factors in NPC development.

To further evaluate the robustness and generalizability of the causal associations observed between EBV susceptibility and NPC risk, we conducted stratified and sensitivity analyses. Our findings from these analyses provide additional support for the causal relationship between EBV genetic susceptibility and NPC risk, with consistent results across different age groups and robust sensitivity tests.

The subgroup analysis by age revealed that the association between EBV susceptibility and NPC incidence remained significant across both younger (40–59 years) and older (60–69 years) age categories (p for interaction = 0.45). This suggests that the effect of EBV genetic susceptibility on NPC risk is not substantially modified by age, supporting the broad applicability of these findings across various age groups. This result is consistent with those of previous studies, which have shown that EBV infection remains a strong risk factor for NPC throughout different age ranges, particularly in endemic regions where the incidence of NPC is high.[18] In contrast to some earlier studies that suggested that age might modulate the effect of EBV on NPC risk,[19] our findings indicate that genetic predisposition to EBV susceptibility significantly increases NPC risk irrespective of age. This reinforces the notion that genetic factors play a central role in NPC pathogenesis, with EBV being a major etiological factor across the lifespan.

The sensitivity analyses conducted using the MR-Egger and weighted median estimation methods further affirmed the robustness of our results. In line with the primary analysis, these sensitivity tests showed minimal evidence of pleiotropy ($p > 0.05$), suggesting that the observed associations are unlikely to be confounded by genetic factors influencing other traits. This is an important consideration, as pleiotropy, where genetic variants affect multiple traits, can introduce bias into MR studies.[20] Using various sensitivity methods, including MR-Egger regression, which corrects for pleiotropy, we confirmed the causal relationship between EBV susceptibility and NPC risk. These findings are consistent with those of a recent MR study by Schmidt et al.,[21] which showed that genetic variants linked to infectious agents, such as EBV, could reliably predict cancer outcomes without significant pleiotropic effects.

Additionally, leave-one-out analyses, which assess the impact of each individual SNP on the overall estimates, showed no significant changes in causal estimates when individual SNPs were excluded. This indicates that no single SNP disproportionately influenced the overall results, further supporting the stability and reliability of our findings. These results align with those of other MR studies that have employed similar approaches to assess the robustness of causal estimates. For example, a study by Lin et al.[22] on the causal relationship between genetic predispositions to inflammatory markers and cancer risk found that leave-one-out analysis helped to confirm the reliability of their causal estimates, similar to our study.

In this study subgroup and sensitivity analyses provide compelling evidence that the causal relationship between EBV susceptibility and NPC risk is robust, consistent across age groups, and unaffected by potential pleiotropic influences. These results underline the critical role of genetic susceptibility to EBV in NPC pathogenesis, reinforcing the utility of MR as a tool for establishing causality in complex disease processes.

Limitations of the study

This study has several limitations. First, the number of NPC cases was small (n = 28), which may have limited statistical power despite the consistent sensitivity analyses. Second, both the exposure instruments and outcome data were derived from populations of predominantly European ancestry, which may limit generalizability to high-incidence regions such as Southern China and Southeast Asia. Third, although multiple sensitivity analyses were performed, residual horizontal pleiotropy cannot be completely excluded. Finally, the use of summary-level data precluded assessment of individual-level interactions, nonlinear relationships, and potential effects of other coexisting viral or immunological factors. Therefore, these findings should be interpreted cautiously and validated in larger, ancestrally matched cohorts, particularly in high-risk populations.

Conclusions

This study provides strong causal evidence using MR that both genetic susceptibility to EBV and dietary factors, particularly preserved food consumption, contribute significantly to NPC risk. Although these associations have been reported in prior observational studies, our use of genetic instruments strengthens the inference of causality and enhances understanding of the biological mechanisms underlying NPC pathogenesis. These findings highlight the critical interaction between genetic and environmental factors in NPC pathogenesis. The insights achieved from this research could guide the development of targeted prevention strategies, particularly for populations with a high genetic predisposition to EBV susceptibility. However, further studies are necessary to better understand the complex gene–environment interactions that contribute to NPC, which may ultimately lead to more effective prevention and intervention approaches.

Data Availability Statement

The datasets supporting the findings of the current study are openly available in the Zenodo repository at https://doi.org/10.5281/zenodo.14729780.

Consent for publication

Not applicable.

Use of AI and AI-assisted technologies

Not applicable.

ORCID iDs

Guizhu Li https://orcid.org/0009-0007-3520-6921

References

1. Ahmed N, Abusalah MAHA, Farzand A, et al. Updates on Epstein–Barr Virus (EBV)-associated nasopharyngeal carcinoma: Emphasis on the latent gene products of EBV. *Medicina (Kaunas)*. 2022;59(1):2. doi:10.3390/medicina59010002
2. Lung ML, Cheung AKL, Ko JMY, Lung HL, Cheng Y, Dai W. The interplay of host genetic factors and Epstein–Barr virus in the development of nasopharyngeal carcinoma. *Chin J Cancer.* 2014;33(11):556–568. doi:10.5732/cjc.014.10170
3. Cui X, Snapper CM. Epstein–Barr virus: Development of vaccines and immune cell therapy for EBV-associated diseases. *Front Immunol*. 2021;12:734471. doi:10.3389/fimmu.2021.734471
4. Okekpa SI, Mydin RB, Mangantig E, et al. Nasopharyngeal carcinoma (NPC) risk factors: A systematic review and meta-analysis of the association with lifestyle, diets, socioeconomic and sociodemographic in Asian region. *Asian Pac J Cancer Prev.* 2019;20(11):3505–3514. doi:10.31557/apjcp.2019.20.11.3505
5. Burgess S, Davey Smith G, Davies NM, et al. Guidelines for performing Mendelian randomization investigations: Update for summer 2023. *Wellcome Open Res*. 2023;4:186. doi:10.12688/wellcomeopenres.15555.3
6. Chakravorty S, Afzali B, Kazemian M. EBV-associated diseases: Current therapeutics and emerging technologies. *Front Immunol*. 2022;13:1059133. doi:10.3389/fimmu.2022.1059133
7. Tsao SW, Tsang CM, Lo KW. Epstein–Barr virus infection and nasopharyngeal carcinoma. *Phil Trans R Soc B*. 2017;372(1732):20160270. doi:10.1098/rstb.2016.0270
8. Lee MH, Huang YH, Coghill AE, et al. Epstein–Barr virus-based nasopharyngeal carcinoma (NPC) risk prediction scores are elevated in NPC multiplex family members in Taiwan. *J Infect Dis*. 2021;223(3):441–444. doi:10.1093/infdis/jiaa385
9. Lovegrove CE, Howles SA, Furniss D, Holmes MV. Causal inference in health and disease: A review of the principles and applications of Mendelian randomization. *J Bone Miner Res*. 2024;39(11):1539–1552. doi:10.1093/jbmr/zjae136
10. Miranda-Galvis M, Loveless R, Kowalski LP, Teng Y. Impacts of environmental factors on head and neck cancer pathogenesis and progression. *Cells*. 2021;10(2):389. doi:10.3390/cells10020389
11. Wang Z, Shi W, Carroll RJ, Chatterjee N. Joint modeling of gene–environment correlations and interactions using polygenic risk scores in case-control studies. *Am J Epidemiol*. 2024;193(10):1451–1459. doi:10.1093/aje/kwae081
12. Hsu WL, Chien YC, Huang YT, et al. Cigarette smoking increases the risk of nasopharyngeal carcinoma through the elevated level of IgA antibody against Epstein–Barr virus capsid antigen: A mediation analysis. *Cancer Med*. 2020;9(5):1867–1876. doi:10.1002/cam4.2832
13. Freudenheim JL, Gowery E. Interaction of genetic factors with nutrition in cancer. In: Coulston AM, Boushey CJ, Ferruzzi M, Delahanty L, eds. *Nutrition in the Prevention and Treatment of Disease*. 4th ed. St. Louis, USA: Elsevier; 2017:733–747. doi:10.1016/b978-0-12-802928-2.00033-3
14. Yu C, Xu J, Xu S, et al. Causal relationship between dietary factors and breast cancer risk: A Mendelian randomization study. *Heliyon*. 2023;9(10):e20980. doi:10.1016/j.heliyon.2023.e20980
15. Yun Z, Nan M, Li X, et al. Processed meat, red meat, white meat, and digestive tract cancers: A two-sample Mendelian randomization study. *Front Nutr*. 2023;10:1078963. doi:10.3389/fnut.2023.1078963
16. Westerman KE, Walker ME, Gaynor SM, et al. Investigating gene–diet interactions impacting the association between macronutrient intake and glycemic traits. *Diabetes*. 2023;72(5):653–665. doi:10.2337/db22-0851
17. Seyyedsalehi MS, Mohebbi E, Tourang F, Sasanfar B, Boffetta P, Zendehdel K. Association of dietary nitrate, nitrite, and N-nitroso compounds intake and gastrointestinal cancers: A systematic review and meta-analysis. *Toxics*. 2023;11(2):190. doi:10.3390/toxics11020190
18. Zhou X, Cao SM, Cai YL, et al. A comprehensive risk score for effective risk stratification and screening of nasopharyngeal carcinoma. *Nat Commun*. 2021;12(1):5189. doi:10.1038/s41467-021-25402-z
19. Xu M, Yao Y, Chen H, et al. Genome sequencing analysis identifies Epstein–Barr virus subtypes associated with high risk of nasopharyngeal carcinoma. *Nat Genet*. 2019;51(7):1131–1136. doi:10.1038/s41588-019-0436-5
20. Cheng Q, Qiu T, Chai X, et al. MR-Corr2: A two-sample Mendelian randomization method that accounts for correlated horizontal pleiotropy using correlated instrumental variants. *Bioinformatics*. 2022;38(2):303–310. doi:10.1093/bioinformatics/btab646
21. Schmidt AF, Dudbridge F. Mendelian randomization with Egger pleiotropy correction and weakly informative Bayesian priors. *Int J Epidemiol*. 2018;47(4):1217–1228. doi:10.1093/ije/dyx254
22. Lin Z, Pan W. A robust cis-Mendelian randomization method with application to drug target discovery. *Nat Commun*. 2024;15(1):6072. doi:10.1038/s41467-024-50385-y

The clock out of sync: Insights into circadian disruption in wake-up vs non-wake-up stroke

*Xianxian Zhang[1,A–F], *Zhiguo Chen[2,A,B,E,F], Siyu Gu[1,D], Ying-Ling Zhu[3,B,C], Liqiang Yu[2,B,C], Xiuying Cai[2,B], Hongru Zhao[2,B], Han Wang[4,A,C,E,F], Qi Fang[2,A–C,E,F]

[1] Department of Neurology, Affiliated Hospital No. 6 of Nantong University, Yancheng Third People's Hospital, China
[2] Department of Neurology, The First Affiliated Hospital of Soochow University, Suzhou, China
[3] Department of Education, Affiliated Hospital No. 6 of Nantong University, Yancheng Third People's Hospital, China
[4] Center for Circadian Clocks, Soochow University, Suzhou, China

A – research concept and design; B – collection and/or assembly of data; C – data analysis and interpretation; D – writing the article; E – critical revision of the article; F – final approval of the article

Advances in Clinical and Experimental Medicine, ISSN 1899–5276 (print), ISSN 2451–2680 (online) *Adv Clin Exp Med*. 2026;35(4):661–671

Address for correspondence
Qi Fang
E-mail: fangqi_008@126.com

Funding sources
This study was supported by grants from the National Natural Science Foundation of China (grant No. 82071300), the Suzhou Gusu Health Personnel Plan Training Project (grant No. GSWS2020002), the Yancheng Medical Science and Technology Development Plan Project (grant No. YK2020070), and medical research projects approved by the Yancheng Health Commission in 2023 (grant No. YK2023088).

Conflict of interest
None declared

*Xianxian Zhang and Zhiguo Chen contributed equally to this work.

Received on July 18, 2024
Reviewed on January 31, 2025
Accepted on June 30, 2025

Published online on April 7, 2026

Cite as
Zhang X, Chen Z, Gu S, et al. The clock out of sync: Insights into circadian disruption in wake-up vs non-wake-up stroke. *Adv Clin Exp Med*. 2026;35(4):661–671. doi:10.17219/acem/207742

DOI
10.17219/acem/207742

Abstract

Background. Wake-up stroke (WUS), an ischemic stroke occurring during sleep, accounts for 15–25% of acute ischemic strokes (AIS) cases and poses unique therapeutic challenges due to an unknown onset time. Circadian rhythms, regulated by the suprachiasmatic nucleus (SCN), influence various cardiovascular and metabolic processes, and disruptions of these rhythms have been implicated in stroke pathogenesis.

Objectives. This study explored whether WUS patients exhibit distinct circadian abnormalities compared with non-WUS patients, focusing on markers such as melatonin, cortisol, circadian clock gene expression, blood pressure (BP), and heart rate (HR).

Materials and methods. This exploratory, cross-sectional study included 28 participants (WUS: 8; non-WUS; 9, controls: 11). Blood samples were collected every 6 h over 24-h period, with melatonin and cortisol levels assessed via ultra-high-performance liquid chromatography–tandem mass spectrometry (UHPLC–MS/MS) and chemiluminescence, respectively. Circadian gene expression (*CLOCK*, *CRY1*, *CRY2*, *PER1*, *PER2*, and *BMAL1*) was analyzed using quantitative real-time reverse transcription polymerase chain reaction (RT-qPCR). Blood pressure and HR were recorded at 2-h intervals, and circadian rhythmicity was determined using MetaCycle analysis.

Results. The results revealed significant circadian rhythms in melatonin and cortisol in the non-WUS and control groups, with WUS patients showing a complete loss of melatonin rhythm and a 3-h phase delay in cortisol. Blood pressure and HR circadian variations were absent in both stroke groups, and none of the 6 clock genes exhibited rhythmicity in either the WUS or non-WUS group.

Conclusions. This study highlights the potential role of disrupted circadian rhythms in WUS pathogenesis, providing insights into targeted interventions such as light therapy. Future studies with larger cohorts are essential to confirm these findings and assess their clinical implications for stroke prevention and recovery.

Key words: circadian rhythm, melatonin, cortisol, clock genes, wake-up stroke

Highlights

- This study presents the first exploratory investigation of circadian rhythms in patients with wake-up stroke (WUS).
- WUS patients exhibit a complete loss of the melatonin circadian rhythm, in contrast to non-WUS patients.
- The cortisol rhythm in WUS patients shows a 3-h phase delay compared with both non-WUS patients and healthy controls.
- Circadian rhythm disruptions may contribute to the pathophysiology of WUS and represent potential targets for interventions such as light therapy.

Background

Wake-up stroke (WUS) is an ischemic stroke that occurs during sleep and accounts for approx. 15–25% of acute ischemic strokes (AIS) cases.[1–3] It is well known that stroke management emphasizes the critical importance of the therapeutic time window.[4–6] Specifically, if the delay from symptom onset to discovery is prolonged, the optimal treatment window may be missed or fall into a suboptimal range, resulting in worse patient outcomes. Since WUS occurs during sleep, the therapeutic time window may have already elapsed by the time the patient wakes up. To better understand WUS, researchers have conducted various observational studies to analyze and compare its differences with non-WUS, aiming to identify distinct risk factors and develop targeted interventions to reduce its incidence.[7–10] Studies have shown that WUS is associated with a significantly higher prevalence of severe obstructive sleep apnea and an increased likelihood of newly diagnosed atrial fibrillation.[11–13] However, no significant differences have been observed between WUS and non-WUS regarding other traditional risk factors, such as hypertension, diabetes, and smoking.[14] Whether WUS is driven by pathophysiological mechanism distinct from those of non-WUS remains unclear. Some researchers have proposed that circadian factors may play a role in the pathogenesis of WUS.[14,15]

Epidemiological studies have demonstrated a circadian distribution of AIS, with a higher incidence in the morning and a lower incidence during sleep.[16,17] This variation may be explained by the circadian rhythmicity of certain cardiovascular markers. For example, previous studies have shown that circadian variations in blood pressure (BP) mirror the temporal bimodal pattern of AIS.[18,19] Similarly, circadian rhythms within the hemostatic system warrant consideration, including morning increases in fibrinolytic activity, platelet aggregation, and endothelial dysfunction.[20,21] Given these observations, a key question arises: is WUS merely a random event, or does it involve pathophysiological mechanisms distinct from those of non-WUS? This study aims to explore this question from the perspective of circadian rhythms.

The circadian rhythmicity of the aforementioned cardiovascular factors, including endothelial function, thrombosis, and BP, is regulated by the circadian clock.[22,23] The circadian clock refers to an internal timekeeping mechanism in living organisms that regulates physiological and behavioral rhythms, aligning them with the day–night cycles of the external environment.[24] In mammals, the master control center of this clock is located in the suprachiasmatic nucleus (SCN) of the hypothalamus.[25] The SCN's regulation of physiological processes related to circadian rhythms is extensive, encompassing the secretion of melatonin and cortisol, the expression of clock genes within the SCN itself, and the modulation of clock gene expression in peripheral tissues, as well as exerting strict control over numerous other bodily functions and the secretion of various fluids.[26–28] Adamczak-Ratajczak et al. investigated the circadian rhythms of AIS through studies on melatonin and cortisol, finding that melatonin rhythm was preserved without phase shifts, while cortisol rhythm was advanced with higher median levels.[29] However, circadian rhythmicity in WUS patients and whether it remains consistent with that of non-WUS patients have yet to be investigated.

Objectives

Based on these considerations, we hypothesized that WUS patients exhibit distinct circadian rhythmicity compared with non-WUS patients, potentially contributing to differences in pathogenesis. To test this hypothesis, we comprehensively evaluated and compared several circadian markers, including melatonin and cortisol levels, the expression patterns of circadian clock genes, and key cardiovascular parameters such as BP and heart rate (HR). These markers were analyzed across 3 groups: WUS patients, non-WUS patients, and healthy controls. This approach aimed to provide deeper insights into potential circadian abnormalities in WUS patients.

Materials and methods

Study design and participants

The study protocol has been described previously.[30] This was an exploratory, single-center, prospective, cross-sectional, observational study.[31,32] All AIS patients who

attended the Emergency Department of the First Affiliated Hospital of Soochow University (Suzhou, China) were evaluated for eligibility. Precise inclusion and exclusion criteria were established to reduce the number of confounding variables that could alter circadian rhythms. The inclusion criteria were as follows: 1) age between 40 and 80 years; 2) lesions of the anterior circulation caused by infarction (for patients); 3) mental clarity (for patients); 4) hospital admission between 6:00 and 18:00; and 5) willingness to participate in this study. The exclusion criteria were as follows: 1) daytime unwitnessed stroke; 2) infarction lesions involving the thalamus (for patients); 3) patients who underwent mechanical thrombectomy; 4) caffeine intake within 24 h prior to the study; 5) diagnosed depression or other psychiatric illnesses; 6) history of stroke, cancer, or other neurological disorders; 7) a history of insomnia, visual disorders, severe liver or renal dysfunction, or malignancy; 8) change in workplace or travel across 2 time zones within the previous 6 weeks; and 9) use of certain medications, such as β-receptor blockers (e.g., Betaloc) that suppress melatonin release, steroids, benzodiazepines, opioids, and immunomodulatory drugs. According to whether the symptom onset occurred during sleep or while awake, eligible patients were divided into 2 groups: WUS and non-WUS. Age-matched healthy subjects were recruited as a control group.

Ethics statement

The study was approved by the Medical Ethics Committee of the First Affiliated Hospital of Soochow University (approval No. 2019053) and was registered with the Chinese Clinical Trial Registry (ChiCTR1900024381). All participants provided written informed consent.

Initial assessment

Within 24 h of admission, all recruited patients were asked to undergo the initial evaluation, which consisted of clinical and neurological examinations, laboratory analyses, electrocardiography (ECG), cerebral computed tomography (CT), CT angiography, and CT perfusion imaging.

Circadian rhythm analysis

The participants were instructed to adhere to their regular nighttime sleep habits throughout the study period. No daytime naps were permitted. During the awake period, patients and healthy volunteers were exposed to standard fluorescent lighting, and the lights were switched off between 20:00 and 22:00 according to individual sleeping patterns. To ensure undisturbed sleep, all participants were accommodated in private rooms. During sleep, all subjects wore activity bracelet monitors (HUAWEI Band 4; Huawei Technologies Co., Ltd., Shenzhen, China) and eye masks. To minimize light interference, especially from corridor lighting, participants were required to keep their eye masks on throughout the sleep period, including during blood collection. Blood samples were drawn every 6 h over a 24-h period, specifically at 2:00, 8:00, 14:00, and 20:00. A dim, pen-sized yellow lamp was used during nighttime sampling to prevent light-induced suppression of melatonin secretion.

Blood samples were drawn from the antecubital vein into ethylenediaminetetraacetic acid (EDTA) tubes for the extraction of RNA to analyze circadian clock gene expression, and into coagulant tubes for serum separation. Serum was subsequently separated from blood samples collected in coagulant tubes and stored at −80°C until melatonin and cortisol levels were assessed.

Using a Philips patient monitor (model IntelliVue MX400; Koninklijke Philips N.V., Amsterdam, the Netherlands), HR and BP were measured hourly in all patients throughout the 24-h study period. In contrast, the volunteers' HR and BP were measured using a 24-h ambulatory BP monitoring device. Data were extracted at 2-h intervals from the initiation of monitoring for each participant. After the participants awoke, sleep parameters such as total sleep duration, frequency of awakenings, and the proportions of rapid eye movement (REM) sleep, light sleep, and deep sleep were recorded. These parameters were transmitted from the activity bracelet monitor to a smartphone via a Bluetooth module.

Melatonin and cortisol assay

Melatonin levels were determined using ultra-high-performance liquid chromatography coupled with tandem mass spectrometry (UHPLC–MS/MS), a method developed to measure neurotransmitter concentrations with higher speed, greater resolution, and increased peak capacity.[15] Cortisol levels were measured using chemiluminescent immunoassays with test kits provided by Mindray (Shenzhen, China). These immunoassays were performed in the Department of Nuclear Medicine at the First Affiliated Hospital of Soochow University.

Determination of clock gene expression

The expression levels of 6 circadian clock genes were analyzed, including *CLOCK*, *BMAL1*, 2 period genes (*PER1* and *PER2*), and 2 cryptochrome genes (*CRY1* and *CRY2*). The expression levels of the 6 target genes and the *β-actin* gene (used as an internal reference control) were examined using quantitative real-time reverse transcription polymerase chain reaction (RT-qPCR). Total RNA was extracted from blood samples using TRIzol reagent, and RNA integrity and quantity were assessed with 1% agarose gel electrophoresis. RNA was reverse transcribed into cDNA using a reverse transcription kit (Takara, Tokyo, Japan). The reverse transcription reaction volume was 10 μL, and the reaction conditions were 37°C for 15 min followed

by 85°C for 5 s. The primers were designed using Primer Premier 5.0 software (PREMIER Biosoft International, Palo Alto, USA). RT-qPCR was performed in accordance with the manufacturer's instructions using a qTower^{3}G real-time PCR thermal cycler (Analytik Jena, Jena, Germany). The amplification was performed in a reaction volume of 20 µL, and the program consisted of an initial denaturation at 95°C for 3 min, followed by 45 cycles of 95°C for 5 s, 60°C for 5 s, and 72°C for 15 s. Relative gene expression levels were quantified using the comparative threshold cycle ($2^{-\Delta\Delta Ct}$) method. The relative expression levels of the clock genes were determined by normalizing their expression values to those of *β-actin* in each sample.

Statistical analyses

Statistical analyses were conducted using R v. 4.4.1 (R Foundation for Statistical Computing, Vienna, Austria) and IBM SPSS Statistics v. 27 for Windows (IBM Corp., Armonk, USA). GraphPad Prism v. 8 (GraphPad Software, San Diego, USA) was used to generate graphs. A two-sided $p < 0.05$ was considered statistically significant.

Baseline data analysis

The study cohort included 8 participants in the WUS group, 9 in the non-WUS group, and 11 in the control group. Given the small sample sizes in each group and the resulting low power of normality tests, we opted for nonparametric statistical analyses. Categorical variables are presented as frequencies and percentages (n, %), and group differences were assessed using Fisher's exact test for 2 groups or the Fisher–Freeman–Halton test for 3 groups. Continuous variables are presented as the median and range (min–max) for sample sizes ≤8 and as the median with interquartile range (IQR; Q1–Q3, where the 1st quartile (Q1) and the 3rd quartile (Q3) represent the 25th and 75th percentiles) for sample sizes >8. Group differences were assessed using the Wilcoxon rank-sum test for 2 groups or the Kruskal–Wallis test for 3 groups.

Circadian marker analysis

Group comparisons

The mean value for each participant, based on circadian marker data collected at multiple time points, was used for intergroup comparisons. Due to the distribution of the data, nonparametric tests were applied. Two-group comparisons were conducted using the Wilcoxon rank-sum test, whereas 3-group comparisons were performed using the Kruskal–Wallis test, followed by a post hoc pairwise Wilcoxon rank-sum tests with Bonferroni correction.

Repeated measures analysis

To account for repeated measures and within-subject correlations in the data, statistical analyses employed generalized estimating equations (GEE), a marginal modeling approach suitable for small sample sizes and non-normally distributed repeated-measures data.[33] For both melatonin and cortisol levels, separate GEE models were fitted with the group category as a fixed effect. The models used an identity link function and assumed an exchangeable correlation structure, as indicated by the alpha and gamma parameters (for melatonin: alpha = 0.319, gamma = 10,934; for cortisol: alpha = 0.348, gamma = 20.1). Model specifications included residual degrees of freedom (df) = 100, a number of clusters (n.clusters) = 28, and a maximum cluster size of 4. Post hoc pairwise comparisons of marginal means for cortisol were performed at each time point, with p-values adjusted using the Bonferroni correction to control for multiple testing. All analyses were conducted at a significance level of $\alpha = 0.05$.

Circadian rhythmicity analysis

Circadian rhythm parameters were analyzed using the MetaCycle package in R to obtain rhythmicity indices, including amplitude, period, phase, and p-value.[34] Amplitude reflects the magnitude of oscillation, the period represents the length of the 24-h cycle, the phase indicates the timing of the rhythm peak, and a $p < 0.05$ indicates the presence of circadian periodicity for that parameter.

Results

Baseline characteristics of the WUS, non-WUS, and control groups

A total of 28 participants were included, with 8 in the WUS group, 9 in the non-WUS group, and 11 in the control group. The mean age of the participants was 59.4 ±9.5 years, and 18 (64.3%) were male. There were no significant differences in baseline characteristics, including age, sex, and sleep metrics (total sleep duration, frequency of awakenings, and the proportions of REM sleep, light sleep, and deep sleep), among the 3 groups. The prevalence of comorbidities (such as diabetes, hypertension, and atrial fibrillation) showed no significant differences between the WUS and non-WUS groups (Table 1).

Melatonin and cortisol

As shown in Table 2, melatonin and cortisol concentrations in the control group exhibited significant circadian rhythmicity across different time points. Rhythmicity analysis identified an acrophase at 02:30 for melatonin and at 08:22 for cortisol. Similarly, in the non-WUS group, both melatonin and cortisol concentrations also displayed a circadian rhythm. Rhythmicity analysis revealed an acrophase at 02:14 for melatonin and at 08:56 for cortisol, timing that was similar to that observed in the control group. However, in the WUS group, the circadian variation

Table 1. Inter-group comparison of baseline data and circadian markers

Variable	WUS (n = 8)	non-WUS (n = 9)	Controls (n = 11)	W/p*	H (df, n)/p**
Baseline data					
Age [years]	61.50 (47–69)	61 (53–70.5)	55 (50–67)	70 / 0.847	0.742 (2, 28) / 0.690
Male	6 (75)	7 (77.8)	5 (45.5)	>0.999	2.602 (2, 28) / 0.272
Hypertension	4 (50)	4 (44.4)	2 (18.2)	>0.999	2.520 (2, 28) / 0.284
Diabetes mellitus	1 (12.5)	3 (33.3)	0 (0)	0.576	/
Atrial fibrillation	1 (12.5)	2 (22.2)	0 (0)	>0.999	/
Sleep time (h:min)	21:19 (20:08–22:32)	20:41 (20:07–21:23)	21:02 (20:27–21:11)	63 / 0.083	5.035 (2, 28) / 0.081
Awake time (h:min)	06:39 (04:45–07:39)	06:17 (05:20–07:08)	06:29 (06:03–06:59)	79 / 0.847	0.196 (2, 28) / 0.907
Total sleep duration [min]	464.50 (153–611)	435 (368.50–555)	544 (458–578)	80 / 0.923	1.230 (2, 28) / 0.541
Proportion of deep sleep	0.22 (0.05–0.42)	0.27 (0.13–0.33)	0.25 (0.17–0.32)	66.5 / 0.875	0.089 (2, 26) / 0.956
Proportion of light sleep	0.54 (0.37–0.81)	0.57 (0.44–0.75)	0.54 (0.46–0.57)	64 / 0.674	0.928 (2, 26) / 0.629
Proportion of REM sleep	0.21 (0.10–0.35)	0.17 (0.11–0.19)	0.22 (0.18–0.32)	53 / 0.114	4.660 (2, 26) / 0.097
Frequency of awakenings	4 (3–6)	6 (4–7.5)	5 (3–5)	55.5 / 0.105	2.585 (2, 28) / 0.275
Circadian markers					
Melatonin [pg/mL]	154 (35–268)	57 (47–79)	57 (44–146)	45.5 / 0.386	1.02 (2, 28) / 0.061
Cortisol [µg/dL]	15.0 (9.5–19.5)	13.0 (11.0–15.0)	6.0 (5.0–8.0)	41.0 / 0.664	18.98 (2, 28) / 0.001
SBP [mm Hg]	146 (135–155)	143 (124–154)	120 (109–130)	43.5 / 0.500	10.11 (2, 28) / 0.006
DBP [mm Hg]	81 (72–91)	79 (76–87)	69 (66–73)	31.5 / 0.699	9.353 (2, 28) / 0.009
HR [bpm]	79 (68–104)	72 (68–82)	72 (67–82)	43.0 / 0.531	0.924 (2, 28) / 0.630

*Comparison between WUS and non-WUS groups; **comparison among all 3 groups. Categorical variables: n (%). Fisher's exact (2 groups) / Freeman–Halton test (3 groups). Continuous variables: median (min–max) for n ≤ 8, median (Q1–Q3) for n > 8. Wilcoxon rank-sum test (2 groups) / Kruskal–Wallis test (3 groups); WUS – wake-up stroke; REM – rapid eye movement; SBP – systolic blood pressure; DBP – diastolic blood pressure; HR – heart rate; min–max – minimal and maximal value; Q1 – 1st quartile (25th percentile); Q3 – 3rd quartile (75th percentile); df – degrees of freedom.

Table 2. Circadian properties of melatonin, cortisol, clock genes, BP, and HR in the WUS, non-WUS, and control groups

Group	Parameters	Melatonin [pg/mL]	Cortisol [µg/dL]	Gene expression levels						SBP [mm Hg]	DBP [mm Hg]	HR [bpm]
				CLOCK	*BMAL1*	*CRY1*	*CRY2*	*PER1*	*PER2*			
WUS	value	90.89 (22.02–257.78)	14.81 (8.99–21.54)	1.38 (1.36–1.40)	1.36 (1.34–1.38)	1.42 (1.40–1.44)	1.36 (1.34–1.39)	1.37 (1.34–1.41)	1.43 (1.40–1.45)	143 (131–157)	79 (70–93)	84.5 (67–103)
	amplitude	85.739	4.578	0.133	0.003	0.005	0.019	0.011	0.024	5.321	0.262	1.060
	acrophase (h:min)	05:41	11:59	13:36	20:59	06:53	17:39	16:49	17:59	17:08	15:08	17:30
	period [h]	23.687	23.566	27.304	25.275	23.333	24.266	26.063	24.220	23.668	22.387	24.787
	p-value	0.316	0.001	0.854	0.932	0.993	0.629	0.823	0.227	0.210	0.928	0.974
Non–WUS	value	45.23 (20.38–120.22)	12.17 (9.19–15.74)	1.42 (1.35–1.46)	1.39 (1.37–1.43)	1.46 (1.42–1.50)	1.43 (1.38–1.46)	1.42 (1.38–1.47)	1.49 (1.43–1.54)	137.5 (122–155)	78 (70–95)	73 (66–83.75)
	amplitude	41.486	3.669	0.021	0.029	0.021	0.040	0.022	0.007	6.877	4.445	2.512
	acrophase (h:min)	02:14	08:56	20:37	18:54	20:28	19:15	20:33	20:09	15:17	13:45	12:48
	period [h]	24.089	23.897	24.352	23.333	26.523	24.249	26.501	22.394	23.878	23.835	25.816
	p-value	0.001	0.002	0.122	0.796	0.932	0.050	0.967	0.331	0.268	0.248	0.948
Control	value	31.63 (16.87–133.52)	5.41 (3.68–8.58)	1.35 (1.32–1.39)	1.33 (1.31–1.37)	1.38 (1.35–1.41)	1.34 (1.31–1.38)	1.37 (1.33–1.41)	1.38 (1.36–1.43)	118 (108–131.75)	69 (62–76)	72 (65–81)
	amplitude	73.707	3.330	0.022	0.016	0.020	0.030	0.020	0.022	6.942	5.284	7.408
	acrophase (h:min)	02:30	08:22	13:26	16:30	03:56	17:39	20:44	19:57	11:00	13:33	12:39
	period [h]	24.094	23.983	24.342	24.061	24.850	24.046	24.322	24.289	23.840	23.533	23.939
	p-value	<0.001	<0.001	0.032	0.289	0.014	0.010	0.002	0.011	<0.001	<0.001	<0.001

Continuous data were presented as median (Q1–Q3). The amplitude, phase, period, and p-values were obtained using the MetaCycle package in R; WUS – wake-up stroke; SBP – systolic blood pressure; DBP – diastolic blood pressure; HR – heart rate; Q1 – 1st quartile (25th percentile); Q3 – 3rd quartile (75th percentile).

Table 3. GEE analysis of melatonin and cortisol concentrations across the WUS, non-WUS, and control groups

Characteristic	β	SE	Statistic	95% CI	p-value
Melatonin					
WUS	–	–	–	–	–
Non-WUS	−133.975	79.263	2.857	−289.327, 21.378	0.091
Controls	−83.141	81.294	1.046	−242.475, 76.193	0.300
Cortisol					
WUS	–	–	–	–	–
Non-WUS	−1.124	2.19	0.264	−5.409, 3.161	0.607
Controls	−6.710	1.91	12.303	−10.459, −2.960	<0.001

Residual df = 100; n.clusters = 28; max.cluster.size = 4. For melatonin: alpha = 0.319, gamma = 10,934; for cortisol: alpha = 0.348, gamma = 20.1.
GEE – generalized estimating equations; 95% CI – 95% confidence interval; SE – standard error; df – degrees of freedom; WUS – wake-up stroke.

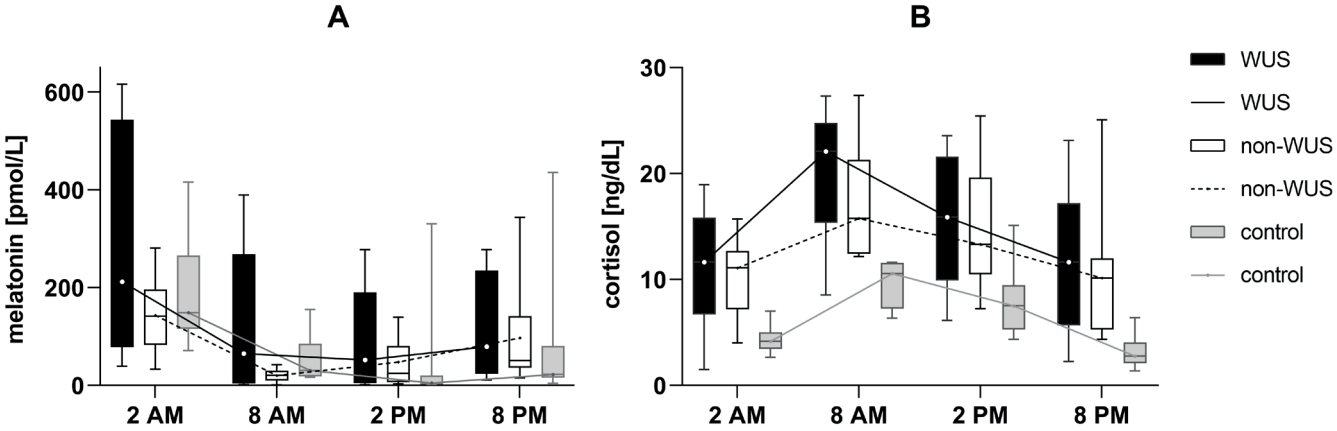

Fig. 1. Melatonin (A) and cortisol (B) concentrations and circadian profiles at 4 time points in the wake-up stroke (WUS), non-WUS, and control groups. The x-axis indicates the time points that blood samples were collected. The y-axis represents the concentration of the corresponding indicator

of melatonin was absent, whereas cortisol maintained its rhythmicity. Rhythmicity analysis showed an acrophase at 11:59 for cortisol in the WUS group, indicating a phase delay of 3 h 37 min compared with the control group. Additionally, overall cortisol concentrations differed significantly among the groups (H = 18.98, p = 0.001). Post hoc Bonferroni tests showed significantly higher cortisol levels in both the WUS (W = 1384, adjusted p < 0.001) and non-WUS (W = 1584, adjusted p < 0.001) groups compared with controls. No significant difference was found between the WUS and non-WUS groups. Descriptive statistics are presented in Table 1, and the full post hoc comparisons are provided in Supplementary Table 1.

The GEE analysis assessed group differences in melatonin and cortisol levels, adjusting for repeated measures and using the WUS group as the reference. Melatonin levels did not differ significantly between the WUS group and either the non-WUS group or control group. Regarding cortisol, no significant difference was found between the WUS and non-WUS groups. However, WUS patients exhibited significantly higher cortisol levels compared with the controls (β = −6.710, p < 0.001). Post hoc Bonferroni-adjusted pairwise comparisons further revealed that, relative to controls, both the WUS group (estimate = 8.472, standard error (SE) = 1.804, adjusted p < 0.001) and the non-WUS group (estimate = 6.836, SE = 1.014, adjusted p < 0.001) had significantly elevated cortisol levels (Table 3; pairwise comparisons are shown in Supplementary Table 2). Figure 1 displays the melatonin and cortisol concentrations at the 4 time points for the 3 groups, with circadian profiles plotted based on their median values.

Circadian clock genes expression

MetaCycle analyses indicated that in the control group, the expression profiles of *C LOCK*, *CRY1*, *CRY2*, *PER1*, and *PER2* exhibited significant circadian rhythmicity, with the exception of *BMAL1*. However, none of the 6 assessed clock genes showed circadian rhythmicity in the WUS or non-WUS groups (Table 2).

Blood pressure and heart rate

In the control group, systolic and diastolic blood pressure (SBP and DBP) and HR exhibited regular circadian rhythmicity (p < 0.001); however, this rhythmicity was absent in both the WUS and non-WUS groups (Table 2).

Group comparisons revealed significant differences in SBP (H = 10.11, p = 0.006) and DBP (H = 9.353, p = 0.009) among the 3 groups. Post hoc analyses with Bonferroni

correction showed that the WUS group had significantly higher SBP than controls (W = 80.5, adjusted p = 0.009), and the non-WUS group had significantly higher DBP than the controls (W = 85, adjusted p = 0.023). All other pairwise comparisons for SBP and DBP yielded nonsignificant results. Descriptive data are presented in Table 1, and the full post hoc results are provided in Supplementary Table 1.

Discussion

In mammals, circadian rhythms are essential for maintaining physiological homeostasis. Disrupted circadian rhythm can contribute to the loss of homeostasis and the development of disease.[35,36] Circadian rhythms are controlled by the SCN in the hypothalamus, which is influenced by a variety of factors. In this study, we explored circadian rhythm indicators in WUS patients to investigate potential associations between WUS and abnormal circadian rhythms. The results revealed disrupted circadian rhythmicity in the WUS group compared with the non-WUS and control groups.

Melatonin is an endogenous neurohormone primarily produced by the pineal gland. It is currently regarded as the most accurate marker of human circadian rhythmicity and SCN function.[37] Its rhythm is minimally, if at all, influenced by environmental factors such as the sleep–wake state, exercise, or emotions. However, known external factors that can affect the melatonin phase include light exposure, posture, and ambient temperature.[38–40] With the onset of darkness, melatonin levels gradually increase throughout the night, peaking in the early morning (between 02:00 and 04:00).

In this study, MetaCycle analyses revealed that melatonin secretion in the non-WUS and control groups exhibited significant circadian rhythmicity, with peak secretion times at 02:14 and 02:30, respectively. These findings suggest that the 2 groups share a similar circadian rhythm for melatonin. The results align with a previous study by Adamczak-Ratajczak et al., which analyzed the circadian phase of AIS based on plasma melatonin and found that the circadian rhythm of melatonin was sustained without any phase shift.[29] However, the WUS group showed a complete loss of melatonin circadian rhythmicity.

Previous studies have established that the majority of humans exhibit a robust and persistent daily melatonin rhythm.[37,41] Therefore, the findings of this study may indicate that WUS patients experience disrupted circadian rhythms, and this discrepancy compared with non-WUS patients suggests that circadian rhythm abnormalities in WUS patients may be present even before stroke onset.

Cortisol, the major end product of the hypothalamic–pituitary–adrenal (HPA) axis,[42] is another important marker for investigating circadian rhythms. Under normal, stress-free conditions, the adrenal cortex produces cortisol, which is then released into the bloodstream in a circadian pattern. Peak cortisol secretion in adults typically occurs between 08:00 and 10:00.[43] In this study, cortisol levels exhibited circadian rhythmicity across all 3 groups. However, in the WUS group, the cortisol rhythm showed an acrophase shift, with an approximate 3-h delay compared with the control and non-WUS groups (the acrophase occurred at 11:59 in the WUS group, compared with 08:22 in the control group and 08:56 in the non-WUS group). This finding supports the conclusion that WUS patients exhibit disrupted circadian rhythms, specifically manifested as a phase delay. In addition, serum cortisol levels in the WUS and non-WUS groups were significantly higher than those in the control group, consistent with previous studies.[44,45] One prior study reported that cortisol levels remain elevated for at least 7 days following stroke in most patients.[45] As a stressor, AIS can stimulate the HPA axis, leading to increased cortisol secretion.[46]

In mammals, circadian rhythms are believed to be governed by a fundamental molecular autoregulatory feedback loop involving key clock genes such as *Period* (*PER1* and *PER2*), Cryptochrome (*CRY1* and *CRY2*), *BMAL1*, and *CLOCK*, along with their protein products.[47] Beyond the central SCN circadian pacemaker, clock genes are expressed in most mammalian cells and organs, including peripheral blood cells.[48,49] In this study, we investigated the circadian rhythmicity in the expression of 6 clock genes in the peripheral blood of the WUS, non-WUS, and control groups. In the control group, all assessed clock genes, except *BMAL1*, exhibited significant rhythmic expression. This observation aligns with previous research suggesting a highly variable daily pattern of *BMAL1* expression across individuals.[50,51] Although *BMAL1* is essential for the regulation of 24-h behavioral cycles, it is not critical for 24-h molecular rhythms at the transcriptional, translational, or post-translational levels, as demonstrated by Ray et al.[52]

In contrast, neither the WUS group nor the non-WUS group showed rhythmic expression of any of the 6 clock genes. Previous studies have shown that the disruption of circadian rhythms increases the risk of stroke by affecting physiological processes such as BP, platelet function, coagulation, and fibrinolysis.[53,54] However, an acute stroke itself can also disrupt circadian rhythms and impair the neuronal clock mechanism. Research has demonstrated that neurons in the SCN have their own clock gene cycles, while astrocytes help synchronize SCN timing by recycling gamma-aminobutyric acid and glutamate.[55–57] During the occurrence of AIS, astrocyte function is altered, potentially disrupting this recycling process and, consequently, impairing the normal rhythmicity of the SCN.[58] Therefore, based solely on these gene expression results, it remains challenging to determine whether circadian rhythm precedes or merely follows stroke onset in WUS patients.

Several physiological processes, including BP and HR, exhibit circadian rhythmicity in humans.[59,60] Analysis

of our control group confirmed this phenomenon. However, our findings revealed a complete loss of circadian variation in BP and HR in both the WUS and non-WUS groups. Previous research has shown that irregular BP rhythms can increase the risk of stroke,[61] and that stroke events themselves can pathologically reduce or abolish circadian BP variation.[62] In a study using spontaneously hypertensive rats prone to malignant stroke, Masaki et al. observed a sudden change in HR, followed by a progressive loss of circadian BP variation occurring just as a stroke began.[63] Consequently, this aspect of the data provided limited insight into the specific circadian rhythms of WUS patients. Additionally, participants in the stroke groups exhibited significantly higher SBP or DBP compared with the control group in our study. This finding may be attributed to the higher prevalence of hypertension among stroke patients, combined with the acute physiological stress induced by the stroke event.

Although an acute stroke itself may cause circadian rhythm disruptions, this study revealed several noteworthy findings. The rhythmicity of the most prominent circadian rhythm marker, melatonin, was completely absent in the WUS group but preserved in the non-WUS group. Additionally, the cortisol rhythm persisted in the WUS group but exhibited a phase delay compared with the non-WUS group. Although other markers showed no differences between the 2 groups, we hypothesize that WUS patients may have preexisting circadian rhythm disruptions before disease onset. For these patients, as well as others with clearly identified circadian rhythm disorders, targeted interventions aimed at regulating circadian rhythms, such as light therapy or pharmacological treatments, could be implemented alongside strategies to prevent stroke recurrence.[64]

These measures may help reduce the occurrence of strokes, particularly WUS. Moreover, research suggests that disruptions in the circadian rhythm system may impair the ability of neural tissue to repair itself, thereby affecting the recovery process.[65] Restoring circadian rhythms after a stroke may also contribute to improved neurological function and overall health outcomes in patients.[65,66]

Limitations of the study

This study has several limitations that should be acknowledged. First, given the exploratory nature of this study, the sample size was relatively small; therefore, the findings should be interpreted with caution, and replication with a larger sample size is needed in future research. Second, due to the limitations inherent to human studies, obtaining repeated blood samples over 2 or 3 consecutive days is challenging, which limits the reproducibility of circadian rhythm analyses and may weaken the robustness of the results. Third, as this was a cross-sectional study, causal relationships cannot be determined. Fourth, the strict exclusion criteria were primarily designed to exclude conditions, dietary factors, medications, or work–rest patterns (e.g., shift work or night work) known to affect circadian rhythms.[67–69]

Such external factors that interfere with circadian rhythms would likely have influenced the results of this study. The comorbidities and medications that were excluded were not specific to stroke and therefore would not bias the study toward a profile unrepresentative of the broader stroke patient population. Nevertheless, patients engaged in shift work or night work were excluded, and examining the influence of circadian rhythms on WUS in these patients would be of interest in future studies. Finally, in this study, sleep was monitored using a smart device. Participants were accommodated in single-occupancy rooms, lights were not permitted, and they were required to wear eye masks during sleep. The only disturbance occurred during nighttime specimen collection. To avoid turning on the room lights, only a dim yellow light from a penlight was used. Efforts were made to minimize exogenous interference, but some confounding factors may still have been present. Despite these limitations, we believe that our work may provide additional insights into the pathogenesis of WUS and serve as inspiration for future studies exploring its potential mechanisms. For example, in future research, when establishing databases for long-term follow-up of high-risk stroke populations, dynamic electrocardiographic and blood pressure data could be included, as these may serve as feasible indicators of circadian rhythms. If a stroke event is observed during follow-up, we would also record the time of stroke onset to further examine the correlation between circadian rhythms and stroke onset time. More research with an adequate sample size is crucial to validate our outcomes.

Conclusions

This study represents the first exploratory investigation of circadian rhythms in WUS patients. Our findings reveal that WUS patients exhibit significant disruptions in circadian rhythms, including the loss of melatonin rhythmicity and a phase delay in cortisol secretion. These alterations differ from those observed in non-WUS patients, in whom some circadian markers, such as melatonin and cortisol, remained intact. Our results suggest that disrupted circadian rhythms may be an intrinsic feature of WUS, possibly predating stroke onset. From a theoretical perspective, this study provides evidence supporting the role of circadian rhythms in stroke pathogenesis, particularly in WUS. For example, light therapy could be optimized for WUS patients by delivering 2,000–10,000 lux of blue-enriched light in the morning (06:00–08:00) to phase-advance delayed rhythms, while minimizing evening light exposure to prevent further disruption.[70,71] Such strategies, combined with pharmacological treatments or lifestyle adjustments, may help regulate circadian rhythms and reduce the risk of stroke recurrence.

These findings underscore the need for larger-scale, longitudinal studies to validate and expand upon the observed associations and to explore the causal mechanisms underlying circadian rhythm disruptions in WUS. By deepening our understanding of the interplay between circadian biology and stroke, this line of research holds promise for the development of novel preventive and therapeutic strategies tailored to the unique characteristics of WUS.

Supplementary data

The supplementary data are available at https://doi.org/10.5281/zenodo.15745360. The package contains the following files:

Supplementary Table 1. Detailed post hoc test results for group comparisons of cortisol, SBP, and DBP using the Kruskal–Wallis test in Table 1.

Supplementary Table 2. Bonferroni-adjusted pairwise comparisons of GEE-estimated marginal means of cortisol concentrations between groups across 4 time points.

Use of AI and AI-assisted technologies

In the preparation of this manuscript, we used ChatGPT, solely for language refinement. The AI tool was employed to assist with language editing and enhancement. However, the author carefully reviewed and ensured that all language revisions accurately conveyed the intended meaning. The authors take full responsibility for the content of the manuscript, including any portions enhanced by AI tools.

Data availability

The datasets generated and/or analyzed during the current study are available from the corresponding author on reasonable request.

Consent for publication

Not applicable.

ORCID iDs

Xianxian Zhang https://orcid.org/0000-0001-5637-507X
Zhiguo Chen https://orcid.org/0000-0003-0232-4992
Siyu Gu https://orcid.org/0009-0003-1516-8738
YingLing Zhu https://orcid.org/0009-0001-0833-8706
Liqiang Yu https://orcid.org/0000-0001-6658-3040
Xiuying Cai https://orcid.org/0000-0002-3496-3281
Hongru Zhao https://orcid.org/0000-0003-2269-9265
Han Wang https://orcid.org/0000-0003-2420-3147
Qi Fang https://orcid.org/0009-0009-0388-6998

References

1. Thomalla G, Boutitie F, Fiebach JB, et al. Stroke with unknown time of symptom onset: Baseline clinical and magnetic resonance imaging data of the first thousand patients in WAKE-UP (Efficacy and safety of MRI-based thrombolysis in wake-up stroke: A randomized, doubleblind, placebo-controlled trial). *Stroke*. 2017;48(3):770–773. doi:10.1161/STROKEAHA.116.015233
2. Moradiya Y, Janjua N. Presentation and outcomes of "wake-up strokes" in a large randomized stroke trial: Analysis of data from the International Stroke Trial. *J Stroke Cerebrovasc Dis*. 2013;22(8):e286–e292. doi:10.1016/j.jstrokecerebrovasdis.2012.07.016
3. Mackey J, Kleindorfer D, Sucharew H, et al. Population-based study of wake-up strokes. *Neurology*. 2011;76(19):1662–1667. doi:10.1212/WNL.0b013e318219fb30
4. Maurer CJ, Egger K, Dempfle AK, Reinhard M, Meckel S, Urbach H. Facing the time window in acute ischemic stroke: The infarct core. *Clin Neuroradiol*. 2016;26(2):153–158. doi:10.1007/s00062-016-0501-8
5. Schellinger PD, Köhrmann M. Current acute stroke trials and their potential impact on the therapeutic time window. *Exp Rev Neurother*. 2012;12(2):169–177. doi:10.1586/ern.11.198
6. Yang H, Huang X, Yang C, et al. Time window for acute stroke management: A cross-sectional study among community healthcare practitioners in primary care. *Int J Gen Med*. 2022;15:4483–4493. doi:10.2147/IJGM.S361189
7. Elfil M, Eldokmak M, Baratloo A, Ahmed N, Amin HP, Koo BB. Pathophysiologic mechanisms, neuroimaging and treatment in wake-up stroke. *CNS Spectr*. 2020;25(4):460–467. doi:10.1017/S1092852919001354
8. Diniz DLDO, Barreto PR, Bruin PFCD, Bruin VMSD. Wake-up stroke: Clinical characteristics, sedentary lifestyle, and daytime sleepiness. *Rev Assoc Med Bras*. 2016;62(7):628–634. doi:10.1590/1806-9282.62.07.628
9. Denny MC, Boehme AK, Dorsey AM, et al. Wake-up strokes are similar to known-onset morning strokes in severity and outcome. *J Neurol Neurol Disord*. 2014;1(1):102. doi:10.15744/2454-4981.1.102
10. Biggs D, Silverman ME, Chen F, Walsh B, Wynne P. How should we treat patients who wake up with a stroke? A review of recent advances in management of acute ischemic stroke. *Am J Emerg Med*. 2019;37(5):954–959. doi:10.1016/j.ajem.2019.02.010
11. Koo BB, Bravata DM, Tobias LA, et al. Observational study of obstructive sleep apnea in wake-up stroke: The SLEEP TIGHT Study. *Cerebrovasc Dis*. 2016;41(5–6):233–241. doi:10.1159/000440736
12. Riccio PM, Klein FR, Pagani Cassará F, et al. Newly diagnosed atrial fibrillation linked to wake-up stroke and TIA: Hypothetical implications. *Neurology*. 2013;80(20):1834–1840. doi:10.1212/WNL.0b013e318292a330
13. Hsieh SW, Lai CL, Liu CK, Hsieh CF, Hsu CY. Obstructive sleep apnea linked to wake-up strokes. *J Neurol*. 2012;259(7):1433–1439. doi:10.1007/s00415-011-6370-9
14. Peter-Derex L, Derex L. Wake-up stroke: From pathophysiology to management. *Sleep Med Rev*. 2019;48:101212. doi:10.1016/j.smrv.2019.101212
15. Wouters A, Lemmens R, Dupont P, Thijs V. Wake-up stroke and stroke of unknown onset: A critical review. *Front Neurol*. 2014;5:153. doi:10.3389/fneur.2014.00153
16. Cheung RTF, Mak W, Chan KH. Circadian variation of stroke onset in Hong Kong Chinese: A hospital-based study. *Cerebrovasc Dis*. 2001;12(1):1–6. doi:10.1159/000047673
17. Chaturvedi S, Adams HP, Woolson RF. Circadian variation in ischemic stroke subtypes. *Stroke*. 1999;30(9):1792–1795. doi:10.1161/01.STR.30.9.1792
18. Smolensky MH, Hermida RC, Castriotta RJ, Portaluppi F. Role of sleep-wake cycle on blood pressure circadian rhythms and hypertension. *Sleep Med*. 2007;8(6):668–680. doi:10.1016/j.sleep.2006.11.011
19. Hermida RC, Ayala DE, Portaluppi F. Circadian variation of blood pressure: The basis for the chronotherapy of hypertension. *Adv Drug Deliv Rev*. 2007;59(9–10):904–922. doi:10.1016/j.addr.2006.08.003
20. Scheer FAJL, Michelson AD, Frelinger AL, et al. The human endogenous circadian system causes greatest platelet activation during the biological morning independent of behaviors. *PLoS One*. 2011;6(9):e24549. doi:10.1371/journal.pone.0024549
21. Shaw E, Tofler GH. Circadian rhythm and cardiovascular disease. *Curr Atheroscler Rep*. 2009;11(4):289–295. doi:10.1007/s11883-009-0044-4
22. Thosar SS, Shea SA. Circadian control of human cardiovascular function. *Curr Opin Pharmacol*. 2021;57:89–97. doi:10.1016/j.coph.2021.01.002
23. Crnko S, Du Pré BC, Sluijter JPG, Van Laake LW. Circadian rhythms and the molecular clock in cardiovascular biology and disease. *Nat Rev Cardiol*. 2019;16(7):437–447. doi:10.1038/s41569-019-0167-4

24. Patke A, Young MW, Axelrod S. Molecular mechanisms and physiological importance of circadian rhythms. *Nat Rev Mol Cell Biol*. 2020; 21(2):67–84. doi:10.1038/s41580-019-0179-2
25. Mohawk JA, Green CB, Takahashi JS. Central and peripheral circadian clocks in mammals. *Annu Rev Neurosci*. 2012;35(1):445–462. doi:10.1146/annurev-neuro-060909-153128
26. Yang MY, Lin PW, Lin HC, et al. Alternations of circadian clock genes expression and oscillation in obstructive sleep apnea. *J Clin Med*. 2019;8(10):1634. doi:10.3390/jcm8101634
27. Steffens S, Winter C, Schloss MJ, Hidalgo A, Weber C, Soehnlein O. Circadian control of inflammatory processes in atherosclerosis and its complications. *Arterioscler Thromb Vasc Biol*. 2017;37(6):1022–1028. doi:10.1161/ATVBAHA.117.309374
28. Mehdipour A, Fateh R, Fuladvand F, Aghaali M, Keykha E, Hadilou M. Association between sleep pattern, salivary cariogenic bacteria and fungi populations, pH and buffering capacity in children: A comparative study. *Dent Med Probl*. 2024;61(2):217–224. doi:10.17219/dmp/167411
29. Adamczak-Ratajczak A, Kupsz J, Owecki M, et al. Circadian rhythms of melatonin and cortisol in manifest Huntington's disease and in acute cortical ischemic stroke. *J Physiol Pharmacol*. 2017;68(4): 539–546. PMID:29151070.
30. Zhang XX, Cai XY, Zhao HR, et al. Circadian rhythms of melatonin, cortisol, and clock gene expression in the hyperacute phase of wake-up stroke: Study design and measurement. *Chin Med J (Engl)*. 2020;133(21):2635–2637. doi:10.1097/CM9.0000000000001111
31. Wang X, Cheng Z. Cross-sectional studies. *Chest*. 2020;158(1 Suppl): S65–S71. doi:10.1016/j.chest.2020.03.012
32. Setia M. Methodology series module 3: Cross-sectional studies. *Indian J Dermatol*. 2016;61(3):261. doi:10.4103/0019-5154.182410
33. Liang KY, Zeger SL. Longitudinal data analysis using generalized linear models. *Biometrika*. 1986;73(1):13–22. doi:10.1093/biomet/73.1.13
34. Wu G, Anafi RC, Hughes ME, Kornacker K, Hogenesch JB. MetaCycle: An integrated R package to evaluate periodicity in large scale data. *Bioinformatics*. 2016;32(21):3351–3353. doi:10.1093/bioinformatics/btw405
35. Yu EA, Weaver DR. Disrupting the circadian clock: Gene-specific effects on aging, cancer, and other phenotypes. *Aging*. 2011;3(5): 479–493. doi:10.18632/aging.100323
36. Gibson EM, Williams WP, Kriegsfeld LJ. Aging in the circadian system: Considerations for health, disease prevention and longevity. *Exp Gerontol*. 2009;44(1–2):51–56. doi:10.1016/j.exger.2008.05.007
37. Benloucif S, Burgess HJ, Klerman EB, et al. Measuring melatonin in humans. *J Clin Sleep Med*. 2008;4(1):66–69. PMID:18350967. PMCID:PMC2276833.
38. Zhao D, Yu Y, Shen Y, et al. Melatonin synthesis and function: Evolutionary history in animals and plants. *Front Endocrinol (Lausanne)*. 2019;10:249. doi:10.3389/fendo.2019.00249
39. Zisapel N. New perspectives on the role of melatonin in human sleep, circadian rhythms and their regulation. *Br J Pharmacol*. 2018;175(16):3190–3199. doi:10.1111/bph.14116
40. St. Hilaire MA, Lockley SW. Measuring dim light melatonin onset in humans. *Methods Mol Biol*. 2022;2550:13–20. doi:10.1007/978-1-0716-2593-4_3
41. Arendt J. Melatonin and human rhythms. *Chronobiol Int*. 2006;23(1–2): 21–37. doi:10.1080/07420520500464361
42. Nicolaides NC, Charmandari E, Chrousos GP, Kino T. Circadian endocrine rhythms: The hypothalamic–pituitary–adrenal axis and its actions. *Ann N Y Acad Sci*. 2014;1318(1):71–80. doi:10.1111/nyas.12464
43. Timmermans S, Souffriau J, Libert C. A general introduction to glucocorticoid biology. *Front Immunol*. 2019;10:1545. doi:10.3389/fimmu.2019.01545
44. Pajediene E, Paulekas E, Salteniene V, et al. Diurnal variation of clock genes expression and other sleep-wake rhythm biomarkers among acute ischemic stroke patients. *Sleep Med*. 2022;99:1–10. doi:10.1016/j.sleep.2022.06.023
45. Barugh AJ, Gray P, Shenkin SD, MacLullich AMJ, Mead GE. Cortisol levels and the severity and outcomes of acute stroke: A systematic review. *J Neurol*. 2014;261(3):533–545. doi:10.1007/s00415-013-7231-5
46. Fassbender K, Schmidt R, Mössner R, Daffertshofer M, Hennerici M. Pattern of activation of the hypothalamic–pituitary–adrenal axis in acute stroke: Relation to acute confusional state, extent of brain damage, and clinical outcome. *Stroke*. 1994;25(6):1105–1108. doi:10.1161/01.STR.25.6.1105
47. Reppert SM, Weaver DR. Coordination of circadian timing in mammals. *Nature*. 2002;418(6901):935–941. doi:10.1038/nature00965
48. Lin C, Tang X, Zhu Z, et al. The rhythmic expression of clock genes attenuated in human plaque-derived vascular smooth muscle cells. *Lipids Health Dis*. 2014;13(1):14. doi:10.1186/1476-511X-13-14
49. Ando H, Ushijima K, Kumazaki M, et al. Influence of age on clock gene expression in peripheral blood cells of healthy women. *J Gerontol A Biol Sci Med Sci*. 2010;65A(1):9–13. doi:10.1093/gerona/glp160
50. James FO, Boivin DB, Charbonneau S, Bélanger V, Cermakian N. Expression of clock genes in human peripheral blood mononuclear cells throughout the sleep/wake and circadian cycles. *Chronobiol Int*. 2007;24(6):1009–1034. doi:10.1080/07420520701800736
51. Teboul M, Barrat-Petit MA, Li XM, et al. Atypical patterns of circadian clock gene expression in human peripheral blood mononuclear cells. *J Mol Med*. 2005;83(9):693–699. doi:10.1007/s00109-005-0697-6
52. Ray S, Valekunja UK, Stangherlin A, et al. Circadian rhythms in the absence of the clock gene *Bmal1*. *Science*. 2020;367(6479):800–806. doi:10.1126/science.aaw7365
53. Fodor DM, Marta MM, Perju-Dumbravă L. Implications of circadian rhythm in stroke occurrence: Certainties and possibilities. *Brain Sci*. 2021;11(7):865. doi:10.3390/brainsci11070865
54. Battaglia S, Schmidt A, Hassel S, Tanaka M. Editorial: Case reports in neuroimaging and stimulation. *Front Psychiatry*. 2023;14:1264669. doi:10.3389/fpsyt.2023.1264669
55. Patton AP, Morris EL, McManus D, et al. Astrocytic control of extracellular GABA drives circadian timekeeping in the suprachiasmatic nucleus. *Proc Natl Acad Sci U S A*. 2023;120(21):e2301330120. doi:10.1073/pnas.2301330120
56. Battaglia S, Nazzi C, Thayer JF. Heart's tale of trauma: Fear-conditioned heart rate changes in post-traumatic stress disorder. *Acta Psychiatr Scand*. 2023;148(5):463–466. doi:10.1111/acps.13602
57. Mazuski C, Abel JH, Chen SP, et al. Entrainment of circadian rhythms depends on firing rates and neuropeptide release of VIP SCN neurons. *Neuron*. 2018;99(3):555–563.e5. doi:10.1016/j.neuron.2018.06.029
58. Xu S, Jia M, Guo J, et al. Ticking brain: Circadian rhythm as a new target for cerebroprotection. *Stroke*. 2024;55(9):2385–2396. doi:10.1161/STROKEAHA.124.046684
59. Douma LG, Gumz ML. Circadian clock-mediated regulation of blood pressure. *Free Radic Biol Med*. 2018;119:108–114. doi:10.1016/j.freeradbiomed.2017.11.024
60. Gubin DG, Weinert D, Rybina SV, et al. Activity, sleep and ambient light have a different impact on circadian blood pressure, heart rate and body temperature rhythms. *Chronobiol Int*. 2017;34(5):632–649. doi:10.1080/07420528.2017.1288632
61. Pierdomenico SD, Pierdomenico AM, Cuccurullo F. Morning blood pressure surge, dipping, and risk of ischemic stroke in elderly patients treated for hypertension. *Am J Hypertens*. 2014;27(4):564–570. doi:10.1093/ajh/hpt170
62. Jain S, Namboodri K, Kumari S, Prabhakar S. Loss of circadian rhythm of blood pressure following acute stroke. *BMC Neurol*. 2004;4(1):1. doi:10.1186/1471-2377-4-1
63. Tabuchi M, Umegaki K, Ito T, Suzuki M, Ikeda M, Tomita T. Disturbance of circadian rhythm in heart rate, blood pressure and locomotive activity at the stroke-onset in malignant stroke-prone spontaneously hypertensive rats. *Jpn J Pharmacol*. 2001;85(2):197–202. doi:10.1254/jjp.85.197
64. Stubblefield JJ, Lechleiter JD. Time to target stroke: Examining the circadian system in stroke. *Yale J Biol Med*. 2019;92(2):349–357. PMID:31249495. PMCID:PMC6585528.
65. Liang X, Bushman FD, FitzGerald GA. Time in motion: The molecular clock meets the microbiome. *Cell*. 2014;159(3):469–470. doi:10.1016/j.cell.2014.10.020
66. Meléndez-Fernández OH, Walton JC, DeVries AC, Nelson RJ. Clocks, rhythms, sex, and hearts: How disrupted circadian rhythms, time-of-day, and sex influence cardiovascular health. *Biomolecules*. 2021; 11(6):883. doi:10.3390/biom11060883

67. Xin M, Bi F, Wang C, et al. The circadian rhythm: A new target of natural products that can protect against diseases of the metabolic system, cardiovascular system, and nervous system. *J Adv Res*. 2025; 69:495–514. doi:10.1016/j.jare.2024.04.005
68. Walker WH, Walton JC, DeVries AC, Nelson RJ. Circadian rhythm disruption and mental health. *Transl Psychiatry*. 2020;10(1):28. doi:10.1038 /s41398-020-0694-0
69. Leng Y, Musiek ES, Hu K, Cappuccio FP, Yaffe K. Association between circadian rhythms and neurodegenerative diseases. *Lancet Neurol*. 2019;18(3):307–318. doi:10.1016/S1474-4422(18)30461-7
70. Barroggi Constantino D, Lederle KA, Middleton B, et al. The bright and dark side of blue-enriched light on sleep and activity in older adults. *GeroScience*. 2025;47(3):3927–3939. doi:10.1007/s11357-025-01506-y
71. Li D, Fang P, Liu H, et al. The clinical effect of blue light therapy on patients with delayed sleep-wake phase disorder. *Nature Sci Sleep*. 2022;14:75–82. doi:10.2147/NSS.S344616

Effects of peribulbar block and incisionless sub-Tenon's block on sleep quality after cataract surgery

Yeliz Kılıç[1,A–D], Haluk Hüseyin Gürsoy[2,B,F], Mustafa Değer Bilgeç[2,B,F], Ali Rıza Ata[1,B,F], Mehmet Sacit Güleç[1,A,F]

[1] Department of Anesthesiology, Eskişehir Osmangazi University, Turkey
[2] Department of Ophthalmology, Eskişehir Osmangazi University, Turkey

A – research concept and design; B – collection and/or assembly of data; C – data analysis and interpretation;
D – writing the article; E – critical revision of the article; F – final approval of the article

Advances in Clinical and Experimental Medicine, ISSN 1899–5276 (print), ISSN 2451–2680 (online) *Adv Clin Exp Med*. 2026;35(4):673–681

Address for correspondence
Yeliz Kılıç
E-mail: yeliz_kilic3@hotmail.com

Funding sources
None declared

Conflict of interest
None declared

Received on September 18, 2024
Reviewed on January 14, 2025
Accepted on June 26, 2025

Published online on March 16, 2026

Abstract

Background. Sleep quality often decreases in patients after surgery and may affect postoperative outcomes.

Objectives. The aim of this study was to compare the effects of peribulbar block and incisionless sub-Tenon's block on postoperative sleep quality.

Materials and methods. Patients who underwent cataract surgery under peribulbar block (n = 36) or incisionless sub-Tenon's block (n = 31) were included in the study. The 2 blocks were compared with each other in terms of eyelid and globe movements, corneal sensation, complications, pain, and postoperative sleep quality (evaluated using the Richard–Campbell Sleep Questionnaire (RCSQ) score).

Results. Sixty-seven patients with a mean age of 67 years were included in the study. At the 15th minute after the block ($p = 0.066$) and at the end of surgery ($p = 0.098$), akinesia was better in the incisionless sub-Tenon's group, with p-values close to the level of statistical significance. Chemosis was found to be significantly lower in the peribulbar block group than in the incisionless sub-Tenon's block group ($p = 0.033$) 3 h after surgery. All minor complications, including chemosis, subconjunctival petechiae, and subconjunctival hemorrhage, were observed less frequently in the peribulbar block group, although the differences were not statistically significant ($p > 0.05$). Pain scores were comparable between the groups ($p > 0.05$). The total RCSQ score ($p = 0.396$) and overall sleep perception ($p = 0.355$) were also comparable between the groups.

Conclusions. The incisionless sub-Tenon's block was superior to the peribulbar block in terms of providing akinesia and reducing the need for maintenance anesthetic medications such as sedatives or analgesics. Although chemosis and subconjunctival hemorrhage occurred more frequently in the incisionless sub-Tenon's group, all events were transient and had no serious clinical significance. The 2 regional techniques were similar in terms of postoperative sleep quality and patient satisfaction.

Key words: cataract surgery, peribulbar block, incisionless sub-Tenon's block, postoperative sleep quality

Cite as
Kılıç Y, Gürsoy HH, Bilgeç MD, Ata AR, Güleç MS. Effects of peribulbar block and incisionless sub-Tenon's block on sleep quality after cataract surgery. *Adv Clin Exp Med*. 2026;35(4):673–681. doi:10.17219/acem/207603

DOI
10.17219/acem/207603

Highlights

- Sleep quality often decreases after surgery and may affect postoperative outcomes.
- The peribulbar block is one of the most commonly used anesthesia techniques for ocular procedures, whereas the incisionless sub-Tenon's block is a newer technique that provides improved akinesia and analgesia.
- This is the first study to compare incisionless sub-Tenon's and peribulbar blocks in terms of postoperative sleep quality.
- Results suggest that incisionless sub-Tenon's and peribulbar blocks result in similar postoperative sleep quality after cataract surgery.

Background

Cataract surgery is among the most commonly performed operations worldwide. It is generally an outpatient procedure, and early return to routine life is an important goal of this surgery.[1] Sleep quality often decreases in patients after surgery, which may affect postoperative outcomes, including conditions such as postoperative delirium, long-term chronic pain, and potentially serious cardiovascular events.[2] In this regard, postoperative sleep quality is highly important. Improving sleep quality accelerates the recovery process and shortens the time required to return to daily life.

Sleep quality after cataract surgery can be affected by several factors, such as sex, anxiety, comorbidities, pain, anesthetic drugs, and perioperative complications. Postoperative pain is one of the leading factors affecting sleep quality and is directly associated with anesthesia.[2,3] Cataract surgery can be performed under local, regional, or general anesthesia. In recent years, regional block techniques, such as peribulbar and sub-Tenon's blocks, have gained popularity because they provide better analgesia and eyeball immobilization than topical anesthesia. In addition, cataract surgery is more frequently performed in older patients with a higher anesthesia risk due to the presence of comorbidities. Therefore, preventing potential problems associated with general anesthesia has made regional block techniques more preferable.[1–4]

The peribulbar block is one of the most commonly used anesthesia methods for ocular procedures because of its low complication rate and ease of application. In contrast, the sub-Tenon's block has recently been increasingly preferred because it provides better akinesia and analgesia and causes less damage to the vasculature and optic nerve.[5–7] Many studies in the literature have compared peribulbar and sub-Tenon's blocks, most of which focused on intraoperative eye movements, postoperative analgesia, and complications.[7,8] However, there are no studies comparing these techniques in terms of postoperative sleep quality.

Objectives

In this study, 2 regional anesthesia techniques, peribulbar block and incisionless sub-Tenon's block, were compared in terms of postoperative sleep quality in patients undergoing cataract surgery.

Materials and methods

Ethics approval

After obtaining approval from the Clinical Research Ethics Committee (approval No. 25.07.2023/6), the study was conducted at the Department of Anesthesiology and Reanimation at Eskisehir Osmangazi University (Turkey) between August 2023 and March 2024, in accordance with Good Clinical Practice guidelines and the principles of the Declaration of Helsinki.

Patient selection

Sixty-seven adult patients who underwent cataract surgery using one of 2 regional anesthesia techniques – peribulbar block (n = 36) or incisionless sub-Tenon's block (n = 31) – were included in the study. All patients were diagnosed with elective cataract by the same surgical team. Inclusion criteria included age ≥18 years, an American Society of Anesthesiologists (ASA) physical status of 1–3, and elective surgery. Patients with intellectual disability, dementia, or psychiatric disorders; those receiving medical therapy affecting the central nervous system, such as benzodiazepines or antipsychotics; and those who developed an allergic reaction to local anesthetics were excluded from the study. All patients were informed in detail about the stages of the study, and written informed consent was obtained from each participant. Patient age, sex, ASA physical status, body mass index (BMI), surgical procedure, and type of regional block were recorded.

Anesthetic management

The patients were taken to the regional block room and monitored using electrocardiography (ECG), pulse oximetry,

and noninvasive blood pressure measurement. Intravenous (IV) access was established using a 20-G cannula placed in a hand vein, and a saline infusion was initiated to maintain vascular access. Premedication included dexmedetomidine (5–10 μg), midazolam (0.5–2 mg), and fentanyl (25–50 μg). Subsequently, proparacaine (1 drop) and 1% povidone–iodine (1 drop) were instilled into the eye. All regional blocks were performed by the 1st author (Y.K.). Thereafter, the patients were transferred to the operating room. Before surgery, IV paracetamol (Partemol 1 g/100 mL; VEM, Ankara, Turkey) was administered to all patients. During the intraoperative period, additional sedoanalgesic medications, including dexmedetomidine (Dekstomid 200 μg/2 mL; Polifarma, Tekirdag, Turkey), fentanyl (Fentanyl-PF 100 μg/2 mL; Polifarma) or midazolam (Zolamid 5 mg/5 mL; VEM), were administered as needed. Additional analgesics were given when the patient reported pain (visual analogue scale (VAS) ≥4) or restlessness (Ramsay sedation score = 1).

Hemodynamic parameters, including heart rate (HR), mean arterial pressure (MAP), and peripheral oxygen saturation (SpO_2), were recorded at 5 time points: before sedation (baseline), 15 min after the regional block, at the end of surgery, 3 h after surgery, and 1 day after surgery.

Block techniques

In the peribulbar block, after the skin was cleaned with alcohol, the technique was performed by inserting a 25-gauge needle through the skin (25 mm for patients with an axial eyeball length of 20–26 mm and for those with an axial length <20 mm) at the junction of the medial $^2/_3$ and lateral $^1/_3$ of the orbital rim. If contact with bone was encountered, the needle was redirected slightly upward. The tip of the needle was maintained in the extraconal peribulbar space. With the patient's eye in a neutral position, a local anesthetic mixture of 0.5% bupivacaine and 2% lidocaine was administered into the extraconal area, with a volume of 4–7 mL adjusted according to the axial length of the eyeball, through the main inferotemporal quadrant.

In the incisionless sub-Tenon's block, a proparacaine eye drop was instilled into the conjunctiva, followed by a drop of aqueous povidone–iodine into the conjunctival sac. A wired eyelid speculum was inserted to separate the eyelids. Thereafter, the conjunctiva and Tenon's capsule were grasped and punctured with forceps 5–8 mm away from the limbus in the inferonasal quadrant, while the patient was looking upward and outward. A disposable plastic cannula (22-gauge) was then advanced along the curvature of the eyeball. After negative aspiration, a local anesthetic mixture of 0.5% bupivacaine and 2% lidocaine, at a volume of 4–7 mL, was administered into the sub-Tenon's space through the cannula.

Outcome measures

The motor effects of the regional blocks included eyelid and globe movements, whereas the sensory effects included corneal sensitivity. Eyelid and globe movements were recorded in 4 primary gaze positions (superonasal, superotemporal, inferonasal, and inferotemporal) at 5 time points (before sedation, 15 min after the regional block, at the end of surgery, 3 h after surgery, and on the first postoperative day) using a 3-point scale (1 – movement, 2 – mild/moderate movement, 3 – akinesia). Corneal sensitivity was assessed based on patients' reported sensation in response to 1% povidone–iodine eye drops at the same time points, using a 3-point scale (0 – no burning, 1 – mild sensation, 2 – strong sensation).

Minor complications included chemosis, subconjunctival petechiae, and hemorrhage and were recorded at 5 time points (before sedation, 15 min after the regional block, at the end of surgery, 3 h after surgery, and 1 day after surgery). These complications were assessed in 4 quadrants of the eye (superonasal, superotemporal, inferonasal, and inferotemporal) using a 2-point scale ranging from 0 (absent) to 1 (present in any quadrant).

Pain was evaluated using a VAS score ranging from 0 (no pain) to 10 (the worst imaginable pain) before sedation, 3 h after the operation, and on the 1st postoperative day. Sleep quality was evaluated using the validated version of the Richard–Campbell Sleep Questionnaire (RCSQ) on the first postoperative day.[9] This questionnaire consists of 6 items that assess depth of sleep, time to fall asleep, frequency of awakenings, time spent awake after awakening, sleep quality, and environmental noise level. Each item is scored on a scale from 0 to 100. The average of the first 5 items was calculated as the total score and represented overall sleep perception.

Overall sleep perception was classified into 4 categories: 0–25 points – very poor sleep perception; 26–50 points – poor sleep perception; 51–75 points – moderate/good sleep perception; and 76–100 points – very good sleep perception. The 6th item evaluates the noise level of the sleeping environment and is not included in the total score. The score obtained from the 6th item was analyzed to determine whether the sleeping environments of the 2 groups were comparable.

Statistical analyses

Because the study population was not fully known (as there are no similar studies in the literature comparing the effects of peribulbar and incisionless sub-Tenon's blocks on postoperative sleep quality), the power and sample size of the present study were calculated based on the study by Duran and Öztürk.[10] A total of 48 patients were required at a power level of 80%. The effect size of the study was 0.35 (medium). Statistical analyses were performed using IBM SPSS Statistics for Windows v. 20.0 (IBM Corp., Armonk, USA). Descriptive statistics are presented as mean and standard deviation (SD) for continuous variables and as frequency and percentage for categorical variables. Data distribution was evaluated using the Shapiro–Wilk test. The Mann–Whitney U test was

Table 1. Comparison of basic patient and surgical characteristics between peribulbar group and incisionless sub-Tenon's group

Characteristics		Peribulbar group	Incisionless sub-Tenon's group	Test name, p-value
Age, mean [years]		66.1 ±13.1 (25–88)	70.1 ±10.2 (40–90)	$z = -1.033$, $p = 0.302$[a]
Gender	female	15 (41.7%)	16 (51.6%)	$\chi^2 = 0.323$, df = 1, $p = 0.570$[b]
	male	21 (58.3%)	15 (48.4%)	
ASA status	ASA 1–2	34 (94.5%)	30 (96.8%)	df = 1, $p > 0.999$[c]
	ASA 3	2 (5.5%)	1 (3.2%)	
BMI [kg/m^2]	under 30	31 (86.1%)	21 (67.7%)	$\chi^2 = 3.112$, df = 1, $p = 0.078$[b]
	above 30	5 (13.9%)	10 (32.3 %)	
Operation side	right eye	19 (52.8%)	17 (54.8%)	$\chi^2 = 0.001$, df = 1, $p = 0.976$[b]
	left eye	17 (47.2%)	14 (45.2%)	
Anticoagulant use		2 (5.6%)	5 (16.1%)	df = 1, $p = 0.236$[c]
Operation time [min]		24.1 ±4.5 (15–35)	26.5 ±8.8 (18–65)	$z = -0.931$, $p = 0.352$[a]

[a] Mann–Whitney U test, [b] continuity correction χ^2 test, [c] Fisher's exact test. All continuous variables were non-normally distributed; therefore, p-values were calculated using nonparametric tests. All categorical variables are presented as frequencies and percentages (%); ASA – American Society of Anesthesiologists; BMI – body mass index; df – degrees of freedom.

Table 2. Comparison of HR, MAP, and SpO_2 values over time between the peribulbar block group and the incisionless sub-Tenon's block group

Parameters		Peribulbar group	Sub-Tenon's group	p-value*	
Heart rate	before sedation	73.7 ±14.7 (45–106)	74.4 ±15.3 (52–119)	0.866	ANOVA (overall test): $F_{(4, 220)} = 0.532$ $p = 0.713$
	15 min after block	68.1 ±14.6 (50–109)	69.2 ±10.4 (50–100)	0.737	
	at the end of the surgery	67.2 ±14.8 (50–111)	65 ±9.9 (49–93)	0.514	
	3 h after surgery	69.1 ±13.7 (50–110)	69.2 ±11.6 (54–98)	0.980	
	1st postoperative day	69.5 ±13.8 (50–109)	65.3 ±14.1 (64–92)	0.330	
Mean arterial pressure	before sedation	105.1 ±15.4 (73–134)	103.1 ±21 (66–153)	0.690	ANOVA (overall test): $F_{(4, 220)} = 2.617$ $p = 0.048$
	15 min after block	93.4 ±14.4 (70–136)	94.4 ±16.3 (67–127)	0.818	
	at the end of the surgery	94.9 ±14.3 (65–131)	92.1 ±14.6 (58–126)	0.505	
	3 h after surgery	93 ±13.3 (72–135)	93.9 ±13.4 (70–125)	0.821	
	1st postoperative day	89.8 ±12.1 (70–132)	94.9 ±12.3 (72–122)	0.162	
Oxygen saturation (SpO_2)	before sedation	96.9 ±2.1 (92–100)	97.8 ±1.7 (93–100)	0.086	ANOVA (overall test): $F_{(4, 220)} = 1.318$ $p = 0.276$
	15 min after block	98.5 ±1.3 (94–100)	99 ±1.1 (95–100)	0.228	
	at the end of the surgery	99 ±0.9 (96–100)	99.2 ±0.8 (97–100)	0.531	
	3 h after surgery	99.2 ±1.4 (96–100)	99.1 ±0.7 (97–100)	0.945	
	1st postoperative day	99.1 ±0.7 (98–100)	99 ±1 (95–100)	0.793	

* Repeated-measures two-way ANOVA with Tukey's honestly significant difference (HSD) post hoc test. All variables were normally distributed and are presented as mean ± standard deviation (minimum–maximum); ns – not significant; HR – heart rate; MAP – mean arterial pressure; ANOVA – analysis of variance.

used to analyze differences in nonparametric continuous variables between groups, and the χ^2 test of independence was used for categorical variables (Table 1). Changes in HR, MAP, and SpO_2 (Table 2), as well as changes in eyelid movement, globe movement (akinesia), and corneal sensation (Table 3) over time in the peribulbar block and incisionless sub-Tenon's block groups, were evaluated separately using two-way analysis of variance (ANOVA) with repeated measures. Post hoc analyses were performed using Bonferroni correction for both within-group and between-group comparisons (Tables 4–7). The results of checking the assumptions for repeated-measures ANOVA (eyelid movement, globe movement, corneal sensation, chemosis, and subconjunctival hemorrhage) are presented as supplementary material (Supplementary Table 1). The subconjunctival petechiae variable could not be analyzed because of the low number of observed cases. The results of assumption testing are presented as supplementary material (Supplementary Table 2). For the analysis of repeated binary outcomes (presence of chemosis or hemorrhage at 4 time points), a generalized linear mixed model was used. The model included time, block type, and their interaction as fixed effects, and patient ID (PROTOCOL) as a random effect.

Table 3. Comparison of eyelid movement, globe movement (akinesia), and corneal sensation scores over time between the peribulbar block group and the incisionless sub-Tenon's block group

Parameters		Peribulbar group	Incisionless sub-Tenon's group	Test statics/p-value*	
Eyelid movement	before sedation	1.00 ±0.00	1.00 ±0.00	N/A	ANOVA (overall test): $F_{(5, 220)} = 0.839$, $p = 0.506$
	15 min after block	2.3 ±1.2 (1–3)	2.4 ±0.8 (1–3)	0.805	
	at the end of the surgery	2.1 ±0.7 (1–3)	2.4 ±0.8 (1–3)	0.227	
	3 h after surgery	2 ±0.6 (1–3)	2 ±0.7 (1–3)	0.858	
	1st postoperative day	1 ±0.2 (1–2)	1 ±0.3 (1–2)	0.573	
Globe movement (akinesia)	before sedation	4.00 ±0.00	4.00 ±0.00	N/A	ANOVA (overall test): $F_{(5, 220)} = 1.663$, $p = 0.170$
	15 min after block	9.4 ±3 (4–12)	10.7 ±2.5 (4–12)	0.066	
	at the end of the surgery	9.5 ±2.8 (4–12)	10.7 ±2.5 (4–12)	0.098	
	3 h after surgery	8.6 ±2.7 (4–12)	8.8 ±2.7 (4–12)	0.793	
	1st postoperative day	4.4 ±1.3 (4–10)	4.5 ±1.5 (4–11)	0.816	
Corneal sensation	before sedation	0.00 ±0.00	0.00 ±0.00	N/A	ANOVA (overall test): $F_{(5, 220)} = 0.884$, $p = 0.351$
	15 min after block	0.2 ±0.1 (0–1)	0.00 ±0.00	0.351	
	at the end of the surgery	0.00 ±0.00	0.00 ±0.00	na	
	3 h after surgery	0.2 ±0.1 (0–1)	0.00 ±0.00	0.351	
	1st postoperative day	0.00 ±0.00	0.00 ±0.00	N/A	

* Repeated-measures two-way analysis of variance (ANOVA) with Tukey's honestly significant difference (HSD) post hoc test. All variables were normally distributed and are presented as mean ± standard deviation (minimum–maximum); N/A – not available (no variability observed).

Table 4. Post hoc analysis (p-values) of eyelid movement, globe movement, and corneal sensation within the peribulbar block group (Tukey's honestly significant difference (HSD) post hoc test)

Parameters		15 min after block	At the end of the surgery	3 h after surgery	1st postoperative day
Eyelid movement	before sedation	<0.001	<0.001	<0.001	0.157
	15 min after block	–	>0.999	>0.999	<0.001
	at the end of the surgery	–	–	>0.999	<0.001
	3 h after surgery	–	–	–	<0.001
Globe movement (akinesia)	before sedation	<0.001	<0.001	<0.001	0.102
	15 min after block	–	0.999	0.999	<0.001
	at the end of the surgery	–	–	0.631	<0.001
	3 h after surgery	–	–	–	<0.001
Corneal sensation	before sedation	0.317	>0.999	0.317	>0.999
	15 min after block	–	0.317	>0.999	0.317
	at the end of the surgery	–	–	0.317	>0.999
	3 h after surgery	–	–	–	0.317

The model was specified as:

model < lmer(move_score ~ time × block + (1 | PROTOCOL), data = long_df).

P-values were calculated using the Satterthwaite approximation for degrees of freedom. A p-value of less than 5% was considered statistically significant.

Results

Sixty-seven adult patients were included in the study (mean age: 67 years; range: 25–90 years). There were 36 men (53.7%) and 31 women (46.3%). Patients were classified into 2 groups according to the anesthesia technique used: peribulbar block (n = 36) and incisionless sub-Tenon's block (n = 31). The 2 groups had similar baseline patient characteristics (Table 1).

Heart rate, MAP, and SpO_2 values measured at all time points (before sedation, 15 min after the block, at the end of surgery, 3 h after surgery, and on the 1st postoperative day) were similar between the peribulbar block group and the incisionless sub-Tenon's block group (Table 2).

Before sedation, eyelid and globe movements were completely normal in all patients. In addition, no corneal sensation was observed in either group. The incisionless sub-Tenon's block provided better akinesia than the peribulbar block, although the difference was not statistically significant

Table 5. Post hoc analysis of eyelid movement, globe movement, and corneal sensation within the incisionless sub-Tenon's block group (Tukey's honestly significant difference (HSD) post hoc test; test statistics and p-values)

Parameters		15 min after block	At the end of the surgery	3 h after surgery	1st postoperative day
Eyelid movement	before sedation	<0.001	<0.001	<0.001	0.083
	15 min after block	–	>0.999	0.003	<0.001
	at the end of the surgery	–	–	0.003	<0.001
	3 h after surgery	–	–	–	<0.001
Globe movement (akinesia)	before sedation	<0.001	<0.001	<0.001	0.102
	15 min after block	–	0.216	0.008	<0.001
	at the end of the surgery	–	–	<0.001	<0.001
	3 h after surgery	–	–	–	<0.001
Corneal sensation	before sedation	>0.999	>0.999	>0.999	>0.999
	15 min after block	–	>0.999	>0.999	>0.999
	at the end of the surgery	–	–	>0.999	>0.999
	3 h after surgery	–	–	–	>0.999

Table 6. Post hoc analysis (p-values) of chemosis, subconjunctival petechiae, and subconjunctival hemorrhage within the peribulbar block group (Tukey's honestly significant difference (HSD) post hoc test; test statistics and p-values)

Parameters		15 min after block	At the end of the surgery	3 h after surgery	1st postoperative day
Chemosis	before sedation	0.083	0.083	0.157	0.317
	15 min after block	–	>0.999	0.317	0.157
	at the end of the surgery	–	–	0.317	0.157
	3 h after surgery	–	–	–	0.317
Subconjunctival petechiae	before sedation	0.317	0.317	>0.999	0.317
	15 min after block	–	>0.999	0.317	0.317
	at the end of the surgery	–	–	0.317	0.317
	3 h after surgery	–	–	–	0.317
Subconjunctival hemorrhage	before sedation	>0.999	0.317	>0.999	0.317
	15 min after block	–	>0.999	>0.999	>0.999
	at the end of the surgery	–	–	>0.999	>0.999
	3 h after surgery	–	–	–	>0.999

Table 7. Post hoc analysis (p-values) of chemosis, subconjunctival petechiae, and subconjunctival hemorrhage within the incisionless sub-Tenon's block group (Tukey's honestly significant difference (HSD) post hoc test)

Parameters		15 min after block	At the end of the surgery	3 h after surgery	1st postoperative day
Chemosis	before sedation	0.004	0.006	0.004	0.016
	15 min after block	–	>0.999	0.480	0.557
	at the end of the surgery	–	–	0.414	0.414
	3 h after surgery	–	–	–	0.197
Subconjunctival petechiae	before sedation	0.102	0.102	0.317	0.180
	15 min after block	–	> 0.999	0.180	0.317
	at the end of the surgery	–	–	0.180	0.317
	3 h after surgery	–	–	–	0.317
Subconjunctival hemorrhage	before sedation	0.008	0.015	0.006	0.023
	15 min after block	–	>0.999	0.414	0.157
	at the end of the surgery	–	–	0.480	0.317
	3 h after surgery	–	–	–	0.102

Table 8. Comparison of the number of patients who developed minor complications (chemosis, subconjunctival petechiae, and subconjunctival hemorrhage) between the peribulbar block group and the incisionless sub-Tenon's block group (generalized linear mixed model)

Parameters		Peribulbar group	Incisionless sub-Tenon's group	p-value
Chemosis	15 min after block	3 (8.3)	11 (35.4)	0.215
	at the end of the surgery	3 (8.3)	10 (32.2)	0.215
	3 h after surgery	2 (5.5)	10 (32.2)	**0.033**
	1st postoperative day	1 (2.7)	8 (25.8)	0.225
Subconjunctival petechiae	15 min after block	1 (2.7)	3 (9.6)	0.658
	at the end of the surgery	1 (2.7)	3 (9.6)	0.658
	3 h after surgery	0 (0)	1 (3.2)	0.940
	1st postoperative day	1 (2.7)	2 (6.4)	0.614
Subconjunctival hemorrhage	15 min after block	0 (0)	7 (22.5)	0.325
	at the end of the surgery	1 (2.7)	7 (22.5)	0.325
	3 h after surgery	0 (0)	9 (29)	0.237
	1st postoperative day	0 (0)	6 (19.3)	0.431

All variables are presented as frequencies and percentages (%). Bold values indicate statistical significance.

($p > 0.05$) (Table 3). Post hoc within-group analyses were performed using the Bonferroni correction (Tables 4,5).

Before sedation, no patient had chemosis, subconjunctival petechiae, or hemorrhage. Chemosis was significantly lower in the peribulbar block group than in the incisionless sub-Tenon's block group ($p = 0.033$) at 3 h after surgery. Although minor complications were less frequent in the peribulbar block group, the differences were not statistically significant ($p > 0.05$). (Table 8). Post hoc within-group analyses were performed using the Bonferroni correction (Tables 6,7).

In both groups, none of the patients reported pain before sedation. Visual analogue scale scores measured at 3 h after the block and on the 1st postoperative day were comparable between the groups ($p > 0.05$). The percentages of patients in the peribulbar block group and the incisionless sub-Tenon's block group were also comparable with regard to the 6th item of the RCSQ (79.2 vs 75.48; $p = 0.843$). The mean total RCSQ score was 381.2 ±56.9 (range: 280–490) in the peribulbar block group, whereas patients in the incisionless sub-Tenon's block group had a mean total RCSQ score of 365.8 ±67.7 (range: 115–500) ($p = 0.396$). Overall sleep perception was comparable between the groups ($p = 0.355$) (Fig. 1). Twenty patients (55.5%) in the peribulbar block group and 15 patients (48.3%) in the incisionless sub-Tenon's block group reported "very good sleep perception." Finally, patient satisfaction was assessed on the 1st postoperative day. Satisfaction levels were comparable between the 2 groups ($p = 0.417$) (Table 9).

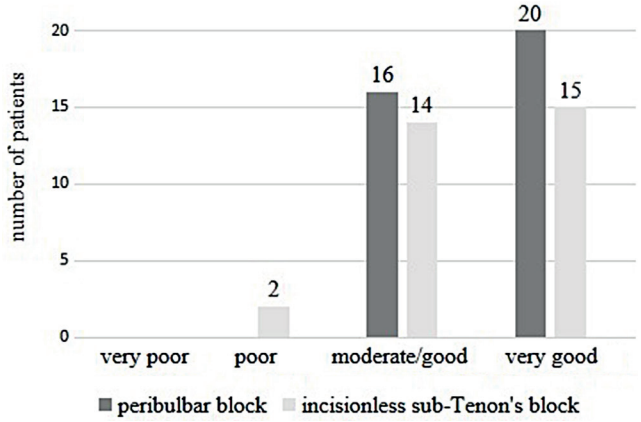

Fig. 1. Categories of overall sleep perception in both groups

Table 9. Comparison of patient satisfaction between the peribulbar block group and the incisionless sub-Tenon's block group (contingency table)

Patient satisfaction	Peribulbar group	Sub-Tenon's group	p-value*
Poor	0 (0)	0 (0)	0.417
Moderate	4 (11.4)	7 (22.6)	
Good	16 (45.7)	13 (41.9)	
Very good	15 (42.9)	11 (35.5)	

* Pearson's χ^2 test. All variables are presented as frequencies and percentages (%).

Discussion

In this study, 2 increasingly used regional anesthesia techniques in cataract surgery – peribulbar block and incisionless sub-Tenon's block – were compared in several aspects, including their ability to provide essential surgical conditions such as eyelid immobilization and akinesia, their associated perioperative complications, and their potential effects on postoperative sleep quality.

Akinesia and eyelid immobility are essential for the safety and success of cataract surgery. In the present study, compared with the peribulbar block, the incisionless sub-Tenon's block was found to be superior in providing akinesia, with p-values close to the level of statistical significance. There are conflicting results in the literature regarding this issue. In a study by Antony et al., the proportion of patients with complete akinesia was found to be significantly greater

in the peribulbar block group than in the sub-Tenon's block group. However, the authors reported that the onset time of akinesia was significantly longer in the peribulbar block group than in the sub-Tenon's block group.[7] We did not measure the onset time of akinesia in our study; however, our findings were consistent with the results of that study. In another study, patients in the sub-Tenon's block group had better akinesia than those in the peribulbar block group.[11] On the other hand, Iganga et al. reported that the 2 regional blocks provided comparable levels of adequate akinesia during cataract surgery.[12] We frequently perform these 2 regional blocks for cataract surgery and many other ocular procedures in our clinic. Based on both the results of our study and our clinical experience, we believe that the sub-Tenon's block provides better akinesia than the peribulbar block.

There is a clear interaction between postoperative pain status and sleep quality.[13] The relationship between pain and sleep disorders, such as short sleep duration or insomnia, has been well established. However, this relationship is bidirectional; while pain disrupts sleep quality, sleep disorders can also exacerbate pain.[3,14] In our study, postoperative pain scores were similar between the peribulbar block and incisionless sub-Tenon's block groups, consistent with previous studies.[12,15,16]

No major complications were observed in the present study. Therefore, minor complications, including chemosis, subconjunctival petechiae, and hemorrhage, were evaluated. According to the results, chemosis and subconjunctival hemorrhage were observed more frequently in the sub-Tenon's block group than in the peribulbar block group. Similar findings have been reported in the majority of previous studies.[12,15,16] In one of the first studies on sub-Tenon's blocks, it was reported that such minor complications were common with this technique but did not cause intraoperative complications.[17] Based on our clinical experience, we agree with this observation, as all of these complications resolved within a few days after surgery and no serious clinical problems developed in any patient.

The primary aim of the present study was to compare the effects of a peribulbar block and an incisionless sub-Tenon's block on postoperative sleep quality. Postoperative sleep disorders are important factors that can negatively affect the recovery process and increase patient morbidity and mortality. Approximately half of patients experience sleep problems during the first days after surgery. The anesthesia technique has also been suggested to be one of the factors affecting postoperative sleep quality.[18,19] Anesthetic drugs can reduce sleep quality by disrupting the normal sleep–wake cycle or affecting the natural rhythm of melatonin, one of the key neurotransmitters involved in the sleep process.[14,20–22] Studies have shown that general anesthesia impairs sleep patterns, and that regional anesthesia is advantageous over general anesthesia with regard to the development of postoperative sleep disorders.[21,23] Despite its importance for surgical success and postoperative recovery, the effect of anesthesia methods on sleep quality has not received sufficient attention. Based on this, the present study investigated the effects of the 2 most commonly used regional block techniques on postoperative sleep quality in patients undergoing cataract surgery, one of the most frequently performed procedures in routine clinical practice.

Statistically, there was no difference in sleep quality between the 2 regional techniques. Sleep is a physiological process that can be influenced by many individual and environmental factors.[20] Therefore, in studies evaluating sleep quality, creating homogeneous patient groups and ensuring environmental conditions that are as similar as possible allow for more reliable statistical outcomes.[14] In our study, the 2 anesthesia groups were similar in terms of baseline patient and surgical characteristics. Noise levels in the sleeping environments were also comparable between the groups.

It should be noted that the need for maintenance anesthetic medications (sedatives and/or analgesics) was greater in the peribulbar block group than in the incisionless sub-Tenon's block group. Considering the effect of postoperative pain levels on sleep quality, the lower requirement for analgesic medication in the sub-Tenon's block group may make this anesthesia technique more favorable, even though statistically both regional blocks had similar effects on postoperative sleep quality. In the present study, all patients were premedicated with dexmedetomidine in addition to midazolam and fentanyl. We routinely use dexmedetomidine in ophthalmic surgeries because of its effectiveness in providing sedoanalgesia and reducing intraocular pressure. Palte et al. also demonstrated in their studies that early administration of a dexmedetomidine bolus (8–20 μg) before midazolam (1–2 mg) and/or low-dose fentanyl (0.5 μg/kg) created ideal conditions for the administration of peribulbar, retrobulbar, or sub-Tenon's blocks. They reported that the use of dexmedetomidine reduced the need for propofol and provided prolonged sedation.[24]

Limitations of the study

Several limitations of this study should be acknowledged. First, it was conducted at a single center, which may limit the generalizability of the results. Second, sleep quality was assessed subjectively rather than objectively, using methods such as polysomnography. Finally, the relatively small sample size may be considered another limitation of this work. However, owing to its prospective design and the fact that it is the first study to compare 2 regional block techniques in terms of postoperative sleep quality, this study remains scientifically valuable.

Conclusions

Incisionless sub-Tenon's block was superior to the peribulbar block in terms of providing akinesia and reducing the need for maintenance anesthetic medications such as sedatives or analgesics. Although minor complications,

including chemosis and subconjunctival hemorrhage, occurred more frequently in the incisionless sub-Tenon's group, all were transient and had no serious clinical significance. The 2 regional techniques were similar with regard to postoperative sleep quality and patient satisfaction.

Supplementary data

The supplementary materials are available at https://doi.org/10.5281/zenodo.13826194. The package contains the following files:

Supplementary Table 1. Test statistics 1.
Supplementary Table 2. Test statistics 2.
Supplementary Table 3. Test statistics 3.
Supplementary Table 4. Test statistics 4.
Supplementary Table 5. Test statistics 5.
Supplementary Table 6. Test statistics 6.
Supplementary Table 7. The results of checking the ANOVA assumptions for repeated measures.
Supplementary Table 8. Test assumption checking.

Data Availability Statement

The datasets supporting the findings of the current study are openly available in Zenodo repository at https://doi.org/10.5281/zenodo.16358814.

Consent for publication

Not applicable.

Use of AI and AI-assisted technologies

Not applicable.

ORCID iDs

Yeliz Kılıç https://orcid.org/0000-0003-1446-7747
Haluk Hüseyin Gürsoy https://orcid.org/0000-0002-9254-4114
Mustafa Değer Bilgeç https://orcid.org/0000-0002-9972-2147
Ali Rıza Ata https://orcid.org/0009-0006-1301-7911
Mehmet Sacit Güleç https://orcid.org/0000-0002-7107-3798

References

1. Lapp T, Wacker K, Heinz C, Maier P, Eberwein P, Reinhard T. Cataract surgery: Indications, techniques, and intraocular lens selection. *Dtsch Arztebl Int*. 2023;120(21):377–386. doi:10.3238/arztebl.m2023.0028
2. Yang D, Yang L, Li Q, Zuo Y. Pharmacotherapy for improving postoperative sleep quality: A protocol for a systematic review and network meta-analysis. *BMJ Open*. 2023;13(2):e069724. doi:10.1136/bmjopen-2022-069724
3. Wei W, Huang X, Zhu J. Effect of acupoint therapies on postoperative sleep quality: A narrative review. *Med Sci Monit*. 2023;29:e938920. doi:10.12659/MSM.938920
4. Palte H. Ophthalmic regional blocks: Management, challenges, and solutions. *Local Reg Anesth*. 2015;8:57. doi:10.2147/LRA.S64806
5. Calenda E, Olle P, Muraine M, Brasseur G. Peribulbar anesthesia and sub-Tenon injection for vitreoretinal surgery: 300 cases. *Acta Ophthalmol Scand*. 2000;78(2):196–199. doi:10.1034/j.1600-0420.2000.078002196.x
6. Coban-Karatas M, Cok OY, Kumar CM. Lacrimal dilator-facilitated incisionless vs standard sub-Tenon's block: A randomized, prospective and non-inferiority comparative study. *Eye*. 2021;35(7):1961–1966. doi:10.1038/s41433-020-01207-0
7. Antony RM, Kamath AR, Jeganathan S, Rodrigues GR. A comparison of sub-tenon block with peribulbar block in small-incision cataract surgery. *Indian J Ophthalmol*. 2022;70(11):3840–3843. doi:10.4103/ijo.IJO_1553_22
8. Alhassan MB, Kyari F, Ejere HO. Peribulbar versus retrobulbar anaesthesia for cataract surgery. *Cochrane Database Syst Rev*. 2008;3:CD004083. doi:10.1002/14651858.CD004083.pub2
9. Karaman Özlü Z, Özer N. Richard–Campbell Sleep Questionnaire validity and reliability study. *J Turk Sleep Med*. 2015;2(2):29–32. doi:10.4274/jtsm.02.008
10. Duran MK, Öztürk Ş. The effect of shoulder massage on shoulder pain and sleep quality in patients after laparoscopic cholecystectomy: A randomized controlled trial. *BMC Nurs*. 2024;23(1):618. doi:10.1186/s12912-024-02264-6
11. Al-Yousuf. Sub-Tenon versus peribulbar anaesthesia for cataract surgery. *Bahrain Med Bull*. 2003;25:115–118. https://bahrainmedicalbulletin.com/September_2003/SubTenon.pdf.
12. Iganga O, Fasina O, Bekibele C, Ajayi BenedictusGK, Ogundipe A. Comparison of peribulbar with posterior sub-tenon's anesthesia in cataract surgery among Nigerians. *Middle East Afr J Ophthalmol*. 2016;23(2):195. doi:10.4103/0974-9233.164609
13. Ohayon MM. Epidemiology of insomnia: What we know and what we still need to learn. *Sleep Med Rev*. 2002;6(2):97–111. doi:10.1053/smrv.2002.0186
14. Lin D, Huang X, Sun Y, Wei C, Wu A. Perioperative sleep disorder: A review. *Front Med (Lausanne)*. 2021;8:640416. doi:10.3389/fmed.2021.640416
15. Parkar T, Gogate P, Deshpande M, Adenwala A, Maske A, Verappa K. Comparison of subtenon anaesthesia with peribulbar anaesthesia for manual small incision cataract surgery. *Indian J Ophthalmol*. 2005;53(4):255. doi:10.4103/0301-4738.18907
16. Adekola O, Aribaba O, Musa K, et al. Regional anesthesia for small incision cataract surgery: Comparison of subtenon and peribulbar block. *J Clin Sci*. 2018;15(1):1. doi:10.4103/jcls.jcls_5_17
17. Roman SJ, Sit DAC, Boureau CM, Auclin FX, Ullern MM. Sub-Tenon's anaesthesia: An efficient and safe technique. *Br J Ophthalmol*. 1997;81(8):673–676. doi:10.1136/bjo.81.8.673
18. Rosenberg J. Sleep disturbances after non-cardiac surgery. *Sleep Med Rev*. 2001;5(2):129–137. doi:10.1053/smrv.2000.0121
19. Ji C, Su X, Gao C, et al. Advances in the use of dexmedetomidine during the perioperative period to improve postoperative sleep quality in patients undergoing surgery. *J Int Med Res*. 2024;52(11):03000605241290715. doi:10.1177/03000605241290715
20. Luo M, Song B, Zhu J. Sleep disturbances after general anesthesia: Current perspectives. *Front Neurol*. 2020;11:629. doi:10.3389/fneur.2020.00629
21. Yuan Y, Song Y, Wang G, et al. Effects of general versus regional anaesthesia on circadian melatonin rhythm and its association with postoperative delirium in elderly patients undergoing hip fracture surgery: Study protocol for a prospective cohort clinical trial. *BMJ Open*. 2021;11(2):e043720. doi:10.1136/bmjopen-2020-043720
22. Zheng F, Zheng ZH, Wang W, Zhu KL, Xing HL, Ding LM. Association between sleep quality and general anesthesia in teenager under elective surgery: A prospective study. *Ir J Med Sci*. 2022;191(5):2297–2303. doi:10.1007/s11845-021-02847-1
23. Yang Y, Zhang Y, Zhou G, Yang Z, Yan H, Zhang J. Efficacy of epidural esketamine on postoperative sleep quality after laparoscopic and robotic lower abdominal surgeries: A study protocol for randomised, double-blind, controlled trial. *BMJ Open*. 2024;14(2):e081589. doi:10.1136/bmjopen-2023-081589
24. Palte H, Masters N. Contemporary anesthesia perspectives for ophthalmic surgery: A brief review. *Med Res Arch*. 2023;11(8):1–9. doi:10.18103/mra.v11i8.4244

Lateral nail entry increases valgus risk, but coronal plane deformity does not affect knee function after femoral locked nailing

Onur Suer[1,A–F], Yusuf Taha Kirmic[1,A–D], Recep Selcuk Eyceyurt[1,A,B,D,E], Meliksah Uzakgider[1,A–D,F], Mesut Tahta[1,A,C–F], Cemil Kayali[1,A,C–F], Kemal Aktuglu[2,A,C–F]

[1] Department of Orthopaedics and Traumatology, Izmir City Hospital, Turkey
[2] Department of Orthopaedics and Traumatology, Faculty of Medicine, Ege University, Izmir, Turkey

A – research concept and design; B – collection and/or assembly of data; C – data analysis and interpretation; D – writing the article; E – critical revision of the article; F – final approval of the article

Advances in Clinical and Experimental Medicine, ISSN 1899–5276 (print), ISSN 2451–2680 (online) *Adv Clin Exp Med*. 2026;35(4):683–691

Address for correspondence
Onur Suer
E-mail: onursuer3434@gmail.com

Funding sources
None declared

Conflict of interest
None declared

Received on February 9, 2025
Reviewed on May 18, 2025
Accepted on July 8, 2025

Published online on April 14, 2026

Abstract

Background. Closed locked intramedullary nailing (IMN) of femoral diaphyseal fractures (FDF) is the gold standard treatment. Postoperative frontal plane deformities can still occur following locked IMN.

Objectives. The primary aim of this study was to evaluate the effect of coronal plane deformities on knee joint function and overall functional outcomes in adults with FDF treated using static locked IMN.

Materials and methods. One hundred and twenty patients treated with locked IMN for FDF were divided into 2 groups based on coronal plane angulation measured on long-leg radiographs: group A (<5° deformity, n = 100) and group B (≥5° deformity, n = 20). Factors potentially influencing coronal plane deformity were compared between the groups. Radiographic parameters, including the mechanical lateral distal femoral angle (mLDFA), mechanical medial proximal tibial angle (mMPTA), and postoperative lower extremity mechanical axis angle (MA), as well as intraoperative factors and complications, were analyzed. Functional outcomes were assessed using the Western Ontario and McMaster Universities Osteoarthritis Index (WOMAC) knee score, the Lower Extremity Functional Scale, and the Kujala patellofemoral scoring system.

Results. There were no significant differences between the groups in terms of age, gender, AO classification, or mechanism of injury. Coronal plane deformity was found to be independent of fracture localization, fracture type, and use of a traction table. However, nails implanted laterally to the greater trochanter were associated with significantly more valgus deformity ($p < 0.001$). No significant differences were observed in postoperative mLDFA, mMPTA, or MA between the groups at the final follow-up. Functional scores also showed no significant differences.

Conclusions. After a minimum follow-up of 5 years, no adverse effects on knee or patellofemoral joint function were observed in patients with coronal plane deformities. Coronal plane deformity following locked IMN for FDF was independent of fracture location, classification, and traction table use. However, lateral entry to the greater trochanter was associated with increased valgus deformity.

Key words: femur diaphyseal fractures, intramedullary nailing, coronal plane malalignment

Cite as
Suer O, Kirmic YT, Eyceyurt RS, Uzakgider M, Tahta M, Kayali C, Aktuglu K. Lateral nail entry increases valgus risk, but coronal plane deformity does not affect knee function after femoral locked nailing. *Adv Clin Exp Med*. 2026;35(4):683–691. doi:10.17219/acem/208062

DOI
10.17219/acem/208062

Highlights

- Coronal plane malalignment after locked intramedullary nailing for femoral diaphyseal fractures was not associated with fracture location, AO/OTA classification, or the use of a traction table.
- A lateral entry point at the greater trochanter significantly increased the risk of postoperative valgus deformity in femoral diaphyseal fractures.
- Coronal plane deformity after intramedullary nailing did not adversely affect long-term knee function or patellofemoral joint outcomes at a minimum 5-year follow-up.

Background

The femur serves as the main weight-bearing bone of the lower extremity, and its fracture can lead to substantial morbidity and mortality. Femoral diaphyseal fractures (FDF) are common fractures in orthopedic practice, frequently seen in young male patients as a result of high-energy trauma, such as traffic accidents, falls from significant heights, or gunshot wounds.[1–3] In this group of patients, transverse or oblique fractures are typically located in the middle third of the femoral shaft.[1–3] These fractures display a bimodal distribution: They occur primarily in younger individuals due to high-energy trauma, while in elderly patients, they are more often the result of low-energy trauma.[4] According to epidemiological studies, the annual incidence of diaphyseal femur fractures is estimated to be around 13 per 100,000 individuals.[5]

Currently, the preferred treatment for FDF is locked intramedullary nailing (IMN) with closed reduction, which is considered the gold standard due to its high union rates, facilitation of early mobilization and weight-bearing, and low complication rates.[6,7] From both biomechanical and clinical perspectives, this method is regarded as superior to extramedullary fixation with plates and external fixators. [6,7] However, malalignment is a well-recognized complication in the literature that may lead to non-union and may require additional surgical intervention after locked IMN.[8,9]

Malalignment can present as angular deformities (such as varus/valgus or flexion/extension) or rotational discrepancies. Postoperative coronal plane deformities following locked IMN are typically defined as frontal plane angulations exceeding 5°, which are generally classified as deformities. A literature review indicates that coronal malalignment is most commonly defined as an angular deformity of either "more than 5 degrees" or "5 degrees or more."[9–12] Studies report that the incidence of such deformities above 5° ranges from 2% to 18%.[9,11,13] While some studies in the literature have explored the impact of rotational deformities on patient functional outcomes following femoral IMN, there is a lack of research examining the effect of coronal deformities on functional status.

Objectives

To our knowledge, this study is the first to directly evaluate the impact of coronal plane malalignment on long-term functional outcomes, including knee and patellofemoral joint function, following locked intramedullary nailing of femoral diaphyseal fractures. The primary aim of this study was to evaluate the effect of coronal plane deformities on knee joint function and overall functional outcomes in adults with FDF treated using static locked IMN. A secondary aim was to identify the factors that contribute to the development of these coronal plane deformities. We hypothesized that coronal plane deformity negatively impacts knee function following femoral locked IMN.

Materials and methods

Study design and patient selection

This retrospective study included patients who underwent locked intramedullary nailing (IMN) for FDF in the Orthopedics and Traumatology Departments of 2 trauma centers. The study received approval from the Medical Research Ethics Committee of İzmir Bozyaka Training and Research Hospital (approval No. 2023/55), and general informed consent was obtained from each participant before the study procedures.

One hundred and twenty patients treated with locked IMN for FDF between February 2012 and February 2019 were included in the study. We excluded patients with open fractures, pathological fractures, additional lower extremity fractures, a history of knee surgery, those over 60 years of age, and those with a follow-up period of less than 5 years. Patients were divided into 2 groups based on coronal plane angulation measurements at the femoral fracture line obtained from orthoroentgenograms: group A, with an angulation of less than 5° (n = 100, 83.4%), and group B, with an angulation of 5° or greater (n = 20, 16.6%). Patient demographics, trauma mechanisms, follow-up duration, type of femoral nail used, and use of a traction table during surgery were obtained from medical records (Table 1).

Assessment of parameters between groups

Fracture localization and the Müller AO classification of fractures were assessed on preoperative femur radiographs. Three orthopedic surgeons independently reviewed and measured the preoperative and postoperative radiographic parameters. Fracture union was evaluated on anteroposterior and lateral femur radiographs obtained during follow-up. Sagittal plane angulations of the femur were assessed using lateral femur radiographs.

Orthoroentgenograms were used to assess femoral length discrepancies, coronal plane angulations (varus/valgus) at the fracture line, mechanical lateral distal femoral angle (mLDFA), mechanical medial proximal tibial angle (mMPTA), and postoperative lower extremity mechanical axis angle (MA), and to compare the sizes of the lesser trochanters on both sides to detect rotational deformity (Fig. 1–3). Coronal plane deformity of the femur was evaluated by drawing one line from the fracture site to the proximal center of the medullary canal and another line from the fracture site to the midpoint of the distal femoral articular surface. The angle between these 2 lines was then measured (Fig. 1C, Fig. 2C).

Functional outcomes were evaluated using the Western Ontario and McMaster Universities Osteoarthritis Index (WOMAC) knee scores, the Lower Extremity Functional Scale, and the Kujala patellofemoral scoring system, and these outcomes were compared between the 2 groups.

Surgical technique

All surgical procedures were performed after patients were medically stabilized and appropriate radiological examinations and consultations were completed. Antegrade locked intramedullary nails were used for all patients. Procedures were conducted either on a traction table in the supine position or on a standard operating table in the lateral position. The insertion point for nail entry was selected based on individual anatomy, with entry sites including the greater trochanter, piriformis fossa, or the lateral aspect of the greater trochanter.

Statistical analyses

Continuous variables with a non-normal distribution are presented as medians and interquartile ranges (IQR; 1st quartile (Q1) and 3rd quartile (Q3) values reported), while categorical variables are presented as percentages. Normally distributed continuous variables are shown as means with standard deviations (SD). Categorical variables were compared between groups using Pearson's

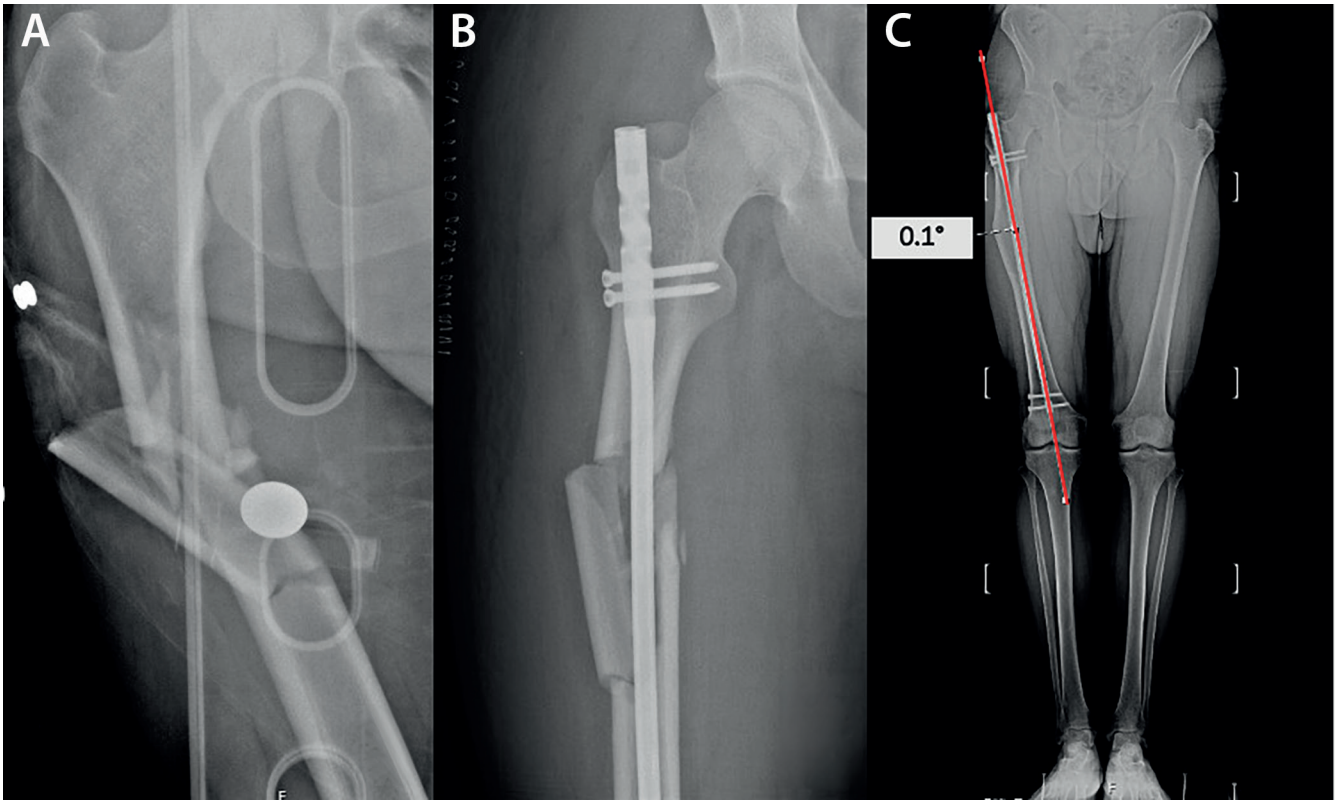

Fig. 1. A 24-year-old male patient in group A with an AO type C femoral fracture. Preoperative (A) and early postoperative x-rays (B). Measurement of coronal plane was performed as follows: To assess the coronal plane deformity of the femur, a line was drawn from the fracture line to the proximal center of the medullary canal, and another line was drawn from the fracture line to the midpoint of the distal femoral joint surface. The angle formed between these 2 lines was then calculated. At the last follow-up, the coronal plane angle in the operated right femur was measured at 0.1°(C)

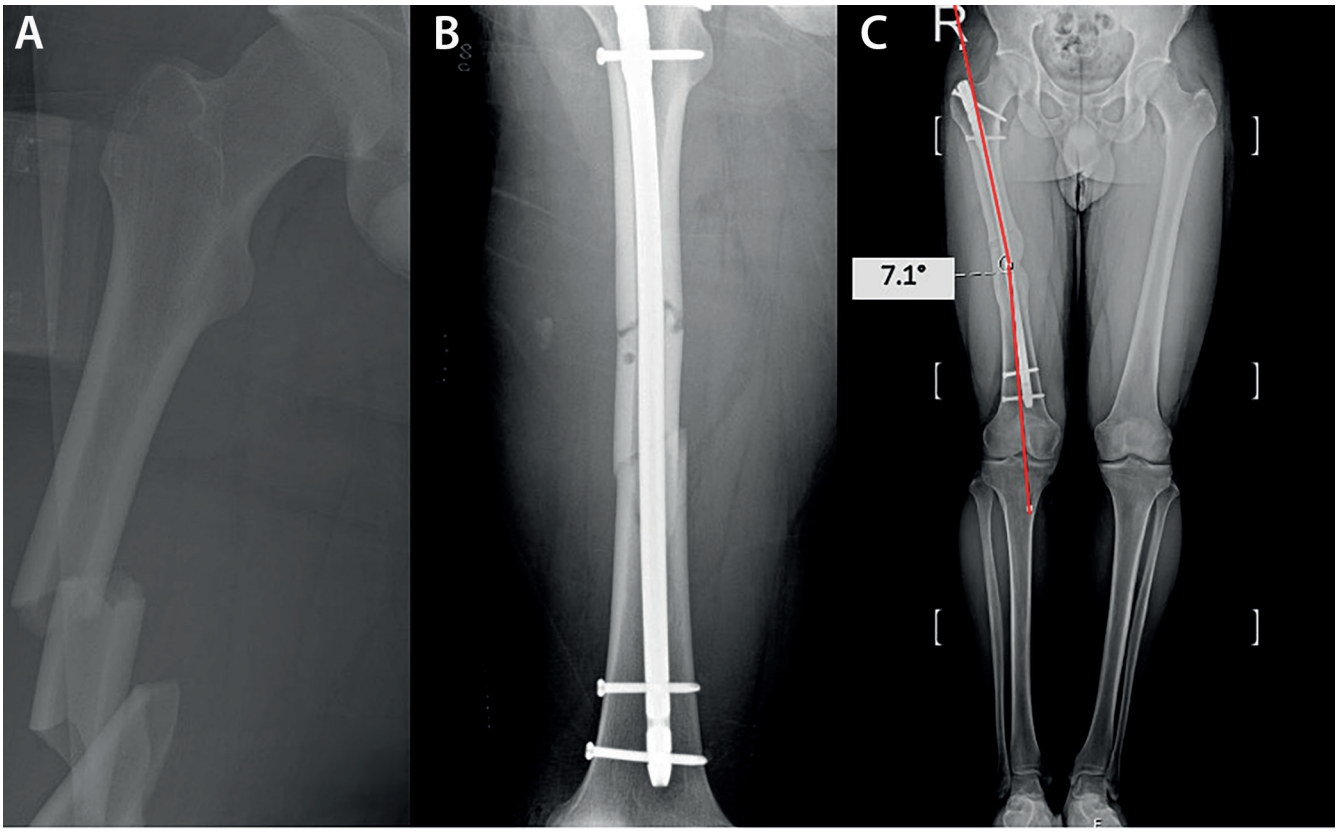

Fig. 2. A 22-year-old male patient in group B with an AO type C femoral fracture. Preoperative (A) and early postoperative x-rays (B). Measurement of coronal plane angle was performed as follows: To assess the coronal plane deformity of the femur, a line was drawn from the fracture line to the proximal center of the medullary canal, and another line was drawn from the fracture line to the midpoint of the distal femoral joint surface. The angle formed between these 2 lines was then calculated. At the last follow-up the coronal plane angle in the operated right femur was measured at 7.1°(C)

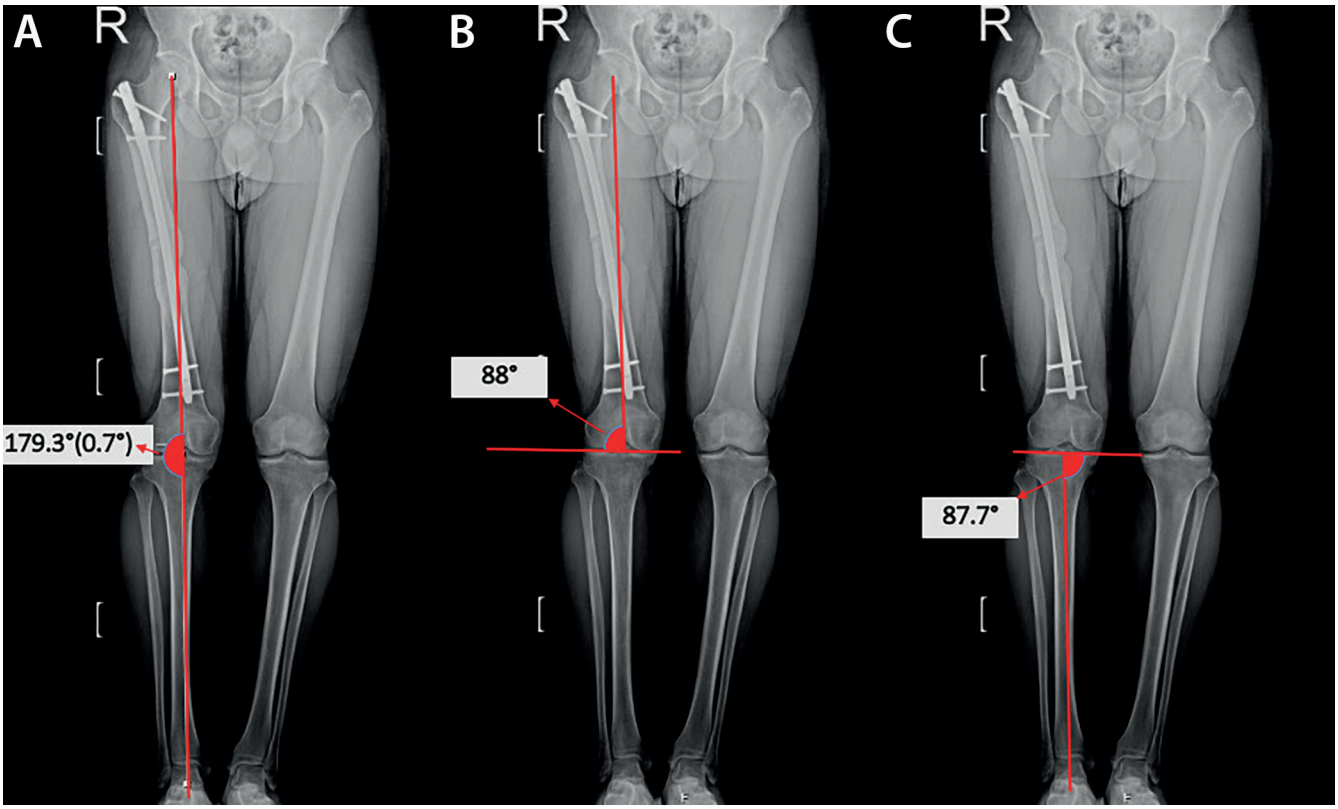

Fig. 3. The mechanical axis angle is defined as the angle formed between a line drawn from the center of the femoral head to the midpoint of the femoral condyles and a line extending from the center of the tibial plateau to the center of the tibial plafond (A). The mechanical lateral distal femoral angle (mLDFA) is defined as the angle created by the line connecting the center of the femoral head to the midpoint of the femoral condyles and the femoral knee joint line (B). The mechanical medial proximal tibial angle (mMPTA) is defined as the angle between the line connecting the center of the proximal tibia to the center of the talar dome and the tibial knee joint line (C)

χ^2 test. The normality of continuous variables was assessed using the Shapiro–Wilk test, and the homogeneity of variances was evaluated using Levene's test.

Comparisons of continuous variables between groups were performed using independent-samples t-tests for normally distributed data, and the Mann–Whitney U test was applied for non-normally distributed data. Interrater reliability was assessed using the intraclass correlation coefficient (ICC; 2-way mixed effects, absolute agreement, 3 raters) at each measurement point.

All statistical analyses were performed using IBM SPSS v. 23.0 (IBM Corp., Armonk, USA), with statistical significance set at $p < 0.05$.

Results

Patients were divided into 2 groups based on the coronal plane angle measurements of the femoral fracture line obtained from orthoroentgenograms: group A, with angulation less than 5° (n = 100, 83.4%), and group B, with angulation of 5° or more (n = 20, 16.6%). In group B, 6 patients (30%) exhibited varus deformity, while 14 patients (70%) displayed valgus deformity. The median coronal plane angle was 1.14° (Q1 = 0.5, Q3 = 2) in group A and 5.74° (Q1 = 5, Q3 = 6.2) in group B.

The median age was 28 years (Q1 = 21, Q3 = 39.25) in group A and 27 years (Q1 = 20, Q3 = 36.75) in group B, with no statistically significant difference (U = 1092, p = 0.519). The median body weight was 77 kg (Q1 = 73, Q3 = 79) in group A and 75.5 kg (Q1 = 73.5, Q3 = 78.25) in group B (U = 1138, p = 0.331). Similarly, the median body mass index (BMI) was 24.64 kg/m^2 (Q1 = 23.71, Q3 = 25.58) in group A and 24.46 kg/m^2 (Q1 = 23.23, Q3 = 25.89) in group B, showing no significant difference (U = 1007, p = 0.963). In terms of gender distribution, group A consisted of 19 women (19%) and 81 men (81%), whereas group B included 4 women (20%) and 16 men (80%), with no significant difference between groups ($\chi^2 = 0.013$, p = 0.918).

Regarding the mechanism of injury, motor vehicle accidents accounted for 73% of cases in group A and 85% in group B, while falls constituted 27% and 15%, respectively. Again, this difference was not statistically significant ($\chi^2 = 1.263$, p = 0.262). The median follow-up time was 78 months (Q1 = 69, Q3 = 90) in group A and 72 months (Q1 = 66, Q3 = 80.5) in group B (U = 1168, p = 0.238) (Table 1).

There was a satisfactory level of agreement among the 3 physicians who independently conducted radiological evaluations for all patients. The ICC values were 0.96, 0.95, and 0.92 for the CP angle; 0.94, 0.92, and 0.93 for mLDFA; 0.91, 0.94, and 0.95 for mMPTA; and 0.90, 0.95, and 0.91 for the MA angle, according to the measurement time points.

None of the 120 patients included in our study showed any signs of clinical rotational deformity. Radiologically, rotational deformity was assessed using orthoroentgenograms by comparing the sizes of the lesser trochanters on both sides. No discrepancies were observed in any patient. Postoperative sagittal plane deformities of the femur were assessed using lateral femur radiographs, and no deformities were identified in any patient.

The femoral diaphysis was divided into 3 equal segments, and fractures were categorized based on their location as proximal third (n = 19; 15.8%), middle third (n = 78; 65%), and distal third (n = 23; 19.2%) fractures. Coronal plane deformities ≥5° were found in 5.3% of proximal third, 17.9% of middle third, and 21.7% of distal third diaphyseal fractures. There were no significant differences between coronal plane deformities and fracture localization ($\chi^2 = 2.297$, p = 0.169) (Table 2).

Table 1. Demographic and clinical characteristics of the 2 groups

Variable		Group A (CP angle <5°)	Group B (CP angle ≥5°)	p-value
n		100	20	–
Age [years], median (Q1, Q3)		28 (21, 39.25)	27 (20, 36.75)	U = 1092 p = 0.519*
Weight [kg], median (Q1, Q3)		77 (73, 79)	75.5 (73.5, 78.25)	U = 1138 p = 0.331*
BMI [kg/m^2], median (Q1, Q3)		24.64 (23.71, 25.58)	24.46 (23.23, 25.89)	U = 1007 p = 0.963*
Gender, n (%)	female	19 (19)	4 (20)	$\chi^2 = 0.013$ p = 0.918#
	male	81 (81)	16 (80)	
Mechanism of injury, n (%)	motor vehicle	73 (73)	17 (85)	$\chi^2 = 1.263$ p = 0.262#
	falling	27 (27)	3 (15)	
Follow-up time [months], median (Q1, Q3)		78 (69, 90)	72 (66, 80.5)	U = 1168 p = 0.238*

The normality of the data was assessed using the Shapiro–Wilk test and the homogeneity of variances was evaluated using Levene's test. *The Mann–Whitney U test was employed to compare age, body weight, BMI, and follow-up duration between the 2 groups. #Pearson's χ^2 test was applied to assess group differences in gender and injury mechanism. CP – coronal plane; BMI – body mass index.

Table 2. Factors that may cause postoperative coronal plane deformity

Variable	Group A (CP angle <5°) n = 100 n (%)	Group B (CP angle ≥5°) n = 20 n (%)	Total n (%)	p-value
Fracture localization				
Proximal diaphysis	18 (94.7)	1 (5.3)	19 (100)	$\chi^2 = 2.297$ p = 0.169
Middle diaphysis	64 (82.1)	14 (17.9)	78 (100)	
Distal diaphysis	18 (78.3)	5 (21.7)	23 (100)	
Fracture classification				
AO type A	65 (82.3)	14 (17.7)	79 (100)	$\chi^2 = 0.332$ p = 0.758
AO type B	27 (87.1)	4 (12.9)	31 (100)	
AO type C	8 (80)	2 (20)	10 (100)	
Nail entry site				
Greater trochanter	36 (97.3)	1 (2.7)	37 (100)	$\chi^2 = 28.092$ p < 0.001
Lateral	12 (50)	12 (50)	24 (100)	
Piriformis fossa	52 (88.1)	7 (11.9)	59 (100)	
Operating table				
Traction table	75 (84.4)	16 (17.6)	91 (100)	$\chi^2 = 0.369$ p = 0.637
Standard operating table	25 (86.2)	4 (13.8)	29 (100)	

Pearson's χ^2 test was used to analyze the association between the groups and variables including fracture type, localization, nail entry point, and surgical table configuration. CP – coronal plane; AO – the Müller AO classification of fractures.

Table 3. Radiological parameters of 2 groups

Variable	Group A (CP angle <5°)	Group B (CP angle ≥5°)	p-value
n	100	20	–
CP angle [°], median (Q1, Q3)	1.14 (0.5, 2)	5.74 (5, 6.2)	U = 0.0 p < 0.001*
Last follow-up mLDFA [°], average ±SD	87,48 ±2.2	87.05 ±1.7	t = 0.778 p = 0.415#
Last follow-up mMPTA [°], average ±SD	88.21 ±3.1	88.8 ±2.4	t = 0.952 p = 0.350#
Last follow-up MA [°], median (Q1, Q3)	2.20 (0.35, 3.85)	1.95 (1.08, 2.93)	U = 1069 p = 0.627*

The normality of the data was assessed using the Shapiro–Wilk test and the homogeneity of variances was evaluated using Levene's test.
*The Mann–Whitney U test was employed to compare CP angle and final follow-up MA between the two groups. #The independent samples t-test was used to compare final follow-up mLDFA and mMPTA between the two groups. CP – coronal plane; mLDFA – mechanical lateral distal femoral angle; mMPTA – mechanical medial proximal tibial angle; MA – lower extremity mechanical axes angle.

Seventy-nine patients (65.8%) had AO 32-A, 31 patients (25.8%) had AO 32-B, and 10 patients (8.5%) had AO 32-C type fractures. Coronal plane deformities ≥5° were found in 17.7% of AO 32-A type fractures, 12.9% of AO 32-B type fractures, and 20% of AO 32-C type fractures. There were no significant differences between coronal plane deformities and fracture types ($\chi^2 = 0.332$, p = 0.758) (Table 2).

Intramedullary nails were placed through the greater trochanter in 37 patients (30.8%), through the piriformis fossa in 59 patients (49.2%), and laterally to the greater trochanter in 24 patients (20%). A coronal plane deformity ≥5° was observed in 2.7% of patients with intramedullary nails inserted through the greater trochanter, 50% of patients with nails inserted via lateral access to the greater trochanter, and 11.9% of patients with nails inserted through the piriformis fossa. It was determined that coronal plane deformity was more frequent in nails inserted from the lateral side of the greater trochanter. This difference was found to be significant ($\chi^2 = 28.092$, p < 0.001) (Table 2).

Ninety-one patients (75.8%) underwent surgery on a traction table, while the remaining 29 patients (24.2%) were operated on a standard operating table. Coronal plane deformities ≥5° were detected in 16 patients (17.6%) who were operated on a traction table and in 4 patients (13.8%) who were operated on a standard operating table. There were no significant differences between surgeries performed on a traction table and those performed on a standard operating table ($\chi^2 = 0.369$, p = 0.637) (Table 2).

The results of the radiological evaluations are shown in Table 3. There was no difference between the 2 groups

Table 4. Evaluation of functional scores

Variable	WOMAC knee score median (Q1, Q3)	LEFS median (Q1, Q3)	Kujala median (Q1, Q3)
Group A (CP angle <5°)	3.12 (1.04, 5.5)	76 (72, 78)	95 (88, 98)
Group B (CP angle ≥5°)	5.2 (3.12, 5.5)	74 (71.5, 76.25)	93 (87.5, 95.25)
p-value	U = 737 p = 0.127	U = 1256 p = 0.061	U =1214 p = 0.067

The Mann–Whitney U test was used to evaluate intergroup differences in WOMAC, LEFS, and Kujala patellofemoral scores. LEFS – lower extremity functional scale; WOMAC – Western Ontario and McMaster Universities Osteoarthritis Index; CP – coronal plane.

in terms of mLDFA, mMPTA, and lower extremity MA angle measured at the last follow-up (t = 0.778, p = 0.415; t = 0.952, p = 0.350; and U = 1069, p = 0.627, respectively).

There was no significant difference between the groups in terms of the WOMAC knee score, the Lower Extremity Functional Scale, and the Kujala patellofemoral score (U = 737, p = 0.127; U = 1256, p = 0.061; and U = 1214, p = 0.067, respectively) (Table 4).

Discussion

The primary aim of this study was to evaluate the effect of coronal plane deformities on knee joint function and overall functional outcomes in adults with FDF treated using static locked IMN. A secondary aim was to identify the factors that contribute to the development of these coronal plane deformities. The results demonstrated that, although coronal plane deformities ≥5° were present in 16.6% of patients, they did not significantly affect functional outcomes, as measured using the WOMAC knee scores, the Lower Extremity Functional Scale, and the Kujala patellofemoral score.

The incidence of coronal plane deformities ≥5° in this study aligns with previous findings, in which deformities above 5° are reported in 2–18% of cases after locked IMN.[9,11,13] Notably, we observed a significantly higher rate of coronal deformities when the nail was inserted laterally to the greater trochanter compared to other insertion points. This result suggests that the choice of nail insertion point may influence postoperative alignment, which could have implications for surgical planning.

Lateral entry points likely alter the trajectory of the nail, making precise alignment more challenging, especially in cases of complex fracture patterns resulting from high-energy trauma. Our findings are consistent with earlier reports suggesting a strong correlation between lateral insertion points and increased varus or valgus angulations.[14] Sadagatullah et al. concluded that there was a higher rate of malalignment in proximal femoral shaft fractures treated with interlocking nails utilizing the greater trochanter entry point.[15] Similarly, Ostrum et al. reported that a lateral starting point led to malalignment and gapping of the femoral cortex with all nails.[16]

Malalignment is a well-recognized complication in the literature that may lead to non-union and may require additional surgical intervention after locked IMN.[8,9] Malalignment can present as angular deformities (such as varus/valgus or flexion/extension) or rotational discrepancies. These deformities may negatively impact knee function following femoral locked IMN. To our knowledge, no previous study has examined the impact of coronal plane deformity on knee functional outcomes following femoral locked intramedullary nailing.

A review of the literature revealed a focus on rotational deformities following femoral locked intramedullary nailing, with studies examining their impact on knee and hip function.[17,18] Karaman et al. showed that femoral rotational malalignment ≥10° is symptomatic for patients and that the hip, knee, and patellofemoral joints are affected.[17] Sharma et al. found worse WOMAC knee and lower extremity functional scores in patients with rotational deformity than in patients without.[18] We found that despite the higher rate of coronal deformities with lateral insertion, functional outcomes were not significantly different between patients with and without deformity. We believe that minor angular deformities may not substantially impact functional performance, particularly in young, active individuals with greater compensatory abilities. However, it is worth noting that our study included a relatively young cohort with an average age of 31.7 years. Older patients or those with pre-existing knee pathology may experience greater functional limitations due to malalignment.

We hypothesized that coronal deformities are more commonly observed in fractures of the proximal and distal thirds of the femoral diaphysis. Khan et al. reported a significant association between proximal femur fractures and malalignment in their study involving 65 patients.[10] Ricci et al. found that fractures in proximal and distal locations are correlated with increased fracture angulation.[11] In our study, coronal deformities were detected in 5.3% of proximal, 17.9% of middle, and 21.7% of distal diaphyseal fractures. In contrast to our initial hypothesis, our study found no statistically significant association between coronal deformities and fracture localization (p = 0.169).

We anticipated that progression from AO type A to type C would involve more complex and fragmented fractures, making coronal alignment more challenging to control. Ricci et al. showed that an unstable fracture pattern is associated with increased fracture angulation.[11] In our study, coronal deformities were identified in 17.7%, 12.9%, and

20% of patients with AO type A, B, and C fractures, respectively. Contrary to our initial hypothesis, our study revealed no statistically significant association between coronal deformities and fracture type (p = 0.758).

Regarding the operative setup, the use of a traction table versus a standard operating table did not significantly impact the incidence of coronal plane deformity. He et al. concluded that, compared with manual traction, the traction table in femoral intramedullary nailing surgery lengthens operative time and preoperative setup time. At the same time, it does not show significant advantages in reducing blood loss volume, fluoroscopy time, or improving prognosis.[19]

Similarly, Sholla et al. found that the lateral decubitus method without a traction table was a safe and effective alternative to the supine method with a traction table in terms of radiological and clinical results.[20] While a traction table is often preferred for better control of fracture reduction, our results suggest that it may not necessarily result in superior coronal alignment. This finding may inform surgical teams that, under certain conditions, a standard operating table may be a viable alternative, especially in facilities without access to traction tables.

Radiographically, there were no significant differences between the groups in terms of mLDFA, mMPTA, or lower extremity mechanical alignment. This outcome highlights that minor deviations in coronal alignment at the fracture site may not translate into large-scale mechanical axis alterations, at least in the short to medium term. This finding may explain why coronal plane deformity does not negatively impact knee function, at least within a 5-year follow-up period. Long-term studies are warranted to evaluate whether these deformities contribute to early degenerative changes, especially in high-functioning individuals.

Limitations of the study

The retrospective nature of this study limits the generalizability of our findings. Future research with a prospective design, larger sample sizes, and longer follow-up periods could provide more insight into the long-term effects of coronal deformities on joint function. An additional limitation of our study is the large difference in the number of patients between the groups. Another limitation was that we could not determine a cut-off point for coronal varus deformity. A key limitation in establishing a definitive "cut-off" for acceptable coronal plane deformity lies in the ethical and clinical need to correct severe malalignments. For instance, high degrees of coronal plane deformity would not be ethically feasible to include in a study or to leave unaddressed in clinical practice. Severe deformities are typically corrected intraoperatively, as leaving a patient with such a misalignment would constitute a deviation from standard care and could lead to legal and medical implications. Consequently, the absence of patients with extreme deformities in our study reflects routine corrective practices rather than a defined clinical threshold for acceptable alignment. This limitation underscores the importance of standardized guidelines and surgical expertise in preventing significant malalignment. Future biomechanical studies could further explore the impact of major coronal plane deformities. Another limitation of our study is that, because the patients were trauma cases with femoral fractures, preoperative evaluation of limb alignment parameters could not be performed. Therefore, it was not possible to compare preoperative measurements with postoperative measurements.

Conclusions

No negative outcomes were detected in the knee or patellofemoral joints of patients with coronal plane deformities after at least a 5-year follow-up. Coronal plane deformity was found to be independent of fracture localization, fracture classification, and whether the fracture was operated on using a traction table. Increased valgus deformity was observed in nails inserted from the lateral aspect of the greater trochanter.

Data Availability Statement

Data sharing does not apply to this article, as all data are already included in the manuscript.

Consent for publication

Not applicable.

Use of AI and AI-assisted technologies

Not applicable.

ORCID iDs

Onur Suer https://orcid.org/0000-0002-6751-0705
Yusuf Taha Kirmic https://orcid.org/0009-0007-5742-4815
Recep Selcuk Eyceyurt https://orcid.org/0000-0002-1451-9896
Meliksah Uzakgider https://orcid.org/0000-0001-7098-2642
Mesut Tahta https://orcid.org/0000-0001-9660-1350
Cemil Kayali https://orcid.org/0000-0002-6260-0744
Kemal Aktuglu https://orcid.org/0000-0001-8058-0364

References

1. Weiss RJ, Montgomery SM, Al Dabbagh Z, Jansson KÅ. National data of 6409 Swedish inpatients with femoral shaft fractures: Stable incidence between 1998 and 2004. *Injury*. 2009;40(3):304–308. doi:10.1016/j.injury.2008.07.017
2. Tscherne H, Regel G, Pape HC, Pohlemann T, Krettek C. Internal fixation of multiple fractures in patients with polytrauma. *Clin Orthop Relat Res*. 1998;(347):62–78. PMID:9520876.
3. Taylor MT, Banerjee B, Alpar EK. The epidemiology of fractured femurs and the effect of these factors on outcome. *Injury*. 1994;25(10):641–644. doi:10.1016/0020-1383(94)90003-5
4. Hedlund R, Lindgren U. Epidemiology of diaphyseal femoral fracture. *Acta Orthop Scand*. 1986;57(5):423–427. doi:10.3109/17453678609014762
5. Wilson CH, Yelton CL, Vesely DG. Intramedullary nailing of femoral fractures. *J Med Assoc State Ala*. 1953;22(10):261–267. PMID:13053110.

6. Fakhry SM, Rutledge R, Dahners LE, Kessler D. Incidence, management, and outcome of femoral shaft fracture: A statewide population-based analysis of 2805 adult patients in a rural state. *J Trauma*. 1994;37(2):255–260; discussion 260–261.
7. Winquist RA. Locked femoral nailing. *J Am Acad Orthop Surg*. 1993; 1(2):95–105. doi:10.5435/00124635-199311000-00004
8. Watanabe Y, Matsushita T. Femoral non-union with malalignment: Reconstruction and biological stimulation with the chipping technique. *Injury*. 2016;47(Suppl 6):S47–S52. doi:10.1016/s0020-1383(16)30839-7
9. Winquist RA, Hansen ST, Clawson DK. Closed intramedullary nailing of femoral fractures: A report of five hundred and twenty cases. *J Bone Joint Surg Am*. 1984;66(4):529–539. PMID:6707031.
10. Khan HN, Ali M, Rashid RH, Mohib Y, Hashmi P. Frequency of angular malalignment after intramedullary nailing for femur shaft fractures: A cross-sectional study. *J Pak Med Assoc*. 2021;71(Suppl 5)(8):S4–S7. PMID:34634006.
11. Ricci WM, Bellabarba C, Lewis R, et al. Angular malalignment after intramedullary nailing of femoral shaft fractures. *J Orthop Trauma*. 2001;15(2):90–95. doi:10.1097/00005131-200102000-00003
12. Majkowski RS, Baker AS. Interlocking nails for femoral fractures: An initial experience. *Injury*. 1991;22(2):93–96. doi:10.1016/0020-1383(91)90062-j
13. Wolinsky PR, McCarty E, Shyr Y, Johnson K. Reamed intramedullary nailing of the femur: 551 cases. *J Trauma*. 1999;46(3):392–399. doi:10.1097/00005373-199903000-00007
14. Strecker W, Suger G, Kinzl L. Local complications of intramedullary nailing [in German]. *Orthopade*. 1996;25(3):274–291. PMID:8766665.
15. Sadagatullah AN, Nazeeb MN, Ibrahim S. Incidence of varus malalignment post interlocking nail in proximal femur shaft fractures comparing two types of entry points. *Malays Orthop J*. 2017;11(3):31–35. doi:10.5704/moj.1711.013
16. Ostrum RF, Marcantonio A, Marburger R. A critical analysis of the eccentric starting point for trochanteric intramedullary femoral nailing. *J Orthop Trauma*. 2008;22(Suppl 3):S25–S30. doi:10.1097/01.bot.0000184145.75201.1b
17. Karaman O, Ayhan E, Kesmezacar H, Seker A, Unlu MC, Aydingoz O. Rotational malalignment after closed intramedullary nailing of femoral shaft fractures and its influence on daily life. *Eur J Orthop Surg Traumatol*. 2014;24(7):1243–1247. doi:10.1007/s00590-013-1289-8
18. Sharma Y, Mugdum G, Prabhakara A. Rotational malalignment after closed intramedullary nailing of femoral shaft fractures and its influence on functional outcome. *Int J Res Med Sci*. 2016;4(7):2802–2808. doi:10.18203/2320-6012.ijrms20161954
19. He YK, Wang YC, Li FF. Is the traction table necessary to treat femoral fractures with intramedullary nailing? A meta-analysis. *J Orthop Surg Res*. 2023;18(1):277. doi:10.1186/s13018-023-03659-y
20. Sholla E, Ertürk C, Doğan N, Büyükdoğan H, Çalışkan G, Şahin A. Is intramedullary nailing of femoral diaphyseal fractures in the lateral decubitus position as safe and effective as on a traction table? *Injury*. 2024;55(6):111516. doi:10.1016/j.injury.2024.111516

Transcriptomic profiling of human corneal epithelial cells exposed to $PM_{2.5}$: Identification of differentially expressed genes and pathways

Yingchao Li[1,A,B], Wenjing Liu[1,B,C], Huijing Bao[1,C,D], *Yibin Ma[1,E,F], *Han Zhang[2,D,E]

[1] Department of Ophthalmology, The Affiliated Taian City Central Hospital of Qingdao University, China
[2] Department of Ophthalmology, Shandong Provincial Hospital Affiliated to Shandong First Medical University, Jinan, China

A – research concept and design; B – collection and/or assembly of data; C – data analysis and interpretation;
D – writing the article; E – critical revision of the article; F – final approval of the article

Advances in Clinical and Experimental Medicine, ISSN 1899–5276 (print), ISSN 2451–2680 (online) *Adv Clin Exp Med*. 2026;35(4):693–701

Address for correspondence
Yibin Ma
E-mail: mybzlj@163.com

Funding sources
This work was supported by the Natural Science Foundation of Shandong Province (grant No. ZR2022LSW011) and the Taian City Science and Technology Innovation Development Project (grants No. 2021NS207, 2022NS203, and 2023NS273).

Conflict of interest
None declared

Acknowledgements
The authors thank Prof. Qing-Jun Zhou of Shandong Eye Institute, Shandong First Medical University and Shandong Academy of Medical Sciences for providing HCECs.

*Yibin Ma and Han Zhang contributed equally to this work.

Received on April 21, 2025
Reviewed on June 24, 2025
Accepted on July 3, 2025

Published online on February 24, 2026

Cite as
Li Y, Liu W, Bao H, Ma Y, Zhang H. Transcriptomic profiling of human corneal epithelial cells exposed to $PM_{2.5}$: Identification of differentially expressed genes and pathways. *Adv Clin Exp Med*. 2026;35(4):693–701. doi:10.17219/acem/207872

DOI
10.17219/acem/207872

Abstract

Background. High levels of $PM_{2.5}$ air pollution pose serious health risks, especially in rapidly urbanizing areas. While its effects on organs such as the heart and lungs are well documented, its effects on the cornea remain less well understood. Emerging evidence links $PM_{2.5}$ exposure to corneal damage through processes such as autophagy, inflammation, and oxidative stress; however, the precise molecular pathways remain largely unknown.

Objectives. This study aimed to identify key genes and signaling pathways in $PM_{2.5}$-exposed human corneal epithelial cells (HCECs) using RNA sequencing and bioinformatics analysis.

Materials and methods. Human corneal epithelial cells were cultured and exposed to 25 μg/mL $PM_{2.5}$ for 24 h. High-throughput sequencing was performed after total RNA extraction and library construction for mRNA and microRNA (miRNA). Clean reads were mapped to the reference genome after filtering out low-quality reads. The Differential Expression Sequencing 2 (DESeq2) R package was used to identify differentially expressed (DE) mRNAs and miRNAs with a fold change ≥ 2 or ≤ 0.5 and a false discovery rate (FDR) ≤ 0.001.. Bioinformatics analyses included hierarchical clustering, protein–protein interaction network construction, target gene prediction, and Gene Ontology (GO) and Kyoto Encyclopedia of Genes and Genomes (KEGG) pathway enrichment.

Results. The analysis identified 45 DE mRNAs, including 14 upregulated and 31 downregulated transcripts, along with 16 upregulated miRNAs. A gene interaction network was constructed comprising nine mRNAs (6 upregulated and 3 downregulated), while a combined miRNA–mRNA network included 14 miRNAs and 21 mRNAs, forming 73 interaction pairs. Functional enrichment analysis of these genes revealed 30 significantly enriched GO terms, as well as 27 KEGG signaling pathways.

Conclusions. This study constructed regulatory networks and identified genes DE in the corneal response to $PM_{2.5}$ exposure, particularly those involved in autophagy, inflammatory responses, and oxidative stress–related pathways. These results lay the groundwork for further research into the effects of $PM_{2.5}$ on ocular surface health and provide insights into the molecular mechanisms underlying $PM_{2.5}$-induced damage to human corneal epithelial cells, potentially guiding the development of targeted diagnostics or therapies to mitigate ocular surface injury caused by $PM_{2.5}$.

Key words: $PM_{2.5}$, bioinformatics analysis, human corneal epithelial cells

Highlights

- Forty-five mRNAs and 16 microRNAs were differentially expressed in human corneal epithelial cells following $PM_{2.5}$ exposure.
- Gene and microRNA–mRNA interaction networks were constructed to elucidate the regulatory mechanisms underlying $PM_{2.5}$-induced corneal damage.
- Functional enrichment analysis identified 30 Gene Ontology terms and 27 Kyoto Encyclopedia of Genes and Genomes pathways associated with inflammation, cellular stress, and immune responses.
- These findings provide novel insights into the molecular effects of air pollution on ocular surface health.
- The results may inform future therapeutic strategies for pollution-related corneal disorders.

Background

Air pollution is a well-established global public health concern.[1] Among its various components, fine particulate matter ($PM_{2.5}$) is considered particularly hazardous.[2,3] In developing nations undergoing rapid industrialization and urban expansion, such as China, $PM_{2.5}$ levels have reached critical thresholds; for instance, the annual average $PM_{2.5}$ concentration in eastern China exceeded 80 $\mu g/m^3$ in 2010.[4,5] Exposure to $PM_{2.5}$ has been widely linked to elevated risks of cancer, respiratory and cardiovascular diseases, and increased mortality.[6–10]

Despite these findings, its effects on the ocular surface, particularly the cornea, which is directly exposed to airborne pollutants, have received less attention. Xiang et al. emphasized the harmful effects of $PM_{2.5}$ on ocular health.[11] Recent studies have suggested that $PM_{2.5}$ may contribute to corneal epithelial damage through mechanisms such as oxidative stress, autophagy dysregulation, and pro-inflammatory responses.[12–16] However, the precise molecular mechanisms involved in these corneal responses remain largely unknown, and whether they mirror those observed in other organs is still unclear.

Objectives

Through comprehensive bioinformatics analysis, this study aims to clarify the key genes and signaling pathways implicated in the effects of $PM_{2.5}$ on the cornea.

Materials and methods

Culture and exposure of human corneal epithelial cells to $PM_{2.5}$

Human corneal epithelial cells (HCECs) were provided by the Shandong Eye Institute, Shandong Provincial Key Laboratory of Ophthalmology, Qingdao, China. The cells were cultured in Dulbecco's modified Eagle's medium (DMEM)/Ham's F12 medium supplemented with 1% penicillin–streptomycin and 10% fetal bovine serum (FBS). The medium was changed every 2 days, and the cultures were maintained at 37°C in an atmosphere containing 5% CO_2.[17–19] Cells were seeded in 6-well plates and cultured for 24–48 h in regular growth medium. The cells were then rinsed with phosphate-buffered saline (PBS) and incubated for 24 h in either control medium or a $PM_{2.5}$ solution at a concentration of 25 μg/mL. The $PM_{2.5}$ used was SRM 1648a (National Institute of Standards and Technology (NIST), Gaithersburg, USA), which was suspended in sterile PBS and sonicated for 30 min in a water-bath sonicator (US-220; Zhongke Scientific Instrument, Beijing, China) to ensure even dispersion before application. Each treatment was replicated 3 times for subsequent RNA extraction. Three biological replicates were used for both mRNA and miRNA sequencing analyses. The cells used for all experiments were between passages 2 and 5. The $PM_{2.5}$ employed was the urban particulate matter reference standard (SRM 1648a), sourced from the NIST and representative of urban environments.

This study did not involve any human participants or animal experiments. Only commercially available human corneal epithelial cell lines were used. Therefore, ethical approval was not required.

Library preparation

RNA library preparation

Total RNA from 2 distinct groups was qualified and quantified using a bioanalyzer (Agilent 2100 Bioanalyzer; Agilent Technologies, Santa Clara, USA) before being randomly fragmented. These fragments then served as templates for 1st-strand cDNA synthesis, followed by 2nd-strand synthesis. The fragments were then purified using the QIAquick polymerase chain reaction (PCR) kit (Qiagen, Hilden, Germany), eluted with elution buffer, end-repaired, adenylated by the addition of a single 'A' base, and ligated to sequencing adapters. The uracil-N-glycosylase (UNG) enzyme (Thermo Fisher Scientific, Waltham, USA) was then used to degrade the 2nd strand. Following fragment

size selection by agarose gel electrophoresis, polymerase chain reaction (PCR) amplification was performed to generate the sequencing library.

microRNA library preparation

RNA concentrations in 6 samples were determined using a bioanalyzer (Agilent 2100 Bioanalyzer; Agilent Technologies). RNAs of different fragment sizes were separated by sodium dodecyl sulfate–polyacrylamide gel electrophoresis (SDS–PAGE), and bands ranging from 18 to 30 nucleotides were excised to recover small RNAs. According to the manufacturer's instructions for T4 RNA ligase (Thermo Fisher Scientific), these RNAs were ligated to 5′ and 3′ adapters before being reverse-transcribed into cDNA molecules. To complete library construction, the PCR products were purified by PAGE and dissolved in ethidium bromide (EB) solution.

RNA-seq method

Raw sequencing reads were subjected to quality control using FastQC v. 0.11.9 (https://www.bioinformatics.babraham.ac.uk/projects/fastqc/) to evaluate metrics such as per-base sequence quality, GC content (the molar ratio of guanine + cytosine bases in DNA), and adapter contamination. Trimmomatic v. 0.39[20] (http://www.usadellab.org/cms/?page=trimmomatic) was employed to remove adapter sequences and low-quality bases, using parameters: ILLUMINACLIP:2:30:10, SLIDINGWINDOW:4:20, and MINLEN:36. Cleaned reads were aligned to the human reference genome (GRCh38/hg38) using HISAT2 v. 2.2.1 (https://daehwankimlab.github.io/hisat2/),[21] a splice-aware aligner. The resulting files of sequence alignment map (SAM) were converted to sorted binary alignment map (BAM) files using SAMtools v. 1.10 (https://www.htslib.org/doc/1.10/samtools.html).[22] Subsequently, transcript assembly and quantification were performed with StringTie v. 2.2.1 (https://ccb.jhu.edu/software/stringtie/).[23] For each sample, transcript abundance was calculated based on the reference gene annotation (GTF) file, and novel transcript isoforms were also predicted. Expression levels were quantified in fragments per kilobase of transcript per million mapped reads (FPKM). Gene-level count matrices were generated using the prepDE.py script provided with StringTie. Differential gene expression analysis was conducted using the DESeq2[24] package v. 1.38.3 in R v. 4.2.2 (R Foundation for Statistical Computing, Vienna, Austria). Raw count data were normalized, and statistical testing was performed using the Wald test with Benjamini–Hochberg correction for multiple comparisons. Genes with an adjusted $p < 0.050$ and $|\log_2 \text{fold change}| \geq 1$ were considered significantly differentially expressed (DE). To interpret the biological significance of the DE genes, Gene Ontology (GO) enrichment and Kyoto Encyclopedia of Genes and Genomes (KEGG) pathway analyses were performed using the clusterProfiler[25] package (v. 4.6.2) in R. Enrichment results were visualized with dot plots and pathway diagrams to identify biological processes and signaling pathways significantly associated with DE genes.

Results

Analysis of 6 samples from both the $PM_{2.5}$ group and the negative control group revealed 45 DE mRNAs (Fig. 1A and Supplementary Table 1), including 14 upregulated and 31 downregulated transcripts. Similarly, analysis of the same sample set identified 16 DE miRNAs, all of which were upregulated (Fig. 1B, Supplementary Table 2). Using Cytoscape software (URL: https://cytoscape.org/), an interaction network of DE mRNAs was constructed, comprising 9 nodes and 7 edges (Fig. 2). This network included 6 upregulated and 3 downregulated genes. These 9 mRNAs were selected for downstream analysis based on their centrality and connectivity within the protein–protein interaction (PPI) network, indicating potential roles as regulatory hubs.

The interaction network included 35 DE genes, consisting of 14 miRNAs and 21 mRNAs, with 73 interaction pairs identified (Fig. 3). Key genes in the miRNA–mRNA network were selected based on overlap in target prediction, consistency of differential expression, and biological relevance to pathways identified through enrichment analysis.

Functional enrichment analysis was performed on the 9 DE mRNAs from the network, revealing enrichment in 30 GO terms, segmented into 3 categories: biological process (BP), cellular component (CC), and molecular function (MF). The top 10 entries from each category are shown in Fig. 4 and Supplementary Table 3. Additionally, 27 signaling pathways were identified through KEGG analysis. The top 20 entries from each category are shown in Fig. 5 and Supplementary Table 4.

Discussion

$PM_{2.5}$ is a complex mixture consisting of various sources, such as automobile exhaust, combustion smoke, soil, and cooking fumes. Its constituents include metals, salts, volatile organic compounds, hydrocarbons, and endotoxins.[26] Owing to this intricate composition, the impact of $PM_{2.5}$ on human health is multifaceted. However, its ocular effects, particularly on the cornea, remain understudied. This study aims to explore the influence of $PM_{2.5}$ on the cornea and to identify key genes and signaling pathways involved.

We identified several novel genes and miRNA candidates not previously associated with $PM_{2.5}$-induced ocular damage. Our study found that several genes in HCECs exhibited differential expression after exposure to $PM_{2.5}$.

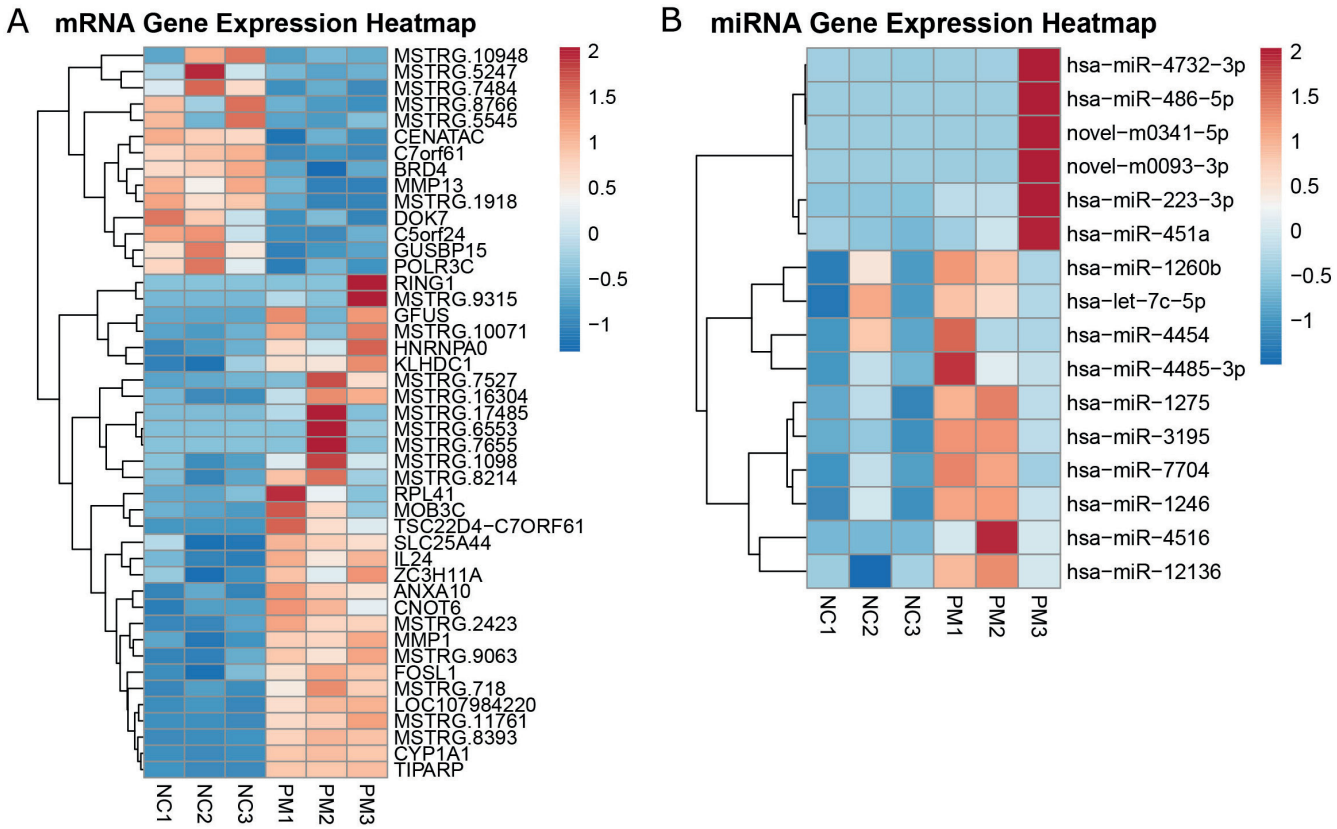

Fig. 1. Heatmap of differentially expressed (DE) genes. A: Heat map of DE mRNAs; B: Heat map of DE miRNAs

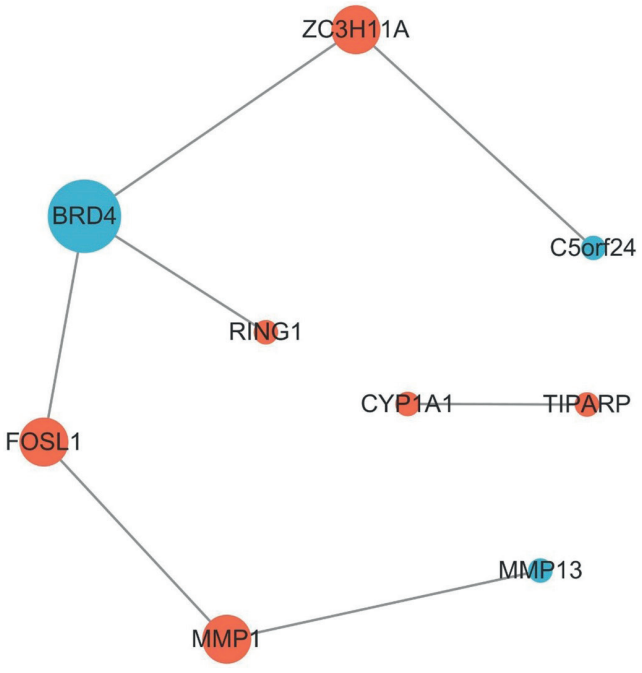

Fig. 2. Interaction network of differentially expressed (DE) mRNAs. Red points represent upregulated genes; blue points indicate downregulated genes. The size of each point correlates with the p-value

These include *BRD4*, *FOSL1*, and *CYP1A1*, which appear to play central roles in regulating oxidative stress, autophagy, and inflammation in the corneal epithelium. *BRD4*, a member of the bromodomain and extraterminal protein family, recognizes and binds to acetylated lysine residues on histone tails.[27] It is implicated in the regulation of various inflammatory cytokines, including interleukin (IL)-1β, IL-6, IL-8, and IL-9, and functions as a transcriptional regulator that modulates autophagy and oxidative stress via lysosomal pathways.[28–30]

FOSL1, a component of the AP-1 transcription factor complex, has been reported to be upregulated following $PM_{2.5}$ exposure in lung epithelial cells and may contribute to autophagy inhibition, inflammation, and oxidative stress.[31,32] Studies have suggested that *FOSL1* can promote apoptosis and inflammation through the AMPK signaling pathway,[33] and that its inhibition leads to reduced pro-inflammatory cytokine expression.[34,35] *FOSL1* also interacts with the Nrf2 pathway, a key regulator of oxidative stress.[36–38]

Cytochrome P450 enzymes (CYPs) are essential for the metabolism of various substances, including heavy metals and drugs.[39] CYP1A1, a cytochrome P450 enzyme, has been shown to be upregulated in corneal epithelial cells following exposure to airborne pollutants such as cigarette smoke and house dust.[11,40] It participates in xenobiotic metabolism and is regulated by the aryl hydrocarbon receptor (AhR) signaling pathway.[39–45] Suppression of CYP1A1 has been linked to reduced reactive oxygen species (ROS) production and oxidative stress.[45] Its co-regulation with TIPARP via AhR signaling underscores its potential importance in pollutant-induced ocular responses

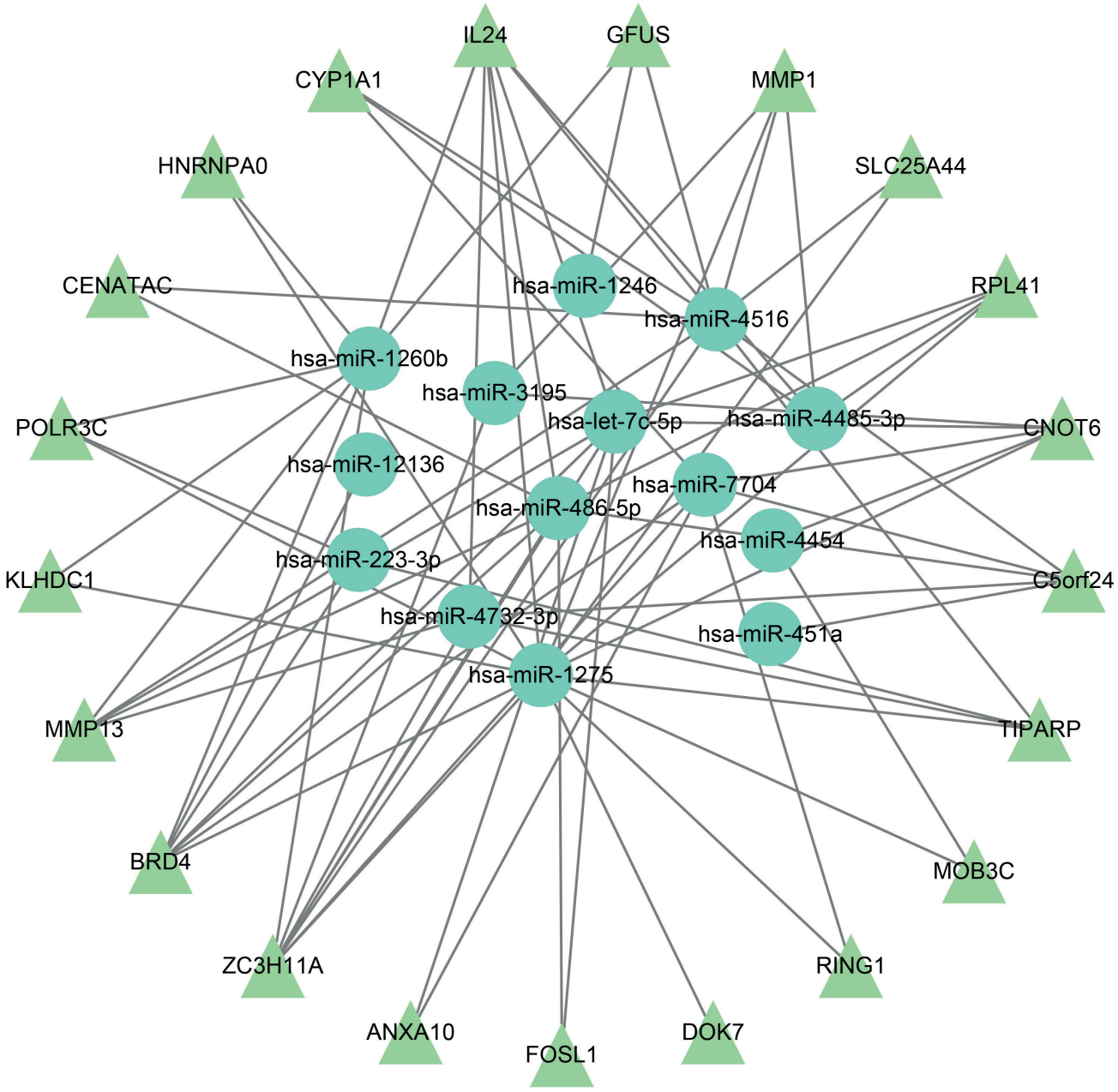

Fig. 3. miRNA-mRNA regulation network, consisting of 35 nodes and 73 edges. Triangles represent mRNAs and circles denote miRNAs

– In addition, we identified 16 DE miRNAs. Among these, several novel miRNA–mRNA interactions potentially relevant to corneal responses to $PM_{2.5}$ were identified:

– miR-1275, predicted to target BRD4 and TIPARP, may regulate autophagy and ROS generation and inflammation when inhibited.[46–48]

– miR-223-3p, also targeting BRD4 and TIPARP, has been linked to the modulation of autophagy and oxidative stress in both ocular and systemic contexts.[49–52]

– *miR-486-5p*, targeting *BRD4* and *FOSL1*, was shown to induce autophagy upon inhibition and reduce inflammation and oxidative damage.[53–55]

– *miR-4516*, associated with *CYP1A1* and *TIPARP*, may regulate autophagic responses to metal components in PM.[56]

– *miR-4454* expression is elevated in PM-exposed populations, although its ocular mechanism is unclear.[57]

– *let-7c-5p*, which may regulate *BRD4* and *FOSL1*, has been implicated in abnormal autophagy in lens epithelial cells.[58]

Gene Ontology analysis and KEGG signaling pathway enrichment were performed for the DE mRNAs. The enriched BP terms were mainly related to nitrogen compound metabolic processes and primary metabolic processes. The enriched CC terms were primarily associated with the nucleoplasm, extracellular matrix (ECM), and mitochondrial membrane. The enriched MF terms were mainly related to enzyme activation or binding, such as metalloendopeptidase activity, metallopeptidase activity, and

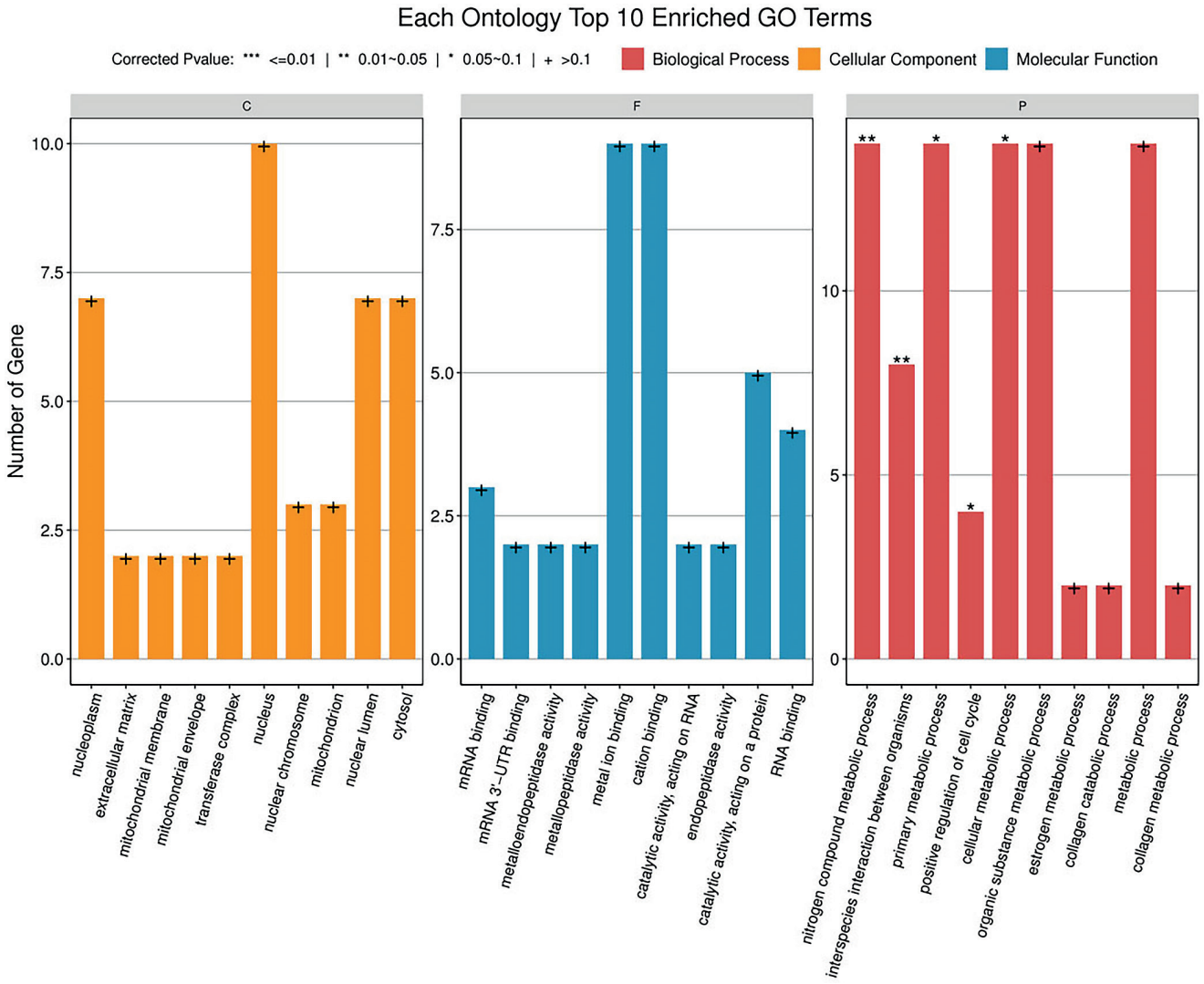

Fig. 4. Gene Ontology (GO) analysis of differentially expressed (DE) mRNAs. GO analysis showing biological process (green points), cellular component (purple points), and molecular function (orange points). The x-axis represents the number of DE mRNAs, and the y-axis lists the pathway names

metal ion binding. The enriched KEGG pathways included the IL-17 signaling pathway, the peroxisome proliferator-activated receptors (PPAR) signaling pathway, tryptophan metabolism, and the metabolism of xenobiotics by cytochrome P450. Interleukin 17 is considered to play a role in regulating corneal inflammatory responses,[59] and the PPAR signaling pathway is thought to be involved in oxidative stress and autophagy.[60]

These enriched pathways, particularly IL-17 and PPAR signaling, further underscore the mechanistic links between $PM_{2.5}$ exposure and oxidative stress, inflammation, and autophagy in the cornea.

Limitations of the study

There are several limitations to this study. First, the fine particulate matter used, SRM 1648a, was not directly collected from ambient air but is a reference material. Its composition therefore differs somewhat from that of actual environmental PM. However, its main components, such as various metals, polycyclic aromatic hydrocarbons, and polychlorinated biphenyl homologues, are similar to those typically adsorbed onto atmospheric PM. Second, the DE RNAs identified in this study require further validation. Despite these limitations, our work provides a foundational transcriptomic dataset and identifies several novel genes, pathways, and miRNA–mRNA interactions that may mediate $PM_{2.5}$-induced corneal damage, thereby laying the groundwork for further elucidation of the underlying damage mechanisms.

Conclusions

Through bioinformatics analysis, we have begun to elucidate genes and signaling pathways responsive to $PM_{2.5}$-induced damage and have constructed regulatory networks that may underlie these processes. These findings provide new insights into the impact of $PM_{2.5}$ on ocular health

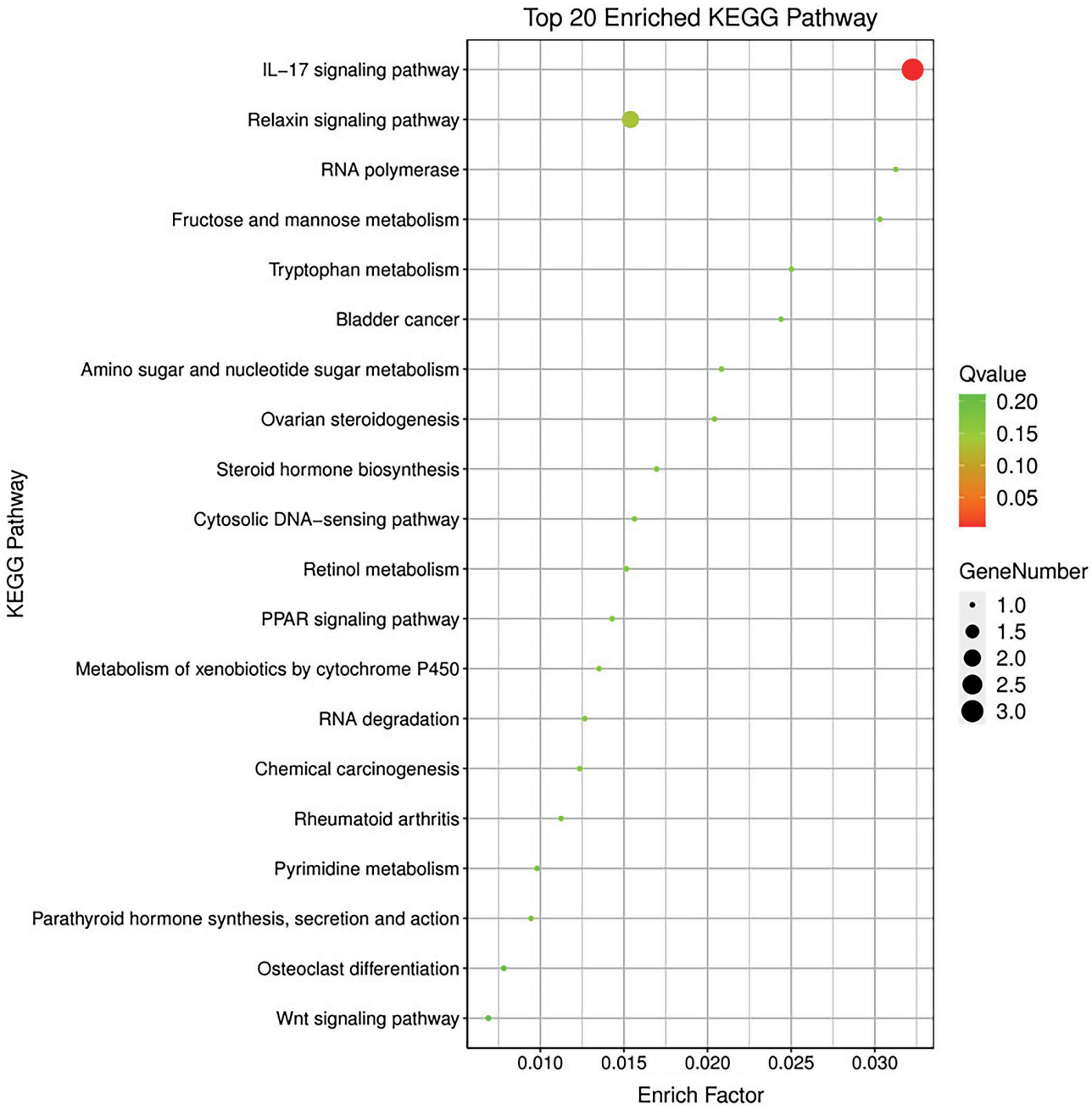

Fig. 5. Kyoto Encyclopedia of Genes and Genomes (KEGG) pathway enrichment analysis of differentially expressed (DE) mRNAs. The x-axis represents the enrichment factor, and the y-axis lists the pathway names. Dot size reflects the number of DE genes involved in each pathway. Color indicates the q value (adjusted p value), with red representing lower q values (higher statistical significance) and green representing higher q values. The top 20 enriched pathways are shown

and serve as a platform for future research in this field, potentially guiding the development of targeted diagnostics or therapies to mitigate $PM_{2.5}$-induced ocular surface damage.

Supplementary data

The supplementary materials are available at https://doi.org/10.5281/zenodo.15245015. The package contains the following files:

Supplementary Table 1. Statistical analysis data of mRNA between the NC group and the $PM_{2.5}$ group.

Supplementary Table 2. Statistical analysis data of miRNA between the NC group and the $PM_{2.5}$ group.

Supplementary Table 3. GO analysis of DE mRNAs.

Supplementary Table 4. KEGG signaling pathways of DE mRNAs.

Data Availability Statement

The datasets generated and analyzed during the current study are available in the NCBI repository. The accession number for these SRA data is PRJNA1233430, and its release date is June 30, 2025.

Consent for publication

Not applicable.

Use of AI and AI-assisted technologies

Not applicable.

ORCID iDs

Yingchao Li https://orcid.org/0000-0001-7766-9026
Wenjing Liu https://orcid.org/0000-0002-4731-3552
Huijing Bao https://orcid.org/0000-0001-9784-5357
Yibin Ma https://orcid.org/0009-0005-5859-8206
Han Zhang https://orcid.org/0000-0003-1575-0595

References

1. Manisalidis I, Stavropoulou E, Stavropoulos A, Bezirtzoglou E. Environmental and health impacts of air pollution: A review. *Front Public Health*. 2020;8:14. doi:10.3389/fpubh.2020.00014
2. Thangavel P, Park D, Lee YC. Recent insights into particulate matter ($PM_{2.5}$)-mediated toxicity in humans: An overview. *Int J Environ Res Public Health*. 2022;19(12):7511. doi:10.3390/ijerph19127511
3. Wang Y, Xiao S, Zhang Y, et al. Long-term exposure to $PM_{2.5}$ major components and mortality in the southeastern United States. *Environ Int*. 2022;158:106969. doi:10.1016/j.envint.2021.106969
4. Ethan CJ, Mokoena KK, Yu Y. Air pollution status in 10 mega-cities in China during the initial phase of the COVID-19 outbreak. *Int J Environ Res Public Health*. 2021;18(6):3172. doi:10.3390/ijerph18063172
5. Shi S, Wang W, Li X, et al. Evolution in disparity of $PM_{2.5}$ pollution in China. *Eco Environ Health*. 2023;2(4):257–263. doi:10.1016/j.eehl.2023.08.007
6. Basith S, Manavalan B, Shin TH, et al. The impact of fine particulate matter 2.5 on the cardiovascular system: A review of the invisible killer. *Nanomaterials*. 2022;12(15):2656. doi:10.3390/nano12152656
7. Guo J, Chai G, Song X, et al. Long-term exposure to particulate matter on cardiovascular and respiratory diseases in low- and middle-income countries: A systematic review and meta-analysis. *Front Public Health*. 2023;11:1134341. doi:10.3389/fpubh.2023.1134341
8. Hayes RB, Lim C, Zhang Y, et al. $PM_{2.5}$ air pollution and cause-specific cardiovascular disease mortality. *Int J Epidemiol*. 2020;49(1):25–35. doi:10.1093/ije/dyz114
9. Krittanawong C, Qadeer YK, Hayes RB, et al. $PM_{2.5}$ and cardiovascular diseases: State-of-the-art review. *Int J Cardiol Cardiovasc Risk Prev*. 2023;19:200217. doi:10.1016/j.ijcrp.2023.200217
10. Moon J, Kim E, Jang H, et al. Long-term exposure to $PM_{2.5}$ and mortality: A national health insurance cohort study. *Int J Epidemiol*. 2024;53(6):dyae140. doi:10.1093/ije/dyae140
11. Xiang P, Liu RY, Sun HJ, et al. Molecular mechanisms of dust-induced toxicity in human corneal epithelial cells: Water and organic extract of office and house dust. *Environ Int*. 2016;92–93:348–356. doi:10.1016/j.envint.2016.04.013
12. Chen ZH, Wu YF, Wang PL, et al. Autophagy is essential for ultrafine particle-induced inflammation and mucus hyperproduction in airway epithelium. *Autophagy*. 2016;12(2):297–311. doi:10.1080/15548627.2015.1124224
13. Han JH, Amri C, Lee H, Hur J. Pathological mechanisms of particulate matter-mediated ocular disorders: A review. *Int J Mol Sci*. 2024;25(22):12107. doi:10.3390/ijms252212107
14. Li T, Yu Y, Sun Z, Duan J. A comprehensive understanding of ambient particulate matter and its components on the adverse health effects based from epidemiological and laboratory evidence. *Part Fibre Toxicol*. 2022;19(1):67. doi:10.1186/s12989-022-00507-5
15. Yu D, Cai W, Shen T, et al. $PM_{2.5}$ exposure increases dry eye disease risks through corneal epithelial inflammation and mitochondrial dysfunctions. *Cell Biol Toxicol*. 2023;39(6):2615–2630. doi:10.1007/s10565-023-09791-z
16. Zhang K. Environmental $PM_{2.5}$-triggered stress responses in digestive diseases. *eGastroenterology*. 2024;2(2):e100063. doi:10.1136/egastro-2024-100063
17. Meng S, Hu H, Qiao Y, et al. A versatile hydrogel with antibacterial and sequential drug-releasing capability for the programmable healing of infectious keratitis. *ACS Nano*. 2023;17(23):24055–24069. doi:10.1021/acsnano.3c09034
18. Sun X, Qiao Y, Zhao L, et al. Application of decellularized porcine sclera in repairing corneal perforations and lamellar injuries. *ACS Biomater Sci Eng*. 2022;8(12):5295–5306. doi:10.1021/acsbiomaterials.2c00972
19. Wang F, Shi W, Li H, et al. Decellularized porcine cornea-derived hydrogels for the regeneration of epithelium and stroma in focal corneal defects. *Ocul Surf*. 2020;18(4):748–760. doi:10.1016/j.jtos.2020.07.020
20. Bolger AM, Lohse M, Usadel B. Trimmomatic: A flexible trimmer for Illumina sequence data. *Bioinformatics*. 2014;30(15):2114–2120. doi:10.1093/bioinformatics/btu170
21. Kim D, Langmead B, Salzberg SL. HISAT: A fast spliced aligner with low memory requirements. *Nat Methods*. 2015;12(4):357–360. doi:10.1038/nmeth.3317
22. Li H, Handsaker B, Wysoker A, et al. The Sequence Alignment/Map format and SAMtools. *Bioinformatics*. 2009;25(16):2078–2079. doi:10.1093/bioinformatics/btp352
23. Pertea M, Pertea GM, Antonescu CM, Chang TC, Mendell JT, Salzberg SL. StringTie enables improved reconstruction of a transcriptome from RNA-seq reads. *Nat Biotechnol*. 2015;33(3):290–295. doi:10.1038/nbt.3122
24. Love MI, Huber W, Anders S. Moderated estimation of fold change and dispersion for RNA-seq data with DESeq2. *Genome Biol*. 2014;15(12):550. doi:10.1186/s13059-014-0550-8
25. Yu G, Li F, Qin Y, Bo X, Wu Y, Wang S. GOSemSim: An R package for measuring semantic similarity among GO terms and gene products. *Bioinformatics*. 2010;26(7):976–978. doi:10.1093/bioinformatics/btq064
26. Li B, Ma Y, Zhou Y, Chai E. Research progress of different components of $PM_{2.5}$ and ischemic stroke. *Sci Rep*. 2023;13(1):15965. doi:10.1038/s41598-023-43119-5
27. Lu X, Zhang H, Wang M, et al. Novel insights into the role of BRD4 in fine particulate matter induced airway hyperresponsiveness. *Ecotoxicol Environ Saf*. 2021;221:112440. doi:10.1016/j.ecoenv.2021.112440
28. Zhang GZ, Chen HW, Deng Y jun, et al. BRD4 inhibition suppresses senescence and apoptosis of nucleus pulposus cells by inducing autophagy during intervertebral disc degeneration: An in vitro and in vivo study. *Oxid Med Cell Longev*. 2022;2022(1):9181412. doi:10.1155/2022/9181412
29. Gong ZG, Zhao Y, Wang ZY, Fan RF, Liu ZP, Wang L. Epigenetic regulator BRD4 is involved in cadmium-induced acute kidney injury via contributing to lysosomal dysfunction, autophagy blockade and oxidative stress. *J Hazard Mater*. 2022;423:127110. doi:10.1016/j.jhazmat.2021.127110
30. Liu H, Wang L, Weng X, et al. Inhibition of Brd4 alleviates renal ischemia/reperfusion injury-induced apoptosis and endoplasmic reticulum stress by blocking FoxO4-mediated oxidative stress. *Redox Biol*. 2019;24:101195. doi:10.1016/j.redox.2019.101195
31. De Noon S, Piggott R, Trotman J, et al. Recurrent *FOSL1* rearrangements in desmoplastic fibroblastoma. *J Pathol*. 2023;259(2):119–124. doi:10.1002/path.6038
32. Zhai X, Wang J, Sun J, Xin L. $PM_{2.5}$ induces inflammatory responses via oxidative stress-mediated mitophagy in human bronchial epithelial cells. *Toxicol Res*. 2022;11(1):195–205. doi:10.1093/toxres/tfac001
33. Zhong L, Fang S, Wang AQ, et al. Identification of the Fosl1/AMPK/autophagy axis involved in apoptotic and inflammatory effects following spinal cord injury. *Int Immunopharmacol*. 2022;103:108492. doi:10.1016/j.intimp.2021.108492
34. Niidome K, Taniguchi R, Yamazaki T, Tsuji M, Itoh K, Ishihara Y. FosL1 is a novel target of levetiracetam for suppressing the microglial inflammatory reaction. *Int J Mol Sci*. 2021;22(20):10962. doi:10.3390/ijms222010962
35. Liang Y, Han D, Zhang S, Sun L. FOSL1 regulates hyperproliferation and NLRP3-mediated inflammation of psoriatic keratinocytes through the NF-kB signaling via transcriptionally activating TRAF3. *Biochim Biophys Acta Mol Cell Res*. 2024;1871(5):119689. doi:10.1016/j.bbamcr.2024.119689
36. Li N, Zhan X. Machine learning identifies pan-cancer landscape of Nrf2 oxidative stress response pathway-related genes. *Oxid Med Cell Longev*. 2022;2022(1):8450087. doi:10.1155/2022/8450087

37. Bathish B, Robertson H, Dillon JF, Dinkova-Kostova AT, Hayes JD. Nonalcoholic steatohepatitis and mechanisms by which it is ameliorated by activation of the CNC-bZIP transcription factor Nrf2. *Free Radic Biol Med*. 2022;188:221–261. doi:10.1016/j.freeradbiomed.2022.06.226
38. Guo S, Ramar V, Guo AA, et al. TRPM7 transactivates the *FOSL1* gene through STAT3 and enhances glioma stemness. *Cell Mol Life Sci*. 2023; 80(9):270. doi:10.1007/s00018-023-04921-6
39. Zhang C, Wang X, Pi S, et al. Cadmium and molybdenum co-exposure triggers autophagy via CYP450s/ROS pathway in duck renal tubular epithelial cells. *Sci Total Environ*. 2021;759:143570. doi:10.1016/j.scitotenv.2020.143570
40. Coelho NR, Pimpão AB, Correia MJ, et al. Pharmacological blockage of the AHR-CYP1A1 axis: A call for in vivo evidence. *J Mol Med*. 2022;100(2):215–243. doi:10.1007/s00109-021-02163-2
41. Yuan J, Sun X, Che S, et al. AhR-mediated CYP1A1 and ROS overexpression are involved in hepatotoxicity of decabromodiphenyl ether (BDE-209). *Toxicol Lett*. 2021;352:26–33. doi:10.1016/j.toxlet.2021.09.008
42. Song Y, Yen S, Southam K, Gaskin S, Hoy RF, Zosky GR. The aryl hydrocarbon receptor pathway is a marker of lung cell activation but does not play a central pathologic role in engineered stone-associated silicosis. *J Appl Toxicol*. 2024;44(10):1518–1527. doi:10.1002/jat.4653
43. Zhan Y, Zhang Z, Liu Y, et al. NUPR1 contributes to radiation resistance by maintaining ROS homeostasis via AhR/CYP signal axis in hepatocellular carcinoma. *BMC Med*. 2022;20(1):365. doi:10.1186/s12916-022-02554-3
44. Alluli A, Fonseca G, Matthews J, Eidelman DH, Baglole CJ. Regulation of long non-coding RNA expression by aryl hydrocarbon receptor activation. *Toxicol Lett*. 2024;391:13–25. doi:10.1016/j.toxlet.2023.11.004
45. Zhang Y, Song M, Bi Y, Lei Y, Sun X, Chen Y. TIPARP is involved in the regulation of intraocular pressure. *Commun Biol*. 2022;5(1):1386. doi:10.1038/s42003-022-04346-0
46. Liang G, Ling Y, Mehrpour M, et al. Autophagy-associated circRNA circCDYL augments autophagy and promotes breast cancer progression. *Mol Cancer*. 2020;19(1):65. doi:10.1186/s12943-020-01152-2
47. Jin Q, Ma X, Wang G, Yang X, Guo F. Dynamics of major air pollutants from crop residue burning in mainland China, 2000–2014. *J Environ Sci*. 2018;70:190–205. doi:10.1016/j.jes.2017.11.024
48. Zeng Z, Ma H, Chen J, et al. Knockdown of miR-1275 protects against cardiomyocytes injury through promoting neuromedin U type 1 receptor. *Cell Cycle*. 2020;19(24):3639–3649. doi:10.1080/15384101.2020.1860310
49. Zhang DM, Deng JJ, Wu YG, et al. MicroRNA-223-3p protect against radiation-induced cardiac toxicity by alleviating myocardial oxidative stress and programmed cell death via targeting the AMPK pathway. *Front Cell Dev Biol*. 2022;9:801661. doi:10.3389/fcell.2021.801661
50. Fernando N, Wong JHC, Das S, et al. MicroRNA-223 regulates retinal function and inflammation in the healthy and degenerating retina. *Front Cell Dev Biol*. 2020;8:516. doi:10.3389/fcell.2020.00516
51. Tang H, Lin Y, Huang L, Hu J. MiR-223-3p regulates autophagy and inflammation by targeting ATG16L1 in *Fusarium solani*-induced keratitis. *Invest Ophthalmol Vis Sci*. 2022;63(1):41. doi:10.1167/iovs.63.1.41
52. Lv P, Liu H, Ye T, et al. XIST inhibition attenuates calcium oxalate nephrocalcinosis-induced renal inflammation and oxidative injury via the miR-223/NLRP3 pathway. *Oxid Med Cell Longev*. 2021;2021(1): 1676152. doi:10.1155/2021/1676152
53. Chang Q, Ji M, Li C, Geng R. Downregulation of miR-486-5p alleviates LPS-induced inflammatory injury, oxidative stress and apoptosis in chondrogenic cell ATDC5 by targeting NRF1. *Mol Med Rep*. 2020;22(3):2123–2131. doi:10.3892/mmr.2020.11289
54. Ma N, Li S, Lin C, Cheng X, Meng Z. Mesenchymal stem cell conditioned medium attenuates oxidative stress injury in hepatocytes partly by regulating the miR-486-5p/PIM1 axis and the TGF-β/Smad pathway. *Bioengineered*. 2021;12(1):6434–6447. doi:10.1080/21655979.2021.1972196
55. Yongprayoon V, Wattanakul N, Khomate W, et al. Targeting BRD4: Potential therapeutic strategy for head and neck squamous cell carcinoma (Review). *Oncol Rep*. 2024;51(6):74. doi:10.3892/or.2024.8733
56. Li X, Lv Y, Hao J, et al. Role of microRNA-4516 involved autophagy associated with exposure to fine particulate matter. *Oncotarget*. 2016;7(29):45385–45397. doi:10.18632/oncotarget.9978
57. Mancini FR, Laine JE, Tarallo S, et al. microRNA expression profiles and personal monitoring of exposure to particulate matter. *Environ Pollut*. 2020;263:114392. doi:10.1016/j.envpol.2020.114392
58. Cao Y, Li P, Zhang G, et al. MicroRNA Let-7c-5p-mediated regulation of ERCC6 disrupts autophagic flux in age-related cataract via the binding to VCP. *Curr Eye Res*. 2021;46(9):1353–1362. doi:10.1080/02713683.2021.1900273
59. Xue Y, Xu P, Hu Y, et al. Stress systems exacerbate the inflammatory response after corneal abrasion in sleep-deprived mice via the IL-17 signaling pathway. *Mucosal Immunol*. 2024;17(3):323–345. doi:10.1016/j.mucimm.2024.02.009
60. Muzio G, Barrera G, Pizzimenti S. Peroxisome proliferator-activated receptors (PPARs) and oxidative stress in physiological conditions and in cancer. *Antioxidants (Basel)*. 2021;10(11):1734. doi:10.3390/antiox10111734

Modulation of NF-κB and oxidative stress pathways in ethanol-induced gastric injury by a multi-component herbal formula: An in vivo study

Shaokai Hou[1,A,B,D], Ji Li[1,2,A–C,E,F]

[1] College of Basic Medicine, Hebei University of Traditional Chinese Medicine, Shijiazhuang, China
[2] College of Basic Medicine, Heilongjiang University of Traditional Chinese Medicine, Harbin, China

A – research concept and design; B – collection and/or assembly of data; C – data analysis and interpretation;
D – writing the article; E – critical revision of the article; F – final approval of the article

Advances in Clinical and Experimental Medicine, ISSN 1899–5276 (print), ISSN 2451–2680 (online) *Adv Clin Exp Med*. 2026;35(4):703–716

Address for correspondence
Ji Li
E-mail: lijilaoshi@sina.com

Funding sources
None declared

Conflict of interest
None declared

Received on December 24, 2024
Reviewed on April 8, 2025
Accepted on July 10, 2025

Published online on March 30, 2026

Abstract

Background. Chronic alcohol consumption can damage the gastric mucosa and increase the risk of severe gastrointestinal disorders, including gastritis, peptic ulcers, and potentially gastric cancer. Modern research has demonstrated that Erchen decoction possesses anti-inflammatory, antioxidant, and gastric mucosal protective properties and has been applied in the treatment of various inflammatory conditions.

Objectives. This study aimed to investigate the effects of Erchen decoction on chronic ethanol-induced gastric injury.

Materials and methods. Seventy-two male Sprague Dawley rats were randomly assigned to the following groups: Con group (control), Mod group (model), OXY group (oxymatrine, 5 mL/kg), ECDH group (high-dose Erchen decoction, 10 mL/kg), ECDM group (medium-dose Erchen decoction, 5 mL/kg), and ECDL group (low-dose Erchen decoction, 2.5 mL/kg). Gastric histopathological changes were evaluated using hematoxylin and eosin (H&E) staining and transmission electron microscopy (TEM). Proliferation of gastric mucosal cells was assessed using immunohistochemical detection of proliferating cell nuclear antigen (PCNA). Serum levels of tumor necrosis factor alpha (TNF-α), interleukin-1 beta (IL-1β), superoxide dismutase (SOD), and malondialdehyde (MDA) were measured using enzyme-linked immunosorbent assay (ELISA) and biochemical analysis. Western blot (WB) was used to analyze protein expression associated with inflammatory pathway activation.

Results. Compared with the Mod group, Erchen decoction significantly alleviated gastric injury and increased PCNA expression in the gastric mucosa. Its therapeutic efficacy decreased in a dose-dependent manner, with weaker effects observed at lower doses. Erchen decoction significantly reduced serum levels of TNF-α, IL-1β, and MDA while enhancing SOD activity; however, these effects were less pronounced in the ECDL group than in the ECDM and ECDH groups. Importantly, Erchen decoction markedly decreased the expression of toll-like receptor 4 (TLR4), nuclear factor kappa-B (NF-κB), NOD-like receptor protein 3 (NLRP3), apoptosis-associated speck-like protein (ASC), cleaved caspase-1, IL-1β, and interleukin-18 (IL-18).

Conclusions. Erchen decoction alleviates ethanol-induced gastric injury by reducing inflammation, attenuating oxidative stress, preserving cellular structural integrity, and regulating the NF-κB signaling pathway.

Key words: ethanol-induced gastric injury, gastric mucosal protection, NF-κB signaling pathway, oxidative stress, TLR4/NLRP3 inflammasome

Cite as
Hou S, Li J. Modulation of NF-κB and oxidative stress pathways in ethanol-induced gastric injury by a multi-component herbal formula: An in vivo study. *Adv Clin Exp Med*. 2026;35(4):703–716. doi:10.17219/acem/208135

DOI
10.17219/acem/208135

Highlights

- Erchen decoction attenuates chronic ethanol-induced gastric injury by improving gastric mucosal pathology, promoting gastric epithelial cell proliferation, reducing inflammatory cytokines (TNF-α, IL-1β) and malondialdehyde (MDA), and enhancing superoxide dismutase (SOD) antioxidant activity.
- Erchen decoction suppresses key inflammatory signaling pathways, including TLR4/NF-κB/NLRP3 inflammasome activation, by downregulating toll-like receptor 4 (TLR4), nuclear factor kappa-B (NF-κB), NOD-like receptor protein 3 (NLRP3), apoptosis-associated speck-like protein(ASC), cleaved caspase-1, interleukin (IL)-1β, and IL-18 expression.
- Regulation of the NF-κB signaling pathway represents a central mechanism underlying the gastroprotective effects of Erchen decoction in chronic alcohol-induced gastric injury.
- Erchen decoction shows potential as a therapeutic strategy for the prevention and treatment of chronic alcohol-related gastric mucosal damage.

Background

Chronic ethanol-induced gastric injury is a common digestive system disorder. Chronic alcohol consumption can damage the gastric mucosa and increase the risk of developing severe gastrointestinal conditions such as gastritis, peptic ulcers, and potentially gastric cancer.[1–3] Alcohol exerts a direct effect on the gastric mucosa, leading to oxidative stress and inflammation, which can impair its protective function and contribute to tissue damage. In addition, the inflammatory process is mediated by interactions among multiple cytokines and signaling pathways.[4–6] Among these, the nuclear factor kappa-B (NF-κB) pathway plays a central role in regulating the inflammatory response.[7–9] Nuclear factor kappa-B is a transcription factor with a wide range of biological functions and regulates the expression of numerous inflammation-related genes. Under physiological conditions, NF-κB remains inactive in the cytoplasm.[10–12] External stimuli, including bacterial or viral infections and inflammatory signals, can activate NF-κB, promoting its translocation to the nucleus and the subsequent initiation of the inflammatory response.[13–15]

Despite advancements in conventional therapies such as proton pump inhibitors (e.g., omeprazole) and histamine 2 (H2) receptor antagonists, their prolonged use is associated with adverse effects, including gastrointestinal disturbances, and incomplete efficacy in mitigating ethanol-related mucosal injury.[16] Therefore, it is important to explore novel therapeutic approaches for alleviating chronic alcohol-induced gastric injury.

Erchen decoction, a classic traditional Chinese medicine (TCM) formula, consists of Pinelliae rhizoma, *Citri exocarpium rubrum*, *Poria*, and *Zingiberis rhizoma recens*, and contains 123 active components, including baicalein, stigmasterol, quercetin, and β-sitosterol.[17] Erchen decoction has traditionally been used to treat headaches and chest tightness attributed to exogenous wind-cold, internal injury, and dampness retention. It has also been widely used in the management of nonalcoholic fatty liver disease (NAFLD) and chronic obstructive pulmonary disease.[18,19] The therapeutic application of Erchen decoction in various inflammatory diseases is largely attributed to its anti-inflammatory and antioxidant properties.[17,20] In recent years, with the increasing focus on the modernization of TCM, the potential therapeutic effects of Erchen decoction in chronic alcohol-induced gastric injury have attracted growing attention. Therefore, this study was undertaken to investigate the therapeutic effects of Erchen decoction in a rat model of chronic ethanol-induced gastric injury and to further explore its underlying mechanisms, thereby addressing existing mechanistic gaps in the current research on its effects in chronic gastric injury.

Advances in microscopy, particularly transmission electron microscopy (TEM), have revolutionized the morphological sciences by providing unprecedented levels of magnification and resolution for the examination of biological samples. Transmission electron microscopy enables detailed visualization of the ultrastructure and organization of cellular components, including the cytoskeleton, membrane systems, and organelles, thereby elucidating structural–functional relationships within cells and tissues.[21] In the context of chronic alcohol-induced gastric injury, TEM has proven to be an invaluable tool for elucidating pathological alterations in gastric mucosal cells, including mitochondrial damage, endoplasmic reticulum stress, and disruption of cellular junctions. These ultrastructural changes are critical for understanding the underlying mechanisms of alcohol-induced gastric injury. Therefore, in this study, hematoxylin and eosin (H&E) staining, immunohistochemistry (IHC), TEM, biochemical assays, and western blot (WB) analysis were used to comprehensively evaluate and characterize the therapeutic effects and underlying mechanisms of Erchen decoction in alcohol-induced gastric injury.

Objectives

The study aims to investigate the effects of Erchen decoction on chronic ethanol-induced gastric injury.

Materials and methods

Animals

Seventy-two healthy male Sprague Dawley rats, aged 8 weeks and weighing approx. 170 g, were obtained from Henan Skbers Biotechnology Co., Ltd. (Zhengzhou, China). The rats were housed in a controlled environment at a room temperature of 20–24°C and relative humidity of 60–80%, with free access to food and water. The standard rat chow was purchased from Henan Huanyu Hekang Biotechnology Co., Ltd. (Zhengzhou, China). It consisted primarily of corn, soybean meal, bran meal, fish meal, macronutrients (vitamins), micronutrients (amino acids), mineral supplements (e.g., ferrous sulfate), edible oil, and salt (0.5% each). This study received ethical approval (No. GENINK-20230029; issued on October 8, 2023) from Tianjin Jinke Bona Biotechnology Co., Ltd. (Tianjin, China). All experiments were conducted in accordance with the Chinese Government's Guidelines for the Care and Use of Laboratory Animals to minimize animal pain and discomfort.[22]

Laboratory reagent

Erchen decoction (Q/BJT 0002S-2020; *Pinelliae rhizoma* 15 g, *Citri exocarpium rubrum* 15 g, *Poria* 9 g, *Glycyrrhizae radix et rhizoma praeparata cum melle* 4.5 g, 7 pieces of *Zingiberis rhizoma recens*, 1 *Mume fructus*; Bozhou Bojiatang Biotechnology Co., Ltd., Bozhou, China); oxymatrine (OXY) solution (1ST40311; Tianjin Alta Technology Co., Ltd., Tianjin, China); H&E staining solution (BA4041–BA4024; Zhuhai BaSO Biotechnology Co., Ltd., Zhuhai, China); anti-proliferating cell nuclear antigen (PCNA) antibody (AF0261; Shanghai Beyotime Biotech Inc., Shanghai, China); serum biochemical factor enzyme-linked immunosorbent assay (ELISA) kits (A001-3-2, A003-1-2; Nanjing Jiancheng Bioengineering Institute, Nanjing, China); Bradford protein quantification kit (P0006; Shanghai Beyotime Biotech Inc.); anti-interleukin-18 (IL-18) antibody (1:2,000; 10663-1-AP; Proteintech, Rosemont, USA); anti-interleukin-1 beta (IL-1β) antibody (1:2,000; 16806-1-AP; Proteintech); anti-caspase-1 antibody (1:1,000; 24232S; Cell Signaling Technology (CST), Danvers, USA); anti-cleaved caspase-1 antibody (1:1,000; 89332S; CST); anti-toll-like receptor 4 (TLR4) antibody (1:1,000; 66350-1-Ig; Proteintech); anti-NF-κB antibody (1:1,000; 10745-1-AP; Proteintech); anti-NOD-like receptor pyrin domain-containing protein 3 (NLRP3) antibody (1:2,000; 68102-1-Ig; Proteintech); and anti-apoptosis-associated speck-like protein containing a CARD (ASC) monoclonal antibody (1:5,000; 10500-1-AP; Proteintech).

Grouping

As shown in Table 1, the study design involved randomly dividing 72 rats into 6 groups: a control group (Con group; n = 12), a model group (Mod group; n = 12), a high-dose Erchen decoction group (ECDH group; n = 12), a medium-dose Erchen decoction group (ECDM group;

Table 1. Overview of experimental design

Group	Number of rats	Ethanol/saline regimen	Additional treatment	Dose and duration	Total study duration	Outcome assessments
Control (Con)	12	8 g/kg normal saline by gavage, once daily for 12 weeks	none	–	12 weeks (plus 1 week acclimatization)	At the end of week 12, rats were fasted overnight (approx. 15 h), then euthanized. Gastric tissues were harvested for: histopathology (H&E staining), IHC (*PCNA*), TEM, biochemical assays (SOD activity, MDA level, TNF-α, IL-1β), and WB (inflammatory/apoptotic proteins: TLR4, NF-κB, NLRP3, ASC, and caspase-1.
Model (Mod)	12	8 g/kg ethanol by gavage, once daily for 12 weeks	none	–	12 weeks (plus 1 week acclimatization)	
High-dose Erchen decoction (ECDH)	12	8 g/kg ethanol by gavage, once daily for 12 weeks	Erchen decoction (high dose: 10 mL/kg)	10 mL/kg/day, administered during the final 4 weeks of ethanol exposure	12 weeks (plus 1 week acclimatization)	
Medium-dose Erchen decoction (ECDM)	12	8 g/kg ethanol by gavage, once daily for 12 weeks	Erchen decoction (medium dose: 5 mL/kg)	5 mL/kg/day, administered during the final 4 weeks of ethanol exposure	12 weeks (plus 1 week acclimatization)	
Low-dose Erchen decoction (ECDL)	12	8 g/kg ethanol by gavage, once daily for 12 weeks	Erchen decoction (low dose: 2.5 mL/kg)	2.5 mL/kg/day, administered during the final 4 weeks of ethanol exposure	12 weeks (plus 1 week acclimatization)	
Oxymatrine (OXY)	12	8 g/kg ethanol by gavage, once daily for 12 weeks	oxymatrine solution (5 mL/kg)	5 mL/kg/day, administered during the final 4 weeks of ethanol exposure	12 weeks (plus 1 week acclimatization)	

H&E – hematoxylin and eosin; IHC – immunohistochemistry; PCNA – proliferating cell nuclear antigen; TEM – transmission electron microscopy; SOD – superoxide dismutase; MDA – malondialdehyde; TNF-α – tumor necrosis factor alpha; IL-1β – interleukin-1 beta; WB – western blot; TLR4 – toll-like receptor 4; NF-κB: nuclear factor kappa-B; NLRP3 – NOD-like receptor thermal protein domain-associated protein 3; ASC – apoptosis-associated speck-like protein.

n = 12), a low-dose Erchen decoction group (ECDL group; n = 12), and an oxymatrine group (OXY group; n = 12). After a 1-week acclimatization period, the Con group received 8 g·kg^{-1} normal saline. Administration was performed 3 times daily for 12 weeks. Other groups received 8 g·kg^{-1} ethanol by gavage for 12 weeks.[23]

The Erchen decoction groups and the OXY group were treated daily during the final 4 weeks of ethanol exposure (weeks 9–12). The ECDH group received 10 mL·kg^{-1} Erchen decoction, the ECDM group received 5 mL·kg^{-1} Erchen decoction, and the ECDL group received 2.5 mL·kg^{-1} Erchen decoction. The OXY group received 5 mL·kg^{-1} OXY solution daily. The above dosages were calculated based on the adult daily dose (1 dose per day, 200 g per dose) and converted to the equivalent rat dose using a standard human body weight of 70 kg.[24] No significant toxicity of Erchen decoction has been reported in previous studies.[25,26] According to common clinical dosages and relevant literature, the dosage used in this study complies with established safety standards for TCM.[4] Animals were fasted overnight for 15 h on the final day of the experiment prior to anesthesia induction and blood sample collection.

Hematoxylin and eosin staining analysis

Rat gastric histopathology was assessed using H&E staining. To preserve tissue structure, gastric tissue samples were immersed in 4% paraformaldehyde for 24 h. After fixation, the samples were dehydrated through a graded ethanol series (70–100%) for approx. 1 h, followed by clearing in xylene. Following dehydration and clearing, the samples were embedded in paraffin and sectioned at a thickness of 4–5 μm. The sections were then dewaxed in xylene, rehydrated through decreasing concentrations of ethanol, and stained with H&E solutions for 3–5 min and 1–2 min, respectively. After staining, the sections were dehydrated again, cleared in xylene, and mounted with sealing medium and a coverslip. Pathological changes, including edema, hemorrhage, epithelial shedding, and inflammatory cell infiltration, were evaluated using light microscopy (model DP26; Olympus Corp., Tokyo, Japan).

Immunohistochemistry analysis

Gastric tissue samples were immersed in 4% formaldehyde for 24 h, dehydrated through a graded series of ethanol solutions, and subsequently embedded in paraffin. The paraffin blocks were sectioned at a thickness of 4–5 μm and mounted onto glass slides. The sections were dewaxed in xylene and rehydrated through decreasing concentrations of ethanol. For antigen retrieval, the sections were heated under high pressure in citrate buffer for 20 min.

The samples were subsequently incubated in a blocking solution containing 5% normal serum and 1% bovine serum albumin (BSA) for 30 min to reduce nonspecific binding. The sections were then incubated overnight at 4°C with a primary antibody against proliferating cell nuclear antigen (PCNA). After washing, the sections were treated with a secondary antibody for 1 h. The chromogenic reaction between the enzyme-labeled secondary antibody and its substrate (typically 5–10 min) was used to visualize antibody binding. Subsequently, hematoxylin was used for nuclear counterstaining, followed by clearing in xylene, and the sections were mounted with a coverslip. PCNA expression in the nuclei was observed and quantitatively analyzed under a light microscope (model DP26; Olympus Corp.) to assess cell proliferation in gastric tissue.

Transmission electron microscopy observation

Gastric tissue was excised and cut into 1 mm^3 pieces, immediately fixed in 2.5% glutaraldehyde followed by 1% osmium tetroxide for 2 h, and then treated with 1% tannic acid for 30 min. The samples were subsequently dehydrated through a graded ethanol series (50–100%), with each step lasting 15 min.

After dehydration, the tissue was infiltrated with acrylic resin by incubation in a mixture of resin and ethanol for 2 h, followed by pure resin overnight, and then subjected to thermal polymerization and embedding in a mold. The cured resin blocks were subsequently sectioned into ultrathin sections (60–90 nm), mounted on copper grids, and stained with lead uranyl acetate for 10 min to enhance contrast. The sections were then placed in the TEM sample holder, and images were acquired for quantitative and qualitative analysis (model HT7800; Hitachi Ltd., Tokyo, Japan).

Serum biochemical detection

The manufacturer's instructions were followed for reagent preparation and microplate handling using the premade ELISA kits. Diluted serum samples and standards were added to the microplate wells, incubated for 1–2 h, and then washed with wash buffer. An enzyme-conjugated secondary antibody was added and incubated, followed by washing and the addition of substrate solution. After 15–30 min, a stop solution was added to terminate the reaction. Absorbance was measured at 450 nm to determine the concentrations of inflammatory markers.

For the determination of superoxide dismutase (SOD) activity and malondialdehyde (MDA) levels, serum samples were added to the prepared reaction mixtures, and absorbance or fluorescence intensity was measured based on the ability of SOD to inhibit substrate oxidation and on the formation of the colored product generated by the reaction of MDA with thiobarbituric acid. Finally, SOD activity and MDA concentrations were calculated by comparison with the standard curve.

Western blot analysis

Sample proteins were extracted using radioimmunoprecipitation assay (RIPA) buffer supplemented with protease inhibitors, followed by centrifugation at 4°C for 10 min to remove insoluble material. A Bradford protein quantification kit (P0006; Shanghai Beyotime Biotech Inc.) was used to determine protein concentration and ensure equal loading onto the sodium dodecyl sulfate–polyacrylamide gel electrophoresis (SDS–PAGE) gel.

The samples were mixed with 5 volumes of loading buffer, boiled for 5 min to achieve denaturation, and then separated by electrophoresis on a 10% SDS–PAGE gel. The separated proteins were transferred onto a polyvinylidene difluoride (PVDF) or nitrocellulose membrane, followed by wet transfer at 100 V for 1–2 h. After blocking in Tris-buffered saline with Tween (TBST) containing 5% skim milk for 1 h, the membranes were incubated with specific primary antibodies, followed by horseradish peroxidase (HRP)-conjugated secondary antibodies.

The membranes were incubated with primary antibodies overnight and with secondary antibodies for 1 h. Finally, an enhanced chemiluminescence (ECL) detection system (GD50202; Monad Biotech. Co. Ltd., Wuhan, China) was used to visualize the signals, and the expression levels of each target protein were quantitatively analyzed based on band intensity.

Statistical analyses

We used IBM SPSS Statistics for Windows v. 22 (IBM Corp., Armonk, USA). Data (n = 3 or n = 9) are presented as the min–max range or as the median (1st and 3rd quartile (Q1, Q3)). The data were derived from 3 or 9 independent replications of a given experiment, and only the aggregate scores in Tables 2,3 represent the sum of scores for sub-indicators. For multiple comparisons involving variability across all groups, the nonparametric Kruskal–Wallis test (n = 3 or n = 9) was used for between-group comparisons, followed by Dunn's test for planned pairwise comparisons.

When the global p-value in a Kruskal–Wallis test is non-significant, pairwise comparisons are not required. However, between-group comparison tests were not performed if any group had all values equal to a constant (n = 3). In cases where only 1 group had constant values (n = 3), 2 groups were directly compared using a one-sample nonparametric Wilcoxon signed-rank test. When both groups showed no variability (n = 3), standard statistical tests were not applied and the results were reported descriptively. In contrast, when both groups showed variation (n = 3), comparisons were performed using the Mann–Whitney U test. The p-values were corrected using the Bonferroni method for both multiple Kruskal–Wallis tests and multiple Dunn's tests. Statistical significance was defined as $p < 0.05$.

Results

Erchen decoction regulates pathological injury of gastric tissue

A comparison of the therapeutic effects of different doses of Erchen decoction based on macroscopic images of ethanol-induced gastric injury in rats showed that gastric tissue in the Con group exhibited no obvious lesions, with uniform coloration and intact structure. The scores for gastric epithelial erosion, ulceration, and hemorrhage were nearly 0, indicating no ethanol-induced damage. In contrast, gastric

Table 2. Score of ethanol-induced gastric injury in rats

Group	Gastric epithelial erosion	Gastric epithelial ulcer	Gastric epithelial hemorrhage focus	Aggregate score
Con	0	0	0–1	0–1
Mod	5	0–5	0–5	10–13*
OXY	0	0	2–4	2–4
ECDH	0	2	1–5	3–7
ECDM	0–5	0–2	2–5	5–9
ECDL	3–5	2–4	2–4	9–11

The lower the score, the less severe the injury.
Gastric epithelial erosion: All samples in Con group scored 0, all samples in Mod group scored 5, and all samples in group OXY and ECDH group scored 0, so no standard statistical test was applied for comparison between these 2 groups due to absence of variability; One-sample nonparametric Wilcoxon signed-rank test: $Z_{Mod\ vs\ ECDM} = 0.000$, $p_{Mod\ vs\ ECDM} = 0.317$; $Z_{Mod\ vs\ ECDL} = 0.000$, $p_{Mod\ vs\ ECDL} = 0.317$.
Gastric epithelial ulcer: one-sample nonparametric Wilcoxon signed-rank test: $Z_{Con\ vs\ Mod} = 3.000$, $p_{Con\ vs\ Mod} = 0.180$; $Z_{OXY\ vs\ Mod} = 3.000$, $p_{OXY\ vs\ Mod} = 0.180$; $Z_{ECDH\ vs\ Mod} = 4.000$, $p_{ECDH\ vs\ Mod} = 0.593$. Mann–Whitney U test: $U_{Mod\ vs\ ECDM} = 2.000$, $p_{Mod\ vs\ ECDM} = 0.400$; $U_{Mod\ vs\ ECDL} = 4.500$, $p_{Mod\ vs\ ECDL} > 0.999$.
Gastric epithelial hemorrhage focus: Kruskal–Wallis test: $H = 5.430$, $df = 5.000$, Adj.p = 0.732. Aggregate score: Kruskal–Wallis test: $H = 15.492$, $df = 5.000$, Adj.p = 0.016. Dunn's test: $Z_{Con\ vs\ Mod} = -13.667$, * $Adj.p_{Mod\ vs\ Con} = 0.010$; $Z_{OXY\ vs\ Mod} = 10.333$, $Adj.p_{OXY\ vs\ Mod} = 0.085$; $Z_{ECDH\ vs\ Mod} = 7.333$, $Adj.p_{ECDH\ vs\ Mod} = 0.455$; $Z_{Mod\ vs\ ECDM} = 5.167$, $Adj.p_{Mod\ vs\ ECDM} > 0.999$; $Z_{Mod\ vs\ ECDL} = 0.500$, $Adj.p_{Mod\ vs\ ECDL} > 0.999$.
*represents statistical significance compared with Con group. Sample n = 3; p-value was adjusted using Bonferroni correction for multiple Kruskal–Wallis tests (n = 2) and multiple Dunn's post hoc tests (n = 5).
Adj.p – adjusted p-value; Con group – control group; Mod group – model group; OXY group – oxymatrine group; ECDH group – high-dose Erchen decoction group; ECDM group – middle-dose Erchen decoction group; ECDL group – low-dose Erchen decoction group; Z – z-score/standard score; p – probability value; U – U-statistic; H – H-index; df – degrees of freedom.

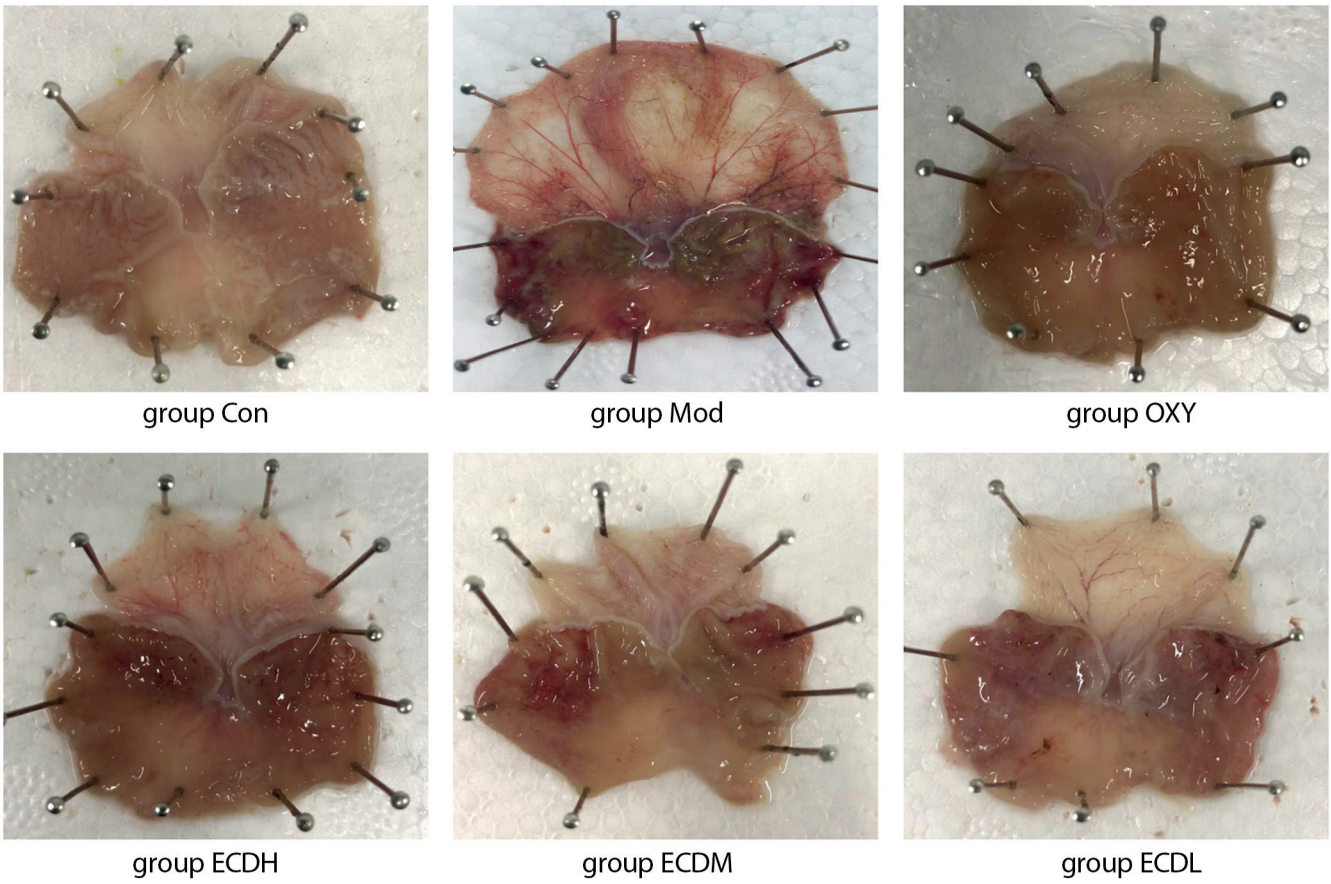

Fig. 1. Gastric tissue status in different treatment groups (n = 3)

Con group – control group; Mod group – model group; OXY group – oxymatrine group; ECDH group – high-dose Erchen decoction group; ECDM group – medium-dose Erchen decoction group; ECDL group – low-dose Erchen decoction group.

tissue in the Mod group displayed marked red hemorrhagic areas, including epithelial erosion, ulceration, and focal bleeding lesions. The Mod group had significantly higher aggregate scores than the Con group (Dunn's test: $Z_{\text{Mod vs Con}} = -13.667$, adjusted $p_{\text{Mod vs Con}} = 0.010$), indicating severe damage induced by 50% ethanol. In the OXY group, gastric tissue damage was mild, hemorrhage was reduced, and the aggregate gastric injury score was lower than that in the Mod group, suggesting that OXY treatment may attenuate ethanol-induced injury. The severity of gastric tissue damage varied among the Erchen decoction dosage groups, with the ECDH group exhibiting the mildest damage, followed by the ECDM group. Compared with the ECDH and ECDM groups, the ECDL group exhibited more severe damage; however, relative to the Mod group, the ECDL group showed improvement, with lower scores for gastric mucosal and epithelial injury. These results indicate that Erchen decoction protects against ethanol-induced gastric injury in a dose-dependent manner (Fig. 1, Table 2).

Erchen decoction regulates gastric injury in a dose-dependent manner

The results demonstrated the gastric tissue status across different treatment groups (Fig. 2, Table 3). In the Con group, the overall gastric architecture was essentially normal: the mucosal layer was intact, the glands were neatly arranged, no epithelial shedding, atrophy, edema, or congestion was observed, and no abnormalities were detected in the submucosa or muscularis. Compared with the Con group, the Mod group exhibited an irregular mucosal layer, disorganized glandular arrangement, mucosal epithelial atrophy, edema and congestion, and submucosal edema accompanied by inflammatory cell infiltration.

The Mod group exhibited an abnormal overall gastric architecture, with a significantly higher aggregate score than the Con group (Dunn's test: $Z_{\text{Mod vs Con}} = -14.667$, adjusted $p_{\text{Mod vs Con}} = 0.005$). Compared with the Mod group, both the OXY and ECDH groups showed improvement in ethanol-induced gastric injury. The general organization of the gastric tissue was largely preserved, with a slightly irregular mucosal layer, relatively well-organized glands, mild mucosal epithelial swelling and hyperplasia with congestion, and limited inflammatory cell infiltration in the submucosa. A reduction in the dose of Erchen decoction was associated with a gradual decrease in therapeutic efficacy against ethanol-induced gastric injury.

Table 3. Score of gastric injury in rats

Group	Mucosa cell edema	Mucosal cell bleeding	Mucosal cell shedding	Inflammatory infiltration	Aggregate score
Con	0	0	0–1	0	0–1
Mod	3	3–4	1–2	1–2	8–11*
OXY	1	1	0–1	1	3–4
ECDH	1	1	0–1	1	3–4
ECDM	1–2	2–3	0–1	0–1	4–5
ECDL	2–3	2–3	1–2	1	6–8

The lower the score, the less severe the injury.
Mucosa cell edema: All samples in Con group scored 0, all samples in the Mod group scored 3, and all samples in the OXY and ECDH groups scored 1, so no standard statistical test was applied for comparison between these 2 groups due to absence of variability; One-sample nonparametric Wilcoxon signed-rank test: $Z_{Mod\ vs\ ECDM} = 0.000$, $p_{Mod\ vs\ ECDM} = 0.102$; $Z_{Mod\ vs\ ECDL} = 0.000$, $p_{Mod\ vs\ ECDL} = 0.157$.
Mucosal cell bleeding: One-sample nonparametric Wilcoxon signed-rank test: $Z_{Con\ vs\ Mod} = 6.000$, $p_{Con\ vs\ Mod} = 0.102$; $Z_{OXY\ vs\ Mod} = 6.000$, $p_{OXY\ vs\ Mod} = 0.102$; $Z_{ECDH\ vs\ Mod} = 6.000$, $p_{ECDH\ vs\ Mod} = 0.102$. Mann–Whitney U test: $U_{Mod\ vs\ ECDM} = 0.500$, $p_{Mod\ vs\ ECDM} = 0.100$; $U_{Mod\ vs\ ECDL} = 1.000$, $P_{Mod\ vs\ ECDL} = 0.200$.
Mucosal cell shedding: Kruskal–Wallis test: $H = 7.942$, $df = 5.000$, $Adj.p = 0.318$.
Inflammatory infiltration: One-sample nonparametric Wilcoxon signed-rank test: $Z_{Con\ vs\ Mod} = 6.000$, $p_{Con\ vs\ Mod} = 0.102$; $Z_{OXY\ vs\ Mod} = 3.000$, $p_{OXY\ vs\ Mod} = 0.157$; $Z_{ECDH\ vs\ Mod} = 3.000$, $p_{ECDH\ vs\ Mod} = 0.157$. Mann–Whitney U test: $U_{Mod\ vs\ ECDM} = 0.500$, $p_{Mod\ vs\ ECDM} = 0.100$. One-sample nonparametric Wilcoxon signed-rank test: $Z_{Mod\ vs\ ECDL} = 3.000$, $p_{Mod\ vs\ ECDL} = 0.157$. Aggregate score: Kruskal–Wallis test: $H = 15.883$, $df = 5.000$, $Adj.p = 0.014$. Dunn's test: $Z_{Con\ vs\ Mod} = -14.667$, * $Adj.p_{Mod\ vs\ Con} = 0.005$; $Z_{OXY\ vs\ Mod} = 10.500$, $Adj.p_{OXY\ vs\ Mod} = 0.075$; $Z_{ECDH\ vs\ Mod} = 9.333$, $Adj.p_{ECDH\ vs\ Mod} = 0.150$; $Z_{Mod\ vs\ ECDM} = 6.167$, $Adj.p_{Mod\ vs\ ECDM} = 0.765$; $Z_{Mod\ vs\ ECDL} = 2.333$, $Adj.p_{Mod\ vs\ ECDL} > 0.999$.
*represents statistical significance compared with Con group. Sample n = 3; p-value was adjusted by Bonferroni correction for multiple Kruskal–Wallis tests (n = 2) and multiple Dunn's tests (n = 5). Adj.p means adjusted p-value.
Adj.p – adjusted p-value; Con group – control group; Mod group – model group; OXY group – oxymatrine group; ECDH group – high-dose Erchen decoction group; ECDM group – medium-dose Erchen decoction group; ECDL group – low-dose Erchen decoction group; Z – z-score/standard score; p – probability value; U – U-statistic; H – H-index; df – degrees of freedom.

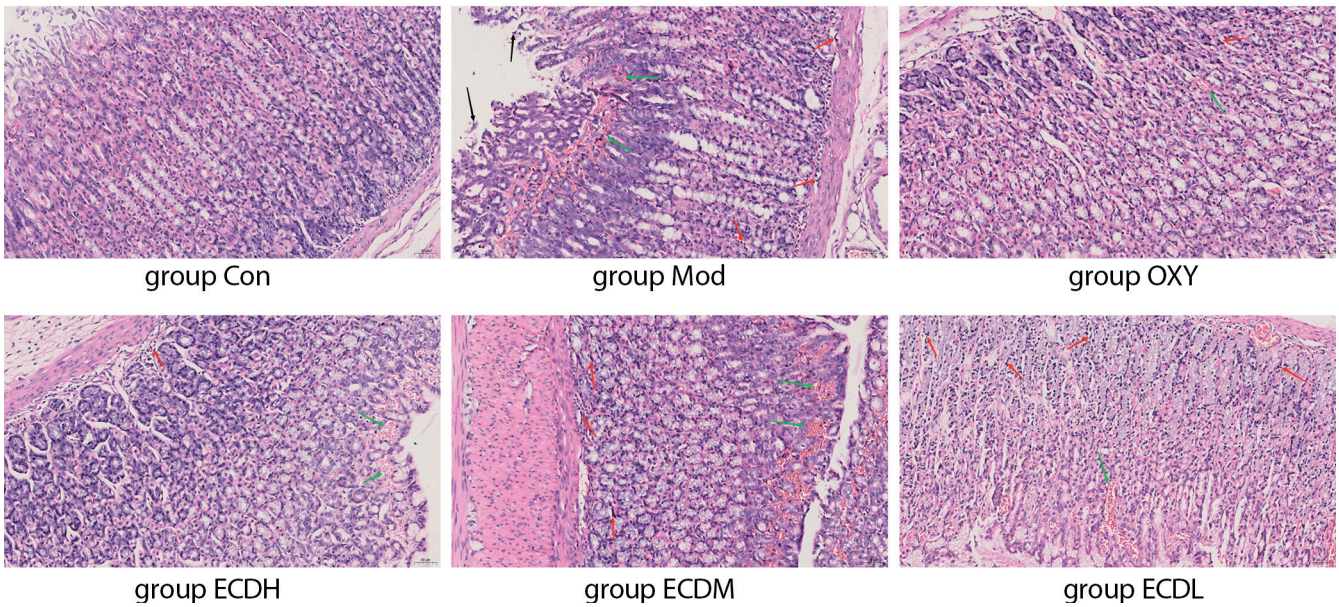

Fig. 2. Hematoxylin and eosin (H&E) staining of rat gastric tissue. Black arrows indicate mucosal epithelial shedding; green arrows indicate inflammatory cell infiltration; red arrows indicate mucosal edema and hemorrhage (n = 3)

Con group – control group; Mod group – model group; OXY group – oxymatrine group; ECDH group – high-dose Erchen decoction group; ECDM group – medium-dose Erchen decoction group; ECDL group – low-dose Erchen decoction group.

Erchen decoction promotes the proliferation of gastric injured cells

Cells in the Con group exhibited strong PCNA staining, indicating normal proliferative activity. In the Mod group, staining intensity was significantly reduced compared with the Con group (Dunn's test: $Z_{Con\ vs\ Mod} = 14.667$, adjusted $p_{Con\ vs\ Mod} = 0.005$), suggesting that ethanol-induced gastric injury may suppress cell proliferation. In contrast to the Mod group, the OXY group demonstrated significantly stronger staining (Dunn's test: $Z_{OXY\ vs\ Mod} = -12.333$, adjusted $p_{OXY\ vs\ Mod} = 0.025$), indicating that OXY treatment may promote the proliferation of damaged cells. Compared with the Mod group, PCNA staining in the Erchen decoction groups increased in a dose-dependent manner. The ECDH group exhibited the most intense staining and highest proliferative activity, whereas the ECDL group showed the lowest proliferative activity (Fig. 3).

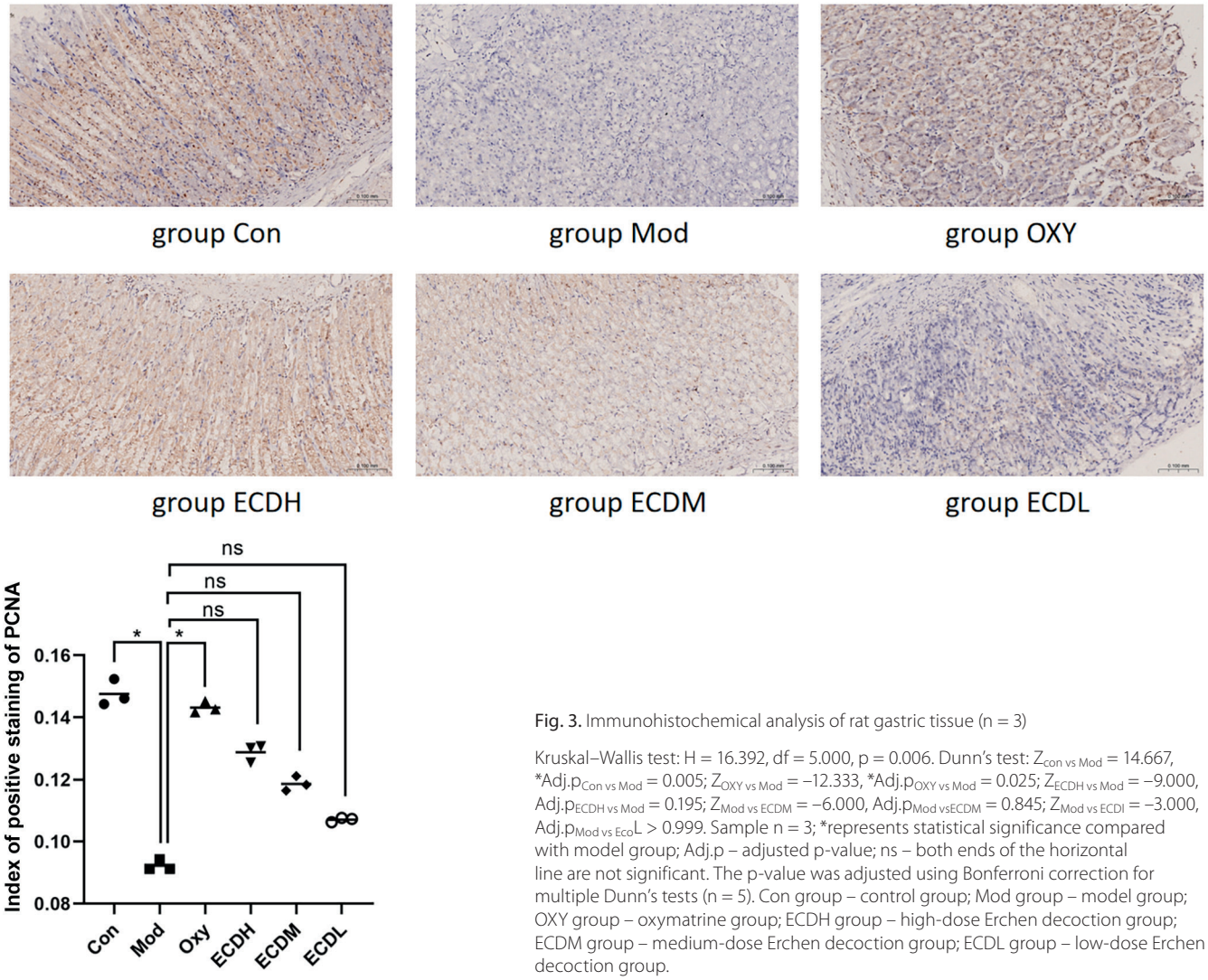

Fig. 3. Immunohistochemical analysis of rat gastric tissue (n = 3)

Kruskal–Wallis test: H = 16.392, df = 5.000, p = 0.006. Dunn's test: $Z_{con\ vs\ Mod} = 14.667$, *Adj.$p_{Con\ vs\ Mod} = 0.005$; $Z_{OXY\ vs\ Mod} = -12.333$, *Adj.$p_{OXY\ vs\ Mod} = 0.025$; $Z_{ECDH\ vs\ Mod} = -9.000$, Adj.$p_{ECDH\ vs\ Mod} = 0.195$; $Z_{Mod\ vs\ ECDM} = -6.000$, Adj.$p_{Mod\ vsECDM} = 0.845$; $Z_{Mod\ vs\ ECDl} = -3.000$, Adj.$p_{Mod\ vs\ EcoL} > 0.999$. Sample n = 3; *represents statistical significance compared with model group; Adj.p – adjusted p-value; ns – both ends of the horizontal line are not significant. The p-value was adjusted using Bonferroni correction for multiple Dunn's tests (n = 5). Con group – control group; Mod group – model group; OXY group – oxymatrine group; ECDH group – high-dose Erchen decoction group; ECDM group – medium-dose Erchen decoction group; ECDL group – low-dose Erchen decoction group.

Erchen decoction improved the structure of gastric damaged cells

The Con group exhibited normal gastric ultrastructure, including well-defined mitochondria and intact cell membranes. Compared with the Con group, the Mod group showed marked mitochondrial swelling and cell membrane damage, indicating inflammation and cellular injury. The OXY and Erchen decoction groups demonstrated attenuation of these pathological changes, particularly in the ECDH group, where cellular architecture was substantially improved compared with the Mod group. Although the ECDM and ECDL groups showed partial structural improvement, these effects were less pronounced than those observed in the ECDH group (Fig. 4).

Erchen decoction inhibited the expression of inflammatory factors

Compared with the Con group, the Mod group exhibited significantly higher levels of tumor necrosis factor alpha (TNF-α; Dunn's test: $Z_{Mod\ vs\ Con} = -44.500$, adjusted $p_{Mod\ vs\ Con} < 0.001$) and IL-1β (IL-1β; Dunn's test: $Z_{Mod\ vs\ Con} = -42.778$, adjusted $p_{Mod\ vs\ Con} < 0.001$), indicating that ethanol administration induced a pronounced inflammatory response. In the OXY group, the levels of these 2 inflammatory markers were comparable to those in the Con group but significantly lower than those in the Mod group (Dunn's test for TNF-α: $Z_{OXY\ vs\ Mod} = 34.500$, adjusted $p_{OXY\ vs\ Mod} < 0.001$; Dunn's test for IL-1β: $Z_{OXY\ vs\ Mod} = 34.944$, adjusted $p_{OXY\ vs\ Mod} < 0.001$), suggesting a significant anti-inflammatory effect of OXY treatment.

Compared with the Mod group, the ECDH group exhibited significantly reduced levels of TNF-α (Dunn's test: $Z_{ECDH\ vs\ Mod} = 28.000$, adjusted $p_{ECDH\ vs\ Mod} < 0.001$) and IL-1β (Dunn's test: $Z_{ECDH\ vs\ Mod} = 27.111$, adjusted $p_{ECDH\ vs\ Mod} = 0.001$), indicating that Erchen decoction decreased inflammation, with a more pronounced effect at higher doses. Compared with the Mod group, the ECDM group showed significantly lower IL-1β levels (Dunn's test: $Z_{Mod\ vs\ ECDM} = 21.167$, adjusted $p_{Mod\ vs\ ECDM} = 0.020$) and intermediate TNF-α levels, whereas the ECDL group

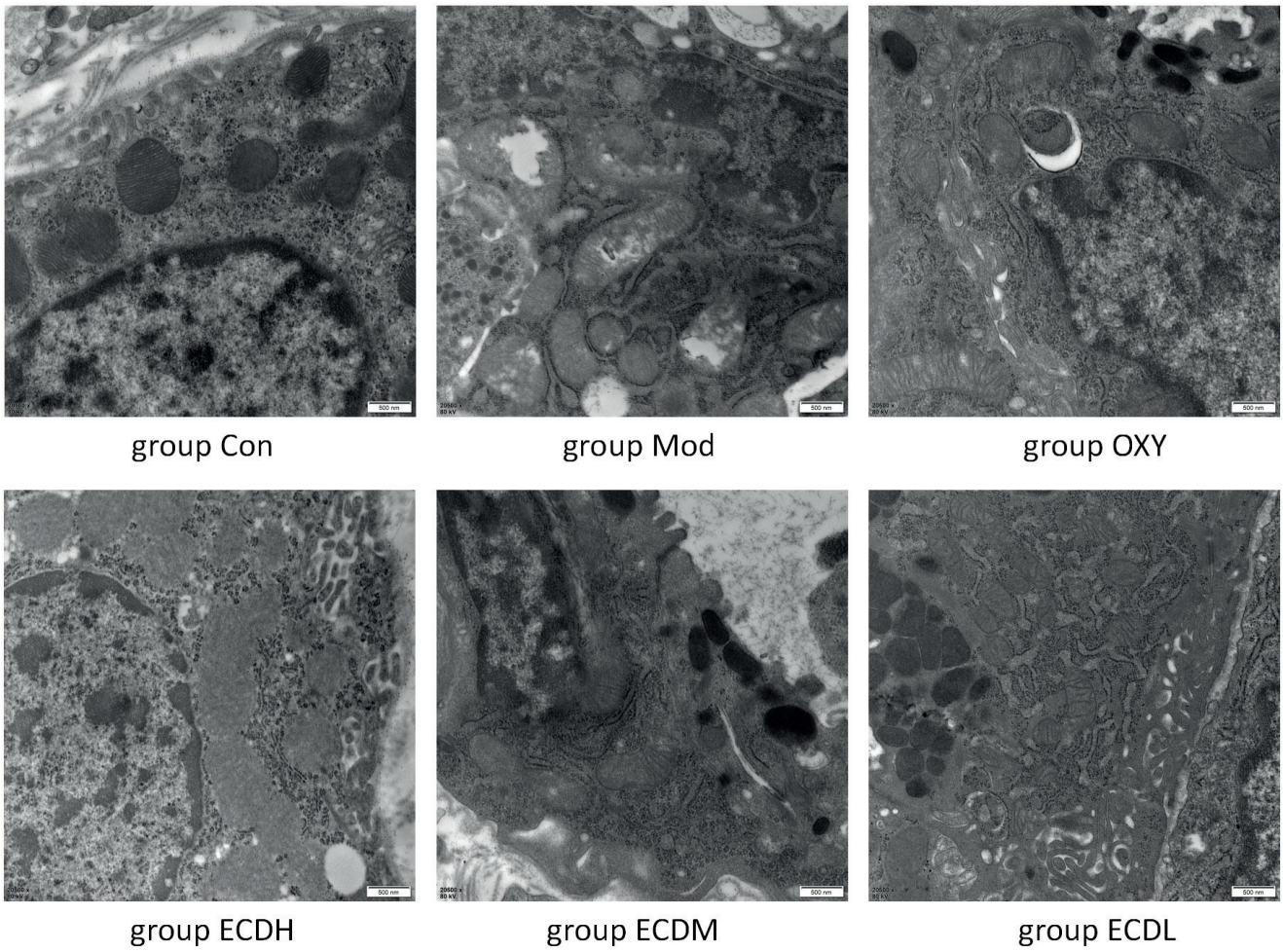

Fig. 4. Ultrastructural morphology of gastric tissue cells in different treatment groups observed by transmission electron microscopy (TEM). The scale bar represents 500 nm (×5,000 magnification; n = 3)

Con group – control group; Mod group – model group; OXY group – oxymatrine group; ECDH group – high-dose Erchen decoction group; ECDM group – medium-dose Erchen decoction group; ECDL group – low-dose Erchen decoction group.

Table 4. Expression of TNF-α and 1L-1β detected with enzyme-linked immunosorbent assay (ELISA)

Group	TNF-α (pg/mL)	IL-1β (pg/mL)
Con	13.7617 (13.3233, 13.9506)	42.3 (41.44, 43.19)
Mod	91.685 (90.6436, 93.0133)*	168.48 (164.78, 170.61)*
OXY	14.9689 (14.5849, 15.2907)$^{\Delta}$	43.56 (42.48, 44.3)$^{\Delta}$
ECDH	16.3317 (16.2662, 16.7924)$^{\Delta}$	44.49 (44.11, 45.06)$^{\Delta}$
ECDM	18.1257 (17.7901, 18.4629)	45.45 (44.68, 45.84)$^{\Delta}$
ECDL	44.3981 (43.3273, 46.056)	86.38 (83.57,89.27)

TNF-α: Kruskal–Wallis test: H = 49.422, df = 5.000, *Adj.p < 0.001. Dunn's test: $Z_{Mod\ vs\ Con} = -44.500$, $Adj.p_{Mod\ vs\ Con} < 0.001$; $Z_{OXY\ vs\ Mod} = 34.500$, $^{\Delta}Adj.p_{OXY\ vs\ Mod} < 0.001$; $Z_{ECDH\ vs\ Mod} = 28.000$, $^{\Delta}Adj.p_{ECDH\ vs\ Mod} < 0.001$; $Z_{Mod\ vs\ ECDM} = 19.000$, $Adj.p_{Mod\ vs\ ECDM} = 0.050$; $Z_{Mod\ vs\ ECDL} = 9.000$, $Adj.p_{Mod\ vs\ ECDL} > 0.999$.
IL-1β: Kruskal–Wallis test: H = 46.492, df = 5.000, Adj.p < 0.001. Dunn's test: $Z_{Mod\ vs\ Con} = -42.778$, $*Adj.p_{Mod\ vs\ Con} < 0.001$; $Z_{OXY\ vs\ Mod} = 34.944$, $^{\Delta}Adj.p_{OXY\ vs\ Mod} < 0.001$; $Z_{ECDH\ vs\ Mod} = 27.111$, $^{\Delta}Adj.p_{ECDH\ vs\ Mod} = 0.001$; $Z_{Mod\ vs\ ECDM} = 21.167$, $^{\Delta}Adj.p_{Mod\ vs\ ECDM} = 0.020$; $Z_{Mod\ vs\ ECDL} = 9.000$, $Adj.p_{Mod\ vs\ ECDL} > 0.999$.
*represents statistical significance compared with Con group; $^{\Delta}$represents statistical significance compared with Mod group. Sample n = 9; p-value was adjusted by Bonferroni correction for multiple Kruskal–Wallis tests (n = 2) and multiple Dunn's tests (n = 5). Adj.p – adjusted p-value;
Con group – control group; Mod group – model group; OXY group – oxymatrine group; ECDH group – high-dose Erchen decoction group; ECDM group – medium-dose Erchen decoction group; ECDL group – low-dose Erchen decoction group; TNF-α – tumor necrosis factor alpha; IL-1β – interleukin-1 beta; Z – z-score/standard score; H – H-index; df – degrees of freedom.

demonstrated intermediate levels of inflammatory markers. These findings suggest a mild anti-inflammatory effect at low and medium doses, which was less pronounced than that observed in the high-dose group (Table 4).

Table 5. SOD activity and MDA detection of serum oxidative stress markers

Group	SOD (U/mL)	MDA (nmol/mL)
Con	17.77 (17.67, 17.93)	2.19 (1.81, 3.23)
Mod	8.91 (8.69, 9.32)*	6.71 (5.81, 7.23)*
OXY	16.54 (15.57, 16.81)$^{\Delta}$	3.1 (1.94, 3.36)$^{\Delta}$
ECDH	15.85 (15.61, 16.26)$^{\Delta}$	2.84 (2.58, 2.84)$^{\Delta}$
ECDM	15.61 (15.59, 15.73)$^{\Delta}$	2.71 (2.58, 3.23)$^{\Delta}$
ECDL	11.88 (11.72, 12.32)	4.52 (4.26, 4.9)

SOD: Kruskal–Wallis test: H = 46.510, df = 5.000, Adj.p < 0.001. Dunn's test: $Z_{Mod\ vs\ Con} = 45.000$, * $Adj.p_{Mod\ vs\ Con} < 0.001$; $Z_{OXY\ vs\ Mod} = -30.111$, $^{\Delta}Adj.p_{OXY\ vs\ Mod} < 0.001$; $Z_{ECDH\ vs\ Mod} = -27.556$, $^{\Delta}Adj.p_{ECDH\ vs\ Mod} = 0.001$; $Z_{Mod\ vs\ ECDM} = -23.333$, $^{\Delta}Adj.p_{Mod\ vs\ ECDM} = 0.010$; $Z_{Mod\ vs\ ECDL} = -9.000$, $Adj.p_{Mod\ vs\ ECDL} > 0.999$. MDA: Kruskal–Wallis test: H = 36.215, df = 5.000, Adj.p < 0.001. Dunn's test: $Z_{Mod\ vs\ Con} = -34.833$, * $Adj.p_{Mod\ vs\ Con} < 0.001$; $Z_{OXY\ vs\ Mod} = 31.222$, $^{\Delta}Adj.p_{OXY\ vs\ Mod} < 0.001$; $Z_{ECDH\ vs\ Mod} = 30.444$, $^{\Delta}Adj.p_{ECDH\ vs\ Mod} < 0.001$; $Z_{Mod\ vs\ ECDM} = 28.611$, $^{\Delta}Adj.p_{Mod\ vs\ ECDM} < 0.001$; $Z_{Mod\ vs\ ECDL} = 9.889$, $Adj.p_{Mod\ vs\ ECDL} = 0.910$. *represents statistical significance compared with Con group; $^{\Delta}$represents statistical significance compared with Mod group. Sample n = 9; p-value was adjusted using Bonferroni correction for multiple Kruskal–Wallis tests (n = 2) and multiple Dunn's tests (n = 5). Adj.p – adjusted p-value; Con group – control group; Mod group – model group; OXY group – oxytmatrine group; ECDH group – high-dose Erchen decoction group; ECDM group – medium-dose Erchen decoction group; ECDL group – low-dose Erchen decoction group; TNF-α – tumor necrosis factor alpha; IL-1β – interleukin-1 beta; SOD – superoxide dismutase; MDA – malondialdehyde; Z – z-score/standard score; H – H-index; df – degrees of freedom.

Erchen decoction enhanced the anti-oxidation of cells

Superoxide dismutase activity in the Mod group was significantly lower than that in the Con group (Dunn's test: Z_Mod vs Con = 45.000, adjusted $p_{Mod\ vs\ Con} < 0.001$), whereas MDA levels were significantly higher (Dunn's test: $Z_{Mod\ vs\ Con} = -34.833$, adjusted $p_{Mod\ vs\ Con} < 0.001$). These findings indicate that ethanol induced pronounced oxidative stress, reduced antioxidant capacity, and increased lipid peroxidation. The OXY, ECDH, and ECDM groups exhibited significantly higher SOD activity than the Mod group (Dunn's test: $Z_{OXY\ vs\ Mod} = -30.111$, adjusted $p_{OXY\ vs\ Mod} < 0.001$; $Z_{ECDH\ vs\ Mod} = -27.556$, adjusted $p_{ECDH\ vs\ Mod} = 0.001$; $Z_{Mod\ vs\ ECDM} = -23.333$, adjusted $p_{Mod\ vs\ ECDM} = 0.010$), along with significantly lower MDA levels (Dunn's test: $Z_{OXY\ vs\ Mod} = 31.222$, adjusted $p_{OXY\ vs\ Mod} < 0.001$; $Z_{ECDH\ vs\ Mod} = 30.444$, adjusted $p_{ECDH\ vs\ Mod} < 0.001$; $Z_{Mod\ vs\ ECDM} = 28.611$, adjusted $p_{Mod\ vs\ ECDM} < 0.001$). These results suggest that these interventions enhanced antioxidant defenses and attenuated oxidative damage. In the Erchen decoction treatment groups, SOD activity in the ECDH and ECDM groups was comparable to that in the Con group, and MDA levels were similarly low, indicating favorable antioxidant effects. Superoxide dismutase activity in the ECDL group also improved; however, the effect was less pronounced than that observed in the ECDH and ECDM groups (Table 5).

Erchen decoction inhibited the expression of inflammation-related proteins

The expression levels of the inflammation- and apoptosis-related proteins TLR4, NF-κB, NLRP3, and ASC were analyzed with WB. Compared with the Con group, the Mod group exhibited higher expression levels of these proteins. In contrast, protein expression in the OXY group was reduced relative to the Mod group, indicating that OXY treatment effectively alleviated ethanol-induced inflammatory activation. Similarly, protein levels in the 3 Erchen decoction-treated groups were lower than those in the Mod group, suggesting that Erchen decoction exerts anti-inflammatory effects (Fig. 5).

Erchen decoction inhibited the expression of proteins related to the activation pathway of inflammatory cells

Western blot analysis demonstrated higher expression of proteins involved in inflammatory pathway activation in the Mod group compared with the Con group, including significantly elevated levels of IL-18 (Dunn's test: $Z_{Con\ vs\ Mod} = -14.667$, adjusted $p_{Con\ vs\ Mod} = 0.005$) and IL-1β (Dunn's test: $Z_{Con\ vs\ Mod} = -14.333$, adjusted $p_{Con\ vs\ Mod} = 0.005$). These findings suggest that ethanol exposure induced a pronounced inflammatory response. Compared with the Mod group, the OXY group exhibited reduced levels of cleaved caspase-1, IL-1β, and IL-18, indicating that OXY treatment suppressed inflammatory activation and associated cell signaling. The levels of cleaved caspase-1, IL-1β, and IL-18 were lower in the ECDH, ECDM, and ECDL groups than in the Mod group. Notably, the reduction in IL-1β levels between the ECDH and Mod groups was statistically significant (Dunn's test: $Z_{ECDH\ vs\ Mod} = 11.333$, adjusted $p_{ECDH\ vs\ Mod} = 0.045$). Although no statistically significant differences were observed among the other Erchen decoction-treated groups, the overall trend was consistent, suggesting that Erchen decoction exerted a dose-dependent suppressive effect on inflammation, with the highest dose (ECDH) showing the most pronounced effect (Fig. 6).

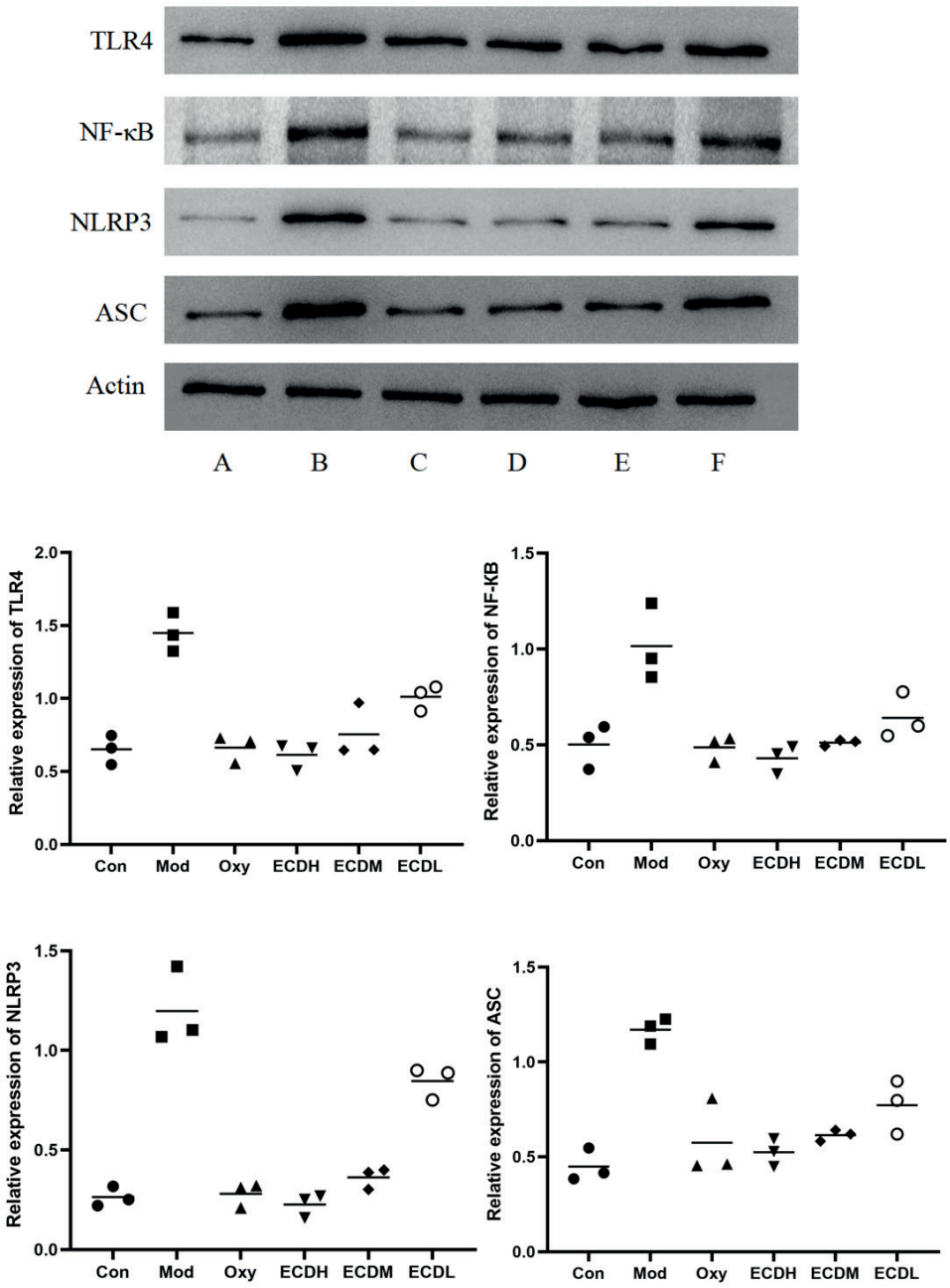

Fig. 5. Western blot analysis of inflammation- and apoptosis-related protein expression. A. Con group; B. Mod group; C. OXY group; D. ECDH group; E. ECDM group; F. ECDL group

Con group – control group; Mod group – model group; OXY group – oxymatrine group; ECDH group – high-dose Erchen decoction group; ECDM group – medium-dose Erchen decoction group; ECDL group – low-dose Erchen decoction group; Adj.p – adjusted p-value.
Toll-like receptor 4 (TLR4): Kruskal–Wallis test: H = 11.713, df = 5.000, Adj.p = 0.156. Nuclear factor kappa-B (NF-κB): Kruskal–Wallis test: H = 13.023, df = 5.000, Adj.p = 0.092. NLR family pyrin domain containing 3 (NLRP3): Kruskal–Wallis test: H = 13.936, df = 5.000, Adj.p = 0.064. Apoptosis-associated speck-like protein (ASC) Kruskal–Wallis test: H = 12.883, df = 5.000, Adj.p = 0.096. Sample n = 3. The p-value was adjusted using Bonferroni correction for multiple Kruskal–Wallis tests (n = 4).

Discussion

Gastric damage caused by excessive alcohol consumption is characterized by bleeding, gastric ulceration, erosion, and related lesions. Injured gastric tissue cells exhibited inflammatory infiltration, accompanied by decreased proliferative activity and increased apoptosis. Under ethanol stimulation, the expression of inflammation-related markers, including TNF-α and IL-1β, was significantly elevated, along with increased oxidative stress levels.

Erchen decoction was first recorded in the well-known Song Dynasty medical text *Taiping Huimin Heji Ju Fang* and has been widely used in TCM. Modern studies have demonstrated that Erchen decoction can reduce inflammatory mediators in tissues and is therefore frequently applied in conditions such as pneumonia, bronchitis, and hepatitis.[27–29] In the present study, we confirmed that Erchen decoction effectively alleviates ethanol-induced gastric injury by regulating inflammatory factors and enhancing antioxidant capacity.

The gastric histopathological findings in the Erchen decoction-treated groups indicated a dose-dependent therapeutic effect, with higher doses producing greater histological improvement. Notably, the high-dose Erchen decoction achieved a therapeutic effect comparable to that of OXY. As a proliferation-associated nuclear antigen, PCNA expression is closely linked to cell proliferation.[30–32] In the Mod group, ethanol exposure resulted in a significant reduction in PCNA expression, suggesting that ethanol not only disrupted the structural integrity of the gastric mucosa but also impaired cellular

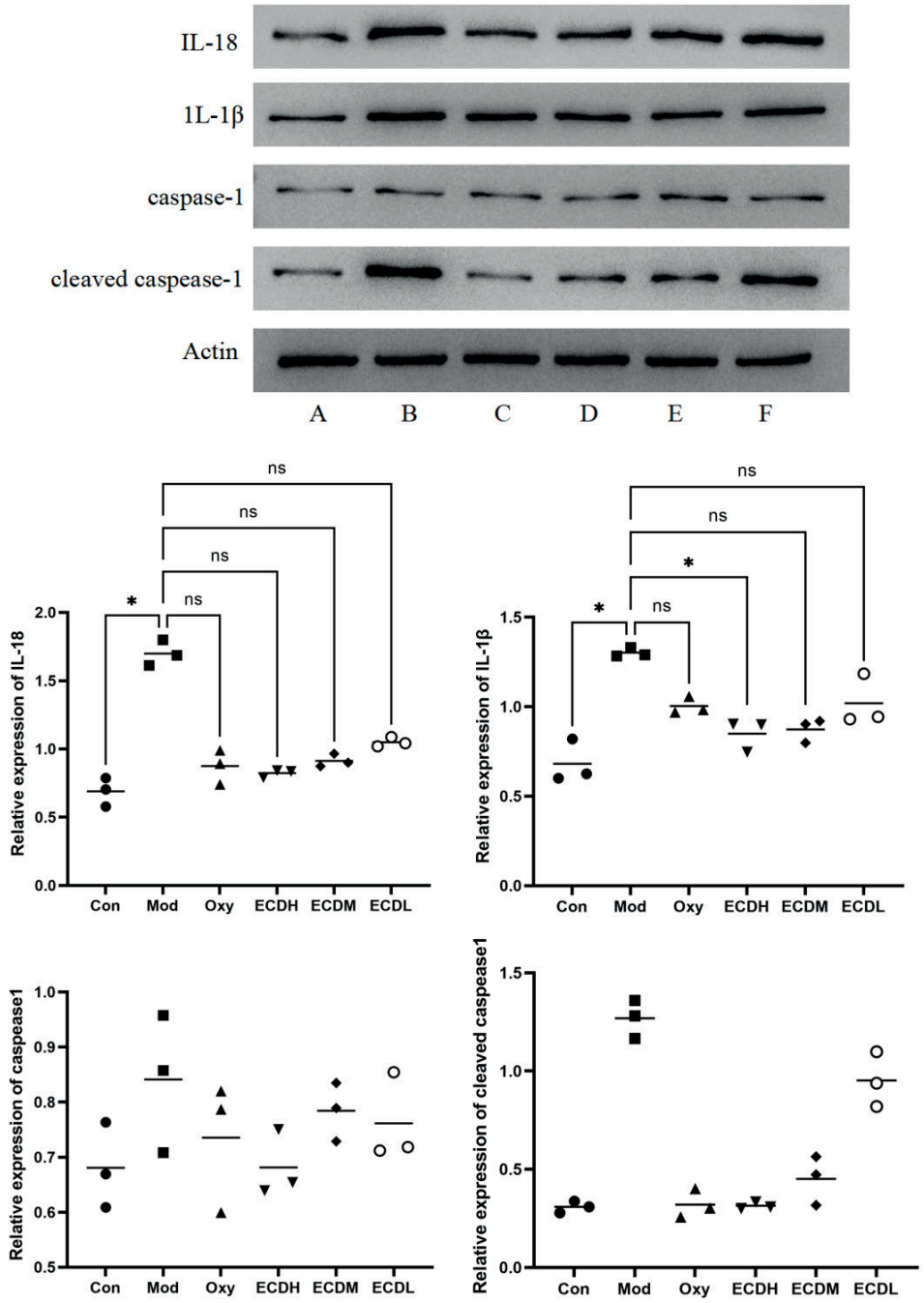

Fig. 6. Western blot analysis of protein expression in the inflammatory signaling pathway. A. Con group; B. Mod group; C. OXY group; D. ECDH group; E. ECDM group; F. ECDL group

Con group – control group; Mod group – model group; OXY group – oxymatrine group; ECDH group – high-dose Erchen decoction group; ECDM group – medium-dose Erchen decoction group; ECDL group – low-dose Erchen decoction group; Adj.p – adjusted p-value. Interleukin-18 (IL-18): Kruskal–Wallis test: H = 14.988, df = 5.000, Adj.p = 0.040. Dunn's test: $Z_{Con\ vs\ Mod}$ = –14.667, *Adj.$p_{Con\ vs\ Mod}$ = 0.005, $Z_{OXY\ vs\ Mod}$ = 9.000, Adj.$p_{OXY\ vs\ Mod}$ = 0.195; $Z_{ECOH\ vs\ Mod}$ = 11.000, Adj.$p_{ECOH\ vs\ Mod}$ = 0.060; $Z_{Mod\ vs\ ECOM}$ = 7.333, Adj.$p_{Mod\ vs\ ECDM}$ = 0.460; $Z_{Mod\ vs\ ECDL}$ = 3.000, Adj.$p_{Mod\ vs\ ECOL}$ > 0.999. Interleukin-1 beta (IL-1β): Kruskal–Wallis test: H = 15.175, df = 5.000, Adj.p = 0.040. Dunn's test: $Z_{Con\ vs\ Mod}$ = –14.333, *Adj.$p_{Con\ vs\ Mod}$ = 0.005; $Z_{OXY\ vs\ Mod}$ = 4.000, Adj.$p_{OXY\ vs\ Mod}$ > 0.999; $Z_{ECDH\ vs\ Mod}$ = 11.333, *Adj.$p_{ECOH\ vs\ Mod}$ = 0.045; $Z_{Mod\ vs\ ECDM}$ = 10.333, Adj.$p_{Mod\ vs\ ECDM}$ =0.090; $Z_{Mod\ vs\ ECDL}$ = 5.000, Adj.$p_{Mod\ vs\ ECDL}$ > 0.999. Caspase 1: Kruskal–Wallis test: H = 5.608, df = 5.000, Adj.p > 0.999. Cleaved caspase 1: Kruskal–Wallis test: H = 13.585, df = 5.000, Adj.p = 0.072. Sample n = 3; *represents statistical significance compared with model group; ns, both ends of the horizontal line are not significant. The p-value was adjusted using Bonferroni correction for multiple Kruskal–Wallis tests (n = 4) and multiple Dunn's post hoc tests (n = 5).

proliferative capacity. Compared with the Mod group, PCNA staining was more intense in the OXY group, indicating that OXY enhanced the proliferation of damaged cells and promoted gastric mucosal repair and regeneration. Similarly, PCNA staining intensity in the Erchen decoction groups increased in a dose-dependent manner.

Among the treatment groups, proliferative activity was greatest in the ECDH group, whereas the ECDL group also showed enhanced proliferation, albeit to a lesser extent. These findings indicate that Erchen decoction not only attenuates ethanol-induced gastric mucosal injury but also promotes the growth and repair of damaged gastric mucosal cells. Erchen decoction treatment reduced mitochondrial swelling and cell membrane disruption, thereby inhibiting cellular injury and the potential subsequent dysfunction or death.[33] Following OXY treatment, the levels of inflammatory markers TNF-α and IL-1β were comparable to those in the Con group and significantly lower than those in the Mod group. Although the high-dose Erchen decoction did not achieve the same magnitude of effect as OXY, it still significantly reduced ethanol-induced inflammation, suggesting that high-dose Erchen decoction exerts a substantial anti-inflammatory effect.

Superoxide dismutase is a key antioxidant enzyme responsible for eliminating harmful superoxide radicals, whereas MDA is a byproduct of lipid peroxidation in cell

membranes and is commonly used as a marker of oxidative damage.[34] Compared with the Con group, the Mod group showed significantly reduced SOD activity and significantly elevated MDA levels. These changes indicate that ethanol exposure markedly impaired antioxidant defense capacity.[11,13,14] Both the OXY group and the ECDH/ECDM/ECDL groups demonstrated varying degrees of improvement. Superoxide dismutase activity increased and MDA levels decreased in all treatment groups compared with the Mod group, suggesting that these interventions enhanced antioxidant defenses and attenuated oxidative damage. Overall, these findings indicate that Erchen decoction alleviates ethanol-induced gastric mucosal injury, at least in part, by increasing SOD activity and reducing MDA levels. Activation of the NF-κB pathway represents a central mechanism in ethanol-induced gastric injury. As a key regulator of the inflammatory response, the NF-κB pathway plays a pivotal role in promoting the expression of pro-inflammatory cytokines.[35,36] Alcohol exposure activates the NF-κB pathway, leading to elevated levels of inflammatory mediators such as TNF-α and IL-1β, thereby exacerbating gastric mucosal inflammation and injury. In the present study, ethanol exposure was associated with increased expression of NF-κB and related inflammatory signaling proteins, including TLR4, NLRP3, and ASC, further indicating activation of the NF-κB pathway in ethanol-induced gastric injury. Notably, this study further explored the regulatory effects of Erchen decoction on this pathway. Erchen decoction effectively suppressed NF-κB activation and the expression of downstream inflammatory mediators, particularly in the ECDH group. In addition, Erchen decoction reduced the levels of cleaved caspase-1, caspase-1, IL-1β, and IL-18, further suggesting that it alleviates ethanol-induced gastric mucosal injury, at least in part, through inhibition of the NF-κB pathway. These findings are important for understanding the mechanisms by which Erchen decoction mitigates chronic ethanol-induced gastric injury and suggest that its protective effects may be mediated by suppression of NF-κB signaling, thereby reducing inflammatory mediator release and inflammatory cell activation.

Limitations of the study

However, we acknowledge that our study has several limitations. Erchen decoction is a complex TCM formulation, and the specific active components and key target proteins responsible for regulating chronic ethanol-induced gastric injury remain unclear. We intend to address this important issue in future investigations.

Conclusions

This study confirmed that Erchen decoction alleviates ethanol-induced gastric injury by reducing inflammation, attenuating oxidative stress, preserving cellular structural integrity, and regulating the NF-κB signaling pathway. These findings not only suggest a potential TCM-based therapeutic approach for ethanol-induced gastric injury but also provide a scientific basis for further investigation of Erchen decoction in the treatment of other inflammation- and oxidative stress-related diseases.

Data Availability Statement

The datasets supporting the findings of the current study are openly available in the Zenodo repository at https://doi.org/10.5281/zenodo.16417628.

Consent for publication

Not applicable.

Use of AI and AI-assisted technologies

Not applicable.

ORCID iDs

Shaokai Hou https://orcid.org/0009-0005-4155-8646
Ji Li https://orcid.org/0009-0003-2110-4618

References

1. Kharbanda KK, Farokhnia M, Deschaine SL, et al. Role of the ghrelin system in alcohol use disorder and alcohol-associated liver disease: A narrative review. *Alcohol Clin Exp Res*. 2022;46(12):2149–2159. doi:10.1111/acer.14967
2. Chao W, Qiong WU, Ping LI, et al. Effect of traditional Chinese medicine combined with Western medicine on blood lipid levels and inflammatory factors in patients with angina pectoris in coronary heart disease identified as intermingled phlegm and blood stasis syndrome: A network meta-analysis. *J Tradit Chin Med*. 2023;43(4):640–649. doi:10.19852/j.cnki.jtcm.20230506.001
3. Yang R, Li J, Xu X, Xu K, Shi J. Preventive and therapeutic effects of *Lactobacillus rhamnosus* SHA113 and its culture supernatant on alcoholic gastric ulcers. *Food Funct*. 2021;12(16):7250–7259. doi:10.1039/d1fo00181g
4. Deng G, Jia H, Li Y, et al. Erchen decoction improves iron homeostasis in mice with non-alcoholic fatty liver disease by regulating iron transport capacity in the spleen [in Chinese]. *Nan Fang Yi Ke Da Xue Xue Bao*. 2023;43(8):1287–1296. doi:10.12122/j.issn.1673-4254.2023.08.04
5. Iskender H, Dokumacioglu E, Terim Kapakin KA, et al. Effects of oleanolic acid on inflammation and metabolism in diabetic rats. *Biotech Histochem*. 2022;97(4):269–276. doi:10.1080/10520295.2021.1954691
6. Lu S, Zhang L, Hu Z, Kong S, Zhang Z, Li G. Optimized preparation of gastric acid-response sulfhydryl functionalized chitosan/alginate /tilapia peptide hydrogel and its protective effects on alcohol-induced liver and brain injury. *RSC Adv*. 2021;11(55):34544–34557. doi:10.1039/d1ra06361h
7. Aziz F, Chakraborty A, Liu K, et al. Gastric tumorigenesis induced by combining *Helicobacter pylori* infection and chronic alcohol through IL-10 inhibition. *Carcinogenesis*. 2022;43(2):126–139. doi:10.1093/carcin/bgab114
8. Thapa K, Khan H, Singh TG, Kaur A. Traumatic brain injury: Mechanistic insight on pathophysiology and potential therapeutic targets. *J Mol Neurosci*. 2021;71(9):1725–1742. doi:10.1007/s12031-021-01841-7
9. Jang J, Jung Y, Chae S, et al. XAV939, a Wnt/β-catenin pathway modulator, has inhibitory effects on LPS-induced inflammatory response. *Immunopharmacol Immunotoxicol*. 2019;41(3):394–402. doi:10.1080/08923973.2018.1536984

10. Fry RC, Navasumrit P, Valiathan C, et al. Activation of inflammation/NF-κB signaling in infants born to arsenic-exposed mothers. *PLoS Genet*. 2007;3(11):e207. doi:10.1371/journal.pgen.0030207
11. Basatinya AM, Sajedianfard J, Nazifi S, et al. Effects of ethanolic extracts of *Quercus*, *Cirsium vulgare* and *Falcaria vulgaris* on gastric ulcer, antioxidant and inflammatory indices, and gene expression in rats. *Physiol Rep*. 2021;9(16):e14954. doi:10.14814/phy2.14954
12. Li Q, Zhu S, Chen G, et al. Exosomal miR-10b derived from protocatechuic acid-treated efferocytic macrophages inhibits endothelial inflammation by targeting MAP3K7/β-TrCP/NF-κB signaling pathway. *Phytomedicine*. 2026;153:157939. doi:10.1016/j.phymed.2026.157939
13. Jafari A, Sadeghpour S, Ghasemnejad-Berenji H, Pashapour S, Ghasemnejad-Berenji M. Potential antioxidative, anti-inflammatory and immunomodulatory effects of ghrelin, an endogenous peptide from the stomach in SARS-CoV2 infection. *Int J Pept Res Ther*. 2021;27(3):1875–1883. doi:10.1007/s10989-021-10217-9
14. Li W, Zhang G, Zhao Z, Zuo Y, Sun Z, Chen S. Exploring the mechanism of Erchen decoction in the treatment of atherosclerosis based on network pharmacology and molecular docking. *Medicine (Baltimore)*. 2023;102(46):e35248. doi:10.1097/md.0000000000035248
15. Sadighi A, Leggio L, Akhlaghi F. Development of a physiologically based pharmacokinetic model for prediction of ethanol concentration-time profile in different organs. *Alcohol Alcohol*. 2021;56(4):401–414. doi:10.1093/alcalc/agaa129
16. Kuna L, Jakab J, Smolic R, Raguz-Lucic N, Vcev A, Smolic M. Peptic ulcer disease: A brief review of conventional therapy and herbal treatment options. *J Clin Med*. 2019;8(2):179. doi:10.3390/jcm8020179
17. Liu H, Xu J, Li H, Zhang L, Xu P. Network pharmacology-based investigation to explore the effect and mechanism of Erchen decoction against the nonalcoholic fatty liver disease. *Anat Rec (Hoboken)*. 2021;304(11):2605–2619. doi:10.1002/ar.24770
18. Ding SS, Zhuang Y, Liao Y, et al. Effect of Erchen decoction on liver mitochondrial function by inhibiting mTORC1/SREBP1/CAV1 pathway in mice with high-fat diet [in Chinese]. *Zhongguo Zhong Yao Za Zhi*. 2024;49(3):763–769. doi:10.19540/j.cnki.cjcmm.20231103.401
19. Deng L, Zhang X, Dong Y, et al. Erchen decoction combined with Sanziyangqin decoction for chronic obstructive pulmonary disease: A protocol for systematic review and meta-analysis. *Medicine (Baltimore)*. 2020;99(40):e22315. doi:10.1097/md.0000000000022315
20. Chen J, Ye C, Yang Z, et al. Erchen decoction to reduce oxidative stress in dyslipidemia phlegm-dampness retention syndrome mice: In vivo mechanism revealed by metabolomics (liquid chromatography–mass spectrometry). *Phytomedicine*. 2023;115:154808. doi:10.1016/j.phymed.2023.154808
21. Bernardi S, Marchetti E, Torge D, Simeone D, Macchiarelli G, Bianchi S. Ultrastructural assessment of human periodontal ligament fibroblast interaction with bovine pericardium membranes: An in vitro study [published online as ahead of print on December 12, 2024]. *Histol Histopathol*. 2024. doi:10.14670/HH-18-860
22. MacArthur Clark JA, Sun D. Guidelines for the ethical review of laboratory animal welfare People's Republic of China National Standard GB/T 35892-2018 [Issued 6 February 2018 Effective from 1 September 2018]. *Anim Models Exp Med*. 2020;3(1):103–113. doi:10.1002/ame2.12111
23. Budinskaya K, Nádeníček J, Stračina T, et al. Mineral water Vincentka and its influence on mucosal ulcers. *Physiol Res*. 2022;71(Suppl 2):S251–S257. doi:10.33549/physiolres.935013
24. Nair AB, Jacob S. A simple practice guide for dose conversion between animals and human. *J Basic Clin Pharm*. 2016;7(2):27–31. doi:10.4103/0976-0105.177703
25. Deng G, Li J, Huang M, et al. Erchen decoction alleviates the progression of NAFLD by inhibiting lipid accumulation and iron overload through caveolin-1 signaling. *J Ethnopharmacol*. 2024;319:117320. doi:10.1016/j.jep.2023.117320
26. Gao Y, Ma K, Zhu Z, et al. Modified Erchen decoction ameliorates cognitive dysfunction in vascular dementia rats via inhibiting JAK2/STAT3 and JNK/BAX signaling pathways. *Phytomedicine*. 2023;114:154797. doi:10.1016/j.phymed.2023.154797
27. Wang Z, Lu J, Liu C, Liang X, Zeng P, Lu F. Erchen decoction alleviates silicosis by attenuating ferroptosis and fibrosis in alveolar macrophages via modulating the P53/HMOX1 pathway. *J Ethnopharmacol*. 2025;352:120227. doi:10.1016/j.jep.2025.120227
28. Chen LP, Cai YM, Li JS. Medication rules of famous veteran traditional Chinese medicine doctor in treatment of chronic bronchitis based on implicit structure model [in Chinese]. *Zhongguo Zhong Yao Za Zhi*. 2017;42(8):1609–1616. doi:10.19540/j.cnki.cjcmm.2017.0052
29. Tai MT, Zhang CF, Fan CW, et al. Intervention effect of Erchen decoction on methionine and choline deficient diet-induced non-alcoholic steatohepatitis in mice [in Chinese]. *Zhongguo Zhong Yao Za Zhi*. 2024;49(5):1310–1317. doi:10.19540/j.cnki.cjcmm.20231013.401
30. Hong M, Sun WH, Lu M, et al. Analysis of the cluster efficacy and prescription characteristics of traditional Chinese medicine intervention for non-small cell lung cancer based on a clustering algorithm. *Technol Health Care*. 2023;31(5):1759–1770. doi:10.3233/thc-220644
31. Meng M, Huo R, Wang Y, et al. Lentinan inhibits oxidative stress and alleviates LPS-induced inflammation and apoptosis of BMECs by activating the Nrf2 signaling pathway. *Int J Biol Macromol*. 2022;222:2375–2391. doi:10.1016/j.ijbiomac.2022.10.024
32. Zhang P, Zhou C, Jing Q, et al. Role of APR3 in cancer: Apoptosis, autophagy, oxidative stress, and cancer therapy. *Apoptosis*. 2023;28(11–12):1520–1533. doi:10.1007/s10495-023-01882-w
33. Xu L, Du X, Zhou Y, et al. Polyaspartic acid-stabilized $CaCO_3$-containing in situ hydrogel for protection and treatment of gastric ulcer. *Mol Pharm*. 2023;20(4):2105–2118. doi:10.1021/acs.molpharmaceut.2c01062
34. Zhang G, Liu M, Chen H, et al. NF-κB signalling pathways in nucleus pulposus cell function and intervertebral disc degeneration. *Cell Prolif*. 2021;54(7):e13057. doi:10.1111/cpr.13057
35. Zheng H, Li H, Du H, et al. Unravelling the mechanisms of Erchen decoction in the treatment of nonalcoholic fatty liver disease (NAFLD): An integrative study combining network pharmacology, molecular docking, molecular dynamics simulation, multi-omics analysis, and experimental validation [published online as ahead of print on July 2, 2025]. *J Ethnopharmacol*. 2025. doi:10.1016/j.jep.2025.120216
36. Ding S, Chen Q, Huang Y, et al. Exploring miRNA-related molecular targets of Erchen decoction against lipid metabolism disorder using a network pharmacologic approach. *Comb Chem High Throughput Screen*. 2022;25(6):986–997. doi:10.2174/1386207324666210302093300

Regulatory T cells and plasmacytoid dendritic cells in drug rash with eosinophilia and systemic symptoms VS maculopapular drug eruption: A serological pilot study

Narachai Julanon[1,B–F], Suteeraporn Chaowattanapanit[1,A–F], Charoen Choonhakarn[1,B,C,E,F], Rachot Wongjirattikarn[1,B,C,E,F], Thapphan Chakrit[2,B,C,E,F], Kanin Salao[2,3,B,C,E,F], Kittisak Sawanyawisuth[1,B,C,E,F]

[1] Division of Dermatology, Department of Medicine, Faculty of Medicine, Khon Kaen University, Thailand
[2] Department of Microbiology, Faculty of Medicine, Khon Kaen University, Thailand
[3] Department of Physiology, Yong Loo Lin School of Medicine, National University of Singapore, Singapore

A – research concept and design; B – collection and/or assembly of data; C – data analysis and interpretation; D – writing the article; E – critical revision of the article; F – final approval of the article

Advances in Clinical and Experimental Medicine, ISSN 1899–5276 (print), ISSN 2451–2680 (online) *Adv Clin Exp Med*. 2026;35(4):717–727

Address for correspondence
Suteeraporn Chaowattanapanit
E-mail: csuteeraporn@yahoo.com

Funding sources
This study was supported by funding from Faculty of Medicine, Khon Kaen University, Thailand (grant No. RR61202).

Conflict of interest
None declared

Acknowledgements
The authors thank the Department of Internal Medicine, Faculty of Medicine, Khon Kaen University, for publication support, and thank Ms. Piyanan Suparattanagool, Clinical Epidemiology Unit, Khon Kaen University, for statistical advice.

Received on October 8, 2024
Reviewed on May 29, 2025
Accepted on June 17, 2025

Published online on February 23, 2026

Cite as
Julanon N, Chaowattanapanit S, Choonhakarn C, et al. Regulatory T cells and plasmacytoid dendritic cells in drug rash with eosinophilia and systemic symptoms VS maculopapular drug eruption: A serological pilot study. *Adv Clin Exp Med*. 2026;35(4):717–727. doi:10.17219/acem/207254

DOI
10.17219/acem/207254

Abstract

Background. Regulatory T (Treg) cells and plasmacytoid dendritic cells (pDCs) are involved in the pathogenesis of drug rash with eosinophilia and systemic symptoms/drug-induced hypersensitivity syndrome (DRESS/DIHS).

Objectives. To compare circulating Treg cells and pDCs at different stages among patients with DRESS/DIHS, patients with maculopapular drug eruption (MPE), and healthy subjects, and to assess circulating Treg cells and pDCs at post-steroid cessation in DRESS/DIHS.

Materials and methods. This was a cross-sectional study that enrolled adult patients diagnosed with DRESS/DIHS and MPE. Blood samples were obtained from the patients at the initial presentation (acute phase), 1 week later (subacute phase), during the 3rd week (resolution phase), and post-steroid cessation for DRESS/DIHS. Healthy subjects' blood samples were also taken. Peripheral blood mononuclear cells were isolated for flow cytometry analysis.

Results. A total of 22 patients participated in this study: patients with DRESS/DIHS (n = 9), patients with MPE (n = 8), and healthy subjects (n = 5). During the acute stage of DRESS/DIHS and MPE, the mean percentage of Treg cells and pDCs significantly decreased compared to healthy subjects. However, Treg cells showed a progressive increase towards the resolution phase in both conditions, while pDCs continued to decrease towards the resolution phase. Following steroid discontinuation in DRESS/DIHS, both Treg cells and pDCs showed a progressive increase in number.

Conclusions. Treg cells and pDCs play a role in DRESS/DIHS and MPE pathogenesis, evidenced by the fluctuation in their percentages at each stage of both conditions. However, increased circulating Treg cells may crucially mitigate inflammation in both conditions.

Key words: regulatory T cells, plasmacytoid dendritic cells, drug-induced hypersensitivity syndrome, drug rash with eosinophilia and systemic symptoms, maculopapular drug eruption

Highlights

- Regulatory T (Treg) cells and plasmacytoid dendritic cell (pDC) levels were significantly reduced during the acute phase of drug rash with eosinophilia and systemic symptoms/drug-induced hypersensitivity syndrome and maculopapular drug eruption compared with healthy controls.
- Regulatory T cells progressively increased during disease resolution, whereas pDCs continued to decline throughout the recovery phase.
- Following steroid withdrawal in drug rash with eosinophilia and systemic symptoms/drug-induced hypersensitivity syndrome, both Treg cell and pDC levels showed a gradual increase.
- Dynamic changes in Treg cell and pDC levels suggest their involvement in immune regulation and inflammatory modulation in drug rash with eosinophilia and systemic symptoms/drug-induced hypersensitivity syndrome and maculopapular drug eruption.

Background

Drug rash with eosinophilia and systemic symptoms/drug-induced hypersensitivity syndrome (DRESS/DIHS) is a severe, delayed-type hypersensitivity reaction. It is characterized by high fever, widespread skin eruptions that are typically morbilliform but may also be pleomorphic, lymphadenopathy, hematologic abnormalities such as atypical lymphocytosis in the early stage and eosinophilia in the later stage, and multiorgan involvement, with liver enzyme elevation being the most common manifestation. Delayed diagnosis can result in significant morbidity and a mortality rate of up to 7%. The diagnosis of DRESS is established using the European RegiSCAR scoring system, which includes 7 clinical features. A score greater than 5 indicates a definite diagnosis of DRESS.[1] The pathogenesis of DRESS is complex and not fully understood. However, several mechanisms have been proposed, including genetic predisposition associated with specific human leukocyte antigen alleles that affect drug metabolism, reactivation of human herpesviruses (HHVs) – particularly HHV-6, cytomegalovirus, and Epstein–Barr virus (EBV) – and dysregulation of the immune response mediated by T cells, all of which are thought to play central roles in the development of DRESS/DIHS.[2]

Regulatory T (Treg) cells and plasmacytoid dendritic cells (pDCs) have been reported to play a role in the pathogenesis of DRESS/DIHS. Treg cells are essential for regulating and suppressing immune responses to self-antigens, promoting peripheral tolerance, preventing autoimmunity, and limiting chronic inflammatory diseases.[3,4] A previous study showed that Treg cells expand during the acute stage of DRESS/DIHS but decrease in both number and function during the resolution phase.[5] These findings suggest a prolonged onset of clinical features, HHV reactivation and the potential development of autoimmunity following recovery from DRESS/DIHS. In contrast, pDCs play a crucial role in antiviral immunity and are also involved in the development of autoimmune and inflammatory diseases.[6] Previous studies demonstrated that the number of circulating pDCs decreases around the time of viral reactivation in DRESS/DIHS compared with other drug eruptions.[7,8] These findings further support the role of viral reactivation in the pathogenesis of DRESS/DIHS.

Objectives

There are limited studies investigating circulating Treg cells and pDCs in DRESS/DIHS at different time points. This study aimed to identify alterations in circulating Treg cells and pDCs at different disease stages in patients with DRESS/DIHS, patients with maculopapular drug eruption (MPE), and healthy subjects, as well as to assess circulating Treg cells and pDCs after steroid cessation in DRESS/DIHS.

Materials and methods

Study design

This was a cross-sectional study conducted from October 2019 to December 2022 at Khon Kaen University's Srinagarind Hospital in Thailand.

Participants

Adult patients aged 18 years or older diagnosed with DRESS/DIHS and/or MPE were recruited. Patients who had received systemic steroids or immunosuppressive drugs before enrollment were excluded. DRESS/DIHS was defined according to the diagnostic criteria established by the European Registry of Severe Cutaneous Adverse Reactions (RegiSCAR) group, including fever >38.5°C, lymphadenopathy, skin rash suggestive of DRESS/DIHS, eosinophilia or atypical lymphocytosis, internal organ involvement, disease duration >15 days, and exclusion of other potential causes.[2] Maculopapular drug eruption, also referred to as exanthematous drug eruption, was

defined as widespread erythematous macules and papules symmetrically distributed over the trunk and extremities, without systemic symptoms or internal organ involvement.

Variables

Demographic data and baseline characteristics, including age, sex, disease onset and duration, RegiSCAR score, and culprit medication, were recorded. Medical comorbidities were also documented and classified as immune abnormalities (such as HIV infection, adult-onset immunodeficiency, and autoimmune diseases) or non-immune abnormalities. Blood samples were obtained at different stages: at the initial presentation (acute phase or visit 1), 1 week later (subacute phase or visit 2), during the 3rd week (resolution phase or visit 3), and after discontinuation of systemic steroids in patients with DRESS/DIHS (visit 4). Blood samples were also collected from 5 healthy subjects as normal controls. Patients with DRESS/DIHS received prednisolone at a dose of 0.5–1 mg/kg/day after the first blood sample was obtained. Patients with MPE were treated with topical corticosteroids and antihistamines. The percentages of Treg cells and pDCs were evaluated by flow cytometry using a BD FACSCanto™ II flow cytometer (BD Biosciences, Franklin Lakes, USA).

Peripheral blood mononuclear cells isolation

A total of 6 mL of venous whole blood was collected from each participant by venipuncture and placed into sodium heparin tubes (cat. No. 367874; BD Biosciences). The whole blood was then diluted with ×1 phosphate-buffered saline (PBS) at a 1:1 ratio. Following dilution, peripheral blood mononuclear cells were isolated using Ficoll–Paque PLUS (density = 1.077 g/mL; cat. No. 71-7167-00 AG; GE Healthcare, Chicago, USA) at a 4:3 ratio and centrifuged at 400 × g for 40 min at 20°C without braking. Subsequently, peripheral blood mononuclear cells (PBMCs) were collected into a new sterile 15 mL centrifuge tube using a sterile plastic dropper. The isolated PBMCs were gently washed twice with 7 mL of 1× PBS and centrifuged for 10 min at 22°C at 500 × g and 260 × g (for platelet removal), respectively. The supernatant was discarded, and the PBMCs were then resuspended in 1 mL of freezing medium consisting of 90% fetal bovine serum (FBS) and 10% dimethyl sulfoxide (DMSO; cat. No. A3672; PanReac AppliChem, Chicago, USA). Cryopreserved cells from all subjects were stored at –80°C until use.

Cell surface markers and intracellular cytokine staining

Isolated PBMCs were gently thawed at 37°C and then stimulated with 100 ng/mL phorbol 12-myristate 13-acetate (PMA; cat. No. P1585; Sigma-Aldrich, Burlington, USA) and 1 µg/mL ionomycin calcium salt (cat. No. I-0634; Sigma-Aldrich). Simultaneously, the cells were incubated with 3 µg/mL brefeldin A (eBioscience, San Diego, USA) at 37°C for 2 h. Subsequently, the cells were washed with R10 medium (RPMI 1640 supplemented with 10% FBS; cat. No. 31800105; Gibco, Waltham, USA) and centrifuged at 400 × g for 10 min. The stimulated PBMCs were then stained with multicolor fluorochrome-conjugated monoclonal antibodies: anti-human CD45 phycoerythrin-cyanine 7 (PE-Cy7; HI30; eBioscience), anti-human CD3 allophycocyanin-eFluor® 780 (APC-eFluor® 780; OKT3; eBioscience), anti-human CD4 eFluor® 450 (RPA-T4; eBioscience), and anti-human CD123 phycoerythrin (PE; 6H6; Abcam, Cambridge, UK). Incubation was carried out for 15 min on ice in the dark. Intracellular staining was performed sequentially after surface staining. Cells were fixed with 4% formaldehyde and permeabilized using fixation and permeabilization buffer (cat. No. 130-090-47; Miltenyi Biotec, Bergisch Gladbach, Germany) for 10 min on ice in the dark. Subsequently, the cells were stained with anti-human FoxP3 peridinin–chlorophyll–cyanine 5.5 (PerCP-Cy5.5; PCH101; eBioscience) for 30 min, followed by washing with staining buffer (×1 PBS containing 2% FBS). Finally, the samples were analyzed using a BD FACSCanto™ II flow cytometer (BD Biosciences). The analysis was performed at the Department of Microbiology, Faculty of Medicine, Khon Kaen University, Thailand.

Gating strategy

Lymphocytes were identified using forward scatter (FSC) and side scatter (SSC). Subsequently, singlet cells were identified based on forward scatter area (FSC-A) and forward scatter height (FSC-H). $CD45^+$ expression was then gated on singlet lymphocytes. Treg cells were identified based on the expression of $CD3^+$ and $CD4^+$, together with intracellular FoxP3. Plasmacytoid dendritic cells were gated as $CD3^-CD123^+$ cells.

Statistical analyses

With respect to baseline characteristics, numerical variables were presented as medians with the 1st and 3rd quartiles (Q1–Q3) and the minimum–maximum range, as the number of subjects in each group was fewer than 10. Comparisons of numerical variables between 2 groups were performed using the Mann–Whitney U test, whereas differences among three groups were assessed using the Kruskal–Wallis test. Categorical variables were reported as numbers (percentages). The Fisher–Freeman–Halton test was used to assess differences in proportions among 2 or 3 groups.

For the percentages of Treg cells and pDCs, a generalized estimating equation (GEE) model with the following parameters was applied: 1) family, Gaussian; 2) link function, identity; and 3) correlation structure, exchangeable.

This model was used to compare the 3 study populations (DRESS/DIHS, MPE and healthy subjects) across 4 visits (visits 1–4). In addition, a subgroup analysis according to immune status was performed for patients with DRESS/DIHS and MPE. The mean (standard deviation (SD)) percentages of Treg cells and pDCs were reported because these variables followed a normal distribution and were analyzed using a GEE model. The regression coefficient, its 95% confidence interval (95% CI), z-value, and p-value for the percentages of Treg cells and pDCs were also reported. Model adequacy was assessed by examining residual plots across the 3 study groups to evaluate the presence of systematic bias, heteroscedasticity or outliers. Statistical analyses were performed using Stata v. 18.0 (StataCorp, College Station, USA). A $p < 0.05$ was considered statistically significant.

Results

Baseline characteristics of the patients and healthy subjects

A total of 22 participants were included in this study: patients with DRESS/DIHS (n = 9), patients with MPE (n = 8) and healthy subjects (n = 5). The baseline characteristics of the participants are presented in Table 1. The DRESS/DIHS group differed significantly from the MPE group in terms of disease onset duration. Among the participants, 4 patients with DRESS/DIHS and 5 patients with MPE had immune abnormalities.

The percentage of Treg cells in DRESS/DIHS, with MPE and healthy subjects at different time points

The mean percentages of Treg cells in patients with DRESS/DIHS, with MPE and healthy subjects at different time points are presented in Table 2.

In the acute stage (visit 1), the mean percentage of Treg cells was significantly lower in DRESS/DIHS compared to healthy subjects ($\beta = -2.10$, 95% CI: −3.44 to −0.75, $z = -3.05$, $p = 0.002$) and also significantly lower in MPE compared to healthy subjects ($\beta = -2.10$, 95% CI: −3.47 to −0.72, $z = -2.99$, $p = 0.003$), as shown in Fig. 1 and Table 3.

In the subacute phase (visit 2), the mean percentage of Treg cells significantly increased in DRESS/DIHS compared to the acute stage ($\beta = 2.16$, 95% CI: 0.97–3.35, $z = 3.56$, $p < 0.001$) and significantly increased in MPE

Table 1. Baseline characteristics of DRESS/DIHS patients, MPE patients, and healthy subjects

Factors		DRESS/DIHS n = 9	MPE n = 8	Control n = 5	p-value
Age [years]	Min Q1 Median Q3 Max	21 30 47 58 69	24 36.5 47.5 60 67	25 26 38 46 58	0.602 (H = 1.02, df = 2)
Male sex, n (%)		5 (55.6)	5 (62.5)	2 (40.0)	0.864
Comorbidities, n (%) HIV AOID UCNTD		4 (44.4) 2 (22.2) 1 (11.1) 1 (11.1)	5 (62.5) 3 (37.5) 2 (25) –	–	0.637
Duration of onset [days]	Min Q1 Median Q3 Max	14 14 21 28 35	5 6 9 11 14	–	<0.001 (z = −3.32)
Causative drugs, n (%) Cotrimoxazole Anti-TB drugs Phenytoin Efavirenz Vancomycin Clarithromycin		9 (100) 4 (44.4) 3 (33.3) 2 (22.2) – – –	8 (100) 2 (25) 2 (25) – 2 (25) 1 (12.5) 1 (12.5)	–	0.328
RegiSCAR score	Min Q1 Median Q3 Max	6 6 6 7 8	–	–	–

AOID – adult-onset immunodeficiency; DRESS/DIHS – drug rash with eosinophilia and systemic symptoms/drug-induced hypersensitivity syndrome; HIV – human immunodeficiency virus; MPE – maculopapular drug eruption; UCNTD – undifferentiated connective tissue disease; RegiSCAR – European Registry of Severe Cutaneous Adverse Reactions; Min – minimal value; Max – maximal value; Q1 – 1st quartile; Q3 – 3rd quartile; H – value of the test statistic of the Kruskal–Wallis test; df – degrees of freedom; z – value of the Mann–Whitney U test.

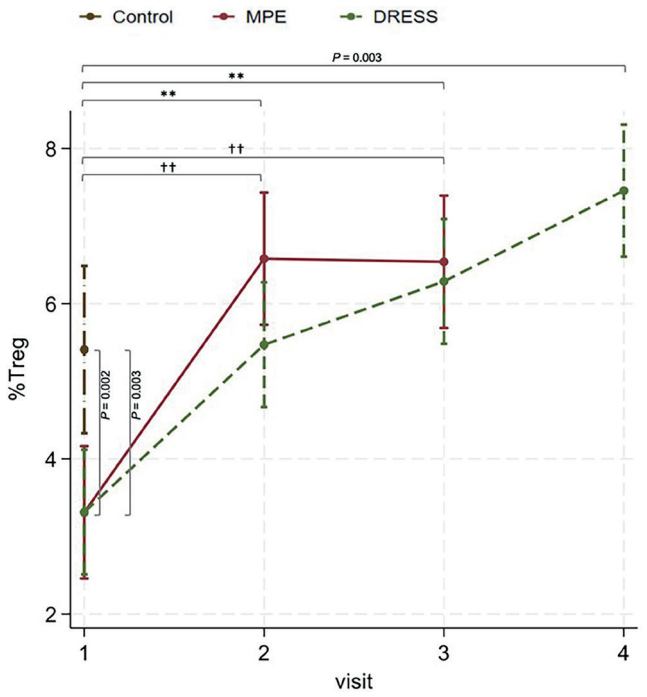

Fig. 1. The percentage of FoxP3+ regulatory T cells (Treg cells) in healthy subjects (control: n = 5), patients with maculopapular drug eruption (MPE, n = 8), and patients with drug rash with eosinophilia and systemic symptoms/drug-induced hypersensitivity syndrome (DRESS/DIHS, n = 9) at different time points: visit 1 – acute phase, visit 2 – subacute phase, visit 3 – resolution phase, and visit 4 – systemic steroids cessation. A significantly low percentage of Treg cells was observed in the acute stage of DRESS/DIHS and MPE. However, the percentage of Treg increased significantly in the subacute to the resolution phase of DRESS/DIHS and MPE when compared to the acute stage. Post-systemic steroid cessation in DRESS/DIHS, the percentage of Treg cells continued rising and was significantly higher than in the control group. No significant differences were detected between the DRESS/DIHS and MPE groups. The data were analyzed as the mean of percentages. All comparisons were computed using a generalized estimating equation (GEE) with multiple comparisons

** $p < 0.001$ between the DRESS/DIHS group; †† $p < 0.001$ between the MPE group, mean difference between the MPE vs healthy subject at visit 1; $p = 0.003$, mean difference between the DRESS/DIHS group vs healthy subjects at visit 1; $p = 0.002$, mean difference between the DRESS/DIHS group at visit 4 vs healthy subjects; $p = 0.003$.

compared to the acute stage (β = 3.27, 95% CI: 2.01–4.53, z = 5.09, p < 0.001).

In the resolution phase (visit 3), the mean percentage of Treg cells showed a tendency to increase in the resolution phase compared to the subacute phase in DRESS/DIHS (β = 0.82, 95% CI: −0.37 to 2.00, z = 1.35, p = 0.178). No significant difference between the subacute and the resolution phases in MPE was observed (β = −0.04, 95% CI: −1.30 to 1.22; z = −0.06, p = 0.949).

In the post-steroid cessation period in DRESS/DIHS (visit 4), the mean percentage of Treg cells showed a further increase compared to the resolution phase (β = 1.17, 95% CI: −0.05 to 2.39, z = 1.88, p = 0.060). The mean percentage of Treg cells was significantly higher after steroid discontinuation compared with healthy controls (β = 2.05, 95% CI: 0.67 to 3.42, z = 2.92, p = 0.003). No significant differences

Table 2. The percentage of FoxP3+ regulatory T cells (Treg cells) and the percentage of CD123+ plasmacytoid dendritic cells (pDCs) in healthy subjects, patients with maculopapular drug eruption (MPE), and patients with drug rash with eosinophilia and systemic symptoms/drug-induced hypersensitivity syndrome (DRESS/DIHS) at the different time points

Factors	Control n = 5	DRESS/DIHS n = 9	MPE n = 8
%Treg cells	5.41 (1.55)	–	–
Visit 1 acute phase		3.31 (0.92)	3.31 (1.09)
Visit 2 subacute phase		5.47 (1.70)	6.58 (0.66)
Visit 3 resolution phase		6.29 (1.23)	6.54 (1.09)
Visit 4 systemic steroid cessation		7.47 (1.91)	–
%pDCs	1.04 (0.21)	–	–
Visit 1 acute phase		0.37 (0.12)	0.48 (0.09)
Visit 2 subacute phase		0.33 (0.09)	0.33 (0.11)
Visit 3 resolution phase		0.35 (0.13)	0.39 (0.12)
Visit 4 systemic steroid cessation		0.84 (0.27)	–

Data are presented as mean (standard deviation (SD)) because they were normally distributed and used in the generalized estimating equation (GEE) model with multiple comparisons.

Table 3. Comparisons of the percentage of FoxP3+ regulatory T cells (Treg cells) in healthy subjects, patients with drug rash with eosinophilia and systemic symptoms/drug-induced hypersensitivity syndrome (DRESS/DIHS), and patients with maculopapular drug eruption (MPE) at the different time points: visit 1 – acute phase, visit 2 – subacute phase, visit 3 – resolution phase, and visit 4 – systemic steroid cessation

Comparisons	Coefficient	95% CI	z-value	p-value
DRESS/DIHS				
Visit 1: vs healthy	−2.10	−3.44, −0.75	−3.05	0.002
Visit 2–visit 1	2.16	0.97, 3.35	3.56	<0.001
Visit 3–visit 1	2.97	1.79, 4.16	4.91	<0.001
Visit 3–visit 2	0.82	−0.37, 2.00	1.35	0.178
Visit 4–visit 1	4.14	2.92, 5.36	6.66	<0.001
Visit 4–visit 2	1.99	0.77, 3.21	3.19	0.001
Visit 4–visit 3	1.17	−0.05, 2.39	1.88	0.060
Visit 4: vs healthy	2.05	0.67, 3.42	2.92	0.003
Visit 1: DRESS/DIHS-MPE	0.003	−1.17, 1.18	0.01	0.996
Visit 2: DRESS/DIHS-MPE	−1.11	−2.28, 0.06	−1.85	0.064
Visit 3: DRESS/DIHS-MPE	−0.25	−1.42, 0.92	−0.42	0.673
MPE				
Visit 1: vs healthy	−2.10	−3.47, −0.72	−2.99	0.003
Visit 2–visit 1	3.27	2.01, 4.53	5.09	<0.001
Visit 3–visit 1	3.23	1.97, 4.49	5.03	<0.001
Visit 3–visit 2	−0.04	−1.30, 1.22	−0.06	0.949

95% CI – 95% confidence interval. All comparisons were performed using a generalized estimating equation (GEE) with multiple comparisons.

were detected between the DRESS/DIHS and MPE groups during the acute phase (β = 0.003, 95% CI: −1.17 to 1.18, z = 0.01, p = 0.996), subacute phase (β = −1.11, 95% CI: −2.28 to 0.06, z = −1.85, p = 0.064), or resolution phase (β = −0.25, 95% CI: −1.42 to 0.92, z = −0.42, p = 0.673).

The percentage of Treg cells in DRESS/DIHS and MPE with and without immune abnormalities

In patients with DRESS/DIHS, a consistent increase in the percentage of Treg cells was observed from visit 1 to visit 4 in both patients with and without immune abnormalities, as shown in Fig. 2 and Table 4. No significant differences were observed between patients with and without immune abnormalities at any visit (visit 1: β = −0.98, 95% CI: −2.48 to 0.52, z = −1.28, p = 0.200; visit 2: β = 0.84, 95% CI: −0.66 to 2.34, z = 1.10, p = 0.271; visit 3: β = 0.59, 95% CI: −0.91 to 2.08, z = 0.77, p = 0.444; visit 4: β = −0.53, 95% CI: −2.02 to 0.97, z = −0.69, p = 0.491), as shown in Table 5.

In patients with MPE, the percentage of Treg cells increased from the acute to the subacute phase in both patients with and without immune abnormalities (Fig. 3, Table 4). During the resolution phase, the percentage of Treg cells increased in patients with immune abnormalities but decreased in those without immune abnormalities; however, this difference did not reach statistical significance (β = 1.34, 95% CI: −0.29 to 2.97, z = 1.61, p = 0.106; Fig. 3, Table 5).

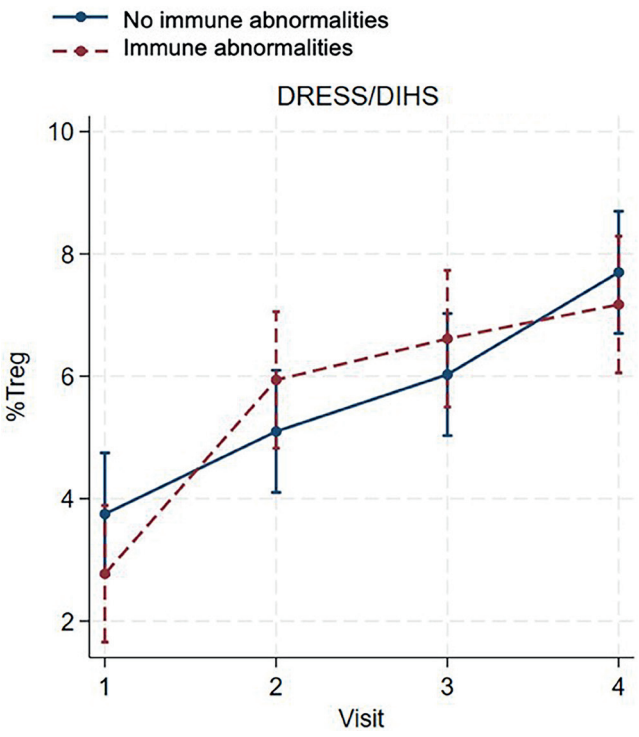

Fig. 2. The percentage of FoxP3+ regulatory T cells (Treg cells) in drug rash with eosinophilia and systemic symptoms/drug-induced hypersensitivity syndrome (DRESS/DIHS) patients without immune abnormalities (n = 5) and with immune abnormalities (n = 4) at different time points: visit 1 – acute phase, visit 2 – subacute phase, visit 3 – resolution phase, and visit 4 – systemic steroids cessation. A trend of continuously increasing percentage of Treg cells was observed in both groups during each visit. No significant differences were observed between the 2 groups in each visit

The percentage of pDCs in DRESS/DIHS, MPE, and healthy subjects at different time points

The mean percentages of pDCs in patients with DRESS/DIHS, with MPE, and in healthy subjects at different time points are shown in Table 2.

In the acute stage, the mean percentage of pDCs was significantly lower in patients with DRESS/DIHS than in healthy subjects (β = −0.67, 95% CI: −0.83 to −0.52, z = −8.64, p < 0.001) and was also significantly lower in patients with MPE than in healthy subjects (β = −0.66, 95% CI: −0.72 to −0.41, z = −7.11, p < 0.001), as shown in Fig. 4 and Table 6.

In the subacute phase, the mean percentage of pDCs was significantly lower than in the acute stage in patients with MPE (β = −0.15, 95% CI: −0.28 to −0.01, z = −2.11,

Table 4. The percentage of FoxP3+ regulatory T cells (Treg cells) and the percentage of CD123+ plasmacytoid dendritic cells (pDCs) in patients with drug rash with eosinophilia and systemic symptoms/drug-induced hypersensitivity syndrome (DRESS/DIHS) and patients with maculopapular drug eruption (MPE) at different time points and with different immune status

Factors	DRESS/DIHS n = 9		MPE n = 8	
	without immune abnormalities (n = 5)	immune abnormalities (n = 4)	without immune abnormalities (n = 3)	immune abnormalities (n = 5)
%Treg cells				
Visit 1 acute phase	3.75 (0.98)	2.77 (0.53)	2.86 (1.27)	3.58 (1.01)
Visit 2 subacute phase	5.10 (1.90)	5.94 (1.56)	6.68 (0.63)	6.52 (0.74)
Visit 3 resolution phase	6.03 (1.42)	6.61 (1.03)	5.70 (1.04)	7.04 (0.84)
Visit 4 systemic steroid cessation	7.70 (1.56)	7.17 (2.24)	–	–
%pDCs				
Visit 1 acute phase	0.33 (0.12)	0.42 (0.13)	0.53 (0.05)	0.44 (0.10)
Visit 2 subacute phase	0.37 (0.10)	0.28 (0.05)	0.29 (0.13)	0.36 (0.10)
Visit 3 resolution phase	0.39 (0.10)	0.30 (0.15)	0.26 (0.08)	0.45 (0.06)
Visit 4 systemic steroid cessation	0.79 (0.31)	0.91 (0.18)	–	–

Data are presented as mean (standard deviation (SD)) because they were normally distributed and used in the generalized estimating equation (GEE) model with multiple comparisons.

Table 5. Comparisons of the percentage of FoxP3+ regulatory T cells (Treg cells) in patient with drug rash with eosinophilia and systemic symptoms/drug-induced hypersensitivity syndrome (DRESS/DIHS) with and without immune abnormalities at different time points and patients with maculopapular drug eruption (MPE) with and without immune abnormalities at different time points: visit 1 – acute phase, visit 2 – subacute phase, visit 3 – resolution phase, and visit 4 – systemic steroid cessation

Comparisons	Coefficient	95% CI	z-value	p-value
DRESS/DIHS with IA vs without IA				
Visit 1	−0.98	−2.48, 0.52	−1.28	0.200
Visit 2	0.84	−0.66, 2.34	1.10	0.271
Visit 3	0.59	−0.91, 2.08	0.77	0.444
Visit 4	−0.53	−2.02, 0.97	−0.69	0.491
MPE with IA vs without IA				
Visit 1	0.72	−0.91, 2.35	0.87	0.384
Visit 2	−0.15	−1.78, 1.48	−0.18	0.853
Visit 3	1.34	−0.29, 2.97	1.61	0.106

IA – immune abnormalities; 95% CI – 95% confidence interval. All comparisons were performed using a generalized estimating equation (GEE) with multiple comparisons.

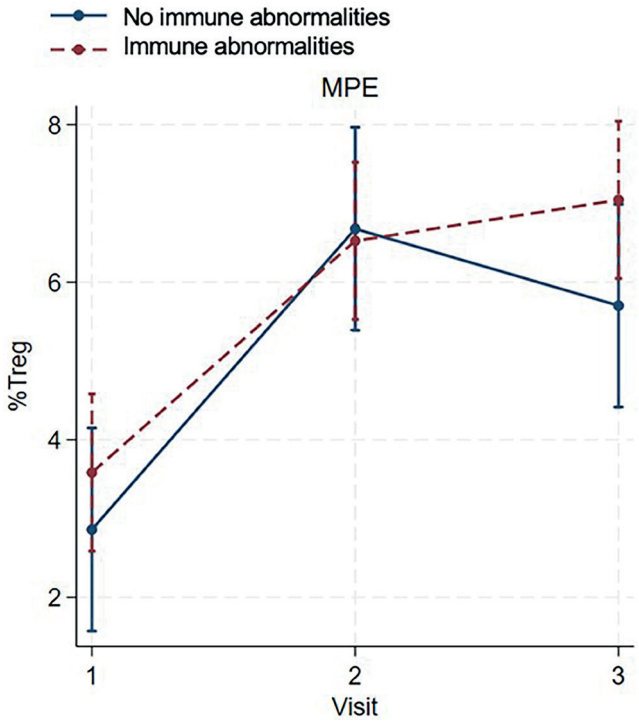

Fig. 3. The percentage of FoxP3+ regulatory T cells (Treg cells) in maculopapular drug eruption patients without immune abnormalities (n = 3) and with immune abnormalities (n = 5) at different time points: visit 1 – acute phase, visit 2 – subacute phase, and visit 3 – resolution phase. An increasing percentage of Treg cells was observed in both groups during the subacute phase. In the resolution phase, the percentage of Treg cells increased in patients with immune abnormalities, while it decreased in patients without immune abnormalities, but there was no statistical significance

p = 0.035), as shown in Table 6. However, no significant difference was detected in the DRESS/DIHS group (β = −0.04, 95% CI: −0.16 to 0.09, z = −0.58, p = 0.559).

Table 6. Comparisons of the percentage of CD123+ plasmacytoid dendritic cells (pDCs) in healthy subjects, patients with drug rash with eosinophilia and systemic symptoms/drug-induced hypersensitivity syndrome (DRESS/DIHS), and patients with maculopapular drug eruption (MPE) at different time points: visit 1 – acute phase, visit 2 – subacute phase, visit 3 – resolution phase, and visit 4 – systemic steroid cessation

Comparisons	Coefficient	95% CI	z-value	p-value
DRESS/DIHS				
Visit 1: vs healthy	−0.67	−0.83, −0.52	−8.64	<0.001
Visit 2–visit 1	−0.04	−0.16, 0.09	−0.58	0.559
Visit 3–visit 1	−0.02	−0.14, 0.11	−0.25	0.804
Visit 3–visit 2	0.02	−0.11, 0.15	0.33	0.738
Visit 4–visit 1	0.47	0.34, 0.60	7.05	<0.001
Visit 4–visit 2	0.51	0.38, 0.64	7.62	<0.001
Visit 4–visit 3	0.49	0.36, 0.62	7.30	<0.001
Visit 4: vs healthy	−0.20	−0.36, −0.04	−2.52	0.012
Visit 1: DRESS/DIHS-MPE	−0.11	−0.24, 0.03	−1.58	0.115
Visit 2: DRESS/DIHS-MPE	0.0003	−0.13, 0.133	0.00	0.996
Visit 3: DRESS/DIHS-MPE	−0.03	−0.16, 0.11	−0.39	0.696
MPE				
Visit 1: vs healthy	−0.66	−0.72, −0.41	−7.11	<0.001
Visit 2–visit 1	−0.15	−0.28, −0.01	−2.11	0.035
Visit 3–visit 1	−0.10	−0.24, 0.04	−1.40	0.160
Visit 3–visit 2	0.05	−0.09, 0.18	0.71	0.480

95% CI – 95% confidence interval. All comparisons were performed using a generalized estimating equation (GEE) with multiple comparisons.

In the resolution phase, the mean percentage of pDCs showed a tendency to increase compared with the subacute phase in both DRESS/DIHS and MPE (β = 0.02, 95% CI: −0.11 to 0.15, z = 0.33, p = 0.738 and β = 0.05, 95% CI: −0.09 to 0.18, z = 0.71, p = 0.480, respectively; Table 6).

In the post-steroid cessation period in DRESS/DIHS, the mean percentage of pDCs was significantly higher after discontinuation of systemic steroids compared with the resolution phase (β = 0.49, 95% CI: 0.36 to 0.62, z = 7.30, p < 0.001). However, the mean percentage of pDCs remained significantly lower after discontinuation of systemic steroids compared with healthy controls (β = −0.20, 95% CI: −0.36 to −0.04, z = −2.52, p = 0.012). No significant differences in the percentages of pDCs between the DRESS/DIHS and MPE groups were detected in the acute (β = −0.11, 95% CI: −0.24 to 0.03, z = −1.58, p = 0.115), subacute (β = −0.0003, 95% CI: −0.13 to 0.13, z = 0.00, p = 0.996), or resolution phases (β = −0.03, 95% CI: −0.16 to 0.11, z = −0.39, p = 0.696).

The percentage of pDCs in DRESS/DIHS and MPE with and without immune abnormalities

In patients with DRESS/DIHS, the percentage of pDCs decreased in those with immune abnormalities during the subacute to resolution phase, while the percentage

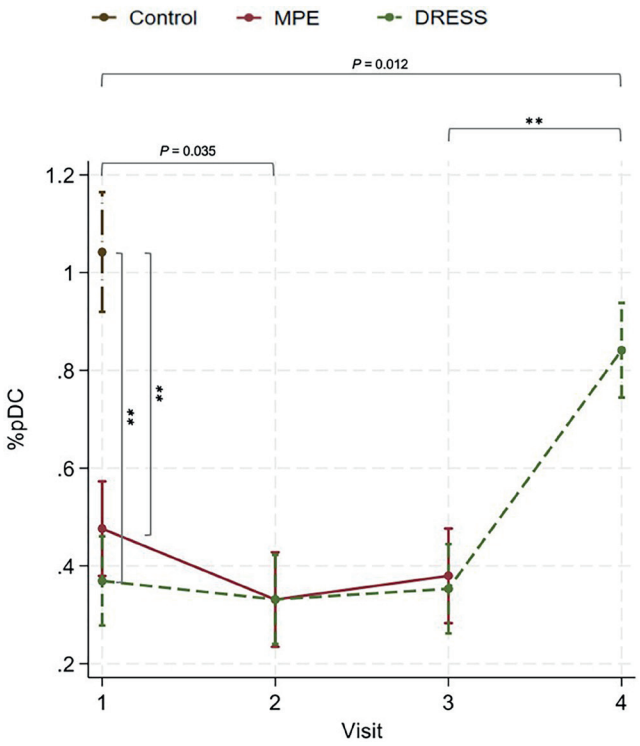

Fig. 4. The percentage of CD123+ plasmacytoid dendritic cells (pDCs) in healthy subjects (control: n = 5), patients with maculopapular drug eruption (MPE, n = 8), and patients with drug rash with eosinophilia and systemic symptoms/drug-induced hypersensitivity syndrome (DRESS/DIHS, n = 9) at different time points: visit 1 – acute phase, visit 2 – subacute phase, visit 3 – resolution phase, and visit 4 – systemic steroids cessation. The percentage of pDCs significantly decreased in the acute stage of both DRESS/DIHS and MPE compared to the control group. Moreover, the percentage of pDCs was significantly lower in the subacute phase of MPE compared to the acute stage, while no significant difference was found in DRESS/DIHS. No significant differences were observed during the subacute to resolution phases of both DRESS/DIHS and MPE. Although the percentage of pDCs increased significantly after systemic steroid cessation in DRESS/DIHS, it was still significantly lower than in the control group. No significant differences were detected between the DRESS/DIHS and MPE groups. The data were analyzed as the mean of percentages; all comparisons were calculated with a generalized estimating equation (GEE) with multiple comparisons

**p < 0.001, mean difference between acute and subacute phase in patients with MPE (p = 0.035), mean difference after discontinuing systemic steroid and healthy controls (p = 0.012).

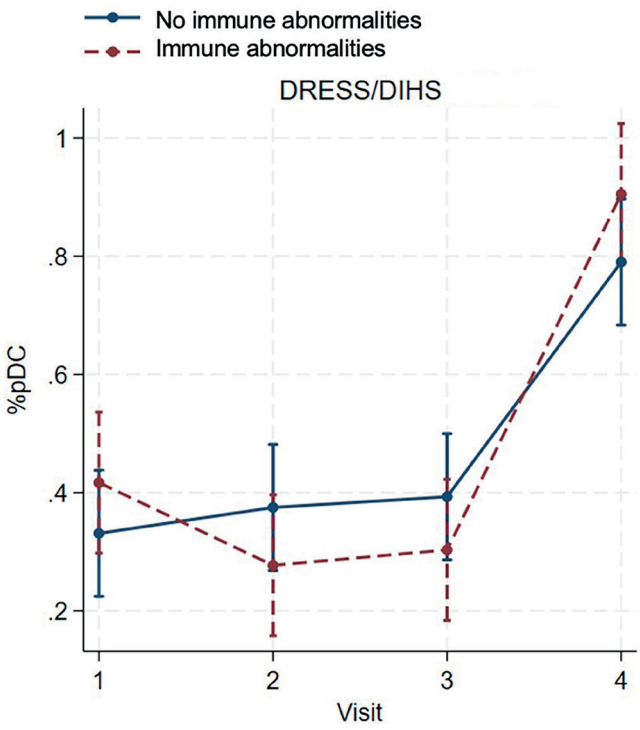

Fig. 5. The percentage of CD123+ plasmacytoid dendritic cells (pDCs) in drug rash with eosinophilia and systemic symptoms/drug-induced hypersensitivity syndrome (DRESS/DIHS) patients without immune abnormalities (n = 5) and with immune abnormalities (n = 4) at different time points: visit 1 – acute phase, visit 2 – subacute phase, visit 3 – resolution phase, and visit 4 – systemic steroids cessation. A decreasing percentage of pDCs was observed in patients with immune abnormalities during the subacute to resolution phase, while the percentage of pDCs tended to increase in patients without immune abnormalities. The percentage of pDCs increased significantly after systemic steroid cessation in both groups. No significant differences were detected between both groups

of pDCs tended to increase in patients without immune abnormalities. The percentage of pDCs increased significantly after systemic steroids cessation in both groups compared to the resolution phase (β = 0.60, 95% CI: 0.44 to 0.76, z = 7.34, p < 0.001 for immune abnormalities; β = 0.40, 95% CI: 0.25 to 0.54, z = 5.41, p < 0.001 for without immune abnormalities; Fig. 5, Table 4). No significant differences were detected between the 2 groups at any visit (visit 1: β = 0.09, 95% CI: −0.07 to 0.25, z = 1.05, p = 0.293; visit 2: β = −0.10, 95% CI: −0.26 to 0.06, z = −1.20, p = 0.231; visit 3: β = −0.09, 95% CI: −0.25 to 0.07, z = −1.10, p = 0.271; visit 4: β = 0.11, 95% CI: −0.05 to 0.27, z = 1.41, p = 0.160), as shown in Table 7.

In patients with MPE, the percentage of pDCs decreased in both groups during the subacute phase. During

Table 7. Comparisons of the percentage of CD123+ plasmacytoid dendritic cells (pDCs) in patients with drug rash with eosinophilia and systemic symptoms/drug-induced hypersensitivity syndrome (DRESS/DIHS) with and without immune abnormalities at different time points and patients with maculopapular drug eruption (MPE) with and without immune abnormalities at the different time points: visit 1 – acute phase, visit 2 – subacute phase, visit 3 – resolution phase, and visit 4 – systemic steroid cessation

Comparisons	Coefficient	95% CI	z-value	p-value
DRESS/DIHS with IA vs without IA				
Visit 1	0.09	−0.07, 0.25	1.05	0.293
Visit 2	−0.10	−0.26, 0.06	−1.20	0.231
Visit 3	−0.09	−0.25, 0.07	−1.10	0.271
Visit 4	0.11	−0.05, 0.27	1.41	0.160
MPE with IA vs without IA				
Visit 1	−0.09	−0.07, 0.25	1.05	0.293
Visit 2	0.07	−0.10, 0.25	0.81	0.416
Visit 3	0.19	0.05, 0.37	2.19	0.029
Visit 4	–	–	–	–

IA – immune abnormalities; 95% CI – 95% confidence interval. All comparisons were performed using a generalized estimating equation (GEE) with multiple comparisons.

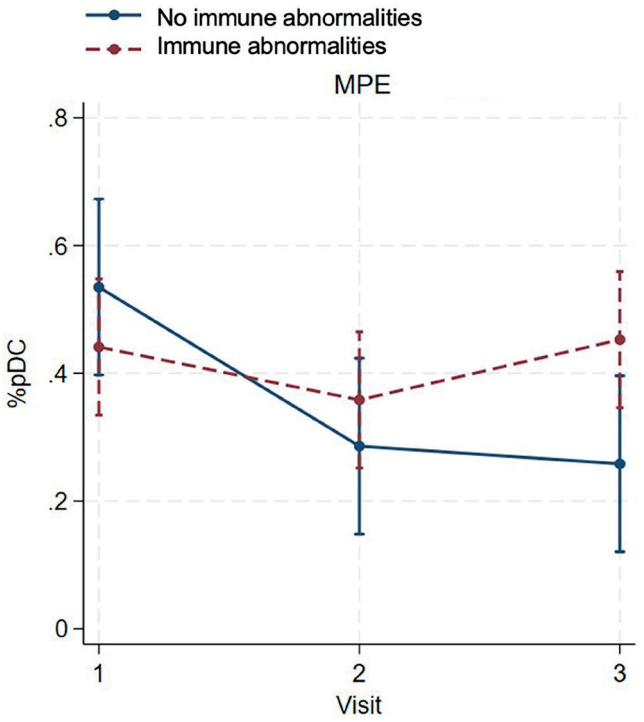

Fig. 6. The percentage of CD123+ plasmacytoid dendritic cells (pDCs) in maculopapular drug eruption patients without immune abnormalities (n = 3) and with immune abnormalities (n = 5) at different time points: visit 1 – acute phase, visit 2 – subacute phase, and visit 3 resolution phase. A decreasing percentage of pDCs was observed in both groups during the subacute phase. In the resolution phase, the percentage of pDCs increased in patients with immune abnormalities, while it decreased in patients without immune abnormalities. This change was significant in the resolution phase

the resolution phase, the percentage of pDCs increased in patients with immune abnormalities but decreased in those without immune abnormalities. At the final visit, the percentage of pDCs was significantly higher in patients with immune abnormalities than in patients without immune abnormalities (β = 0.19, 95% CI: 0.05 to 0.37, z = 2.19, p = 0.029; Fig. 6, Table 7).

To assess model adequacy, residuals for Treg cells and pDCs from the GEE model were plotted against the control, MPE and DRESS/DIHS groups (Supplementary Fig. 1–4). Across all 3 groups, the residuals were approximately centered around 0, with no evidence of systematic bias. The spread of residuals was relatively consistent across groups, although a few outliers were observed.

Discussion

The pathogenesis of DRESS/DIHS remains complex and incompletely understood. Dysregulation of the immune response, particularly T cell-mediated immunity, plays a crucial role in the onset and progression of the disease. This study demonstrated a significant reduction in the mean percentages of Treg cells and pDCs during the acute stage of both DRESS/DIHS and MPE compared with healthy subjects. However, Treg cells showed a progressive increase toward the resolution phase in both conditions, whereas pDCs continued to decrease toward the resolution phase. After discontinuation of systemic steroids in DRESS/DIHS, both Treg cells and pDCs demonstrated a progressive increase. Nevertheless, Treg cell levels were significantly higher than those in the control group, while pDC levels remained significantly lower than those in the control group. No significant differences were observed in Treg cells or pDCs between patients with and without immune abnormalities in both DRESS/DIHS and MPE, except for pDCs during the resolution phase in MPE. These findings enhance our understanding of the immunological alterations associated with DRESS/DIHS, highlighting the dynamic changes in Treg cells and pDCs across different stages of the disease and its treatment.

Treg cells play a crucial role in maintaining immunological tolerance to both self and foreign antigens, preventing autoimmunity and controlling inflammation.[3,4] In a previous study, significantly increased frequencies of Treg cells were observed during the acute stage of DRESS/DIHS compared with healthy controls and the resolution phase; however, this pattern was not observed in toxic epidermal necrolysis (TEN) or MPE.[5] In contrast, our study revealed a significant reduction in the number of Treg cells during the acute stage of both DRESS/DIHS and MPE compared with healthy subjects and the resolution phase. Moreover, no significant differences in Treg cell numbers were observed between patients with DRESS/DIHS or MPE who had immune abnormalities and those without. This discrepancy may be attributable to differences in the ethnic backgrounds of the study populations, which could influence immune response development. During acute inflammation, various soluble mediators, such as cytokines, acute-phase proteins, and chemokines, are released, promoting the migration of inflammatory cells to the site of inflammation.[9] Previous studies have shown that Treg cells are significantly more abundant in the skin lesions of patients with DRESS/DIHS compared with those with TEN, graft-versus-host disease, and MPE.[5,10] Another recent study demonstrated that Treg cells become highly migratory during the first 3 days of skin inflammation, leading to increased Treg abundance in the dermis. Subsequently, Treg levels return to baseline by day 6.[11] This migratory behavior may account for the reduced number of circulating Treg cells observed during the acute phase of DRESS/DIHS and MPE, as these cells are recruited to suppress cutaneous inflammation. Our study demonstrated a progressive increase in circulating Treg cells during the subacute phase (approx. 1 week after the acute stage) in both DRESS/DIHS and MPE, which aligns with the reported timeframe of normalized Treg migratory behavior. Furthermore, circulating Treg cell levels continued to rise during the resolution phase and following discontinuation of systemic corticosteroids in patients with DRESS/DIHS. Glucocorticoids exert complex effects

on T cells, both promoting and suppressing T-cell-mediated immunity depending on the immunological context.[12] Previous reports have shown that glucocorticoids can induce the expansion of Treg cells in autoimmune conditions, including systemic lupus erythematosus, immune thrombocytopenic purpura, and asthma, as well as in healthy individuals receiving long-term dexamethasone treatment.[13] This suggests that the expansion of Treg cells in the post-acute stage of DRESS/DIHS may result from the resolution of inflammation, glucocorticoid therapy, or a combination of both. The expansion of Treg cells likely plays a pivotal role in limiting disease progression and severity, while also preventing the subsequent development of autoimmunity.

Plasmacytoid dendritic cells represent a distinct subset of dendritic cells that specialize in the production and secretion of large amounts of type I interferons (IFNs). They play a crucial role in antiviral immunity and also contribute to the development of autoimmune and inflammatory diseases. The association between DRESS/DIHS and HHV-6 reactivation suggests the potential involvement of pDCs in the pathogenesis of this condition. A previous study reported a significant decrease in circulating pDCs around 3–4 weeks after the onset of DRESS/DIHS, with frequencies lower than those in patients with MPE and healthy subjects.[8] Another study found decreased frequencies of circulating pDCs during the initial 1–2 weeks of disease onset in DRESS/DIHS compared to MPE patients.[7] Our results were consistent with these findings, demonstrating a significant reduction in the mean percentage of pDCs from the acute stage through the resolution phase (3 weeks after the initial presentation) in patients with DRESS/DIHS compared with healthy controls. This reduction in pDCs during the acute stage may be attributable to their migration and infiltration into skin lesions, a phenomenon observed in inflammatory skin diseases such as cutaneous lupus erythematosus and psoriasis.[14] Additionally, a previous study reported higher pDC detection in the dermis of patients with DRESS/DIHS compared with those with MPE and healthy subjects.[8] Unlike Treg cells, our study did not identify significant differences in the percentage of pDCs between DRESS/DIHS and MPE from the acute through the resolution phases, except after discontinuation of systemic steroids in DRESS/DIHS. Notably, glucocorticoids have been shown to significantly reduce IFN-α production and decrease the number of circulating pDCs.[15,16] These effects are reversible and typically return to baseline within days after steroid cessation.[15,16] During inflammatory periods, the reduction in circulating pDCs likely serves to limit inflammation and promote clinical immunosuppression. This dynamic interplay underscores the complexity of the immunological mechanisms involved in DRESS/DIHS and highlights the role of pDCs in modulating the immune response.

Notably, our study did not identify significant differences in the percentages of Treg cells and pDCs between DRESS/DIHS and MPE from the acute to the resolution phase, which contrasts with findings from previous studies.[5,8] This discrepancy may be attributable to the small sample size of our study or to the lack of assessment of HHV-6 reactivation in patients with DRESS/DIHS. Further investigations incorporating larger cohorts and systematic evaluation of HHV-6 reactivation are warranted to achieve a more comprehensive understanding of the immunological differences between DRESS/DIHS and MPE.

Limitations of the study

This study had some limitations. First, the number of participants in the study was relatively small, as this was a pilot study, and sample size calculation was not performed. Second, the functions and subsets of circulating Treg cells and pDCs were not examined. Third, skin biopsies to evaluate the numbers and functions of Treg cells and pDCs were not conducted. Lastly, reactivation of HHV-6, cytomegalovirus, and EBV was not evaluated in this study. However, this study successfully monitored dynamic changes in the numbers of Treg cells and pDCs throughout the course of DRESS/DIHS and MPE. Further studies assessing HHV reactivation and incorporating genetic testing may enhance the understanding of disease pathogenesis.

Conclusions

This study demonstrated the dynamic interplay between Treg cells and pDCs in the pathogenesis of DRESS/DIHS and MPE. The acute stage of both conditions exhibited a significant decrease in Treg cells and pDCs, suggesting their potential involvement in immune dysregulation during disease onset. However, Treg cells showed a significant increase in the resolution phase of both DRESS/DIHS and MPE, while pDCs continued to decrease until the resolution phase in both conditions. This suggests that Treg cells are likely to play a crucial role in preventing further inflammation in both DRESS/DIHS and MPE.

Supplementary data

The supplementary materials are available at https://doi.org/10.5281/zenodo.15682125. The package contains the following files:

Supplementary Fig. 1. Residuals of Treg cells from the GEE model across the 3 groups at each visit.

Supplementary Fig. 2. Residuals of Treg cells from the GEE model at each visit, comparing patients with and without immune abnormalities across MPE and DRESS/DISH groups.

Supplementary Fig. 3. Residuals of pDCs from the GEE model across the 3 groups at each visit.

Supplementary Fig. 4. Residuals of pDCs from the GEE model at each visit, comparing patients with and without immune abnormalities across MPE and DRESS/DISH groups.

Data Availability Statement

The datasets supporting the findings of the current study are openly available in Zenodo at https://doi.org/10.5281/zenodo.14210150.

Consent for publication

Not applicable.

Use of AI and AI-assisted technologies

Not applicable.

ORCID iDs

Narachai Julanon https://orcid.org/ 0000-0002-4374-1170
Suteeraporn Chaowattanapanit https://orcid.org/0000-0002-8954-7672
Charoen Choonhakarn https://orcid.org/0000-0002-3417-6210
Rachot Wongjirattikarn https://orcid.org/0000-0002-5172-5250
Thapphan Chakrit https://orcid.org/0000-0002-1873-0744
Kanin Salao https://orcid.org/0000-0003-4731-9556
Kittisak Sawanyawisuth https://orcid.org/0000-0003-3570-8474

References

1. Kroshinsky D, Cardones ARG, Blumenthal KG. Drug reaction with eosinophilia and systemic symptoms. *N Engl J Med*. 2024;391(23):2242–2254. doi:10.1056/NEJMra2204547
2. Cho YT, Yang CW, Chu CY. Drug reaction with eosinophilia and systemic symptoms (DRESS): An interplay among drugs, viruses, and immune system. *Int J Mol Sci*. 2017;18(6):1243. doi:10.3390/ijms18061243
3. Vignali DAA, Collison LW, Workman CJ. How regulatory T cells work. *Nat Rev Immunol*. 2008;8(7):523–532. doi:10.1038/nri2343
4. Grover P, Goel PN, Greene MI. Regulatory T cells: Regulation of identity and function. *Front Immunol*. 2021;12:750542. doi:10.3389/fimmu.2021.750542
5. Takahashi R, Kano Y, Yamazaki Y, Kimishima M, Mizukawa Y, Shiohara T. Defective regulatory T cells in patients with severe drug eruptions: Timing of the dysfunction is associated with the pathological phenotype and outcome. *J Immunol*. 2009;182(12):8071–8079. doi:10.4049/jimmunol.0804002
6. Ye Y, Gaugler B, Mohty M, Malard F. Plasmacytoid dendritic cell biology and its role in immune-mediated diseases. *Clin Transl Immunol*. 2020;9(5):e1139. doi:10.1002/cti2.1139
7. Hsu SH, Yang CW, Hsieh YC, et al. Plasmacytoid dendritic cells diminution in peripheral blood is prevalent in drug reaction with eosinophilia and systemic symptoms and may precede human herpesvirus 6 reactivation. *Dermatol Sin*. 2021;39(4):175–181. doi:10.4103/ds.ds_37_21
8. Sugita K, Tohyama M, Watanabe H, et al. Fluctuation of blood and skin plasmacytoid dendritic cells in drug-induced hypersensitivity syndrome. *J Allergy Clin Immunol*. 2010;126(2):408–410. doi:10.1016/j.jaci.2010.06.004
9. Hannoodee S, Nasuruddin DN. Acute inflammatory response. In: *StatPearls*. Treasure Island, USA: StatPearls Publishing; 2025:Bookshelf ID: NBK556083. PMID:32310543.
10. Morito H, Ogawa K, Fukumoto T, et al. Increased ratio of FoxP3$^+$ regulatory T cells/CD3$^+$ T cells in skin lesions in drug-induced hypersensitivity syndrome/drug rash with eosinophilia and systemic symptoms. *Clin Exp Dermatol*. 2014;39(3):284–291. doi:10.1111/ced.12246
11. Norman MU, Chow Z, Snelgrove SL, Prakongtham P, Hickey MJ. Dynamic regulation of the molecular mechanisms of regulatory T cell migration in inflamed skin. *Front Immunol*. 2021;12:655499. doi:10.3389/fimmu.2021.655499
12. Taves MD, Ashwell JD. Glucocorticoids in T cell development, differentiation and function. *Nat Rev Immunol*. 2021;21(4):233–243. doi:10.1038/s41577-020-00464-0
13. Cari L, De Rosa F, Nocentini G, Riccardi C. Context-dependent effect of glucocorticoids on the proliferation, differentiation, and apoptosis of regulatory T cells: A review of the empirical evidence and clinical applications. *Int J Mol Sci*. 2019;20(5):1142. doi:10.3390/ijms20051142
14. Dias De Oliveira NF, Santi CG, Maruta CW, Aoki V. Plasmacytoid dendritic cells in dermatology. *An Bras Dermatol*. 2021;96(1):76–81. doi:10.1016/j.abd.2020.08.006
15. Shodell M, Siegal FP. Corticosteroids depress IFN-α-producing plasmacytoid dendritic cells in human blood. *J Allergy Clin Immunol*. 2001;108(3):446–448. doi:10.1067/mai.2001.117928
16. Shodell M, Shah K, Siegal FP. Circulating human plasmacytoid dendritic cells are highly sensitive to corticosteroid administration. *Lupus*. 2003;12(3):222–230. doi:10.1191/0961203303lu362xx

Assessing the stability of drugs of abuse and pharmaceuticals in postmortem blood samples

Guido Pelletti[1,2,A,D], Susan Mohamed[1,A–C], Rafael Boscolo-Berto[3,C,D], Alessia Giampietro[1,B,E], Arianna Giorgetti[1,C,E], Jennifer Pascali[1,C,E], Jacopo Lenzi[4,C,E], Susi Pelotti[1,E,F]

[1] Department of Medical and Surgical Sciences, Unit of Legal Medicine, University of Bologna, Italy
[2] Azienda Unità Sanitaria Locale di Bologna, Italy
[3] Department of Neurosciences, Institute of Human Anatomy, University of Padova, Italy
[4] Department of Hygiene and Public Health, University of Bologna, Italy

A – research concept and design; B – collection and/or assembly of data; C – data analysis and interpretation; D – writing the article; E – critical revision of the article; F – final approval of the article

Advances in Clinical and Experimental Medicine, ISSN 1899–5276 (print), ISSN 2451–2680 (online) *Adv Clin Exp Med*. 2026;35(4):729–734

Address for correspondence
Rafael Boscolo-Berto
E-mail: rafael.boscoloberto@unipd.it

Funding sources
None declared

Conflict of interest
None declared

Received on March 24, 2025
Reviewed on June 29, 2025
Accepted on July 10, 2025

Published online on March 16, 2026

Abstract

Background. Reliable toxicological analysis is crucial for accurate forensic and clinical interpretation; however, pre-analytical factors such as handling and storage can significantly alter drug concentrations in postmortem (PM) samples, potentially leading to misinterpretation. Postmortem degradation, influenced by enzymatic and microbial activity, can change drug levels, making it essential to understand drug stability in biological matrices.

Objectives. This preliminary study investigates the long-term stability of drugs of abuse and psychoactive substances in PM blood samples from drug-related deaths stored at –20°C for 29 months.

Materials and methods. Postmortem blood samples were analyzed using ultra-performance liquid chromatography–tandem mass spectrometry (UPLC–MS/MS) following the routine methodology currently in use in the forensic toxicology laboratory. Stability was assessed by measuring concentration changes between analyses performed shortly after sample collection and reanalyses conducted after 6–29 months. Regression analyses were used to relate percentage variation in concentration to elapsed time.

Results. A strong correlation was found between the percentage reduction in drug concentration and storage time for all tested molecules, including morphine, cocaine, methadone, ketamine, benzodiazepines, antidepressants, antipsychotics, and lidocaine. Regression curve analysis revealed a reduction in concentration beginning within the initial months, with high variability.

Conclusions. The study highlights the significant impact of long-term storage on drug concentrations in PM blood, emphasizing the need for careful consideration of storage intervals when reanalysis of samples is requested for forensic purposes. The findings underscore the importance of understanding degradation patterns for the accurate interpretation of toxicological results in medicolegal investigations.

Key words: forensic toxicology, long-term storage, UPLC-MS/MS, postmortem stability, drug degradation

Cite as
Pelletti G, Mohamed S, Boscolo-Berto R, et al. Assessing stability of drugs of abuse and pharmaceuticals in postmortem blood samples. *Adv Clin Exp Med*. 2026;35(4):729–734. doi:10.17219/acem/208126

DOI
10.17219/acem/208126

Highlights

- This study investigates the stability of drugs in postmortem (PM) blood samples stored at –20°C.
- Ultra-performance liquid chromatography–tandem mass spectrometry (UPLC-MS/MS) was used to analyze 44 PM samples that were stored without preservatives.
- A strong correlation was observed between concentration loss and storage time for most substances.
- The substances analyzed included cocaine, morphine, methadone, ketamine, benzodiazepines, antipsychotics, and antidepressants.
- Stability is crucial for ensuring accurate interpretations in judicial proceedings.

Background

One of the fundamentals of forensic toxicology is the accurate and reproducible analysis of biological samples. Reliable qualitative and quantitative toxicological analysis is essential for sound toxicological judgment in both clinical and forensic toxicology, as unreliable results may lead to misinterpretations, unwarranted conclusions, or incorrect treatment.[1] For this purpose, forensic toxicologists implement rigorous quality control procedures, method validation, and optimization procedures to ensure analytical quality and achieve the highest degree of accuracy.

However, even the most accurate and precise methods reflect drug detection and quantification only at the time of analysis.[2,3] This issue is particularly important when sample re-testing is required for forensic purposes in judicial proceedings. In fact, the majority of "laboratory errors" have been found to originate from the pre-analytical phase rather than from problems related to the analytical process; handling and storage conditions can significantly alter concentrations, especially in samples collected postmortem (PM).[4]

The degradation of compounds that occurs in PM samples can be caused by several factors, including residual enzymatic or microbial activity or spontaneous hydrolysis.[5] Enzymatic activity may degrade drugs into byproducts that are not detected in toxicological analyses or may increase parent drug levels through metabolite hydrolysis. Some microorganisms produce unique nonhuman metabolites, while others are unable to metabolize specific drugs.[6] Consequently, assessed PM drug concentrations usually do not reflect drug levels at the time of death, even when analyzing matrices less influenced by PM redistribution, such as peripheral blood.[7] Therefore, studying drug stability in biological matrices during storage is of the utmost importance when assessing suspected drug-related crimes.[8]

Levine and Smith[9] were the first to review the stability of compounds of toxicological interest in blood, plasma, serum, urine, oral fluid, and tissue samples. Despite the rising volume of experimental and laboratory research published in forensic toxicology,[10,11] in most studies stability has been investigated using fresh or PM spiked blood samples[12–15] or simulated matrices.[16] Fewer experiments have examined the stability of compounds of forensic interest in real samples collected PM.[17] The presence of multiple analytes, which is very common in drug-related death cases, can influence the stability of some compounds; however, this issue has rarely been taken into consideration.[18]

The Guidelines for Sample Collection Postmortem[19] recommend the collection of blood in tubes containing both preservatives and no preservatives. The addition of preservatives, such as fluoride at concentrations of up to 2%, to collected matrices has been shown to increase the stability of analytes over time. One of the main reasons for this practice is to prevent PM degradation of molecules, which may occur even under storage conditions. Since the Guidelines[19] state that sampling can also be performed without preservatives, it is necessary to understand the stability of these compounds for medico-legal purposes. Nevertheless, in routine forensic casework, most laboratories analyze samples within a short time frame, making the addition of preservatives unnecessary. In this context, the re-testing of samples stored for a prolonged period without preservatives presents greater complexity in terms of interpretation.

Objectives

Our experimental study aimed to investigate the long-term stability of drugs of abuse and psychoactive substances in real, unpreserved PM samples from drug-related deaths stored at –20°C over a period of 29 months.

Materials and methods

Chemicals and reagents

Cocaine, benzoylecgonine, cocaethylene, morphine, codeine, methadone, 2-ethylidene-1,5-dimethyl-3,3-diphenylpyrrolidine (EDDP), opioid analgesics, ketamine, norketamine, and the standards of all included drugs (antipsychotics, antidepressants, benzodiazepines),[20] nordiazepam-d5, and ammonium formate were purchased from Sigma-Aldrich® (Steinheim, Germany). Ultra-pure water was obtained by filtration using a Purelab® Chorus 1 Elga

system (High Wycombe, UK). Formic acid, acetonitrile, 2-isopropanol, and methanol were purchased from Merck® (Darmstadt, Germany).

Instrumentation

Chromatography was performed using an Acquity UPLC® System (Waters Corporation, Milford, USA) equipped with an Acquity UPLC® HSS C18 column (2.1 × 150 mm, 1.8 µm; Waters Corporation) set at 50°C. The mobile phase consisted of an aqueous solution of 5 mM ammonium formate with 0.1% (v/v) formic acid (A) and acetonitrile with 0.1% (v/v) formic acid (B). The UPLC system was coupled to a Waters triple quadrupole detector (Xevo TQD®) with electrospray ionization (ESI) in positive mode, and data acquisition was carried out in Multiple Reaction Monitoring (MRM) mode. Data acquisition and analysis were performed using MassLynx v. 4.2® software (Waters Corporation), whereas quantitation was performed using the TargetLynx application (Waters Corporation).

Sample collection

The analysis in this study was conducted on 44 PM blood samples collected in 10-mL Vacutainer tubes without any additive or preservative and analyzed for medico-legal purposes at the Laboratory of Forensic Toxicology of the University of Bologna (Italy) between January 2022 and November 2023, according to standardized procedures.[21] The cohort comprised 33 men and 11 women. All specimens were stored at –20°C before and after analysis. In May 2024, 1 tube from each sample was reanalyzed under the same instrumental conditions. The time intervals for reanalysis were heterogeneous, ranging from 6 to 29 months.

Sample preparation and analysis

The sample pre-treatment consisted of protein precipitation with ice-cold acetonitrile added to 100 µL of blood. After centrifugation and dilution with mobile phase A, 5 µL was injected into the ultra-performance liquid chromatography–tandem mass spectrometry (UPLC-MS/MS) instrument. The analytical procedure for both the original analyses and the subsequent reanalyses was the same and consisted of a method for the simultaneous detection of drugs of abuse (cannabinoids, cocaine and metabolites, opiates and methadone, amphetamine-like drugs, ketamine) and 68 commonly prescribed antidepressants, benzodiazepines, neuroleptics, and their metabolites in whole blood.[20]

Statistical analyses

Stability was defined as the ability of a drug concentration to remain unchanged during storage over time. Stability was measured as the change in concentration from the time of the first analysis to the time of reanalysis and was expressed either as the absolute difference in concentration or as the percentage change. The following drugs (or classes of drugs) were assessed: morphine and codeine, cocaine, benzoylecgonine, cocaethylene, methadone, EDDP, ketamine, norketamine, benzodiazepines, antidepressants, antipsychotics, and lidocaine.

For each molecule, we computed the average monthly decrease in concentration by dividing the absolute difference between T0 and T1 by the number of elapsed months. Confidence intervals (CIs) were estimated using nonparametric bootstrapping (1,000 replications) with the bias-corrected and accelerated (BCa) method to account for the small sample size, potential outliers, and heteroskedasticity in the estimates.[22] A 95% CI entirely below zero was interpreted as evidence of a statistically significant monthly decrease at the 5% level.

The same analysis was replicated in percentage terms using the monthly compounded degradation rate. This was calculated from the ratio T_1/T_0 under the assumption that the molecule concentration decreases each month by a constant proportion, consistent with an exponential decay model. This yielded the formula

$$[(T_1/T_0)^{(1/m)} - 1] \times 100,$$

where "m" denotes the number of elapsed months.

While exploratory regressions (e.g., applying square-root or log transformations of time) were initially considered, we refrained from formal modeling due to the small sample sizes (ranging from 4 for norketamine to 19 for benzodiazepines), the lack of repeated measurements or grouping structures, and the absence of theoretical support for a specific degradation law. We therefore prioritized robustness, interpretability, and minimal reliance on distributional assumptions. As a secondary analysis, we computed Kendall's τ_b correlations between the overall percentage decrease in concentration and the number of elapsed months. We used Kendall's τ_b rather than Spearman's ρ because it is more robust in small samples and provides a stricter correction for tied ranks in either variable. Given the frequency of ties in elapsed time and the limited sample size, τ^b offered a more appropriate nonparametric correlation measure for our analysis.[23]

As this was an exploratory study, no corrections for multiple comparisons were applied. Each molecule was analyzed separately, and no formal comparisons were made across substances. Nevertheless, we acknowledge that multiple hypothesis testing may inflate the type I error rate, and the results should be interpreted accordingly. All analyses were conducted using Stata/SE v. 18 (StataCorp LLC, College Station, USA).

Results

Absolute and relative estimates of average monthly degradation for all tested molecules are reported in Table 1. The results of the T_1/T_0 analysis for all samples are reported in Supplementary Table 1 and 2.

Table 1. Average monthly degradation of various drugs of abuse and psychoactive substances in postmortem (PM) samples from drug-related deaths (absolute and relative estimates)

Abused drugs and pharmaceuticals	Number of samples	Months (range)	Average monthly change [mg/mL]		Average monthly change [%]	
			mean	95% CI	mean	95% CI
Morphine and codeine	12	6–25	–4.42	–14.57, –1.47	–4.4	–7.1, –2.7
Cocaine	13	6–28	–14.38	–36.52, –3.58	–4.4	–6.4, –3.2
Benzoylecgonine	17	6–26	–46.59	–83.11, –26.17	–5.5	–7.9, –3.9
Cocaethylene	8	9–26	–1.51	–3.62, –0.19	–3.9	–7.2, –2.4
Methadone	11	6–28	–17.63	–25.17, –12.24	–5.9	–9.9, –3.9
EDDP	11	6–28	–4.39	–9.16, –2.13	–6.4	–9.9, –4.3
Ketamine	5	7–23	-4,92	-19.65, –7.00	–13.8	–21.5, –6.4
Norketamine	4	7–23	–52.67	–152.48, –2.32	–9.2	–11.5, –5.8
Benzodiazepines	19	6–29	–2.95	–8.16, –1.38	–6.5	–9.9, –4.0
Antipsychotics	10	6–28	–2.11	–5.55, –0.84	–5.4	–9.1, –2.8
Antidepressants	10	6–29	–21.33	–51.27, –10.83	–7.4	–12.1, –4.5
Lidocaine	8	6–21	–1.38	–4.74, –0.39	–5.4	–11.3, –2.6

95% CI – 95% confidence interval; EDDP – 2-ethylidene-1,5-dimethyl-3,3-diphenylpyrrolidine.

Discussion

The interpretation of toxicological results in PM samples remains a widely debated topic in forensic toxicology, primarily due to artificial increases or decreases in PM blood concentrations. The main factor responsible for increased concentrations is PM redistribution, a well-known phenomenon describing site- and time-dependent changes in drug levels after death. Drugs bound to tissues can be released from areas of higher concentration, such as the lungs, liver, or stomach contents, and subsequently move along concentration gradients, leading to an artificial rise in PM blood concentrations.

Conversely, drug concentrations may decrease due to tissue uptake, metabolism, or instability and degradation resulting from decomposition or bacterial activity.[24] These processes can significantly affect the interpretation of toxicological results and may lead to misjudgment of the toxicological significance of drug concentrations in medicolegal investigations. Besides PM redistribution, stability may also lead to alterations in PM concentrations. In fact, the time between the initial analysis and any subsequent reanalysis can be prolonged, sometimes lasting months or even years, depending on the legal context. Therefore, PM stability is a critical factor that must be systematically evaluated in forensic toxicology. We addressed this issue by investigating concentration changes in drugs of abuse (cocaine and its metabolites, opiates, ketamine and its metabolites, methadone) and pharmaceuticals (benzodiazepines, antidepressants, antipsychotics) in PM blood stored at –20°C without preservatives for up to 29 months.

The analytical results demonstrate absolute and relative reductions in concentration over time for all tested molecules, beginning within the initial months. The results of the secondary analysis (Supplementary Table 1) highlight the limitations of raw time-to-decrease correlations in this context and support the use of normalized degradation rates that explicitly account for time as a key component of the phenomenon under investigation. These rates are not adjusted post hoc but intrinsically incorporate time through their construction formula, which expresses degradation per unit of time under the assumption of constant proportional loss.

This approach is especially appropriate when the time intervals between the 1st and 2nd analyses are highly variable, as in our study (ranging from 6 to 29 months), and when the sample size for each molecule is small, thereby limiting the robustness of traditional regression models. By calculating monthly compounded degradation rates and estimating their uncertainty via bootstrapping, we were able to identify consistent and significant degradation patterns across all molecules, even in the absence of a strong linear or monotonic correlation between elapsed time and percentage decrease.

Morphine and codeine showed an average monthly percentage change of 4.4%, with significant variability among samples. In fact, 5 out of 12 samples demonstrated very good stability, with reductions below 20% at 6, 11, and 19 months, while 3 samples showed reductions greater than 30% starting at 5 months. In the forensic literature, the stability of morphine in real samples has been primarily studied using spiked blank matrices obtained from living subjects.[1,9] In a study performed by Høiseth et al.,[25] the stability of opiates in 37 PM blood samples obtained from deaths following heroin intake was investigated. They observed good stability in PM samples (–12% for morphine and –11% for codeine over 4–9 years), which was lower than that observed in samples from living individuals. The results suggest that, for extended storage periods, the use of preservatives for opioids is strongly recommended.

Given the high number of cocaine-positive samples and its metabolites, cocaine, benzoylecgonine, and cocaethylene were studied separately. Similar average monthly

percentage changes were observed for all 3 molecules (4.4%, 5.5%, and 3.9%, respectively). Studies assessing the stability of cocaine in real casework include only a small number of cases. Kiszka et al.[26] tested the stability of cocaine for up to 90 days in PM blood obtained from 5 corpses. They observed degradation of up to 7% of the initial concentration in frozen samples without preservatives, whereas samples containing preservatives (NaF, CH_3COOH, and NaF + CH_3COOH) showed good stability.[26] Although stability in real samples with preservatives was not studied over longer time intervals, these findings suggest that preservatives slow degradation and should be considered during sampling, especially when reanalysis is performed after months or years. Methadone showed an average monthly percentage change of 5.9%. Notably, several samples demonstrated significant decreases even after short time intervals (5–10 months). Methadone has shown very good stability in clinical plasma samples[27]; however, despite being increasingly detected in drug-related deaths, particularly in cases of co-administration, there is a lack of stability studies on methadone in PM samples. Benzodiazepines (6.5%), antidepressants (7.4%), and antipsychotics (5.4%) exhibited significant reductions over time, even during early periods. Melo et al.[28] conducted an experimental study on unpreserved PM blood spiked with benzodiazepines, observing reductions of up to 13% at 6 months. The wide variability and marked degradation observed in our study may be attributable to the longer study intervals and the heterogeneity of the drugs examined. Additionally, very high variability was observed within this class of molecules, with concentration reductions ranging from 26% to 92% at 28 months. Similar results were observed for antidepressants (–60.4%), whereas antipsychotics showed greater stability, albeit with high inter-sample variability. For ketamine (13.8%) and lidocaine (5.4%), the limited sample size precluded firm conclusions, although significant long-term reductions in stability were observed for these molecules.

In general, although a strong relationship between percentage reduction and elapsed time was observed for all molecules, it is not possible to formulate a model for back-calculating the time elapsed since the initial analysis, as significant inter-sample variability was observed that cannot be predicted using a single model. Therefore, the results should be interpreted in terms of likely concentration reductions upon reanalysis, with careful consideration of quantitative findings.

The differences in stability among samples may be attributed to several factors. First, the initial concentrations of the molecules in the starting samples varied, which may influence the degradation rate.[1] Additionally, heterogeneity in the composition of PM samples may account for the fact that PM blood typically exhibits a lower pH compared with blood collected from living individuals, thereby promoting hydrolysis. This pH may vary depending on the PM interval (PMI), and its effect on analytes differs according to the molecular structure of the drug.[4]

Moreover, biological sex may represent an additional source of variability. It is well established in forensic toxicology that sex influences drug pharmacokinetics and pharmacodynamics; however, little is known about the influence of sex on the decrease in drug concentrations in PM samples.[29] Therefore, future studies should also consider sex as a variable, both when defining PM redistribution as a function of PMI and when assessing stability.

Regrettably, given the limited number of cases included in this preliminary analysis, subgroup analyses were precluded due to insufficient statistical power. Finally, based on the current literature, sample stability in tubes containing preservatives appears to be superior and more reliable over extended periods. However, in the absence of comparative experimental studies on real-world samples employing a study design analogous to the present investigation, this hypothesis requires further experimental validation.

Limitations of the study

This study has several unavoidable limitations in the forensic context. Primarily, the subjects from whom the samples were collected had varying PMIs, potentially leading to differential degradation patterns. Consequently, future research could benefit from conducting multiple analyses on single-sample aliquots. However, this approach would introduce the confounding effect of freeze–thaw stability. Furthermore, in this study, most samples tested positive for multiple drugs, as is commonly observed in real forensic casework, and there may be unknown interactions that warrant further investigation. In addition, the influence of the subject's sex on the decrease in drug concentrations in PM samples warrants further examination. This analysis was not feasible in the current preliminary study due to the limited number of cases included.

Conclusions

The lack of stability observed in this preliminary study highlights the critical importance of considering storage conditions and biochemical variations when evaluating re-testing results in forensic investigations. Potential interactions between different compounds within the blood matrix may affect the stability of individual target analytes, thereby complicating the interpretation of toxicological results. This underscores the necessity for comprehensive analytical strategies that account for PM alterations to ensure reliable and legally defensible results.

Supplementary data

The supplementary materials are available at https://doi.org/10.5281/zenodo.15737109. The package contains the following files:

Supplementary Table 1. The results of the analysis at T_1/T_0 for all samples are reported.

Supplementary Table 2. Kendall's τb correlations between the overall percent decrease in molecule concentration and the number of elapsed months.

Data Availability Statement

The datasets supporting the findings of the current study are openly available in Zenodo at https://doi.org/10.5281/zenodo.15082513.

Consent for publication

Not applicable.

Use of AI and AI-assisted technologies

Not applicable.

ORCID iDs

Guido Pelletti https://orcid.org/0000-0003-3263-1758
Susan Mohamed https://orcid.org/0000-0003-3311-1404.
Rafael Boscolo-Berto https://orcid.org/0000-0001-7556-1943
Alessia Giampietro https://orcid.org/0009-0005-0272-5309
Arianna Giorgetti https://orcid.org/0000-0002-0441-9787
Jennifer Pascali https://orcid.org/0000-0002-1363-3400
Jacopo Lenzi https://orcid.org/0000-0003-2882-4223
Susi Pelotti https://orcid.org/0000-0003-2214-8885

References

1. Peters FT. Stability of analytes in biosamples: An important issue in clinical and forensic toxicology? *Anal Bioanal Chem*. 2007;388(7):1505–1519. doi:10.1007/s00216-007-1267-2
2. Boscolo-Berto R. Challenges and future trends of forensic toxicology to keep a cut above the rest. *Adv Clin Exp Med*. 2024;33(5):423–425. doi:10.17219/acem/185730
3. Giorgetti A, Pascali JP, Pelletti G, et al. Optimizing screening cutoffs for drugs of abuse in hair using immunoassay for forensic applications. *Adv Clin Exp Med*. 2024;34(1):75–82. doi:10.17219/acem/183124
4. Skopp G. Preanalytic aspects in postmortem toxicology. *Forensic Sci Int*. 2004;142(2–3):75–100. doi:10.1016/j.forsciint.2004.02.012
5. Butzbach DM. The influence of putrefaction and sample storage on postmortem toxicology results. *Forensic Sci Med Pathol*. 2010;6(1):35–45. doi:10.1007/s12024-009-9130-8
6. Martínez-Ramírez JA, Strien J, Walther G, Peters FT. Search for fungi-specific metabolites of four model drugs in postmortem blood as potential indicators of postmortem fungal metabolism. *Forensic Sci Int*. 2016;262:173–178. doi:10.1016/j.forsciint.2016.03.006
7. Castle JW, Butzbach DM, Walker GS, Lenehan CE, Reith F, Kirkbride KP. Microbial impacts in postmortem toxicology. In: Carter DO, Tomberlin JK, Benbow ME, Metcalf JL, eds. *Forensic Microbiology*. Hoboken, USA: Wiley; 2017:212–244. doi:10.1002/9781119062585.ch9
8. Pelletti G, Garagnani M, Rossi F, Roffi R, Banchini A, Pelotti S. Safe drugs in drug facilitated crimes and acute intoxications in Northern Italy. *Forensic Sci Med Pathol*. 2018;14(4):442–449. doi:10.1007/s12024-018-0010-y
9. Levine B, Smith ML. Stability of drugs of abuse in biological specimens. *Forensic Sci Rev*. 1990;2(2):147–157. PMID:26266841.
10. Viel G, Boscolo-Berto R, Cecchi R, Bajanowski T, Vieira ND, Ferrara SD. Bio-medicolegal scientific research in Europe: A country-based analysis. *Int J Legal Med*. 2011;125(5):717–725. doi:10.1007/s00414-011-0576-3
11. Ferrara SD, Bajanowski T, Cecchi R, Boscolo-Berto R, Viel G. Bio-medicolegal scientific research in Europe: A comprehensive bibliometric overview. *Int J Legal Med*. 2011;125(3):393–402. doi:10.1007/s00414-010-0538-1
12. Kahl JH, Gonyea J, Humphrey SM, Hime GW, Boland DM. Quantitative analysis of fentanyl and six fentanyl analogs in postmortem specimens by UHPLC–MS-MS. *J Anal Toxicol*. 2018;42(8):570–580. doi:10.1093/jat/bky054
13. Kosecki PA, Canonico E, Abbott L. Ethanol stability in unpreserved refrigerated antemortem blood. *J Forensic Sci*. 2023;68(2):682–687. doi:10.1111/1556-4029.15189
14. Skopp G, Pötsch L, Klingmann A, Mattern R. Stability of morphine, morphine-3-glucuronide, and morphine-6-glucuronide in fresh blood and plasma and postmortem blood samples. *J Anal Toxicol*. 2001;25(1):2–7. doi:10.1093/jat/25.1.2
15. Truver MT, Swortwood-Gates MJ. Long-term stability of novel synthetic opioids in blood. *Forensic Sci Int*. 2020;308:110175. doi:10.1016/j.forsciint.2020.110175
16. Castle JW, Butzbach DM, Reith F, et al. Investigations into the stability of 17 psychoactive drugs in a "simulated postmortem blood" model. *Drug Test Anal*. 2022;14(7):1200–1222. doi:10.1002/dta.3239
17. Moretti M, Freni F, Tomaciello I, et al. Determination of benzodiazepines in blood and in dried blood spots collected from postmortem samples and evaluation of the stability over a three-month period. *Drug Test Anal*. 2019;11(9):1403–1411. doi:10.1002/dta.2653
18. Atanasov VN, Stoykova S, Runiov A, et al. Stability of diazepam in blood samples at different storage conditions and in the presence of alcohol. *Forensic Sci Int*. 2012;215(1–3):159–163. doi:10.1016/j.forsciint.2011.04.005
19. Flanagan RJ, Connally G, Evans JM. Analytical toxicology: Guidelines for sample collection postmortem. *Toxicol Rev*. 2005;24(1):63–71. doi:10.2165/00139709-200524010-00005
20. Barone R, Giorgetti A, Cardella R, et al. Development and validation of a fast UPLC–MS/MS screening method for the detection of 68 psychoactive drugs and metabolites in whole blood and application to postmortem cases. *J Pharm Biomed Anal*. 2023;228:115315. doi:10.1016/j.jpba.2023.115315
21. Pelletti G, Rossi F, Garagnani M, et al. Optimization of cloned enzyme donor immunoassay cut-offs for drugs of abuse in postmortem whole blood. *Forensic Sci Int*. 2020;312:110291. doi:10.1016/j.forsciint.2020.110291
22. Efron B. Better bootstrap confidence intervals. *J Am Stat Assoc*. 1987;82(397):171–185. doi:10.1080/01621459.1987.10478410
23. Kendall MG. The treatments of ties in ranking problems. *Biometrika*. 1945;33(3):239–251. doi:10.1093/biomet/33.3.239
24. Mantinieks D, Gerostamoulos D, Glowacki L, et al. Postmortem drug redistribution: A compilation of postmortem/antemortem drug concentration ratios. *J Anal Toxicol*. 2021;45(4):368–377. doi:10.1093/jat/bkaa107
25. Høiseth G, Fjeld B, Burns ML, Strand DH, Vindenes V. Long-term stability of morphine, codeine, and 6-acetylmorphine in real-life whole blood samples, stored at –20°C. *Forensic Sci Int*. 2014;239:6–10. doi:10.1016/j.forsciint.2014.03.008
26. Kiszka M, Buszewicz G, Mądro R. Stability of cocaine in blood and in other tissues. *Z Zagadnień Nauk Sądowych*. 2001;45:16–35. https://arch.ies.gov.pl/images/PDF/2001/vol_45/45_kiszka.pdf.
27. López ML, Baño MD, Guillén JL. Long-term stability of methadone in clinical plasma samples stored at –20°C. *J Anal Toxicol*. 2002;26(4):236–238. doi:10.1093/jat/26.4.236
28. Melo P, Bastos ML, Teixeira HM. Benzodiazepine stability in postmortem samples stored at different temperatures. *J Anal Toxicol*. 2012;36(1):52–60. doi:10.1093/jat/bkr008
29. Giorgetti A, Boscolo-Berto R. Investigating gender dynamics in forensic toxicology: The role of masculinity and femininity in alcohol and drug abuse. *Adv Clin Exp Med*. 2025;34(1):5–8. doi:10.17219/acem/199712

The PassTrue® technique for evaluating the needle/tissue mechanical interaction in a medicolegal simulation setting

Rafael Boscolo-Berto[1,2,A–F], Martina Contran[1,2,B,F], Alessandro De Cassai[3,4,C–F], Raffaele De Caro[1,2,C–F], Veronica Macchi[1,2,C,E,F], Andrea Porzionato[1,2,C–F]

[1] Institute of Human Anatomy, Department of Neurosciences, University of Padova, Italy
[2] Veneto Region Reference Center for the Preservation and Use of Donated Bodies, Padova, Italy
[3] Department of Medicine (DIMED), University of Padova, Italy
[4] Anesthesia and Intensive Care Unit, University Hospital of Padova, Italy

A – research concept and design; B – collection and/or assembly of data; C – data analysis and interpretation; D – writing the article; E – critical revision of the article; F – final approval of the article

Advances in Clinical and Experimental Medicine, ISSN 1899–5276 (print), ISSN 2451–2680 (online) *Adv Clin Exp Med*. 2026;35(4):735–740

Address for correspondence
Rafael Boscolo-Berto
E-mail: rafael.boscoloberto@unipd.it

Funding sources
None declared

Conflict of interest
None declared

Acknowledgements
The authors express their deepest gratitude to the individuals who participate in the University of Padova body donation program, thanks to whom this research was made possible. We hope that the results of these efforts are useful to the entire scientific community and, in doing so, honor the memory of those who donate their bodies. Furthermore, the authors thank Valentina Manzo for her valuable technical support.

Received on December 22, 2025
Reviewed on April 10, 2026
Accepted on April 13, 2026

Published online on April 21, 2026

Cite as
Boscolo-Berto R, Contran M, De Cassai A, De Caro R, Macchi V, Porzionato A. The PassTrue® technique for evaluating the needle/tissue mechanical interaction in a medicolegal simulation setting. *Adv Clin Exp Med*. 2026;35(4):735–740. doi:10.17219/acem/220612

DOI
10.17219/acem/220612

Abstract

Background. The increasing availability of body donations and the expansion of reference centers provide forensic clinical anatomy with the opportunity to experimentally reproduce, in ex vivo settings, the effects of specific interactions on the human body, such as needle–tissue interaction in medical procedures.

Objectives. The primary objective of this study was to develop a reproducible, standardized benchtop methodology that enables the identification of the trajectory traveled by the needle when piercing soft tissue, causing detectable iatrogenic tissue damage.

Materials and methods. Skeletal muscle tissue samples were harvested from a fresh-frozen 78-year-old male body housed at our Reference Center, Center for Body Donation. Needle transfixions were then tested using a novel technique designed for this purpose (PassTrue® methodology): full-thickness tissue transfixion by a needle, insertion into the needle of a coaxial thread, grasping the thread with forceps, and needle withdrawal, so that the in-place thread indicates the route of transfixion. This procedure was tested against the control procedure without a thread.

Results. Microscopic analysis revealed a pattern consistent with the needle's course during transfixion in all cases with the PassTrue® technique (10/10), but not in controls (0/10).

Conclusions. Our novel methodology improves the efficiency of assessing needle–tissue interactions, enabling identification of the needle's trajectory within biological tissues.

Key words: medical malpractice, legal medicine, body donation, cadaver lab, clinical anatomy

Highlights

- PassTrue® methodology enables precise tracking of needle trajectory in soft tissue.
- A standardized ex vivo model supports reproducible analysis of needle–tissue interactions.
- Microscopic validation confirms reliable detection of needle pathways in biological tissue.
- PassTrue® methodology may improve research, training, and patient safety in medical procedures.

Background

A substantial proportion of medical procedures entail the use of needles to inject or aspirate fluids, and this practice inherently constitutes a potential source of tissue trauma.[1] The ensuing tissue injury may plausibly have clinically relevant consequences and, as an adverse effect of medical interventions, can prompt patients to pursue compensation claims or initiate criminal proceedings.[2] In response, there has been a marked and growing concern among clinicians regarding the medicolegal ramifications of their professional activities on patients' health, extending even to seemingly routine needle-based procedures involving tissue penetration. This phenomenon has frequently been described as a "medicolegal epidemic," a characterization mirrored by the expanding body of literature on these issues internationally.[3,4] Nonetheless, with specific regard to tissue damage caused by needle use, the current evidence base remains limited. Although several research papers have examined needle–tissue interaction during medical procedures, particularly focusing on parameters such as velocity of needle insertion and pressure of fluid injection, no consistent, experimentally robust, and reproducible findings have yet been established.

More recently, some authors have focused on iatrogenic tissue injury arising from needle insertion, employing heterogeneous, non-standardized methodologies with limited demonstrable validity and substantial variability in microscopic outcomes, with the fundamental problem of the loss of the tract during histological fixation. These developments have significant implications for clinical risk management and for the formulation of policies guiding the selection of specific invasive techniques among multiple available options. Given the extraordinarily high volume of procedures involving needle–tissue interaction across all medical specialties, this topic is of considerable relevance and warrants systematic, standardized investigation.

Objectives

The primary objective of this pilot study was to develop a reproducible, standardized benchtop methodology that would allow the trajectory of the needle to be identified in tissue.

Materials and methods

Research ethics

All procedures were conducted on human bodies from the "Donation to Science" body donation program of the University of Padova (Italy) and the Veneto Region/National Reference Center for the preservation and use of donated bodies. These procedures adhered to national laws and the ethical standards set by regional and national research committees, as well as the Declaration of Helsinki of 1964, including its later amendments or comparable ethical standards. Participants provided their written informed consent to join the Body Donation Program, which is consistent with ISO 9001:2015 (registration No. IT-62435-16764). The privacy rights of all human subjects were and will always be respected. Informed consent was obtained from all participants involved in the study, in accordance with the procedure for collecting and donating anatomical material.

In accordance with the regulations of the Body Donation Program of the Institute of Human Anatomy (University of Padova), a skeletal muscle tissue specimen (2 × 2 × 1 cm) was harvested from a fresh-frozen male body aged 78 years, housed at our Reference Center.[5–7] As a certified standard, we use a routine protocol according to which we receive the bodies 48 h after death, and on the same day, they are frozen at –20°C with a remote temperature control system until they are used with programmed thawing, approx. 1 month after death.

The donor had no documented diseases that could interfere with the study's objectives. In particular, the donor did not suffer from age-related pathological or physiological cachexia and had a normal build. He was not bedridden and had documented normal mobility consistent with his age. The tissue was fully thawed to room temperature prior to transfixion. On the bench, transfixion of the sample was performed 10 times using the PassTrue® technique.

It consisted of a multistep procedure. Initially, a full-thickness, side-to-side tissue transfixion was performed using a 22-gauge needle (BD Microlance; Becton Dickinson (BD), Oslo, Norway) oriented perpendicular to the tissue plane (Fig. 1A). A coaxial polypropylene monofilament suture (Prolene 3/0; Ethicon, Raritan, USA) was subsequently advanced through the lumen of the needle and grasped on the opposite side with forceps, which maintained traction

on the thread while the needle was carefully withdrawn from the tissue along a trajectory opposite to that of insertion (Fig. 1A). This resulted in the placement of a reference thread indicating the tissue route created by the needle during transfixion (Fig. 1B). A control procedure was performed with 10 free transfixions using the same materials and steps on a comparable control specimen, except for the use of the reference thread passed inside the needle.

Following completion of the procedures, the skeletal muscle tissue specimens were immersed in a 4% m/v formalin solution and stored at room temperature. After 5 days of formalin fixation, they were sectioned at 5-mm intervals, processed according to standard microscopic protocols, and embedded in paraffin. From each sample, sequential 5 µm-thick sections were systematically cut and stained with hematoxylin and eosin (H&E) (W01030708; BioOptica, Milan, Italy) for microscopic characterization.

To perform both the 5-mm and 5 µm-thick sections, the cut plane was consistently aligned with the needle path, which followed a trajectory perpendicular to the skeletal muscle tissue specimen.

The sections were dipped in xylene for deparaffinization, immersed in a graded series of alcohol solutions for hydration, and stained with the kit dyes. Subsequently, dehydration through immersion in an increasing series of alcohol solutions, clarification in xylene, and mounting with Eukitt medium (09-00250; BioOptica) were performed on all tissue sections. Hematoxylin and eosin staining was performed to observe the tissue morphology and architecture of each section of the skeletal muscle tissue samples.

Discussion

Over the past several years, forensic medicine has undergone significant development, particularly in relation to the evaluation of alleged cases of medical malpractice. Within this framework, the subspecialty of forensic clinical anatomy has emerged to investigate the forensic implications of anatomical alterations and variants in the context of assessing iatrogenic injuries and quantifying personal damage.[8,9] The increasing availability of body donations and the expansion of reference centers provide forensic clinical anatomy with the opportunity to experimentally reproduce, in ex vivo settings, the effects of specific interactions on the human body, including those involving medical procedures (e.g., needle–tissue interaction, novel techniques, and innovative tools).[10–12] The interest of legal medicine in this procedure within a hypothetical medical malpractice setting could, e.g., be experimental in nature, relating to the study of the injury a needle could cause when inserted into tissue. In this case, the procedure described in the present paper allows for further investigation of this aspect by precisely tracking the needle's path within the tissue and identifying any consequent vascular or nerve injuries. This allows for better interpretation and analysis of specific clinical conditions, e.g., in the field of anesthesiology, where, in the case of peripheral nerve blocks, nerve injury caused by needle insertion during an anesthetic procedure is possible. Such investigations were previously feasible only in an anecdotal manner in living subjects and were substantially limited by ethical constraints.

The literature exhibits substantial heterogeneity regarding the types of procedures performed, the materials employed, and the biological specimens utilized to investigate needle–tissue interactions. Our novel methodology improves the efficiency of assessing needle–tissue interactions, both in detecting them and in analyzing the needle's trajectory within biological tissues and the consequent structural alterations. Indeed, in the control experiments, no needle tracts (0/10) were identified, even when carefully examining tissue slices corresponding to surface changes that suggested the exact point of needle penetration into the sample (Fig. 1C,D). By contrast, using the PassTrue® procedure, the thread acts as a "wick" that prevents the natural elastic recoil of tissue during fixation, which would otherwise lead to fading of the needle path during transfixion. For this reason, the thread simply keeps the passageway created by the needle open and does not cause any structural alteration or distortion of the tissue. Consequently, a microscopic pattern consistent with needle transfixion was identified in all cases (10/10) in which the PassTrue® procedure was used (Fig. 1E,F). Furthermore, the entire trajectory of the needle was visualized in substantial portions of its course, together with the associated partial tissue removal. The procedure has therefore proven to be valid for testing the muscles of an elderly individual. We expect that in younger subjects, the effect is even greater than in the muscles of an elderly individual. The trophism and the greater presence of elastic fibers in younger subjects would result in a greater probability of obscuring the needle tracks after the needle has passed if a reference thread is not used, as proposed in this procedure.

Overall, based on a literature review, we identified a number of biomechanical studies based on computational simulations, relying on mathematical models and mechanical representations, which we intentionally excluded, restricting our analysis exclusively to studies employing biological material. In several instances, the investigations employed biological material derived from various animal species, including bovine tissue,[13–15] porcine tissue,[16] rabbit tissue,[17] rat tissue,[18,19] and canine tissue.[20] Human biological material (placental tissue) was utilized in only a single study.[21] Moreover, the tissues collected for the experimental analyses were heterogeneous across species, as in each case a different anatomical structure was utilized, including segments of the carotid artery,[13] brain,[16,18,19] sciatic nerve,[17] skeletal muscle,[14] liver,[15] kidney,[20] and placenta.[21] The comparability and reproducibility of experimental results are further compromised by the heterogeneity of microscopic assessment protocols applied to tissues obtained

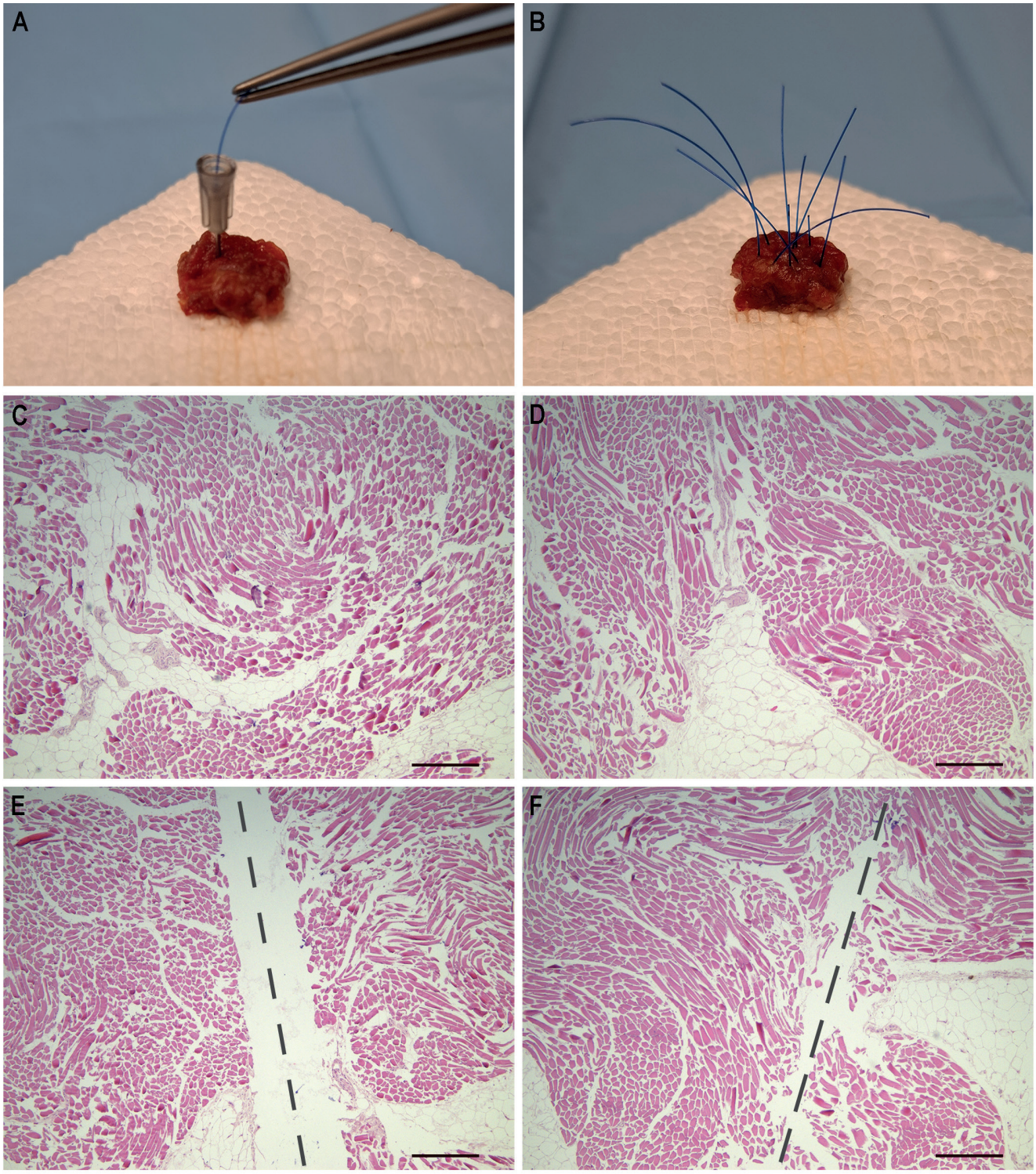

Fig. 1. Key procedural steps and morphological analysis. A. Transfixion of side-to-side tissue using a 22-gauge needle perpendicular to the tissue plane, with a coaxial polypropylene monofilament suture advanced through its lumen; B. Overall placement of reference threads that indicate the tissue routes created by the needle during transfixions; C,D. Microscopic analysis (hematoxylin and eosin (H&E); scale bar 300 µm) of controls. The procedure was performed without the use of the reference thread passed inside the needle. There is no evidence of detectable needle passage; E,F. Microscopic analysis (H&E; scale bar 300 µm) after using the PassTrue® procedure. A microscopic pattern consistent with needle transfixion (dotted line) was detected. The trajectory of the needle was visualized in substantial portions of its course, together with associated partial tissue removal. The tissue removal area corresponds to the white space surrounding the dotted line along the path of the needle in the tissue

following mechanical interaction with the needle. For accurate identification of the needle tract and a more reliable evaluation of the associated tissue injury, histological sectioning should be performed in a longitudinal plane parallel to the needle's major axis,[16,20] rather than in a transverse orientation.[14,15,17–19,21] Notably, in at least 1 study,

morphological characterization using light microscopy was not conducted.[13]

In any case, among all these experimental investigations on needle–tissue interactions, no established method has yielded a defined and reproducible standard that approximates, even remotely, the features of the current PassTrue® technique, and in particular the positioning of a reference thread within the needle trajectory that allows the route to be kept open during the fixation and embedding steps of the tissue sample.

Our findings indicate that the PassTrue® technique constitutes an efficient, standardized, rapid, and cost-effective method that facilitates inter-study comparability, provided that investigations are conducted on the same tissue type within the same species. Within this framework, research involving human biological material assumes particular importance for addressing both clinical and forensic questions, and in this setting, forensic clinical anatomy occupies a pivotal position.

Limitations of the study

Our pilot study presents limitations that warrant consideration. First, while the control demonstrates the usefulness of the thread for visualization, it does not confirm whether the thread maintains the fidelity of the original injury geometry, although it has a smaller diameter than the needle used for transfixion, and we do not expect any significant inconsistencies. Second, this technique has currently only been tested in muscle tissue harvested from a single donor, and the needle interaction observed here using the PassTrue® technique may differ in tissues with different collagen densities, for which specific experimental tests will be necessary. Third, the use of skeletal muscle samples obtained from a deceased individual allows us to demonstrate only the trajectory traveled by the needle when piercing soft tissue, causing iatrogenic mechanical damage to the tissue, without capturing potential in vivo biological or immunological responses to injury. This may be of clinical interest but is beyond the scope of this paper, which focuses on the development of an innovative experimental model. Fourth, the exclusive use of sharp needles does not fully encompass the spectrum of clinical scenarios, given that non-cutting needles are sometimes preferred for specific procedures. Similarly, different needle diameters and tissue thicknesses could yield slightly different results, although the effectiveness of the innovative approach is expected to be independent of these circumstantial factors, which are probably irrelevant but need to be verified.

Conclusions

The present pilot study showed that the novel PassTrue® technique improves the efficiency of assessing needle–tissue interactions, allowing the needle trajectory to be identified within biological tissues. The methodology is standardized, rapid, and cost-effective. It provides a potential common framework for future medicolegal simulations on cadavers and facilitates comparability across studies addressing similar research questions. However, further studies will be needed to evaluate the suitability of this new procedure across different combinations of needle type, needle diameter, tissue type, and tissue thickness.

Registered trademark

PassTrue® is a trademark registered by the University of Padova on behalf of Prof. Rafael Boscolo-Berto, using his personal funds.

Consent for publication of personal information

Not applicable.

Use of AI and AI-assisted technologies

Not applicable.

ORCID iDs

Rafael Boscolo-Berto https://orcid.org/0000-0001-7556-1943
Martina Contran https://orcid.org/0000-0002-3709-8414
Alessandro De Cassai https://orcid.org/0000-0002-9773-1832
Raffaele De Caro https://orcid.org/0000-0002-8991-7610
Veronica Macchi https://orcid.org/0000-0003-2335-6897
Andrea Porzionato https://orcid.org/0000-0003-3025-4717

References

1. Torrano V, Anastasi S, Balzani E, et al. Enhancing Safety in Regional Anesthesia: Guidelines from the Italian Society of Anesthesia, Analgesia, Resuscitation and Intensive Care (SIAARTI). *J Anesth Analg Crit Care*. 2025;5(1):26. doi:10.1186/s44158-025-00245-y
2. Members of the IALM Working Group on Personal Injury and Damage; Ferrara SD, Baccino E, Boscolo-Berto R, et al. Padova Charter on personal injury and damage under civil-tort law: Medico-legal guidelines on methods of ascertainment and criteria of evaluation. *Int J Legal Med*. 2016;130(1):1–12. doi:10.1007/s00414-015-1244-9
3. Ferrara SD, Bajanowski T, Cecchi R, Boscolo-Berto R, Viel G. Bio-medicolegal scientific research in Europe: A comprehensive bibliometric overview. *Int J Legal Med*. 2011;125(3):393–402. doi:10.1007/s00414-010-0538-1
4. Giorgetti C, Giorgetti A, Boscolo-Berto R. Establishing new boundaries for medical liability: The role of AI as a decision-maker. *Adv Clin Exp Med*. 2025;34(10):1601–1606. doi:10.17219/acem/208596
5. Porzionato A, Macchi V, Stecco C, et al. Quality management of body donation program at the University of Padova. *Anat Sci Ed*. 2012;5(5):264–272. doi:10.1002/ase.1285
6. Boscolo-Berto R, Porzionato A, Stecco C, Macchi V, De Caro R. Reference centers for tissue and body donations: Compulsory requirements in Italy. *Clin Anat*. 2023;36(3):465–470. doi:10.1002/ca.23990
7. Boscolo-Berto R, Porzionato A, Stecco C, Macchi V, De Caro R. Body donation in Italy: Lights and shadows of law No. 10/2020. *Clin Anat*. 2020;33(6):950–959. doi:10.1002/ca.23623
8. Porzionato A, Macchi V, Stecco C, Loukas M, Tubbs RS, De Caro R. Forensic clinical anatomy: A new field of study with application to medicolegal issues. *Clin Anat*. 2017;30(1):2–5. doi:10.1002/ca.22796
9. Porzionato A, Macchi V, Stecco C, et al. Clinical anatomy and medical malpractice: A narrative review with methodological implications. *Healthcare (Basel)*. 2022;10(10):1915. doi:10.3390/healthcare10101915

10. Boscolo-Berto R, Macchi V, Tubbs RS, et al. The transversoclasiotome: A novel instrument for examining the vertebral artery. *Forensic Sci Med Pathol*. 2023;20(2):325–334. doi:10.1007/s12024-023-00638-x
11. Boscolo-Berto R, Maggiolo A, Emmi A, Macchi V, Navalesi P, De Cassai A. Morphological findings in the sciatic nerve after intraneural injection. *J Clin Anesth*. 2025;104:111868. doi:10.1016/j.jclinane.2025.111868
12. De Cassai A, Santonastaso DP, Coppolino F, et al. Perineural dexamethasone: Neurotoxicity or neuroprotection? A systematic review of preclinical evidence. *J Anesth Analg Crit Care*. 2025;5(1):50. doi:10.1186/s44158-025-00271-w
13. Ross EA, Verlander JW, Koo LC, Hawkins IF. Minimizing hemodialysis vascular access trauma with an improved needle design. *J Am Soc Nephrol*. 2000;11(7):1325–1330. doi:10.1681/ASN.V1171325
14. Tsumura R, Takishita Y, Fukushima Y, Iwata H. Histological evaluation of tissue damage caused by rotational needle insertion. *Annu Int Conf IEEE Eng Med Biol Soc*. 2016;2016:5120–5123. doi:10.1109/EMBC.2016.7591879
15. Gidde STR, Acharya SR, Kandel S, Pleshko N, Hutapea P. Assessment of tissue damage from mosquito-inspired surgical needle. *Minim Invasive Ther Allied Technol*. 2022;31(7):1112–1121. doi:10.1080/13645706.2022.2051718
16. Lehocky C, Fellows-Mayle W, Engh J, Riviere CN. Tip design for safety of steerable needles for robot-controlled brain insertion. *Robot Surg*. 2017;4:107–114. doi:10.2147/RSRR.S141085
17. Maruyama M. Long-tapered double needle used to reduce needle stick nerve injury. *Reg Anesth*. 1997;22(2):157–160. doi:10.1016/S1098-7339(06)80035-0
18. Casanova F, Carney PR, Sarntinoranont M. Effect of needle insertion speed on tissue injury, stress, and backflow distribution for convection-enhanced delivery in the rat brain. *PLoS One*. 2014;9(4):e94919. doi:10.1371/journal.pone.0094919
19. Casanova F, Carney PR, Sarntinoranont M. In vivo evaluation of needle force and friction stress during insertion at varying insertion speed into the brain. *J Neurosci Methods*. 2014;237:79–89. doi:10.1016/j.jneumeth.2014.08.012
20. Majewicz A, Marra SP, Van Vledder MG, et al. Behavior of tip-steerable needles in ex vivo and in vivo tissue. *IEEE Trans Biomed Eng*. 2012;59(10):2705–2715. doi:10.1109/TBME.2012.2204749
21. Gratacós E, Devlieger R, Decaluwé H, Wu J, Nicolini U, Deprest JA. Is the angle of needle insertion influencing the created defect in human fetal membranes? Evaluation of the agreement between specialists' opinions and ex vivo observations. *Am J Obstet Gynecol*. 2000;182(3):646–649. doi:10.1067/mob.2000.103218